

https://dspace.org/

Verifying the Quality and Performance of Grout Using Sensor Technology

Hadebe, Menzi Bright

2023-10
University of the Witwatersrand, Johannesburg
https://hdl.handle.net/10539/38916
Hadebe, Menzi Bright. (2023). Verifying the Quality and Performance of Grout Using Sensor Technology. [Master's dissertation, University of the Witwatersrand, Johannesburg]. WIReDSpace. https://hdl.handle.net/10539/38916

Downloaded from a DSpace repository. https://dspace.org/

School of Mining Engineering



UNIVERSITY OF THE
WITWATERSRAND,
JOHANNESBURG

VERIFYING THE QUALITY AND PERFORMANCE OF GROUT USING SENSOR TECHNOLOGY

Menzi Bright Hadebe

A research report submitted to the Faculty of Engineering and the Built Environment, University of the Witwatersrand, Johannesburg, in partial fulfilment of the requirements for the degree of Master of Science in Engineering.

Johannesburg, 2023

DECLARATION

I declare that this report is my own, unaided work. I have read the University Policy on Plagiarism and hereby confirm that no plagiarism exists in this report. I also confirm that there is no copying nor is there any copyright infringement. I willingly submit to any investigation in this regard by the School of Mining Engineering and I undertake to abide by the decision of any such investigation.

Menzi Bright Hadebe
_____ 30/10/2023

Signature of Candidate Date

ABSTRACT

Underground mines systematically install ground support to stabilize excavations and provide safe working environments. Support units, such as rock bolts and cables, are commonly filled with cementitious grout to effectively prevent corrosion, maintain bonding behaviour between the support unit and grout, and enhance the load transfer between the grout and surrounding rock mass. The grouting process is however time-consuming and labour-intensive, which leads to haphazard installations. These substandard grout installations are only observed after rock fall instabilities occur when the quality and extent of grouting inside a support hole are exposed and can be observed.

The need to monitor grout installations increased (provide assurance) but remained a challenge due to the invisibility of grout inside the support hole. The invisibility of the grout column inside the support hole renders the routine quality control inspections of installed support units ineffective. This ineffectiveness of quality control inspections has led to a growing need to monitor grout installations with smart technologies to provide quality assurance of full-column grouting.

In its current state, grout technology in the mining industry can only measure the extent of grout inside a support hole directly after installation (limited battery life). It cannot measure the loss of grouting material into near-borehole fractures, shrinkage, quality of grout inside the support hole or its

impact on support performance. These factors are critical to the success of an effective support system and pose a significant safety risk when overlooked.

This research report will describe how grout sensor technology data was recorded and used to verify the extent and quality of cementitious grout inside support hole installations at laboratory and deep-level mine study sites. Grout sensor technology, in practice, utilizes several grout sensors placed at predetermined positions along a support unit with a receiver attached to the collar of the support hole. Electrical resistivity data from each sensor is collected using a grout detector. Depending on the position of each grout sensor, the extent of grout inside a support hole can be confirmed, hence eliminating the need for speculative and ineffective visual observations.

The non-destructive verification and prediction of the quality and performance of grout inside support holes using sensor technology forms an invaluable strata control tool that can be used to identify sub-standard grouting operations and significantly improve safety at underground mines. This novel and innovative technology is a mining industry first.

DEDICATION

I dedicate this work to my late mother Peggy Zanele, my fiancé Thabile Sonke, and my daughter Mpilenhle Zamahlubi.

ACKNOWLEDGMENTS

I would like to acknowledge Gold Fields for funding my studies and permitting me access to the South Deep gold mine. I would like to give special thanks to Rabele, Tshimangadzo and the rest of the Technical Services Department at the South Deep gold mine for assisting with the underground visits and data recording.

I would also like to thank Fabchem Mining for providing me with the research materials as well as permitting me to access their laboratory facilities. A special word of thanks to Freddy (Director Fabchem), Jaco and Elvis for their technical advice and assistance with underground visits.

Last but not least, I would like to thank my Wits supervisor, Prof R. Mitra, for supervising me and for making countless hours available to go through my MSc chapters. I am profoundly grateful.

TABLE OF CONTENTS

DECLARATION i

ABSTRACT ii

DEDICATION iv

ACKNOWLEDGMENTS v

LIST OF FIGURES x

LIST OF EQUATIONS xx

LIST OF TABLES xx

LIST OF APPENDIX TABLES xxiii

LIST OF SYMBOLS xxiv

1 INTRODUCTION 1

1.1 Project Background 1

1.2 Problem Statement 4

1.3 Research Questions and Hypothesis 4

1.4 Research Methodology 5

1.5 Significance of the Study 5

1.6 Report Structure 7

2 SOUTH DEEP MINE OVERVIEW 8

2.1 Introduction 8

2.2 Locality and Overview 8

2.3 Geology and Mining Method 10

2.4 Quality Control of Support Units 11

3 LITERATURE SURVEY 12

3.1 Introduction 12

3.2 Cable Bolting in Mining 12

3.2.1 Elements of the cable bolt system 17

3.2.2 Corrosion prevention and load transfer-mechanism 19

3.3 The Grouting of Cable Bolts 23

3.3.1 The breather-tube grouting method 27

3.3.2 The grout-tube grouting method 28

3.4 Shrinkage Studies of Cementitious Materials 29

3.4.1 Shrinkage test conditions 32

3.4.2 Testing standards and variations of ASTM 35

3.5 Pull-Out Testing of Support Units 43

3.5.1 Cable bond strength 48

3.5.2 Factors affecting pull-out testing 50

3.5.3 Simulating failure modes 53

3.5.4 Corrosion studies using pull-out testing 56

3.5.5 Modelling pull-out testing 57

3.6 Mining Smart Sensor Technologies 59

3.6.1 Strain-gauge and other methods 61

3.6.2 Ultrasonic-guided waves 67

3.6.3 Optical-fibre methods 72

3.7 Electrical Resistivity Technology 75

3.7.1 Portland cement hydration and electrical resistivity 79

3.7.2 Curing temperatures 84
3.7.3 Water-cement ratio 89
3.7.4 Compressive strength 94
3.8 Chapter Summary 101
4 RESEARCH METHODOLOGY 110
4.1 Introduction 110
4.2 Grout Shrinkage 112
4.3 SEPT 115
4.4 Grout Sensor Technology 119
4.4.1 Laboratory Grout Sensor Data Recording 126
4.4.2 Underground Grout Sensor Data Recording 128
5 RESULTS AND DISCUSSION 134
5.1 Introduction 134
5.2 Grout Shrinkage 134
5.2.1 Grout shrinkage summary 140
5.3 SEPT 140
5.3.1 SEPT Summary 148
5.4 Grout Sensor Technology 148
5.4.1 Grout quality 149
5.4.2 Grout quality summary 167
5.4.3 The setting of grout 168
5.4.4 The setting of grout summary 176
5.4.5 The effectiveness of grout 177

5.4.6 The effectiveness of grout summary 193
5.5 Shortcomings of Grout Sensor Technology 194
5.5.1 Grout sensor technology shortcomings summary 199
6 CONCLUSIONS AND RECOMMENDATIONS 201
6.1 Introduction 201
6.2 Grout Shrinkage 201
6.3 SEPT 203
6.4 Grout Sensor Technology 204
6.5 Research Limitations 209
6.6 Recommendations 209
6.7 Further Work 210
REFERENCE LIST 212
APPENDIX 229

LIST OF FIGURES

Figure 1.5-1. Graph of fatalities recorded in South African mines between 2000 and 2021 (Minerals Council, 2021). 6

Figure 2.2-1. Locality map of the South Deep gold mine (Gold Field Mineral Resource and Mineral Reserves Supplement, 2020)..... 9

Figure 2.3-1. A 3D view geological map of the South Deep gold mine (Gold Field Mineral Resource and Mineral Reserves Supplement, 2020). 10

Figure 3.2-1. An illustration of longitudinal and cross-sections of the diverse types of cable bolt configurations (Hutchison and Diederichs, 1996, pp.11) 14

Figure 3.2-2. An illustration of the use of cable bolting for support in underground mines (Hutchison and Diederichs, 1996, pp.6) 16

Figure 3.2-3. A diagram illustrating the elements of the cable bolt system (Modified from Li, 2017, pp. 17) 17

Figure 3.2-4. Photos of a fall of ground in an underground tunnel, (left) A fall of ground attributed to corroded support anchors, and (right) Heavily corroded support anchors sticking out from fallen blocks of rocks (Dorion, 2019)..... 21

Figure 3.2-5. A drawing illustrating the concept of the load transfer mechanism (Thompson and Villaescusa, 2014) 22

Figure 3.3-1. A plot of UCS versus the w/c ratio of grout (Hutchison and Diederichs, 1996, pp.66)..... 25

Figure 3.3-2. The breather (left) and grout tube grout (right) installation methods (Hoek et al., 1980) 28

Figure 3.3-3. An illustration of an underground cable bolt installed using the grout tube method (Reny et al., 2019) 29

Figure 3.4-1. A plot of ten-hour cured OPC shrinkage values versus curing age in hours under three different test conditions (Newlands et al., 2008) 34

Figure 3.4-2. A digital length comparator and a three-gang shrinkage mould equipment used to measure shrinkage (Kucharczykova et al., 2017) 37

Figure 3.4-3. (a) A plot of relative length change versus curing age in days for different sets of test specimens, and (b) A plot of relative mass loss for the different test specimens (Kucharczykova et al., 2017) 38

Figure 3.4-4. A plot of micro-strain shrinkage versus drying time in days measured in an (a) 0.45 w/c ratio shotcrete mixture and in an (b) 0.60 w/c ratio shotcrete mixture (Menu et al., 2017) 40

Figure 3.4-5. A plot of total and autogenous shrinkage deformation strain and changes in length for pre-blended grouts five and six versus curing age, post-demoulding, in days (Mohan et al., 2021) 42

Figure 3.5-1. A diagram of a pull-out testing hydraulic jack (Littlejohn and Bruce, 1975) 45

Figure 3.5-2. A rock bolt pull-out test schematic (ASTM D4435-08) 46

Figure 3.5-3. A plot of the critical embedment length and mean rebar–grout bond strength (Li et al., 2016) 50

Figure 3.5-4. An illustration of the routed anchor models used to assess three diverse types of rock anchors and two anchorage lengths (Benmokrane et al., 1995) 51

Figure 3.5-5. A diagram of the device used for constrained axial and shear testing of cable bolts (Bawden et al., 1994) 54

Figure 3.5-6. A plot of load versus displacement that compares the standard and SINTEF pull-out testing benches (Hagen et al., 2020) 55

Figure 3.5-7. 3DEC modelling of cable bolts output showing the variation of pull-out load with the length of grouted and non-grouted cable anchors (Singh and Srivastava, 2021)..... 58

Figure 3.5-8. FLAC3D model showing the angled strain-gauge instrumented rock bolt installations and a dipping geological structure for a room and pillar mining method (Singh et al., 2022) 59

Figure 3.6-1. A diagrammatical representation of the non-destructive monitoring of cables and rock bolts using wave-propagation methods (Liu et al., 2022)..... 61

Figure 3.6-2. A picture of a strain gauge device used for the measurement of cable bolt tension values (Chekired et al., 1997) 62

Figure 3.6-3. A smart rock bolt installation in a mine (Eliasson et al., 2014) 64

Figure 3.6-4. The use of the smart rock bolt to detect nearby drilling activity (Eliasson et al., 2014) 64

Figure 3.6-5. A diagrammatical representation of the Cavimeter system comprising of a hand-held readout unit, a Cavimeter backpack housing a gas container, and a plastic tube for installation into a support hole (Gustafsson et al., 2016)..... 65

Figure 3.6-6. A diagram showing a rock bolt installation and the set-up of the guided wave method (Beard and Lowe, 2003)..... 68

Figure 3.6-7. Plots of the bottom-sensor (PZT1) stress-wave signals recorded from different grouting simulations (Jiang et al., 2016) 70

Figure 3.6-8. An illustration of (a) The incorporation of FGB sensors into a rock bolt and (b) An instrumented rock bolt installation in a mine (Tang et al., 2018)..... 73

Figure 3.7-1. Diagrams and classification of electrical resistivity measurements (Sang et al., 2022)..... 77

Figure 3.7-2. A diagrammatical illustration of the non-contact electrical resistivity measurement technique (Lu et al., 2018)..... 78

Figure 3.7-3. A schematic illustration of the setting of OPC paste and the effect on electrical resistivity (a) Early-age cement paste permits the easy flow of electrical current = low resistivity values, and (b) Late-age cement paste restricts the easy flow of electrical current = high resistivity values. (Modified from Wei et al., 2012)..... 81

Figure 3.7-4. A plot of the idealised OPC and cementitious grout resistivity versus curing age profile. 82

Figure 3.7-5. Plots of electrical conductivity versus hydration time of (a) Silica fume blended OPC and (b) Slag blended OPC. 86

Figure 3.7-6. A plot of initial and final setting time plots of OPC mixtures with different amounts of added silica fumes and slag cured at different temperatures (Morsy, 1999) 87

Figure 3.7-7. A plot of electrical resistivity versus curing age of normal and titanium oxide-modified cement pastes cured at different temperatures over a 28-day interval (Teixeira et al., 2016). 88

Figure 3.7-8. A non-electrode electrical resistivity mould and measurement device (Dong et al., 2016) 90

Figure 3.7-9. A plot of electrical resistivity measurements versus curing age in seconds shows the effect of an increasing w/c ratio on the electrical resistivity values (Dong et al., 2016). 91

Figure 3.7-10. A plot of resistivity values recorded from different w/c ratio CSA mixtures over the first 24 hours of curing (Zhang and Li, 2017) 92

Figure 3.7-11. A plot of resistivity values recorded from different w/c ratio OPC mixtures over the first 24 hours of curing (Zhang and Li, 2017) 93

Figure 3.7-12. A diagram of a non-contact transformer-based electrical resistivity measurement equipment (Wei et al., 2012) 94

Figure 3.7-13. A plot of electrical resistivity recorded over 24 hours in eight different cement mixtures with a w/c ratio of 0.4 (Wei et al., 2012) 95

Figure 3.7-14. A plot of the 28-day cement mortar compressive strength against the 24-hour electrical resistivity values (Wei et al., 2012)..... 96

Figure 3.7-15. A plot of electrical conductivity recorded from three-cement grout stabilized sands with a w/c ratio of 1.5 (Choo et al., 2021) 97

Figure 3.7-16. Plots of UCS versus curing age for different cement stabilized sands mixed at different w/c ratios (Choo et al., 2021) 99

Figure 3.7-17. A plot of electrical resistivity against the UCS of cement grout stabilized sand (Choo et al., 2021)..... 100

Figure 4.2-1. A three-gang mould apparatus (left), the casting of shrinkage samples (middle), and the curing of grout shrinkage samples (right).... 113

Figure 4.2-2. A temperature and humidity-controlled curing chamber used to cure shrinkage test prisms. 114

Figure 4.3-1. A schematic of a short-encapsulation pull-out testing sample (not to scale). 117

Figure 4.3-2. Pictures of the SEPT samples prepared in the laboratory. 118

Figure 4.3-3. A picture of the 25-tonne pull-out testing bench. 119

Figure 4.4-1. A sample of the novel grout sensor technology. Yellow circles indicate exposed positive and negative terminals that are used to record grout resistivity signals. 120

Figure 4.4-2. A diagrammatical representation of the installation of grout sensor technology. 121

Figure 4.4-3. A picture of the GDT100 grout detector meter (Fabchem Mining Product Brochure, 2022). 123

Figure 4.4-4. A picture of the simulated support holes in the laboratory showing grout tubes and grout sensor positioning. 127

Figure 4.4-5. A mine map of the testing site (red arrow) at South Deep. 128

Figure 4.4-6. Diagram of the underground 1.2 m and 4.5 m support test holes. 130

Figure 4.4-7. A picture showing grout sensor technology installations at the South Deep gold mine. 131

Figure 4.4-8. Pictures of the GDT100 meter in use during underground grouting operations. 132

Figure 5.2-1. A plot of the linear change of length in grouts A and B samples. 136

Figure 5.2-2. A plot of the linear change of length in grout C and Portland cement samples. 137

Figure 5.3-1. Pictures showing the failure of the grout column during short encapsulation pull-out testing of grout test samples, (a) Grout B fair-quality mixture sample, and (b) Grout A good-quality mixture sample. 141

Figure 5.3-2. A plot of the cable anchor to grout bond strengths for grouts A and B with different w/c ratios. Curvilinear, linear and stepwise relationships between the w/c and bond strength are indicated. 144

Figure 5.3-3. A plot of the cable anchor to grout bond strengths for grout C and Portland cement with different w/c ratios. Curvilinear and stepwise relationships between the w/c and bond strength are indicated. 145

Figure 5.4-1. Electrical resistivity recorded from good, fair, and bad-quality grout A mixtures in 4 m long simulated support holes in the laboratory. 151

Figure 5.4-2. Electrical resistivity recorded from good, fair, and bad-quality grout A mixtures in 1.2 m long underground support holes. 152

Figure 5.4-3. Electrical resistivity recorded from good, fair, and bad-quality grout A mixtures in 4.5 m long underground support holes. 152

Figure 5.4-4. Electrical resistivity recorded from good, fair, and bad-quality grout B mixtures in 4 m long simulated support holes in the laboratory. 155

Figure 5.4-5. Electrical resistivity recorded from good, fair, and bad-quality grout B mixtures in 1.2 m long underground support holes. 155

Figure 5.4-6. Electrical resistivity recorded from good, fair, and bad-quality grout B mixtures in 4.5 m long underground support holes. 156

Figure 5.4-7. Electrical resistivity recorded from good, fair, and bad-quality grout C mixtures in 4 m long simulated support holes in the laboratory. 158

Figure 5.4-8. Electrical resistivity recorded from good, fair, and bad-quality grout C mixtures in 1.2 m long underground support holes. 159

Figure 5.4-9. Electrical resistivity recorded from good, fair, and bad-quality grout C mixtures in 4.5 m long underground support holes. 159

Figure 5.4-10. Electrical resistivity recorded from good, fair, and bad-quality Portland cement mixtures in 4 m long simulated support holes in the laboratory. 162

Figure 5.4-11. Electrical resistivity recorded from good, fair, and bad-quality Portland cement mixtures in 1.2 m long underground support holes. 162

Figure 5.4-12. Electrical resistivity recorded from good, fair, and bad-quality Portland cement mixtures in 4.5 m long underground support holes. 163

Figure 5.4-13. A plot of the average resistivity differences between good-quality grout mixtures recorded from underground support holes to those recorded in the laboratory over a three-month period. 169

Figure 5.4-14. A plot of the average resistivity differences between fair-quality grout mixtures recorded from underground support holes to those recorded in the laboratory over a three-month period. 170

Figure 5.4-15. A plot of the average resistivity differences between fair-quality grout mixtures recorded from underground support holes to those recorded in the laboratory over a three-month period. 171

Figure 5.4-16. Grout resistivity measurements conducted on good-quality grout A, B, and C as well as Portland cement mixtures grouted into 4 m long simulated support holes over 35 curing days. 173

Figure 5.4-17. Grout resistivity measurements conducted on good, fair, and bad-quality grout C mixtures grouted into 1.2 m long underground support holes over 35 curing days. 174

Figure 5.4-18. Grout resistivity measurements conducted on good-quality grout A, B and C mixtures grouted into 4.5 m long underground support holes over 35 curing days. 175

Figure 5.4-19. Electrical resistivity recorded from a good-quality Portland cement mixture in an underground 4.5 m long support hole. 181

Figure 5.4-20. Support hole two-dimensional drawing showing the shrinkage of grout. 184

Figure 5.4-21. A plot of the lower, middle, and upper sensor resistivity versus the grout–cable anchor bond strength in all good-quality grout mixtures. 186

Figure 5.4-22. A plot of the lower, middle, and upper sensor resistivity versus the grout–cable anchor bond strength in all fair-quality grout mixtures. 189

Figure 5.4-23. A plot of the lower, middle, and upper sensor resistivity versus the grout–cable anchor bond strength in all bad-quality grout mixtures. 191

Figure 5.5-1. A generic length support hole schematic showing potentially unmonitored occurrences of in-support hole shrinkage (A) top support hole grout shrinkage; (B) bottom support hole grout shrinkage; and (C) grout shrinkage between sensor locations. 195

Figure 5.5-2. A comparison of grout A good (yellow) and bad (brown) quality mixture to grout-water solution (blue) resistivity values recorded from an underground 1.2 m support hole. 199

LIST OF EQUATIONS

Equation 3.4-1..... 35

Equation 4.3-1..... 116

Equation 5.4-1..... 187

LIST OF TABLES

Table 3.6-1. Descriptions and measurement functions of the Cavisensor programs..... 66

Table 3.7-1. Silica fume cement mixture compositions (Adapted from Morsy, 1999)..... 85

Table 3.8-1. Summary of the factors that impact electrical resistivity measurements in cement-based materials. 109

Table 4.1-1. Factors contributing to ineffective grouting installations, impact, investigation method, and study site. 110

Table 4.1-2. Descriptions and w/c ratio ranges of the grouts and Portland cement mixtures used in this study. 112

Table 4.4-1. The placement of sacrificial grout sensors in different-length support holes. 122

Table 4.4-2. Laboratory grout sensor technology data recording methodology. 126

Table 4.4-3. Underground grout sensor technology data recording. 129

Table 5.2-1. A table showing measured grout linear shrinkage and expansion values in cm. Naming convention = shrinkage/sample name. 135

Table 5.2-2. Lengths of grout columns after 28 curing days in different length support holes. Green shading = no shrinkage, red shading = maximum shrinkage, and asterisk (*) = net expansion. 139

Table 5.3-1. Grouts A, B, C and Portland cement cable anchor to grout bond strength on the first curing day. 142

Table 5.3-2. Bond strengths for the first curing day in different length support holes. 143

Table 5.3-3. The gain in bond strength by different quality grout mixtures over curing intervals as a percentage of the 35-day bond strength..... 147

Table 5.4-1. Grout recordings sample naming convention (recording location/sample name/support hole length). 149

Table 5.4-2. Grout A quality signature identified from laboratory and underground grout sensor recordings. 154

Table 5.4-3. Grout B quality signature identified from laboratory and underground grout sensor recordings. 157

Table 5.4-4. Grout C quality signature identified from laboratory and underground grout sensor recordings. 161

Table 5.4-5. Portland cement quality signature identified from laboratory and underground grout sensor recordings. 164

Table 5.4-6. The performance of grout sensor technology in the laboratory and underground over a three-month observation period. 178

Table 5.4-7. A grout sensor technology excel sheet compiled from laboratory support hole resistivity recordings. 180

Table 5.4-8. A grout sensor technology excel sheet compiled from the underground 4.5 m long support hole recordings showing an OPEN grout detection status on all sensors on the 3rd week following grouting operations. 183

Table 5.4-9. Good-quality grout linear regression trendline correlation confidence and MAPE. 188

Table 5.4-10. Fair-quality grout linear regression trendline correlation confidence and MAPE. 190

Table 5.4-11. Bad-quality grout linear regression trendlines, correlation confidence and MAPE. 192

Table 5.5-1. Unmonitored lengths in support and experimental support holes equipped with grout sensor technology. 195

Table 5.5-2. A grout sensor technology datasheet showing short-circuiting in the upper grout sensor. 197

LIST OF APPENDIX TABLES

Table_A-1. Grout sensor technology datasets recorded in the laboratory and underground..... 229

LIST OF SYMBOLS

Ω – S.I. symbol for electrical resistance.

∑ - Mathematical symbol that expresses the sum of all items.

K – A letter that represents the number one thousand and is derived from the Greek word “kilo.”

1 INTRODUCTION

1.1 Project Background

Underground mines systematically install support units of various lengths to stabilize excavations and provide safe working environments. These support units, such as rock bolts and cables, are commonly installed into support holes followed by the pumping of a full column of cementitious grout. The full-column grouting of support units entails that the entire mechanical cable anchor be immersed in the grout to be considered a successful installation. The full-column grouting of support units prevents corrosion, maintains a strong bond between the support unit and rock mass, and enhances the load transfer mechanism between the support unit and the surrounding rock mass.

However, the grouting process of long support units is time-consuming and labour-intensive, which can lead to miners conducting sub-standard grout installations. These sub-standard grout installations are only observed after rock instabilities or rock falls when the quality and extent of grouting inside a support hole are exposed and can be observed. This has led to a growing need to monitor grout installations with smart technologies to provide quality assurance of full-column grouting. Yet, the monitoring and quality assurance of fully grouted support holes has remained a challenge due to the invisibility of grout inside the support hole.

In response, in-support hole sensor solutions have been developed for the mining industry. These sensors, however, use complex and limited battery life tools to excite a signal and obtain a reading from a support hole. Furthermore, these sensors cannot measure the loss of grouting material into near-borehole fractures, the quality of grout inside the support hole, or its impact on support performance. Crucially, the knowledge of the extent of the column of grout and its performance inside the support hole is critical to the success of support units and poses a significant safety risk when overlooked.

In-hole sensor technology initially developed for civil engineering uses has been adapted for underground applications to form novel grout sensor technology evaluated in this research report. In practice, a small number of grout sensors are placed at predetermined positions alongside a support unit with a receiver attached to the collar of the support hole. Depending on the position of each grout sensor the extent and quality of grout inside a support role can be confirmed thus eliminating the need for ineffective visual observations.

Diagnostic grout data from each sensor is read by a hand-held grout detector meter (GDT100) connected through signal receiver wires located at the collar of each support hole. The GDT100 meter can be used to record and store in memory up to 2500 grout detection operations of underground support holes. The GDT100 meter can also be used as a datalogger to

monitor grout columns in support holes for a period of up to three months. This novel and innovative grout sensor technology is a mining industry first.

Another important, but often overlooked, aspect of fully grouted support units is the amount of grout shrinkage taking place inside the support hole. In underground mines, there are rarely evaluations and reports of grout shrinkage and it is often assumed that all supplied grouts have minimal to no shrinkage. However, it is important to study grout shrinkage as a shrunken grout column offers limited corrosion prevention in support units. Corroded support units have lower supportive capacities and can potentially lead to undesirable falls of ground when loaded by seismic events and mining activities.

The bonding behaviour of the support unit to the grout installed inside the support hole is another critical aspect of fully grouted support units. The quality and thus the performance of the grout inside the support hole can be assessed through the bond strength of the grout column to the support unit. This bonding behaviour value can be calculated from axial-pull-out resistance values recorded from short-encapsulation pull-out testing (SEPT). Regular pull-out testing of grouted support units forms an important part of the quality control of fully grouted support units.

This research report describes how diagnostic grout data were collected using a combination of grout sensor recordings, grout shrinkage measurements and short encapsulation pull-out testing. Further, this

research report also describes how diagnostic grout data was analysed and interpreted to verify the quality and performance of cementitious grout inside support holes.

1.2 Problem Statement

The quality of the cementitious grout, the length over which the grout extends, as well as areas where grout may be missing due to grout underfilling, shrinkage and loss into near-borehole fractures, are important but often overlooked considerations during the installation and long-term quality control of fully grouted support units.

The creation of voids around support units due to grout shrinkage, loss of grout into fractures, and inefficient grouting practices permit the entry of mine groundwater into the support hole resulting in the development of acute corrosion in support units. When severely corroded, support units have a weakened bond to the cementitious grout leading to a loss of supportive capacity and falls of ground, and thus pose significant health and safety risks to miners in underground working areas.

1.3 Research Questions and Hypothesis

This research report aimed to address three key research questions. Firstly, can grout sensor technology differentiate between good and poor-quality grout? Secondly, how accurate or sensitive is grout sensor technology to

the setting of grout? And thirdly, can grout sensor technology be used to determine the effectiveness of grout over time?

It is hypothesized that the data required to answer these research questions are being recorded by grout sensor technology in the 'background,' however, this needs to be analysed in more detail. It is further hypothesized that the different quality grout mixes evaluated in this study have different grout sensor data signatures that indicate their quality.

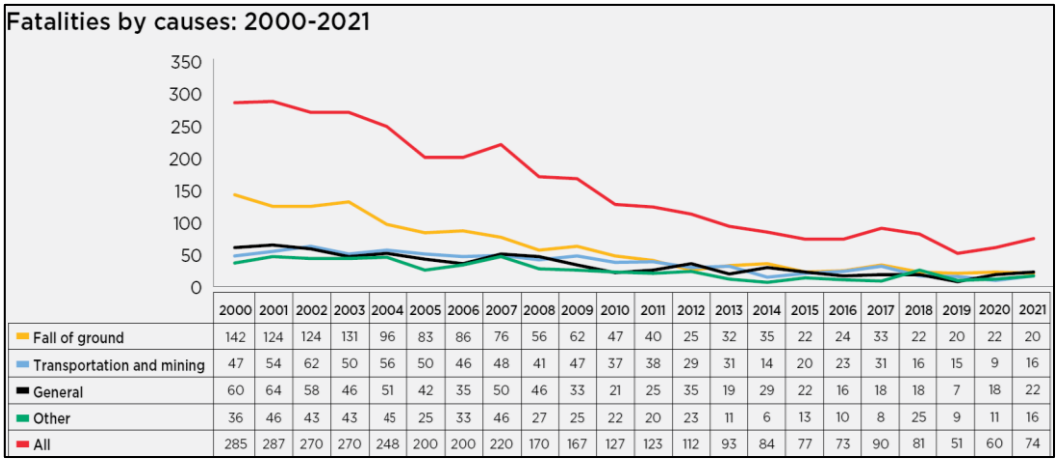
1.4 Research Methodology

This research conducted tests at a laboratory site as well as at the South Deep gold mine in Johannesburg, South Africa. The laboratory facilities have been utilized to conduct short-encapsulation pull-out tests and grout shrinkage measurements. Grout sensor technology data were recorded both in the laboratory as well as underground.

1.5 Significance of the Study

Numerous incidents of rock fall in underground mines are recorded year after year and account for many fatalities. Between 2000 and 2021, the reported fatalities have been shown to have reduced significantly. Yet, many fatalities are reported year on year. A total of seventy-four fatalities were reported in the South African mining industry where 30 percent were caused by FOG's incidents. It is surmised that a substantial percentage of these incidents of rock falls can be traced back to ineffectively grouted support

units. Figure 1.5-1 shows fatalities by cause recorded in South African mines between 2000 and 2021.



	2000	2001	2002	2003	2004	2005	2006	2007	2008	2009	2010	2011	2012	2013	2014	2015	2016	2017	2018	2019	2020	2021
Fall of ground	142	124	124	131	96	83	86	76	56	62	47	40	25	32	35	22	24	33	22	20	22	20
Transportation and mining	47	54	62	50	56	50	46	48	41	47	37	38	29	31	14	20	23	31	16	15	9	16
General	60	64	58	46	51	42	35	50	46	33	21	25	35	19	29	22	16	18	18	7	18	22
Other	36	46	43	43	45	25	33	46	27	25	22	20	23	11	6	13	10	8	25	9	11	16
All	285	287	270	270	248	200	200	220	170	167	127	123	112	93	84	77	73	90	81	51	60	74

Figure 1.5-1. Graph of fatalities recorded in South African mines between 2000 and 2021 (Minerals Council, 2021).

This research report will study the quality and performance of grout using a combination of novel grout sensor technology, grout shrinkage measurements, and short-encapsulation pull-out tests as a first study of its kind in the South African mining fraternity. This research report will contribute to a better understanding of the quality and performance of in-support hole grout, grout loss and shrinkage, as well as the bond strength of fully grouted support units.

It is anticipated that the novel grout sensor technology evaluated in this research report can help to reduce sub-standard grouting practices and

eliminate ineffective visual observations of grouted support units in underground mines. The outcomes of this report have significant implications for health and safety in underground mines and can help make inroads into making safer the extraction of mineral resources underground.

1.6 Report Structure

This research report includes six chapters. Chapter one outlines the research background, the problem statement and briefly introduces the research methodology. Chapter 2 is a brief introduction of the South Deep mine where the underground tests were conducted. Chapter 3 is a literature survey of all relevant research work on cable bolting, grouting methods, shrinkage studies, pull-out testing as well as smart sensors technologies that is applicable to this research report. Chapter 4 presents the research methodology where all tests conducted in this research are described. Chapter 5 presents and critically discusses the results of the tests described in Chapter 4. Chapter 6 presents the research conclusions, limitations, and recommendations as well as makes suggestions for further work.

2 SOUTH DEEP MINE OVERVIEW

2.1 Introduction

The overview and locality, geology and mining method as well as the quality control of support units at the Gold Fields South Deep gold mine are introduced in this chapter.

2.2 Locality and Overview

South Deep is a Gold Fields operated (100%) mechanised deep-level gold mine located in the Witwatersrand Basin approximately 50 km to the South-West of the city of Johannesburg in South Africa. The location of the South Deep gold mine is shown in Figure 2.1-1. Entry to underground workings is provided by a double shaft system comprising a ventilation and a main shaft. The main shaft, in a single-pass, extends down to approximately 3000 m below ground.

Another shaft system (three sub-vertical shafts) towards the South of the mining boundary is also utilised to access underground workings. These three shafts service different mining levels and extend down to approximately 2800 m below ground. Gold Fields estimates that the gold reserves at South Deep will be fully exploited by the year 2106 (Gold Field Mineral Resource and Mineral Reserves Supplement, 2020).



Figure 2.2-1. Locality map of the South Deep gold mine (Gold Field Mineral Resource and Mineral Reserves Supplement, 2020).

2.3 Geology and Mining Method

The exploited gold ore is situated within the Central Rand Group (CRG) in the Witwatersrand Basin between 2700 and 3000 metres below ground. Immediately overlying this geological supergroup is the Ventersdorp Lava formation. The main exploited orebodies at South Deep are the Ventersdorp contact reef and Elsburg reef. The Elsburg reef sub-crops against the VCR towards the west of the mining area and thickens into a wedge (greater than 120 m wedge was confirmed by infill and exploration drilling) towards the west of the mining area. The main geological subdivisions encountered within the South Deep mining right boundary are illustrated in a 3D isometric view in Figure 2.3-1.

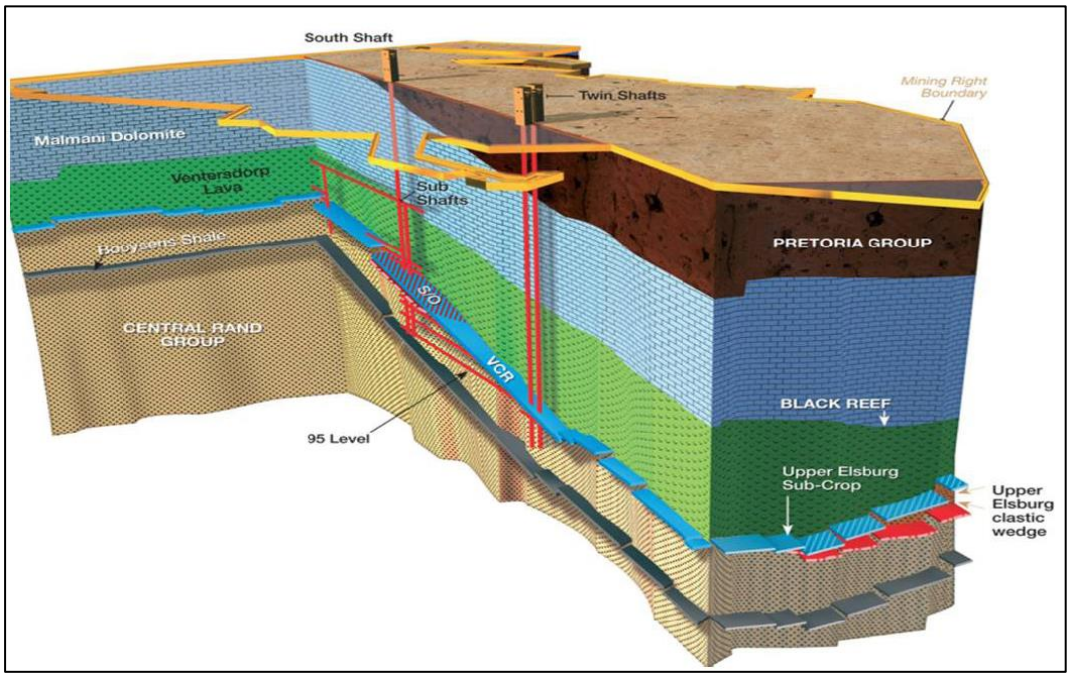


Figure 2.3-1. A 3D view geological map of the South Deep gold mine (Gold Field Mineral Resource and Mineral Reserves Supplement, 2020).

A conventional mining method was used at the mine before 1998. After 1998, the conventional mining method was replaced by a low-profile mechanised destressed method. In 2015, the low-profile mechanised was replaced by a high-profile (5 m x 6 m excavations) destress and long-hole stoping mining method. Six main mining corridors with 180 m spans are used to access the reef with 60 m regional pillars used for regional support.

2.4 Quality Control of Support Units

There is extensive primary support (yielding bolts) installed at the mine. This support is designed to cope with dynamic loading conditions frequently encountered in the Witwatersrand Basin. The secondary support of underground workings consists of 4.3 m and 6.8 m long fully grouted mechanical cable anchors. Quality control of installed ground support units is performed during routine underground visits where visual observations are used to confirm the number, installation pattern and full-column grouting of support units. These quality control measures have, however, been found to be ineffective as the column of grout and its quality inside the support hole cannot be inspected and confirmed. Thus, sub-standard grouting practices cannot be detected, until observed where the support system failed and resulted in large-scale rock mass instability. The evaluation of grout sensor technology in this report is designed to assess the suitability of this technology to address the shortfall of visual observations at South Deep. The next chapter presents the literature of all relevant publications used in the preparation of this research report.

3 LITERATURE SURVEY

3.1 Introduction

The sections presented in this chapter collate and critically review engineering research on important aspects of fully grouted support units with a particular focus on cable bolts. Section 3.2 reviews the use of cable bolts to support and stabilize mining excavations, the main elements of the cable bolt system and a short discussion of the load-transfer mechanism and grout corrosion preventive ability. This is followed by Section 3.3 which covers the grouting methods used when installing cable bolts. Mid-sections 3.4 and 3.5 review different standardized tests and studies of shrinkage in cementitious materials as well as the in-situ and laboratory pull testing of support units. Later Sections, 3.6 and 3.7, briefly review the emergence of smart sensor technology and the use of electrical resistivity for long-term assessment of cementitious grout, respectively. A summary of the chapter is provided at the end.

3.2 Cable Bolting in Mining

Mining excavations and tunnelling operations of various sizes are well documented and spread out globally with a long history of usage in the mining and civil engineering industries (Bawden et al.,1994; Kilic et al., 2002; Thenevin et al., 2017; Chen et al., 2020). The mining and civil engineering industries have developed cable bolts to support underground excavations.

Cable bolts have become one of the most common means of stabilizing rock strata over their allocated usage and life span (Villaescusa et al., 2008; Singh et al., 2016; Dorion, 2019). Cable bolts work by utilizing the in-situ rock strength and deformation characteristics to allow a rock mass to support itself (Hudson and Harrison, 1997; Ryder and Jager, 2002; Kim et al., 2019).

The mining and civil engineering industries install cable bolts numbering in the millions around the world with the consumption set to increase year on year (Song et al., 2017). The mining and civil engineering industries have made extensive use of these cable anchors due to their flexibility, cost-efficiency, and ease of application and installation (Windsor, 1997; Thenevin et al., 2017; Bohloli et al., 2019; Li et al., 2022). Figure 3.2-1 illustrates the diverse types of cable bolts, their longitudinal profile drawings, and cross-section cut-aways for each cable bolt type.

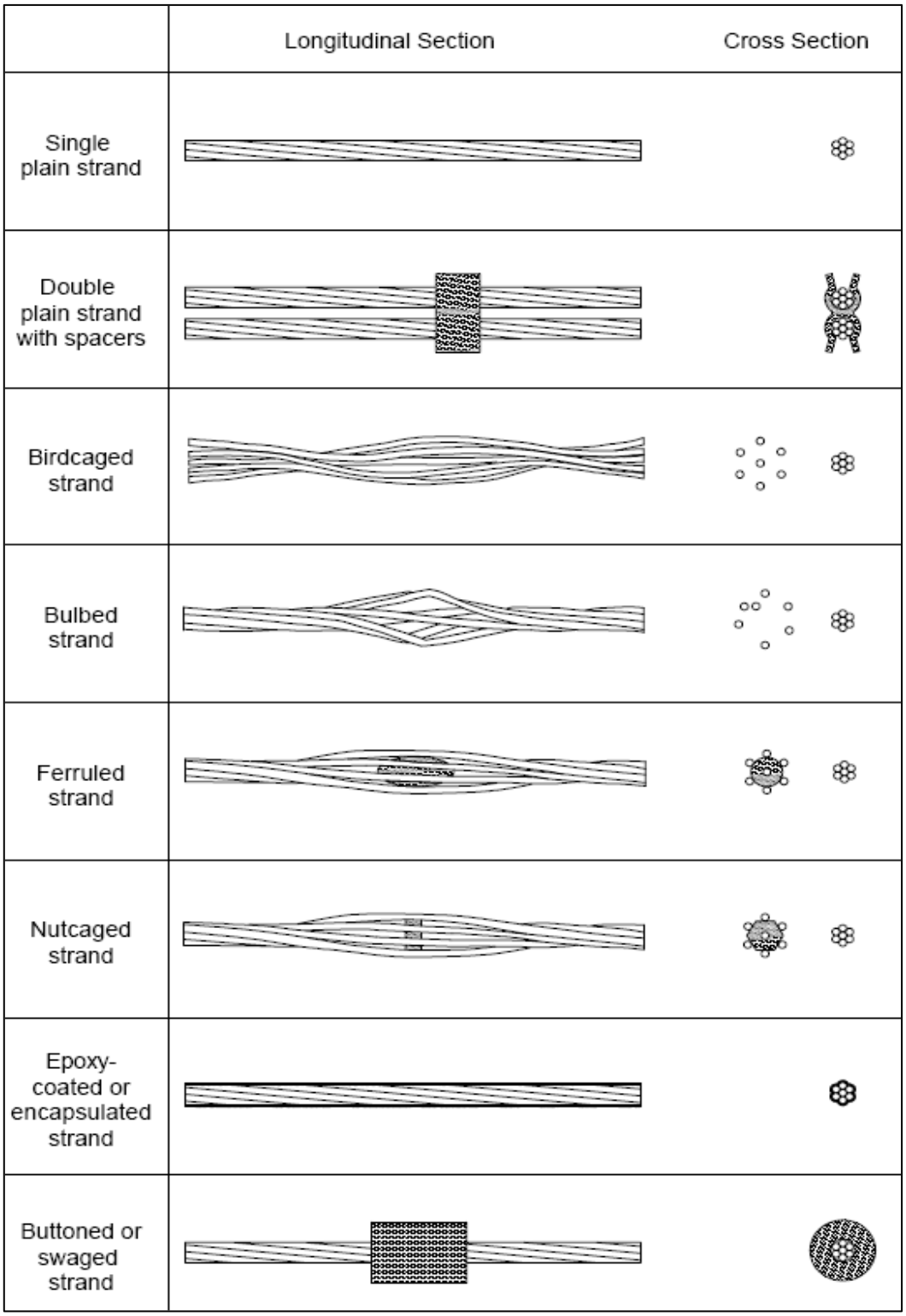


Figure 3.2-1. An illustration of longitudinal and cross-sections of the diverse types of cable bolt configurations (Hutchison and Diederichs, 1996, pp.11).

The stability of mining excavations is of foremost importance as any collapse may lead to loss of life and major financial consequences (Windsor, 1997; Singh et al., 2016; Dorion, 2019). Cable bolts experience various changes in stress due to mining operations, and thus maintaining the operational integrity of these cable bolts is imperative to allow for the safe extraction of ore underground, and the protection of mine personnel and mining equipment (Vallati et al., 2020; Craig et al., 2021).

Manufacturers produce single-strand cable bolts from six very flexible steel wires. The production process involves twisting and coiling these wires around a larger central wire (colloquially called the king-wire). Manufacturing variations produce diverse types of strands for a wide range of rock reinforcement applications; however, most mining applications use the single-strand seven-wire cable bolt variation (Hutchison and Diederichs, 1996).

Cable bolts have a wide range of mining uses. Mining personnel can install cable bolts from development headways before mining the stopes to support large potentially unstable zones in the rock mass thus making cable bolts very handy for rock mass reinforcement in tight spaces (Hoek and Wood, 1987). Figure 3.2-2 illustrates the use of cable bolts in areas such as tunnel intersections, stoping areas, and stope draw points.

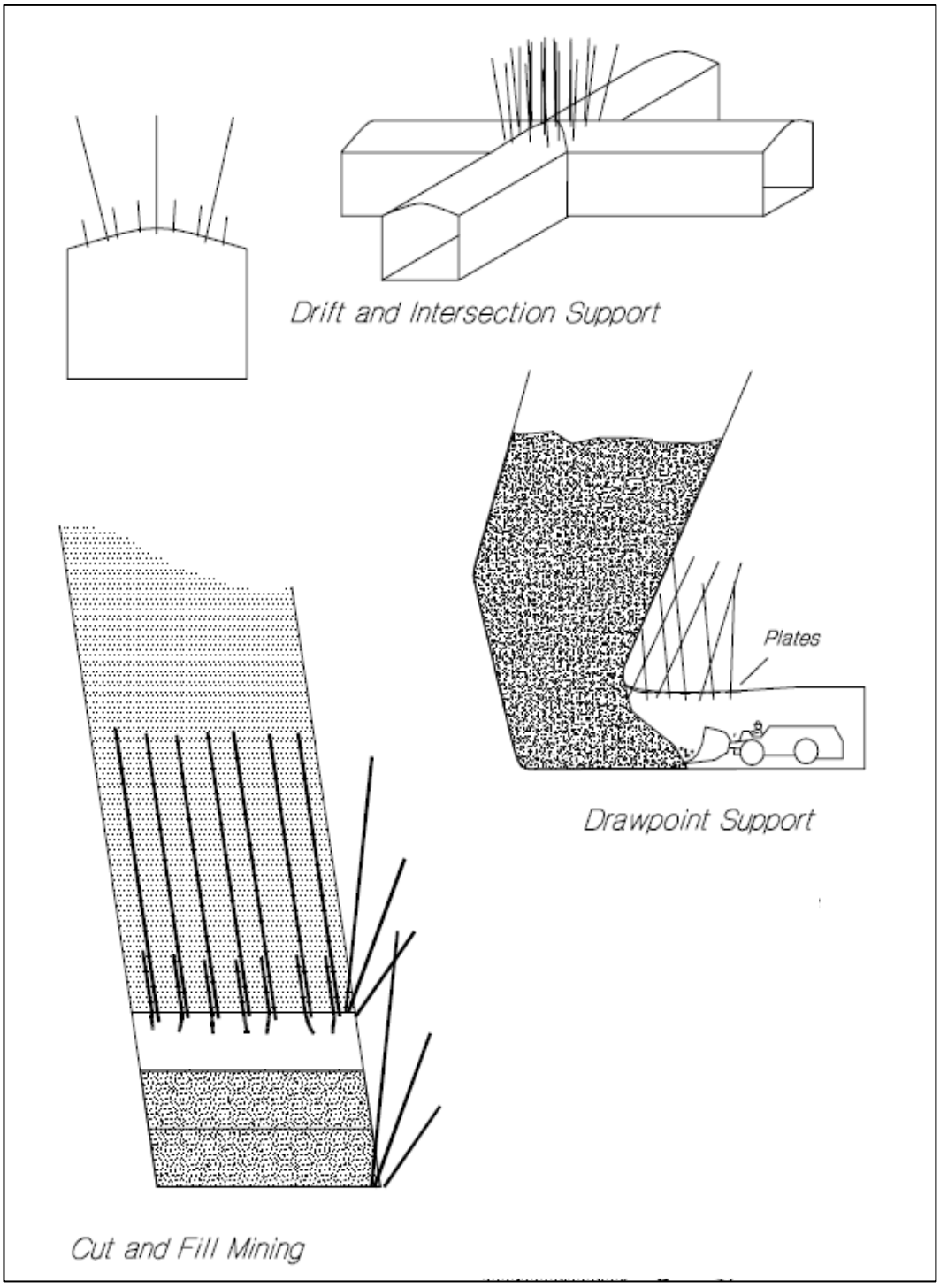


Figure 3.2-2. An illustration of the use of cable bolting for support in underground mines (Hutchison and Diederichs, 1996, pp.6).

3.2.1 Elements of the cable bolt system

The cable bolt system comprises the surrounding rock mass, cable bolt unit, cementitious or resin grout, and an expansion shell or hook mechanism. A steel faceplate, as well as a fastening nut, are used as external fixtures to secure the cable bolt to the surface of the rock mass. Figure 3.2-3 illustrates a cable bolt system that comprises twin cables installed into one support hole and fully encapsulated with cementitious grout.

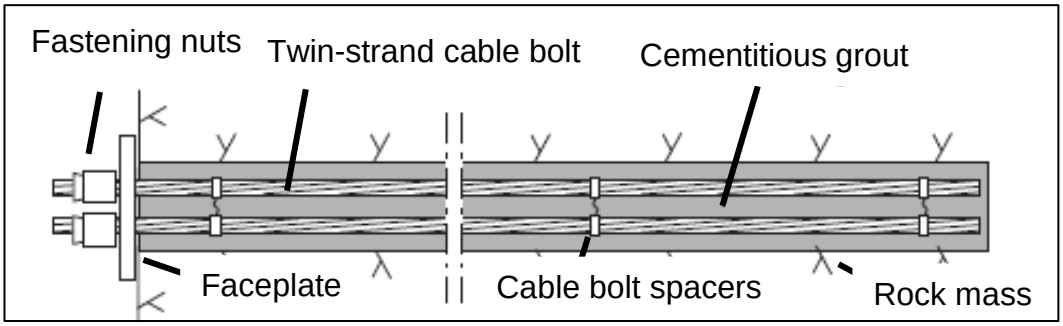


Figure 3.2-3. A diagram illustrating the elements of the cable bolt system (Modified from Li, 2017, pp. 17).

In Figure 3.2-3 the cable bolts are kept separated using spacer clips to allow for better movement of grout around the cables. The two cable strands are each secured at the support hole collar with a nut and faceplate.

Underground mining crews install cable bolts in combination with surface retainment elements such as shotcrete and mesh wires that hold together exposed loose rock pieces (Villaescusa et al., 2008; Vallati et al., 2020). Steel plates connect the cable bolt system to wire mesh and shotcrete

surface retainment elements. All the rock support system elements work together in sharing rock deformation loads thus allowing for better support of the rock mass (Stacey, 2012).

Underground mining crews install cable anchors by drilling an appropriately sized support hole into the roof or sidewalls of an excavation and fitting the cable anchor. Mine support requirements can also necessitate installing two cable bolts into a single support hole to increase the load-bearing capacity of the cable bolt installation (Hutchison and Diederichs, 1996). Cable anchors are installed by mining crews in a pre-designed pattern or a spot arrangement depending on rock support requirements (Windsor, 1997).

Buys et al (2009) similarly noted that the longevity and stability of excavations depend on the installation quality and pattern density of cable anchors. In addition, the required cable bolt pattern design in a particular mine can be based on previous experiences, empirical design numbers, and numerical modelling techniques (Zhao et al., 2019). Furthermore, the capacity of the cable bolt support system is determined based on the volume of the unstable rock mass to be supported by the cable bolts to prevent rock falls (Ryder and Jager, 2002).

Underground crews install cable anchors with or without the application of a tensioning load. Pre-tensioning is the process of applying a tensile force to the reinforcement system during cable bolt installation to improve the cable bolt's ability to reinforce the rock mass (Windsor, 1997; Singh et al.,

2016). Tensioning to about 70 percent of the ultimate load-bearing capacity of the cable bolt helps the cable lock and firmly hold together any loose rock mass blocks and helps stop any other rock blocks and pieces from coming loose (Hoek and Wood, 1987).

3.2.2 Corrosion prevention and load transfer-mechanism

Engineering crews pump an entire column of grout when installing support anchors. Grout prevents the corrosion of the steel anchor and enhances the load transfer mechanism during rock movement and loading (Mark et al., 2003; Villaescusa et al., 2008; Song et al., 2017; Chen et al., 2020). The location of gaps due to absent or inefficient grout around cable anchors and the locations of acute corrosion are well correlated thus highlighting the importance of decent-quality grout operations in underground mines (Permeh et al., 2021). Corroded rock reinforcement systems can lose their reinforcement capacity.

This loss of capacity poses a threat to the safety of mining personnel and may result in collapses with major negative financial implications for the mine. Research work on corroded rock tendons includes those by Dorion (2019), Preston et al (2019) and Permeh et al (2021). Dorion (2019) studied corroded ground anchor units at the Raglan mine in Canada where the authors devised a corrosion assessment program and employed pull-out tests to quantify the reduction in rock bolt support capacity.

Preston et al (2019), in their study of corroded rock anchors, recommended establishing baselines and continuous sampling of water to identify the spatial distribution of corrosion. The authors further stated that water samples are to be evaluated in the laboratory to pinpoint the occurrence of ions that contribute to the corrosion of rock reinforcement units and overall underground mine infrastructure.

Permeh et al (2021) studied the changes, evolution, and lamination of charged ions as well as the change in moisture concentrations in tendon ducts used in civil bridge elements. The authors used post-tensioned 4.57 m long anchors cast in clear polyvinyl chloride (PVC) pipes held at a 30-degree incline.

Permeh et al (2021) found that moisture and ions concentrations in the grout from the top parts of the simulated support holes tended to be higher than the moisture and ions concentrations sampled from the lower part of the support hole simulations. This study found that the upwards migration of moisture and higher ion concentrations in the top parts of support holes can result in severely weakened and corroded cables posing a safety threat to

civil engineering structures and mining operations. Figure 3.2-4 shows photos taken at an underground mine.



Figure 3.2-4. Photos of a fall of ground in an underground tunnel, (left) A fall of ground attributed to corroded support anchors, and (right) Heavily corroded support anchors sticking out from fallen blocks of rocks (Dorion, 2019).

The fall of ground shown in Figure 3.2-4 was attributed to heavily corroded support. Support anchors can be seen sticking out of the fallen blocks of rocks. The load transfer mechanism describes the transfer of load from unstable parts of the rock mass via the grout medium to the cable bolt, and the final transfer back to more stable parts of the rock mass. Figure 3.2-5

illustrates the concept of the load transfer mechanism for a rock mass loaded by gravity.

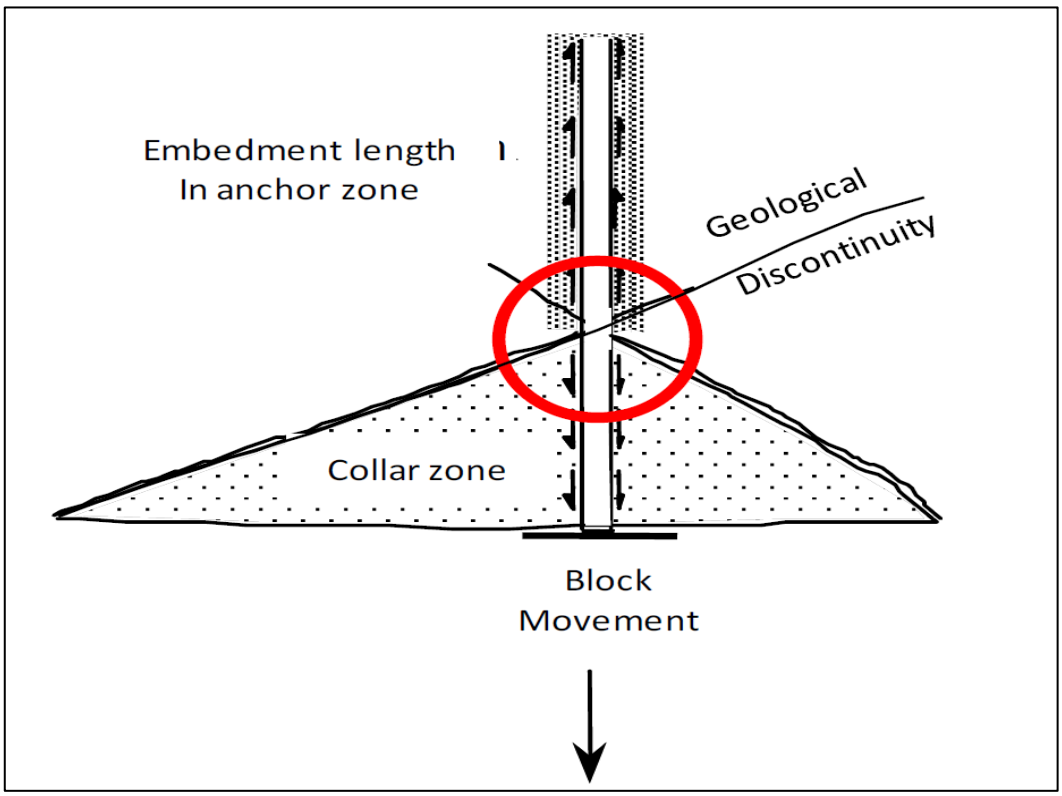


Figure 3.2-5. A drawing illustrating the concept of the load transfer mechanism (Thompson and Villaescusa, 2014).

In Figure 3.2-5, an unstable rock block under gravitational loading is prevented from falling out from the roof of excavation by the transfer of its unstable load to a more stable region of the rock mass through frictional resistance provided by the rock mass–grout–rock interfaces.

Jalalifar's (2011) study showed that load transfer between a cable bolt, rock mass, and grout is dependent on factors such as the annular space available between the supporting tendon and rock mass, strength of the grout, and the supporting tendon profile, as well as the roughness and strength of the rock mass over the support hole section.

Chen et al (2020) studied the placement of loads in rock bolts during the load transfer mechanism using a closed-form solution mathematical model calibrated by in-situ pull-out tests. The authors found that axial pull-out loads were higher in the loaded parts of the rock bolts and decreased rapidly to the exposed section at all pull-out loads.

3.3 The Grouting of Cable Bolts

Cable bolts are full column grouted to eliminate gaps between the rock mass and the cable bolt thus preventing the corrosion of cable bolts as well as enhancing the load transfer mechanisms from weaker rock layers to more stable parts of the supported rock mass via the rock mass to grout and grout to cable anchor interfaces.

One of the most important but often overlooked considerations in cable bolt installations is the quality of the grout, the length over which the grout extends, as well as areas where grout may be missing due to grout underfilling, shrinkage and loss into near-borehole rock mass fractures. The quality of the cement grout mix used to grout cable anchors determines the

cable anchor's efficiency to support the rock mass and is also often overlooked.

There are diverse types of cement grouts available for use in the mining industry. Most cementitious grouts contain Ordinary Portland Cement (OPC) and cement admixtures in different percentages. Cement admixtures are added to enhance the Portland cement's physical, chemical, and mechanical attributes without causing an increase in water demand or diminishing the strength or corrosion prevention abilities of the cement grout (Heikal et al., 2000).

The most salient property of Portland cement grouts is the water-to-cement (w/c) ratio (Hutchison and Diederichs, 1996). Vasumithran et al (2020), in their study of grout mechanical properties, asserted that the inherent strength of cementitious grouts is affected most by the w/c ratio. These lower w/c grouts thus require the addition of admixture to ensure these thick grouts can flow into tight spaces.

Hutchison and Diederichs (1996); Satyarno et al (2014) asserted that the w/c ratio of cement grouts needs careful regulation to ensure flowability and a good bond to the rock mass. Hyett et al (1992) advocate for the use of grouts with w/c ratios between 0.35 and 0.40 for optimal enhancement of the cable bolt load-carrying capacity, and optimal pumpability, as well as the enhancement of the grout compressive strength. Figure 3.3-1 shows the variation of the uniaxial compressive strength (UCS) with the grout w/c ratio

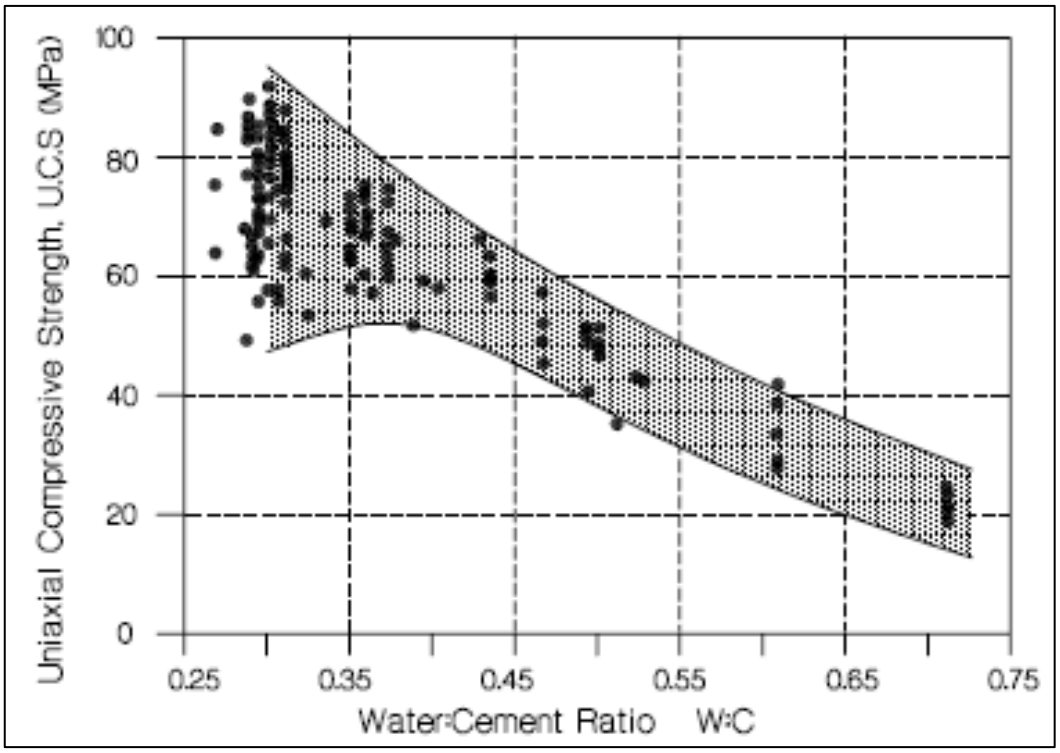


Figure 3.3-1. A plot of UCS versus the w/c ratio of grout (Hutchison and Diederichs, 1996, pp.66).

The UCS can be seen to decrease with an increase in the grout w/c in Figure 3.3-1. It can also be observed in Figure 3.3-1 that there is a large data scatter at the high UCS – low w/c values.

Cable bolts are often poorly installed; poor-quality grout installations affect the capacity of the cable bolt support systems and are not easily identifiable in situ where the only visible elements of the anchor system are the faceplate, fastening nut and the short length of the cable bolt (Villaescusa et al., 2008; Vallati et al., 2020). Poor-quality grout installation practices include incorrectly sized support hole diameters and depths, very watery

grout mixtures, grout loss through cracks in the support hole and the pumping of insufficient grout to encapsulate the entire length of a cable bolt (Kelly and Jager, 1996).

Research work from Villaescusa et al (2008) as well as Maepa and Zvarivadza (2017) also demonstrated that cable bolt installations often fail due to ineffective grout mixing, resulting in low grout strength. Researchers such as Mark et al (2003); Zou et al (2010); Stacey (2012); and Kim et al (2019) cited poor-quality installation practices, improperly sized borehole annulus, and the use of poor-quality grout as the main factors that contribute to the failure of fully grouted cable bolt installations. Twin cable strand support holes can also experience ineffective grouting where the grout has not penetrated the full column of the support hole. Ryder and Jager (2002) also stated that it is particularly hard to fully grout long cable anchors, especially if the excavation roof is full of fractures or when there is groundwater present and should be performed by experienced installation crews.

Ineffective grouting practices and the use of low-quality grouts are also known to result in the occurrence of significant amounts of grout shrinkage, and the formation of non-grouted spaces between the support hole and cable anchor. As a consequence, non-grouted spaces can result in an ineffective load distribution during rock mass movement, a reduction of the cable anchor support capacity, as well a loss of corrosion protection. The breather tube and grout tube techniques are the two main methods of

grouting a support hole. The breather tube method is the most widely used in underground mines for grouting cable anchors. Hutchison and Diederichs (1996) stated that rock engineers can successfully use the breather tube grout installation method for vertical support holes whereas the grout tube method is applicable for most support hole orientations.

It is important to note that the success of support holes is largely dependent on correctly drilled and sized diameter and length support holes as well as the use of correctly regulated w/c ratio, and flowable grout. Support holes slightly longer than the length of the cable to be installed are required to facilitate grout movement and the application of pre-tensioning force to the cable anchor inside the support hole.

3.3.1 The breather-tube grouting method

The breather tube method uses two tubes during grouting operations, a grout and a breather tube. The grout (short length, larger diameter) and breather tubes (longer length, smaller diameter) are inserted into the support hole beside the cable anchor. Grout is then pumped through the grout tube while the trapped air escapes through the breather tube, ensuring the grout can be set without air bubbles. The occurrence of air bubbles in pumped grout can lower the cable anchor installation quality. The base of the support hole is plugged tightly to stop grout from flowing out of the support hole. The breather tube method is disadvantaged by the difficulty of recognizing when the support hole has been full-column grouted (Kelly and Jager 1996; Hoek et al., 2000).

3.3.2 The grout-tube grouting method

The grout tube method only uses a grout tube to install grout into a support hole. This grout tube is inserted into the support hole alongside the cable anchor. A small gap towards the collar of the borehole is left for the grout mixture to travel out of the pipe and downwards. The grout breather tube and grout tube installation methods in upright support holes are illustrated in Figure 3.3-2.

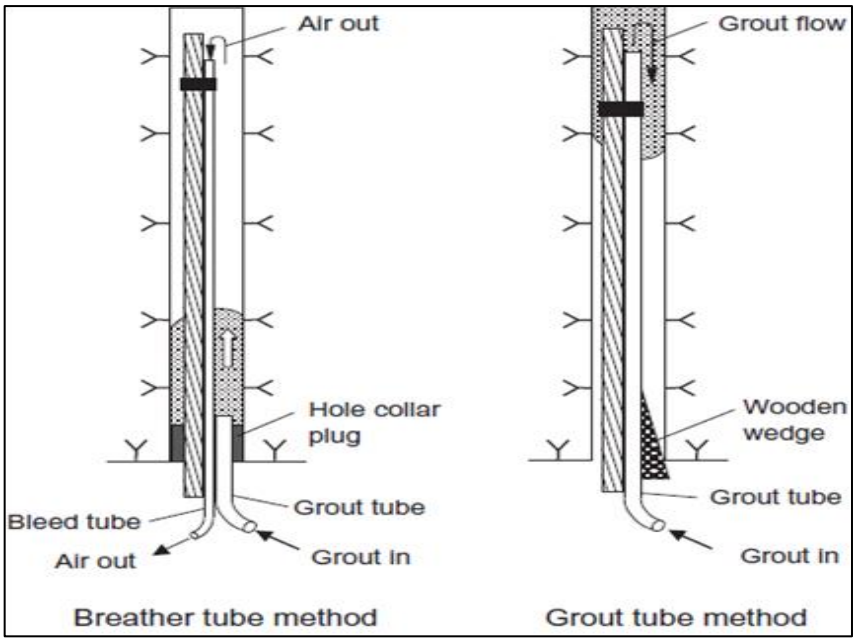


Figure 3.3-2. The breather (left) and grout tube grout (right) installation methods (Hoek & Brown, 1980).

A wooden wedge is commonly used during the grouting process to stop the grout mixture from flowing out of the support hole as well as to secure in

place the grout tube. The grout mixture appears at the support hole collar when the hole is fully grouted and grout pumping may stop (Hutchison and Diederichs, 1996). The grout tube method is illustrated in Figure 3.3-3.

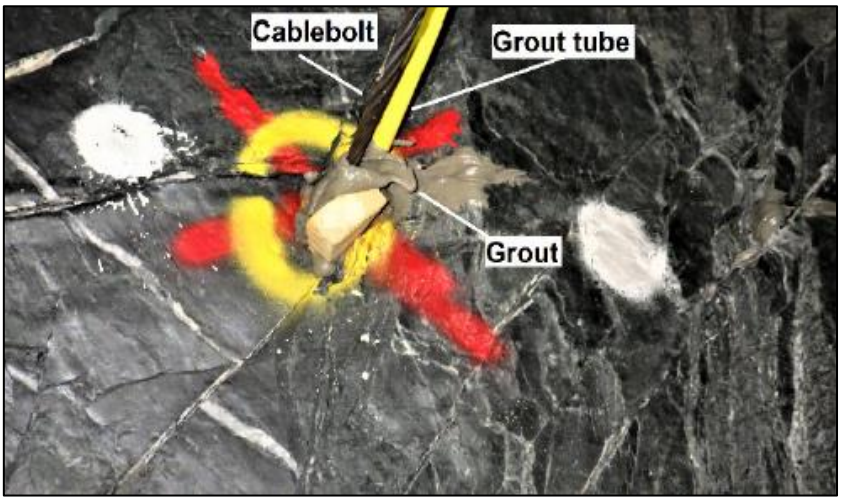


Figure 3.3-3. An illustration of an underground cable bolt installed using the grout tube method (Reny et al., 2019).

Figure 3.3-3 shows an underground cable bolt installation where the grout was pumped using the grout tube method, a wedge piece to plug the borehole and grout tube can be seen.

3.4 Shrinkage Studies of Cementitious Materials

This section reviews studies of cement-based materials shrinkage organized by grout shrinkage research topics that are directly applicable to this research report. Studies of autogenous shrinkage are important as they relate to the field performance of cement-based materials such as cement grouts in underground mines. Furthermore, the mining and civil engineering

fraternity rarely evaluate and report autogenous shrinkage values for cementitious grouts (Bentz et al., 2015).

Cementitious grouts are used for filling the borehole annulus in support holes used in underground mines and prefabricated civil engineering structures (De la Varga and Graybeal, 2016; De la Varga et al., 2018). These cementitious grouts, to be effective, need to flow consistently, have low levels of shrinkage, possess high inherent strength, as well as have long-term longevity (De la Varga et al., 2018; Mohan et al., 2021). Cementitious grouts are, however, known to suffer appreciable levels of shrinkage (Newlands et al., 2008; De la Varga and Graybeal, 2016; De la Varga et al., 2018).

Zhang et al (2019) asserted that grout shrinkage is responsible for the loss of bonding ability of grout to the substrate and the development of cracks in hardened grouts. Portland cement products will crack if they cure under tight spaces or constrained conditions due to the development of tensile forces (expansion strain deformation) thus lowering their quality (Yoo et al., 2017; Lecieux et al., 2018; De la Varga et al., 2018). Authors such as Menu et al., 2017; Terzioglu et al., 2018; and Shamsuddoha et al., 2019; as well as Mohan et al., 2021 have studied the development of cracks in cementitious grouts as they undergo shrinkage and correlated these grout cracks to areas of water penetration and corroded steel tendons.

Autogenous shrinkage can be described as the volume change of cement-based material when cured under sealed conditions. Autogenous shrinkage is caused by chemical shrinkage through the hydration reactions of Portland cement that result in a volume reduction (a combination of net expansion and shrinkage) of the cement paste (Lura et al., 2003; Yoo et al., 2017; De la Varga et al., 2018). The Portland-cement hydration process is a complex superposition of exothermic chemical reactions, the released heat of hydration impacts a further thermal strain on the cement grout installation.

The cement grout hardens with increasing curing age, the autogenous shrinkage process slows down and a process of drying shrinkage takes over. Drying shrinkage in grout results from relative changes in humidity and the development of small pore spaces between the hardened cement particles when the water contained in these pores has evaporated (self-desiccation) (Yoo et al., 2017; Lecieux et al., 2018).

Lower levels of relative humidity curing conditions under which grouts are installed may result in the occurrence of a higher percentage of grout shrinkage whereas high humidity levels result in the swelling of the cement grout thus outlining the importance of noting humidity levels when evaluating grout shrinkage (Lura et al., 2003; Menu et al., 2017; Shamsuddoha et al., 2019).

3.4.1 Shrinkage test conditions

Lura et al (2003) assessed a numerical model that predicts autogenous shrinkage by measuring the autogenous deformation, internal relative humidity, and elastic modulus, as well as the isothermal heat evolution. The authors continuously measured the evolution of relative humidity in 0.37 w/c ratio OPC samples for one week following mixing with demineralized water as well as measured the elastic modulus of the hardening cement paste. These measured properties formed inputs into the determination of the autogenous deformation under the capillary tension methodology.

The capillary tension method is concerned with the formation of meniscus curvature (which is particularly prevalent at higher levels of relative humidity) between the air and water surrounding partly empty cement particles as Portland cement undergoes the hydration process. Rock engineers can obtain cement paste relative humidity values which can be used to determine the capillary tension meniscus curve and indirectly determine the slope of the autogenous shrinkage curve.

Lura et al (2003) noted a change in autogenous deformation and elastic modulus approximately eight hours after the testing began. The relative humidity dropped at approximately 12 hours of curing. This delayed change in relative humidity is attributed to the influence of dissolved salts in the cement paste and the formation of the meniscus layer in the cement paste pore fluid.

The experimental data was input into numerical equations; one equation was used to separate the contribution to relative humidity from the effects of dissolved salts and meniscus layer formation. Another equation was used to calculate cement paste deformation. The calibrated (separated dissolved salts and meniscus contributions) numerical simulations under-estimated the measured autogenous deformation at decreasing values of relative humidity. The numerical simulations of autogenous shrinkage showed good alignment with measured autogenous shrinkage values at higher relative humidity values. This study showed the value of the capillary tension approach when using numerical codes to model autogenous shrinkage in cement-based materials.

Newlands et al (2008) developed a linear early-age concrete testing technique. The sensitivity of the developed testing technique was evaluated under changing temperature, humidity, and wind speed testing conditions. The linear testing technique comprised a triangle-shaped steel mould with a linear variable differential transducer (LVDT) attached to an adjustable end of the steel mould. A data logger was connected to the LVDT and allowed for continuous logging of shrinkage results. The test results showed that the proposed method retained enough sensitivity to be able to capture changing environmental conditions during linear shrinkage testing. The proposed method was further shown to be repeatable outlining its future potential as a reliable linear shrinkage testing technique. Figure 3.4-1 shows

a plot of shrinkage versus curing age in hours under different test conditions from Newlands et al (2008).

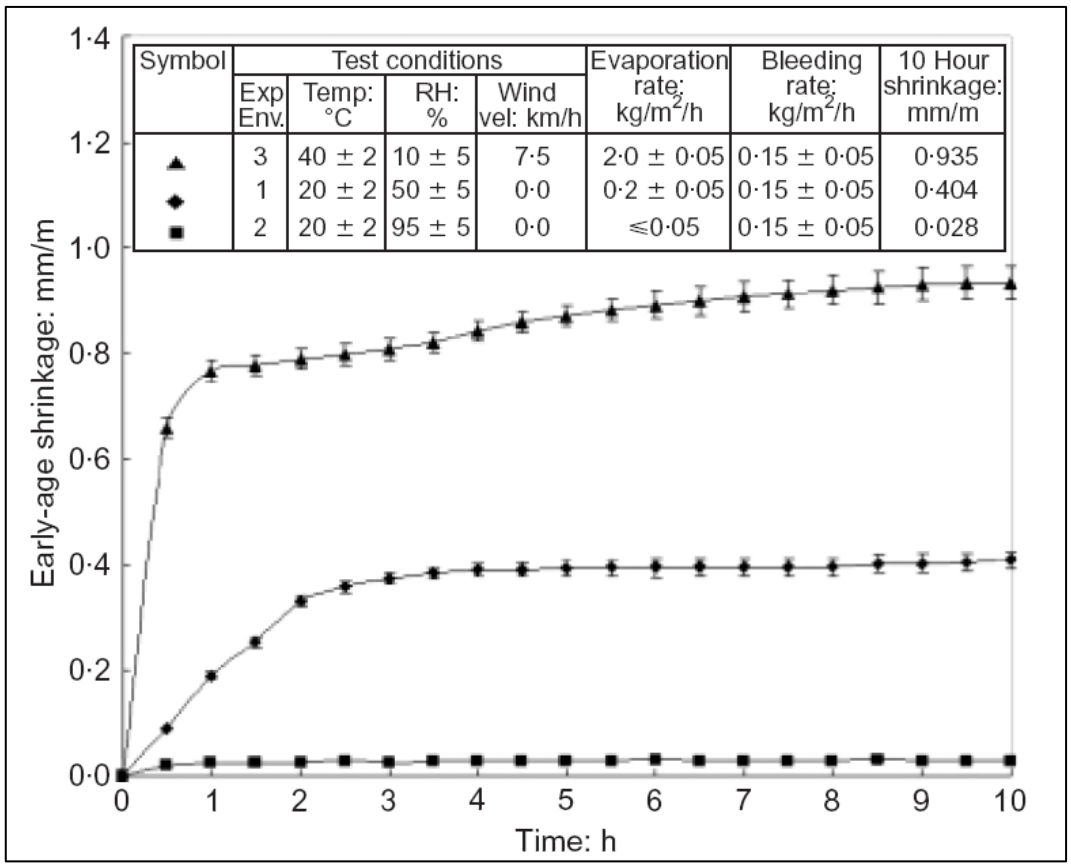


Figure 3.4-1. A plot of ten-hour cured OPC shrinkage values versus curing age in hours under three different test conditions (Newlands et al., 2008).

The differentiation between different test conditions in the shrinkage results can be observed in Figure 3.4-1, thus outlining the importance of noting environmental conditions during shrinkage measurements.

3.4.2 Testing standards and variations of ASTM

The ASTM C 157/C 157M is a standardized test that evaluates the change of length under carefully controlled temperature and relative humidity conditions in cured cement mortars and concrete (and by extension cementitious grouts) while eliminating the effects of external forces and curing temperature fluctuations. The change in length of cured and solidified cement-based material can be due to either shrinkage or expansion and in the absence of the influence of external forces and temperature fluctuations, can be a useful parameter that can be used to compare different cement-based materials. The standard prescribes the use of a drying room kept at a temperature and relative humidity of 23 ± 2 degrees Celsius and 50 percent, respectively. Steel moulds and a length comparator are used to cast the prism specimens and to measure the length change after four, seven, 14, and 28 days of curing.

The change of length formula can be written as:

$$\Delta L_x = \frac{\Delta\, CRD - \Delta\, CRD\ _{initial}}{CGL}\, x\ 100 \qquad \textit{Equation 3.4-1}$$

Where CRD = Difference in length comparator and reference rod readings at any curing age, $CRD_{initial}$ = Initial difference in length comparator and reference rod readings, and CGL = Mould gage length (a 250 mm gauge is marked in mm fractions).

Kucharczykova et al (2017) compared and contrasted two methods of measuring polymer cement mortars' relative change in length (shrinkage). The first evaluated method was the European standard for measuring cement-based product shrinkage and expansion (CSN EN 12617-4). The authors prepared two sets of 40 x 40 x 160 mm test prism samples; one set followed the standard requirements (set one). Set one was further split using methods of specimen drying; set 1a specimens were coated with PE foil whilst set 1b specimens were not protected from drying. Another set of prism specimens used a modified procedure for the curing conditions to form test set two.

The second evaluated procedure used was the Austrian standard (OENORM B 3329:2009-06-01). For the Austrian standard shrinkage moulds of size 100 x 60 x 1000 mm were prepared to form set three (cured in the same manner as set two). Markers were placed in the shrinkage moulds to measure the long-term relative deformation. The loss of mass was recorded by placing the moulds onto a specialized weighing table. The study found that the largest changes in length and mass loss were recorded in the first 20 days of curing. Thereafter, only slight increases in shrinkage and relative mass loss were recorded. Figure 3.4-2 shows the shrinkage

mould and the digital length comparator used to cast the shrinkage test specimens and measure the relative length changes.

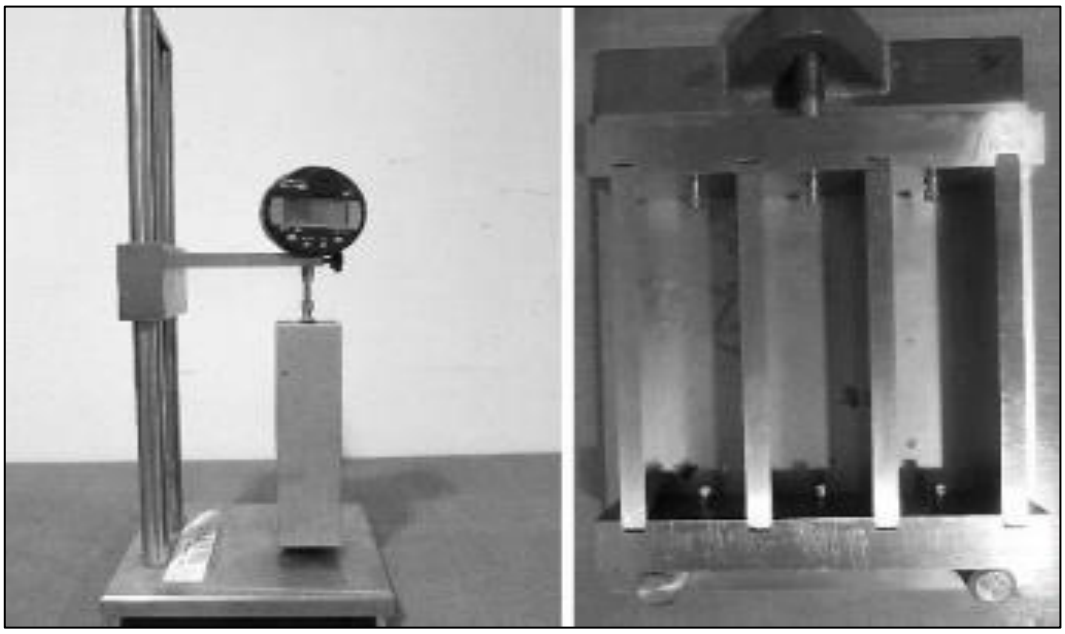


Figure 3.4-2. A digital length comparator and a three-gang shrinkage mould equipment used to measure shrinkage (Kucharczykova et al., 2017).

In Figure 3.4-2, studs in the three-gang shrinkage mould are used to hold each mould in place as well as fit snuggly into the length comparator for ease of length change measurements. Figure 3.4-3 is a plot of the relative length changes against curing age in days.

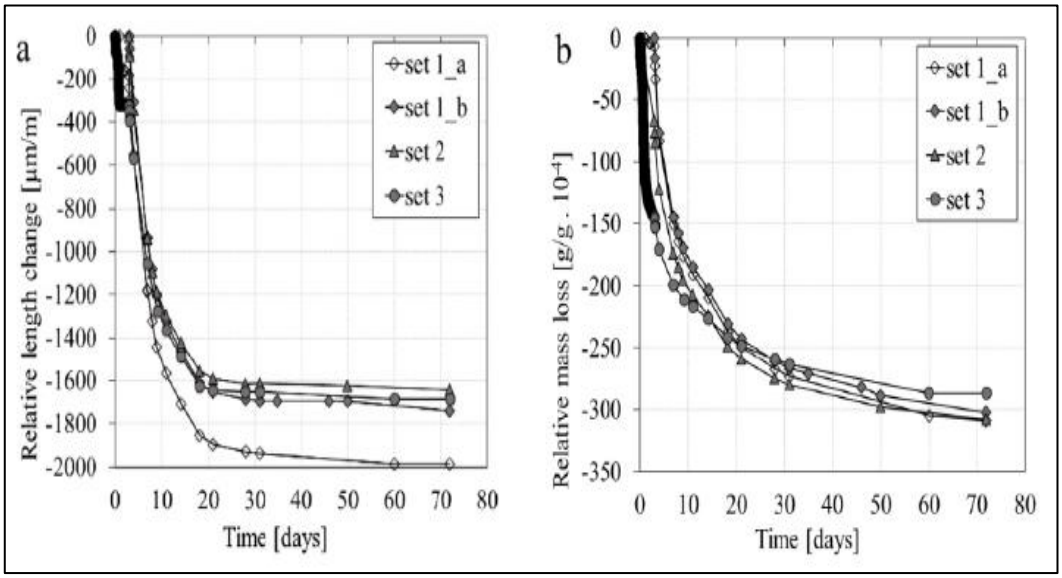


Figure 3.4-3. (a) A plot of relative length change versus curing age in days for different sets of test specimens, and (b) A plot of relative mass loss for the different test specimens (Kucharczykova et al., 2017).

The plot shown in Figure 3.4-3 captured the differences between the different testing methods and the influence of the different curing conditions. Kucharczykova et al (2017) were able to show that different shrinkage values will be obtained for the same test specimens if the curing conditions specified by standardized tests differ markedly. Thus, it may be informative in shrinkage studies to follow a standardized method and a slightly different curing methodology to assess the impact of curing conditions on measured changes in length.

Menu et al (2017) sought to explore how the free ring shrinkage testing procedure impacted the measured shrinkage values of shotcrete used to determine its durability with time. The research further looked into

understanding the influence of the geometry of test specimens, the surface area to volume ratio exposed to drying, as well as the sealing methods on measured shrinkage values.

The authors prepared radial test specimens of size 152 x 152.5 x 228.5 mm (height x inner radius x outer radius) for free ring shrinkage measurements. A set of prismatic test specimens of size 75 x 75 x 285 mm were also prepared for linear shrinkage measurements under a modified ASTM C 157 standard length change test. Two methods of drying for the prismatic and radial specimens were used to investigate the influence of the surface to volume ratio on measured shrinkage values (axial and radial drying for the free ring specimens and drying at all surfaces and no exposed drying surfaces for the prismatic specimens).

A 0.60 w/c ratio shotcrete mixture with no admixtures was used to cast the test specimens. A second shotcrete mixture for test specimens was prepared under a 0.45 w/c ratio with an addition of a super-plasticizer and air-entraining agent to make the mixture workable at the low w/c ratio. Both shotcrete mixtures were prepared as concrete mixtures using up to a maximum of 10 mm coarse aggregates to form the concrete.

The results of the compressive strength testing showed an increase in compressive strength with increasing curing age and in contrast, a decrease in compressive strength with an increasing w/c ratio. The drying shrinkage values were seen to increase with an increase in the specimen surface to volume exposed to drying thus highlighting that a test specimen surface area to volume ratio has a significant impact on shrinkage testing. Figure 3.4-4 shows the modified ASTM C 157 shrinkage micro-strain values measured in 0.45 and 0.60 w/c ratio shotcrete mixtures.

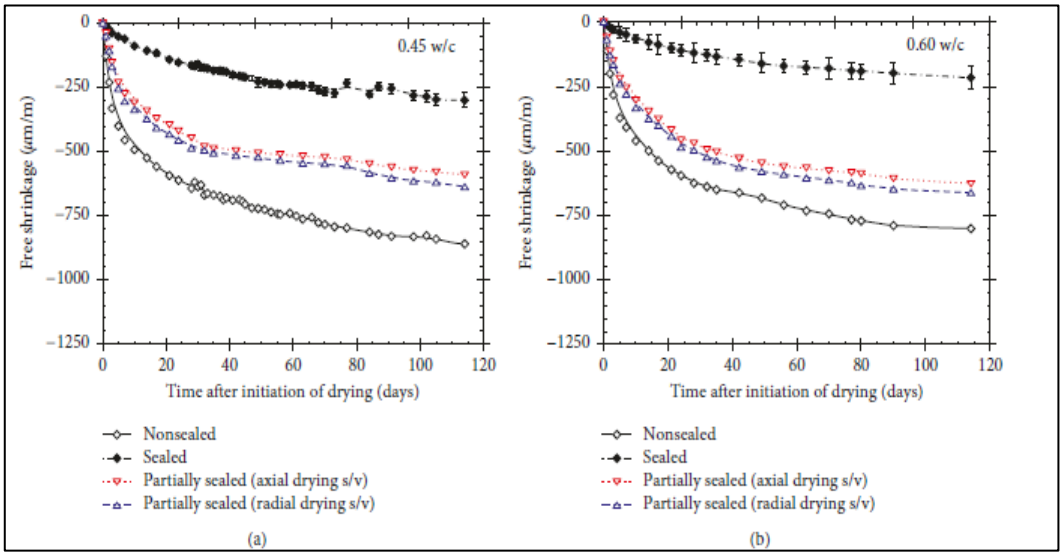


Figure 3.4-4. A plot of micro-strain shrinkage versus drying time in days measured in an (a) 0.45 w/c ratio shotcrete mixture and in an (b) 0.60 w/c ratio shotcrete mixture (Menu et al., 2017).

Figure 3.4-4 illustrates the effect of different drying conditions on measured shrinkage values, this effect is illustrated by distinct curves of shrinkage. The free shrinkage ring specimens that were dried radially recorded higher

shrinkage than those dried axially, the difference in shrinkage values was caused by the higher exposed surface to volume ratio of the radially dried specimens. The free shrinkage ring specimens' shrinkage values were also found to be markedly different from those of the prismatic specimens and thus a specimen's geometry has a considerable influence on measured shrinkage values. This study highlighted the influence imposed on measured shrinkage values by the surface to volume ratio exposed to drying, the test specimen geometry, and drying methods. Thus, when assessing the long-term durability of cementitious material to reduce shrinkage the test method will have a large bearing on measured shrinkage values.

Mohan et al (2021) initiated a study to develop a high-performance premixed grout mixture from a combination of fly ash, chemical admixtures, and OPC. The authors utilized a three-phased approach to systematically assess the performance and physical properties of formulated grouts. The final grout mixture was mixed in an industrial complex and its composition by volume was 52 percent OPC and 48 percent fly ash with appropriate doses of chemical admixtures. This final composition grout minimized cement grout bleeding and shrinkage and was thus suitable for grouting post-tensioned support strands for protection against corrosion.

The ASTM C 157 standard was followed for the measurement of total and autogenous shrinkage, 25 x 25 x 285 mm sized prisms were cast and covered with plastic sheets to prevent moisture loss. Drying shrinkage was

prevented by double wrapping the test prisms with foil wrap thereby only allowing autogenous shrinkage to occur in the curing samples.

The total shrinkage (autogenous and drying shrinkage) test prisms were de-moulded after one curing day and measured for a change of length. These prisms were then stored at 25 degrees Celsius and 65 percent relative humidity for seventy days and autogenous and total shrinkage was measured using an accurate extensometer. Figure 3.4-5 shows plots of the total autogenous shrinkage curves with and without the addition of admixtures.

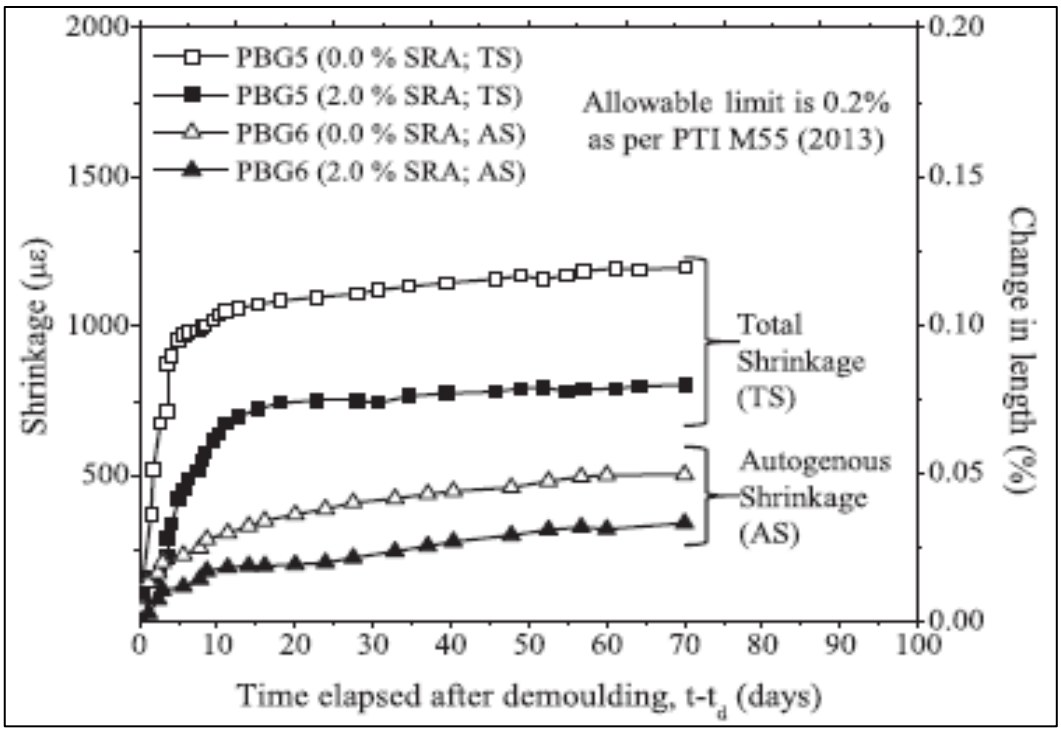


Figure 3.4-5. A plot of total and autogenous shrinkage deformation strain and changes in length for pre-blended grouts five and six versus curing age, post-demoulding, in days (Mohan et al., 2021).

The reduction in autogenous and total shrinkage can be observed (black-filled squares and triangles) in Figure 3.4-5. The results showed that the addition of the optimum amounts of shrinkage-reducing admixtures (two percent) reduced total and autogenous shrinkage values by around 34 percent and 31 percent, respectively. Furthermore, the reduction of autogenous shrinkage in the optimal grout mixture did not affect its flowability and grout bleeding prevention characteristics.

3.5 Pull-Out Testing of Support Units

Geotechnical engineers have long sought to understand the behaviour of rock support anchors under rock loading through laboratory and field pull-out tests, as well as through numerical modelling tools (Bawden et al., 1994; Benmokrane et al., 1995; Singh et al., 2016; Chen et al., 2020; Li et al, 2022). Pull-out testing is a conventional approach for assessing the integrity of rock support anchors. This method takes a long time to set up and destroys the installed rock anchor support (Zou et al., 2010; Song et al., 2017).

Rock masses are naturally dissected by abundant discontinuities that form potential sliding and release surfaces for rock blocks during rock falls (Windsor, 1997). Therefore, geotechnical practitioners have designed laboratory tests of rock anchors to mimic potential in-situ failures. The four loading conditions under which cables and rock bolts are commonly evaluated in the laboratory include axial loading (tension), shear loading,

axial and shear loading, as well as compression loading (Tomasone et al., 2020). Bawden et al (1994), on loading conditions, stated that axial and shear loading conditions are generally not encountered in underground mines and that a combination of all loading conditions is more common.

Pull-out test samples are prepared by casting rock bolts or cables into cylinders of suitable height comprised of suitable grout or concrete mixture to simulate the support hole and the surrounding rock mass confinement. These pull-out samples can be evaluated on a pull-out bench or pull-out apparatus. Engineers have developed a multitude of pull-out test apparatuses; most variations contain circular openings to insert the cable or rock bolt housed in a hydraulic jack cylinder. Mining personnel use a pressure line to provide high air pressures that drive the hydraulic mechanisms. A housing or loading frame is used to attach the head of the cable or bolt to the pull-out jack. Pull-test apparatus manually or digitally record the rock bolt/cable head displacement; rock engineers report this parameter alongside the applied load.

ASTM D4435-08 describes a standardized method for testing cement grout or resin-grouted rock bolt capacity. The ASTM D4435-08 method prescribes the pull-testing, using a hydraulic device, of a rock bolt installed into a material that is similar to what the rock bolt will be installed into under mining conditions. The rock bolt is pulled axially until the anchoring mechanism fails or the anchor material (rock mass or concrete cast) fails. The ultimate load-bearing capacity is determined from the load versus displacement output

results. Figure 3.5-1 details a manually operated pull-out and pre-stressing jack device.

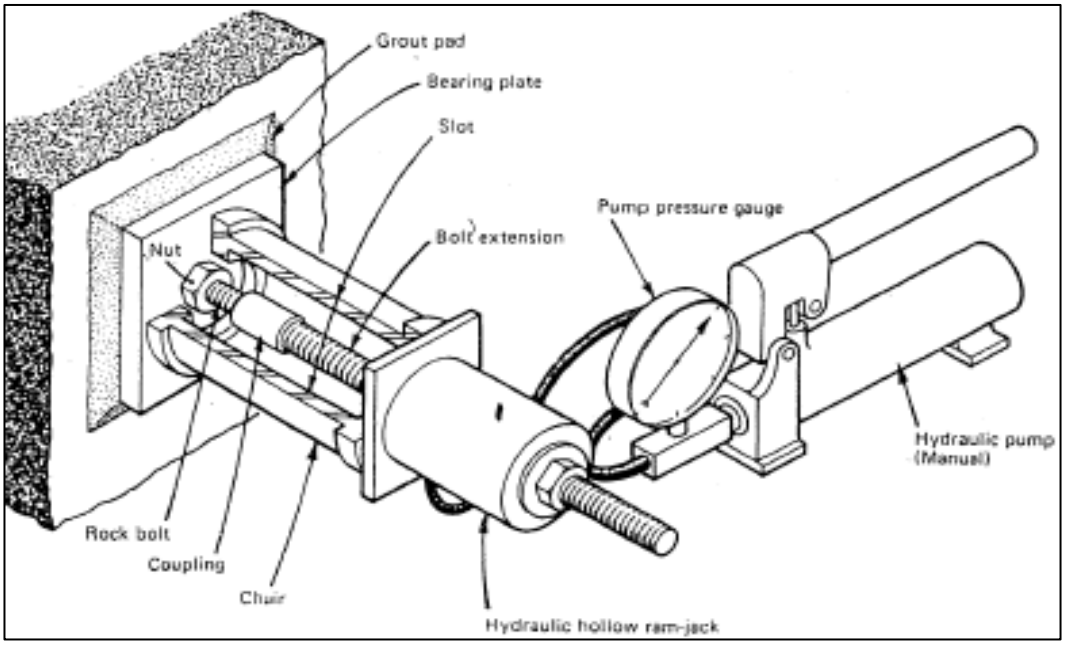


Figure 3.5-1. A diagram of a pull-out testing hydraulic jack (Littlejohn and Bruce, 1975).

In Figure 3.5-1 the cut-away shows the inner working mechanism of the tensioning jack. The recorded axial resistance of rock anchors from pull-testing is an amalgamation of the rock mass to grout and anchor-to-grout interface bond strengths as well as the ultimate tensile capacity of the cable or rock bolt. Understanding these interfaces is key to a better understanding of the cable-to-rock load transfer mechanism (Martin et al., 2013; Singh et al., 2022). Figure 3.5-2 is a diagrammatical representation of the ASTM D4435-08 method.

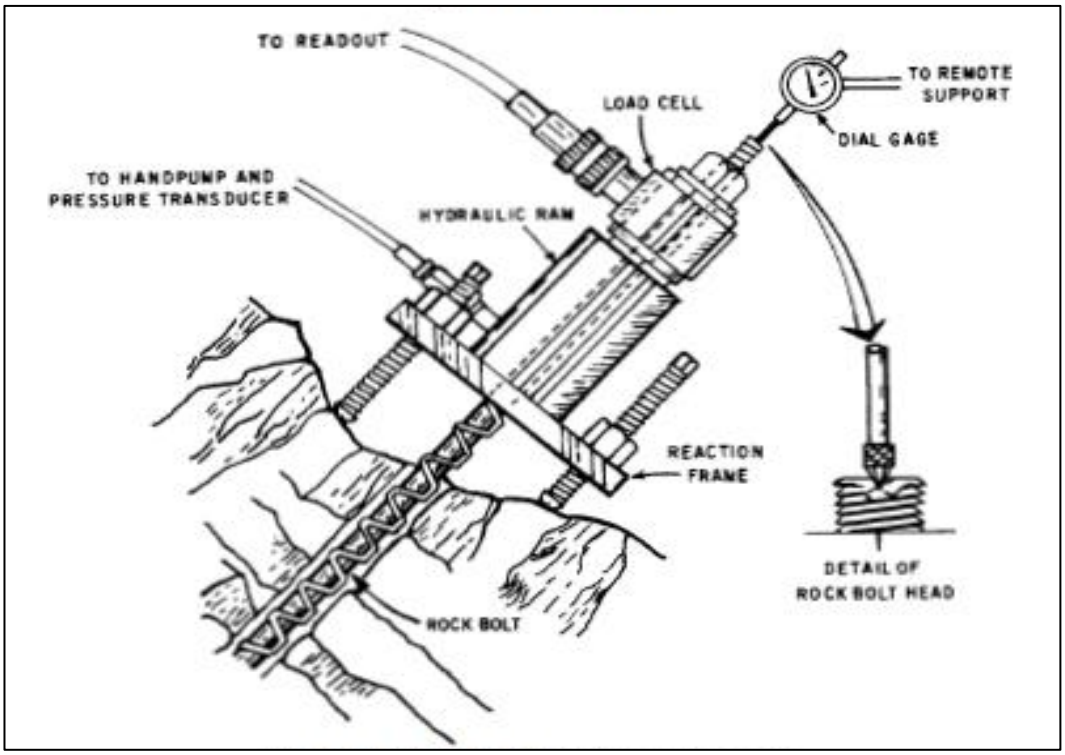


Figure 3.5-2. A rock bolt pull-out test schematic (ASTM D4435-08).

Figure 3.5-2 shows the connection lines for the hydraulic jack and read-out units as well as details of the rock bolt head. Engineers use pull-test results as input to further refine the design of rock bolts and cable capacity as well as to assess the mechanical performance of cable bolts (Hadjigeorgiou and Tomasone, 2018). Other uses include the investigation of expected cable bolt failure mechanisms and the assessment of the effects of pre-tensioning (Li et al., 2022).

Skrzypkowski et al (2020) also outlined how pull tests can be used to evaluate the effect of different embedment lengths on the load-bearing

capacity of the cable bolt. Furthermore, rock engineers use pull testing to double-check the listed axial loads of new cable bolts as advertised. When performed regularly, pull testing can help rock engineers monitor cable bolt behavioural changes (Tomasone et al., 2020).

Pull tests do have limitations. The use of concrete/geo-materials pull-test samples cannot fully replicate the bond stress between cables or bolts and the in-situ rock masses in underground mines. Another limitation of pull testing is the measurement of the load and displacement information at only the externally accessible portion of a rock anchor. The load and bond stress distributions along the partially or fully grouted length of the rock anchor may be non-uniform. This is a major drawback of pull testing as the non-uniformity of load and bond stress distributions does not constitute a good test of the efficiency of the grout-to-rock anchor bond strength (Forbes et al., 2020).

Jalalifar (2011) also stated that pull-testing load and displacement information is of limited use and forms a non-unique solution when assessing the efficiency of the anchor-to-grout bond strength. This is because the stress distribution in the cable anchor to grout interface is affected by a combination of factors that include the shape of the cable bolt, the installation borehole roughness, as well as the nature of the cement grout.

3.5.1 Cable bond strength

Hyett et al (1992) studied factors that control the bond strength of full-column grouted cables using a combination of laboratory and field testing. This study, using Portland cement pastes and standard seven-wire cable strands, found that the capacity of cables is most affected by the cement grout w/c ratio, and the embedded length of the cables, as well as the radial, restrain acting on the grout.

Yazici and Kaiser (1992), in their ground-breaking cable bond study, developed a theoretical model for full-column grouted cables that describes the bond strength developed between the cable and grout boundary. This study was able to describe the development of the bonding behaviour of cables through frictional forces between the grout and cable interface. The bonding behaviour was also shown to be controlled by the pressure developed at this interface.

Furthermore, this study outlined that the cable-to-grout dilatational pressure is controlled by the mechanical and elastic attributes of the rock mass and grout, the roughness of the support hole, and the cable bolt surface profile. This study found that a stronger grout-to-cable bond is formed by stiffer rocks and grouts, higher compressive strength grouts, and a higher degree of frictional resistance between the grout and cable. Finally, Yazici and Kaiser (1992), explained the occurrence of a sudden decrease in axial loads during short encapsulation testing as caused by the erratic spreading of cracks.

Kilic et al (2002) detailed how cementitious grout material properties affect rock support anchors. The authors obtained lower ultimate compressive and shear strengths in high w/c ratio grout mixes. The pull-out test results also showed a linear increase in pull-out load with increasing embedded rock anchor sections. Furthermore, this study showed a rapid increase of rock anchor bond strength in the first seven days of curing with a gradual increase thereafter until a full cure of the cement grout after 28 days.

Li et al (2016) conducted laboratory pull-out tests to determine the critical embedment length (CEL) of cement grouted 20 mm rebar rock bolts under three different w/c ratios. Li et al (2016) also conducted UCS testing on 100 x 100 mm cubic grout specimens whereas the pull-testing was conducted on rebar rock bolts cast into holes drilled into a solid concrete block.

Li et al (2016) found a linear relationship to exist between grout w/c ratio, grout UCS, and the CEL of cement grouted 20 mm rebars. Li et al (2016) then calculated the bond strength of grout to rebar rock bolt as the average shear strength of this interface. The bond strength was shown to be linearly correlated to the grout UCS as well as shown to increase with the CEL of the rebar rock bolts. Figure 3.5-3 is a plot of the CEL, UCS, and mean bond strength.

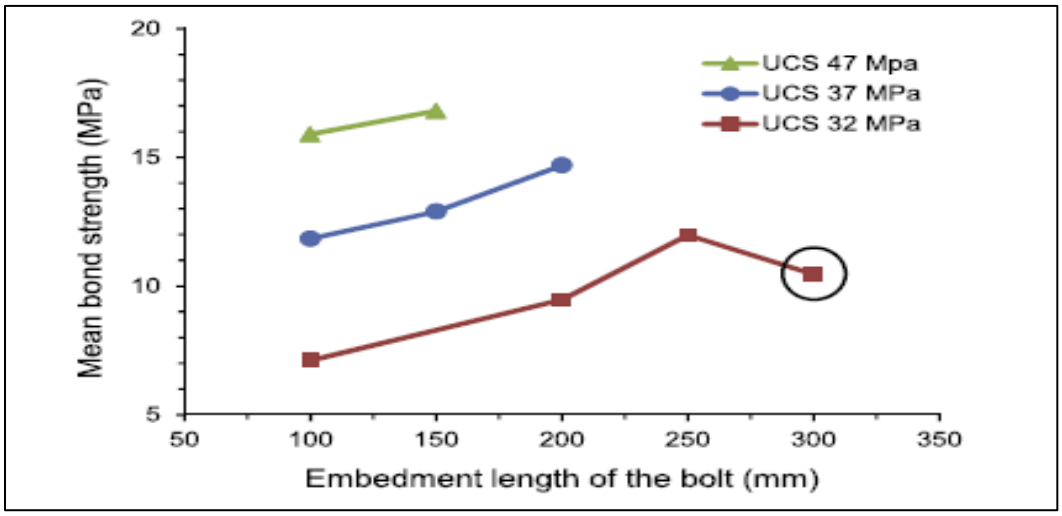


Figure 3.5-3. A plot of the critical embedment length and mean rebar–grout bond strength (Li et al., 2016).

Figure 3.5-3 shows a near-linear grout UCS and bond strength relationship. The circled point represents a rebar bolt that failed at its shank when its tensile capacity was exceeded and thus shows a lower bond strength.

3.5.2 Factors affecting pull-out testing

Benmokrane et al (1995) found in their laboratory study of different cement grouts and different cable anchor types under different embedment lengths that pull-out load increased linearly with anchorage length for each anchor type and cement grout type. The grouted anchor models (models A and B) used by Benmokrane are illustrated in Figure 3.5-4.

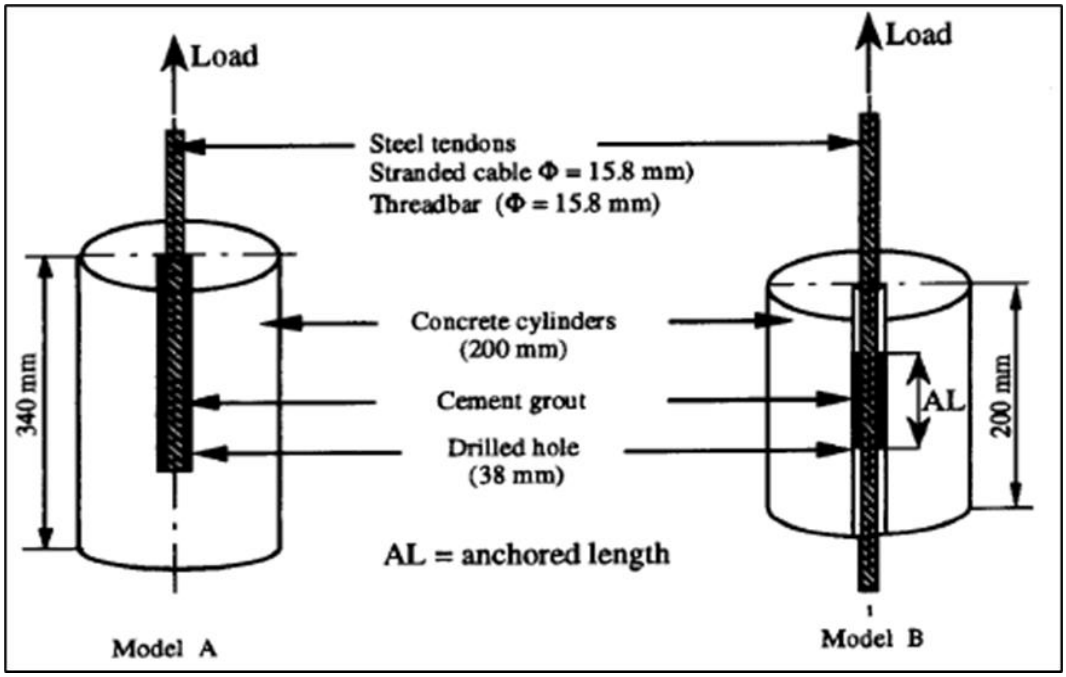


Figure 3.5-4. An illustration of the routed anchor models used to assess three diverse types of rock anchors and two anchorage lengths (Benmokrane et al., 1995).

Martin et al (2013) conducted a detailed study of the rock bolt-to-grout interface. They performed pull-out testing of three distinct types of rock bolts to attain insights into the behavioural characteristics of the rock bolt-to-grout interface under the influence of confining pressure, bolt type and surface profile, as well as boundary conditions of constant confining pressure and constant radial stiffness. Martin et al (2013) concluded that the pull-out testing axial displacement versus axial load is mostly affected by the boundary condition of constant radial stiffness.

Chen et al (2016) conducted testing of the axial loading performance of a broad range of cable bolts using a newly built laboratory for short encapsulation pull testing at the School of Mining Engineering, University of New South Wales, Australia. This study used 300 mm artificial geomaterial cylinders to simulate the rock mass into which these researchers installed cable bolts. The authors left the upper parts of the cable anchors to move around freely promoting shear failure of the rock mass–grout–cable anchor interfaces. The authors found in their research that embedment length and peak load capacity of cable bolts both increase linearly about each other for specimens of diameter 360 mm or less.

Singh et al (2016) investigated the performance of un-tensioned fully grouted rock bolts installed in competent rock mass in an Indian underground metal mine. 30 rock bolts were grouted using a 0.36 w/c ratio grout and pull-tested under variable embedment lengths and curing ages. The load-displacement profiles from pull-testing were analysed and showed that the main rock bolt failure mode was debonding of the rock bolt to the grout interface. The field pull-out tests study was complemented with finite difference modelling (FLAC3D code) to assess stress re-distribution at 150 m mining depth. A safety factor was developed for an unsupported rock mass using load-displacement profiles developed from the in-situ SEPT. Singh et al (2016) concluded that the evaluated un-tensioned fully grouted rock bolts can be safely used to support underground excavations at this mine.

Feng et al (2017) investigated anchorage performance in layered rock strata using pull-out tests of rock bolts inserted into segmented steel tubes. This study showed that the rock anchor performance is affected by factors such as how well bonded the grout is to the rock anchor, grout-to-rock mass interface bond properties, rock bolt and faceplate mechanical properties, and whether a pre-tensioning force is applied or not.

Thenevin et al (2017) detailed a new pull-out testing bench used to evaluate parameters such as confining pressure, length of rock bolt embedment, borehole wall roughness, and the thickness of grout as well as the failure of rock bolt to grout interface. They concluded the pull-out response was most affected by the length of the rock bolt embedment and the confining pressure.

3.5.3 Simulating failure modes

Bawden et al (1994) conducted constrained axial and shear testing of normal and modified cable bolts. They built a laboratory contraption to recreate the in-situ shear and joint displacement failure modes encountered during gravitational rock mass sliding (Figure 3.5-5).

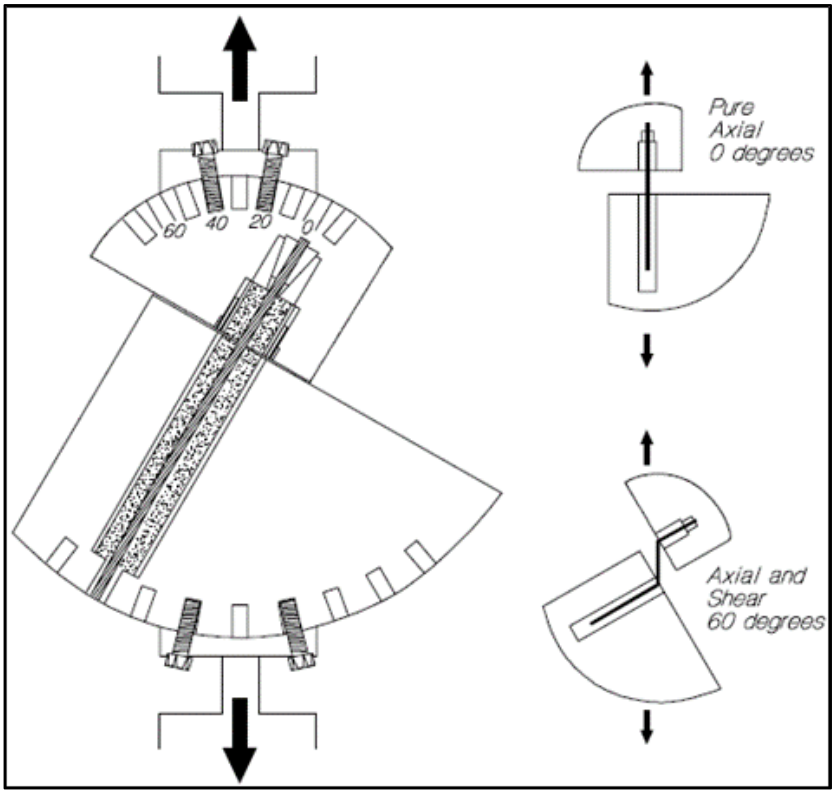


Figure 3.5-5. A diagram of the device used for constrained axial and shear testing of cable bolts (Bawden et al., 1994).

It can be seen in Figure 3.5-5 that the device is comprised of two freely rotating semi-circular steel discs that hold the cable bolt and can be rotated to the desired angle as well as permitted to slide about each other. Bawden et al (1994) found a change in the failure mode of standard cable bolt samples from bond failure to cable rupture with an increase in pull-test angle, and an increase in the peak load capacity of the cable bolts with an increase in pull-test angle, as well as a decrease in the cable bolt stiffness with an increase in pull-test angle. The modified cable bolts also showed a

similar change of failure mode, however, the peak load-bearing capacities of the cable bolts and their stiffness decreased for steep pull test angles.

Hagen et al (2020) detailed how the SINTEF and the Norwegian University of Science and Technology (NTNU) rock mechanics labs in Norway have developed a rock bolt testing rig that can evaluate cement and resin grouted cable anchors and rock bolts simulating pull, shear, and combinations of pull to shear testing mechanisms under fully controlled and monitored conditions. Hagen et al (2020) demonstrated that the SINTEF/NTNU testing rig can better approximate underground loading conditions by testing rock and cable bolts to higher failure and displacement values when compared to standard pull-out testing benches. Figure 3.5-6 is a plot of pull-out load versus displacement from the Hagen et al (2020) study.

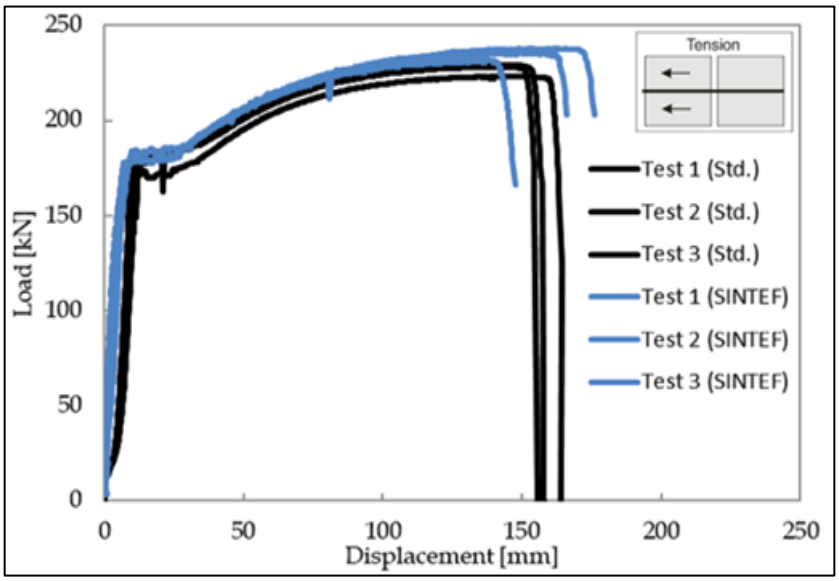


Figure 3.5-6. A plot of load versus displacement that compares the standard and SINTEF pull-out testing benches (Hagen et al., 2020).

Figure 3.5-6 shows that the SINTEF testing bench obtained higher average values of load and displacement (blue lines) compared to standard testing (black lines).

3.5.4 Corrosion studies using pull-out testing

Thompson (2004) studied, through laboratory pull-out tests, the performance of barrel and wedge cable bolts at installation and through their service life. This study showed how corrosion impacted the barrel and wedge mechanism. Pull-out tests of the barrel and wedge cables showed a slip failure of the wedge-cable strand interface at loads less than the designed capacities. Thus, barrel and wedge cables can provide less than the required support capacity if large periods pass between the installation of the cables and events of rock mass loading.

Villaescusa et al (2008) conducted a study to better understand the loss of supportive capacity by corroded full-column cement grouted cables under a controlled corrosive environment. Pull-testing was conducted at different time intervals for different corrosion environments simulated through custom-built corrosion chambers. These researchers used cable loads and displacements that were far below the material's tensile strength so that failures could be related to corrosion effects. The study estimated that cable strands, under the most intense corrosive environments, last for about a year. Furthermore, barrel and wedge cable strands installed without corrosion coating were estimated to only last seven months.

This study outlined how full-column grouted cables can still get corroded and lose their supportive capacity over time due to water seepage in areas of cracked grout. This finding is in line with the information presented in section 3.4 on the studies of grout shrinkage further cementing the importance of pull-testing and grout shrinkage studies.

3.5.5 Modelling pull-out testing

Jalalifar (2011) developed an analytical model to describe the development of load along rock bolts installed in elastoplastic rock conditions. The model was used to predict the transfer of loads by using rock bolts with and without end plate features as well as using different rock mass characteristics. Stress changes due to mining activities were found to be a significant factor that controls the strength of the grout-to-rock bolt-to-rock mass bond in a study by Jalalifar (2011).

Singh and Srivastava (2021) employed the 3DEC distinct element software code and studied the influence of factors such as cable bolt diameter, cable bolt length, and grout thickness on grouted and non-grouted cable bolts. They observed a non-linear relationship between pull-out load and cable bolt length for grouted cable bolts whilst non-grouted cable bolts exhibited a linear relationship to pull-out load. Singh and Srivastava (2021) also showed that grouted cable bolts have a linear association of the pull-out resistance with the thickness of the grouting material further outlining the importance of fully grouting support anchors to ensure enough thickness of grout. Figure 3.5-7 shows the 3DEC modelling outputs.

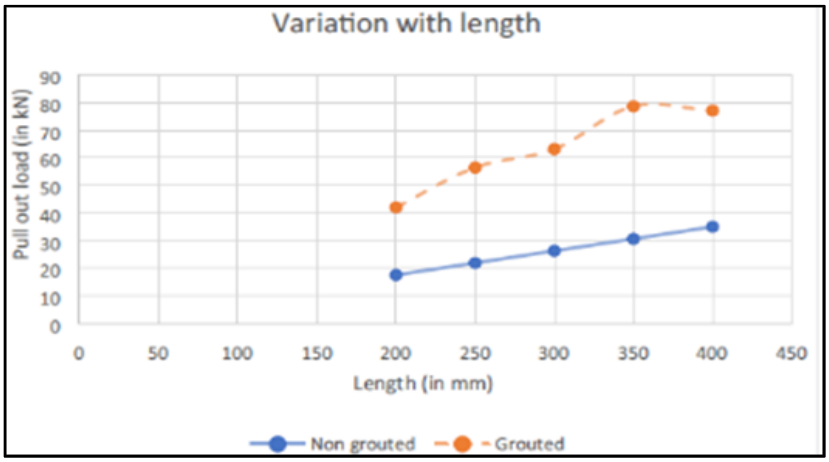


Figure 3.5-7. 3DEC modelling of cable bolts output showing the variation of pull-out load with the length of grouted and non-grouted cable anchors (Singh and Srivastava, 2021).

The variation of pull-out load with grouted and non-grouted cable length is illustrated in Figure 3.5-7. Both non-linear and linear relationships can be observed. Singh et al (2022) presented a study on the identification of rock structural fabric from strain gauge instrumented rock bolt installations and a methodology for calibrating a rock bolt FLAC3D model with in-situ rock bolt strain data. These researchers utilized optical strain gauge instrumented rock bolts to obtain high-resolution strain data.

The instrumented rock bolts were shown to accurately capture bending strain impacted on the rock bolt by shear loading events; bending strains are useful for locating and resolving the orientation of localized rock mass discontinuities. Figure 3.5-8 shows a snapshot of the FLAC3D numerical model used by Singh et al (2022).

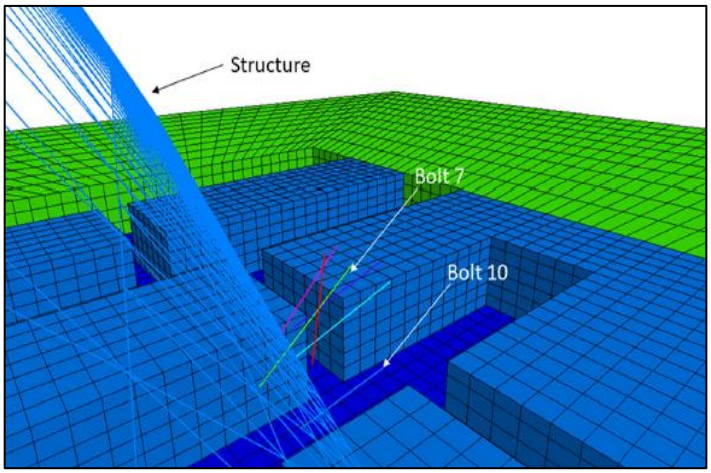


Figure 3.5-8. FLAC3D model showing the angled strain-gauge instrumented rock bolt installations and a dipping geological structure for a room and pillar mining method (Singh et al., 2022).

Strain-sensor instrumented rock bolts are shown in Figure 3.5-8 to be installed at various angles to the dipping geological structure in the mine.

3.6 Mining Smart Sensor Technologies

Rock anchors experience differing loads in their field-use lifetimes and thus require long-term monitoring (Bacic et al., 2018). There have been advances made in the field of smart sensors in search of non-destructive testing methods to assess the quality of grout and the support unit's integrity in situ. Smart sensors for monitoring cable bolts are being commercialized and can monitor and detect exerted axial loads, support hole non-grouted spaces and grout defects, as well as collect strain data to calibrate numerical models (Song et al., 2017; Singh et al, 2022). Bacic et al (2018), however, argue there are still deficiencies in instrumented cable data

interpretation and correct application in the practice of smart sensor technology in the mining industry.

Smart-sensor methods that have been evaluated by the mining industry include direct radar waves, fibre-optic instrumentation, and guided ultrasonic wave measurements forming the so-called non-destructive measurement techniques. Smart sensor cable anchor monitoring technologies are currently challenged by the harsh operating environments normally found in underground mines and the inability to perform long-term monitoring of cable and rock bolt installations.

Smart sensor technologies are founded on strong theoretical research backgrounds. These smart sensors are, however, prone to abuse, misuse, and incorrect application in situ for the monitoring of underground rock reinforcement units (Song et al., 2017; Bacic et al., 2018). Smart sensor cable anchor technologies are also found lacking in the ability to perform constant and long-term monitoring with an easy method of data collection and processing (Eliasson et al., 2014). Figure 3.6-1 is a diagrammatical representation of a strain-gauge instrumented cable bolt.

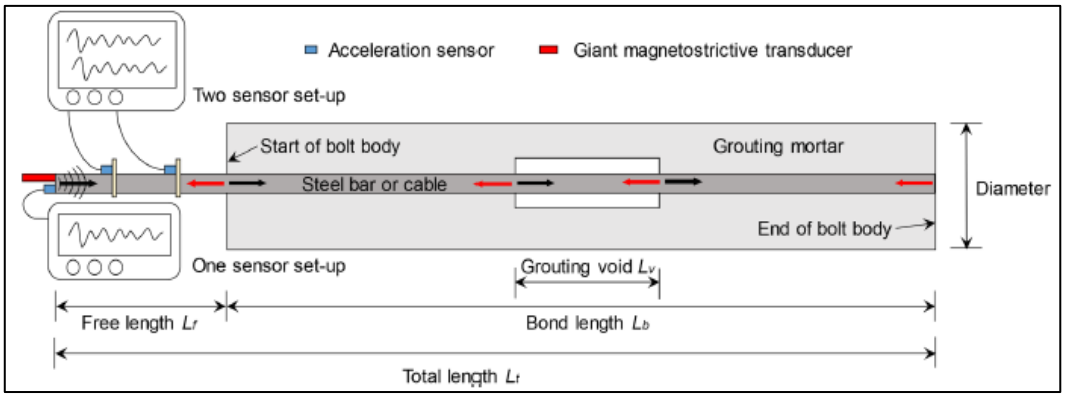


Figure 3.6-1. A diagrammatical representation of the non-destructive monitoring of cables and rock bolts using wave-propagation methods (Liu et al., 2022).

Figure 3.6-1 shows the placement of strain gauges and the connection to a readout meter. The subsequent sub-sections review research work on distinct types of smart sensor technology used for monitoring cable bolts.

3.6.1 Strain-gauge and other methods

Chekired et al (1997) outlined how they developed and evaluated a device capable of measuring cable anchor tension values using a set of vibrating wire strain gauges fastened at two points on the cable. The authors used an experimental pull-out test to mimic the effect of cable bolts undergoing tensioning when installed into a rock mass to evaluate the strain-gauge instrumented cable bolts.

Cable bolt samples were grouted into mortar moulds and pull-tested. The device, as can be seen in Figure 3.6-2, was shown to accurately record the

load versus displacement experienced by the cable bolt samples. The results obtained were comparable to commercially available gauges. Figure 3.6-2 shows the strain-gauge device installed around a cable anchor; a pencil is used for scale.

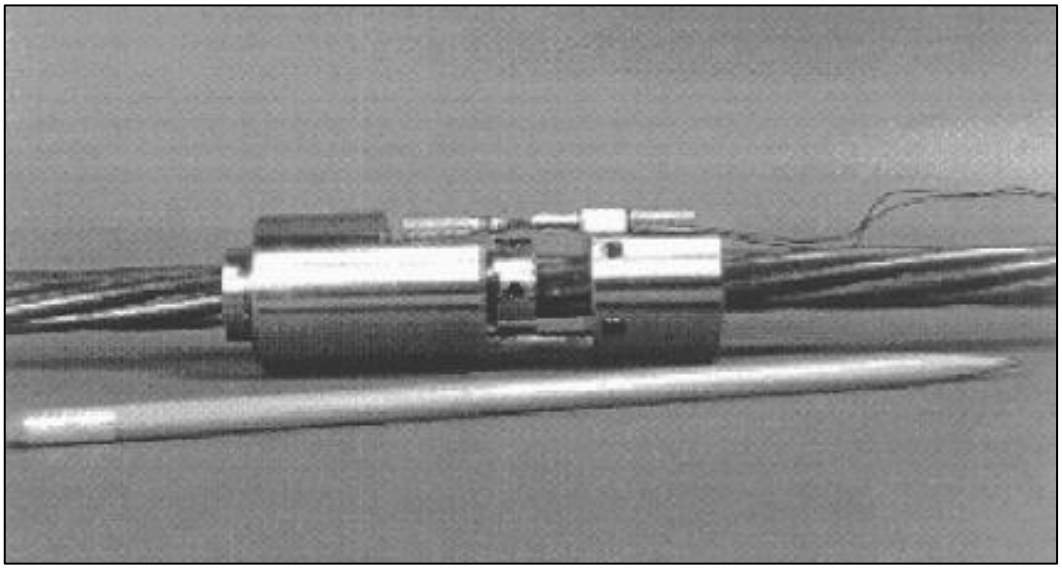


Figure 3.6-2. A picture of a strain gauge device used for the measurement of cable bolt tension values (Chekired et al., 1997).

Martin et al (2002) investigated the physical properties of fully grouted cable bolts during pull testing by replacing the traditional king-wire of cable bolts with a modified strain-gauge king-wire to help advance knowledge and understanding of load-deformation behaviour of grouted cable bolts. The authors conducted three tests on 1.83 m long cable anchors grouted into 0.91 m long pull-tube cylinders. A total of 20 strain gauges were installed along the length of the tested cable bolts.

Pull testing provides cable bolt load values that are averaged over the entire length of a cable bolt. In contrast, the strain-gauge instrumented cable bolts tested by Martin et al (2002) were able to provide a repeatable point of load measurements along the entire length of a cable bolt. The authors thus showed load measurements taken along the entire length of a cable bolt can be used to assess the behaviour of cables under loading conditions as well as help better understand the rock mass to grout to cable interface complex load transfer mechanisms.

Eliasson et al (2014) detailed a smart rock bolt with buried strain sensors and the capability to process and transmit recorded data wirelessly fully taking advantage of the concept of the Internet of Things (IoT). The authors showed how the smart rock bolt can initiate a wireless network to transmit data via a numbered address to detect a computer or network interface with a further option for data encryption. The smart rock bolt can appraise strain and seismic energy values in underground excavations in real time. Figures 3.6-3 and 3.6-4 show an underground installation of the smart rock bolt as well as the acceleration versus time output from a smart rock bolt.



Figure 3.6-3. A smart rock bolt installation in a mine (Eliasson et al., 2014).

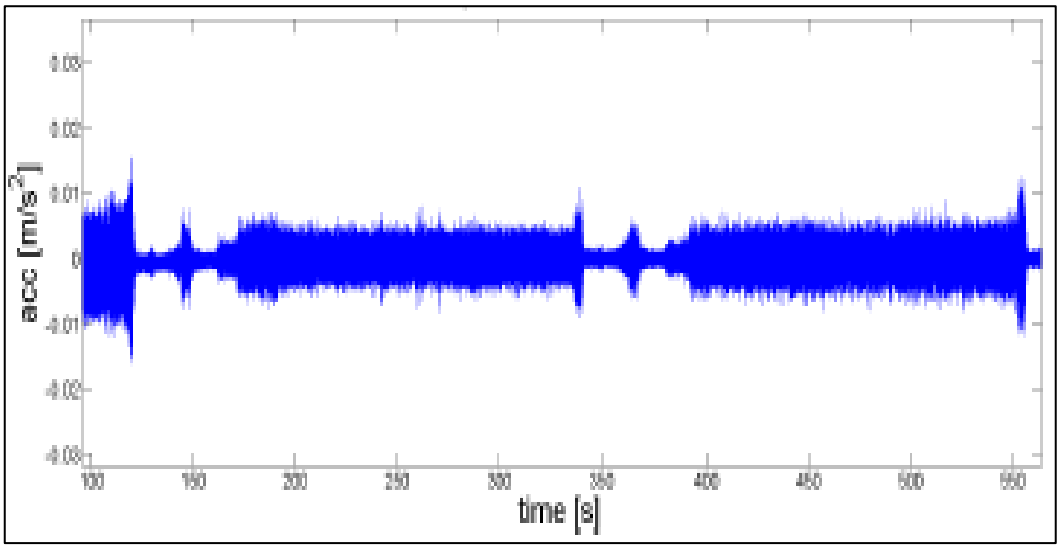


Figure 3.6-4. The use of the smart rock bolt to detect nearby drilling activity (Eliasson et al., 2014).

The acceleration data was used to detect nearby drilling activity, the change in drilling tools is shown as apparent breaks in the acceleration signal in Figure 3.6-4. Gustafsson (2016) developed sensor systems to check the status of grout installation (non-grouted, half-grouted, and full-column grouted) and the development of micro-cracks in a support hole. The first system developed is the Cavimeter system. This system is used to check whether a support hole has been fully grouted or not. The Cavimeter uses a pressurized plastic pipe wrapped around the rock bolt that will expand into non-grouted gaps in the support hole, the volume of air in the expanded plastic pipe can be used to calculate the volume of un-grouted cavities using the Cavimeter system. In the Cavimeter system, the volume by which the plastic pipe expands is proportional to the volume of the non-grouted space inside of the support hole. The Cavimeter system is illustrated in Figure 3.6-5.

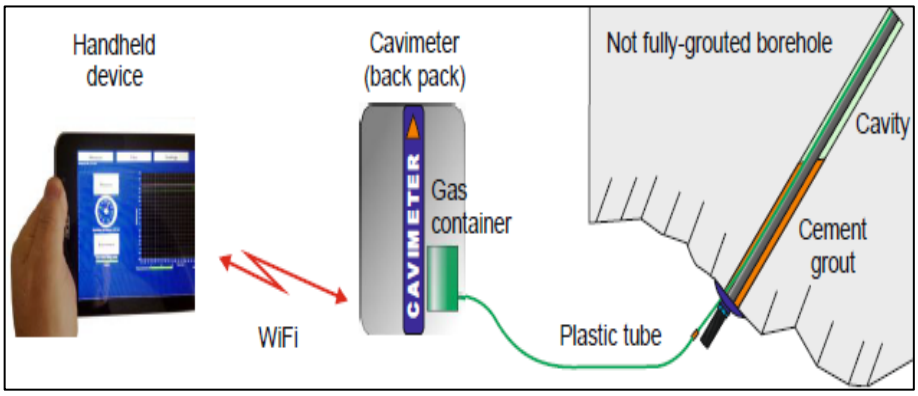


Figure 3.6-5. A diagrammatical representation of the Cavimeter system comprising of a hand-held readout unit, a Cavimeter backpack housing a gas container, and a plastic tube for installation into a support hole (Gustafsson et al., 2016).

Figure 3.6-5 shows the working premise of the Cavimeter system and the transmission of data to a readout unit. Furthermore, the authors have developed the Cavisensor system. The Cavisensor program line-up includes the CaviBasic, CaviLight, CaviSens, and CaviCom sensor systems. Each program is a step up from the previous program with more technical detail added, the Cavisensor program line-up is outlined in Table 3.6-1.

Table 3.6-1. Descriptions and measurement functions of the Cavisensor programs.

Sensor	Description	Measurement
CaviBasic	Extensometer attached to rock bolt	Rock bolt elongation and rupture
CaviLight	CaviBasic and flashing red LED light attached to the sensor	Rock bolt elongation and rupture
CaviSens	CaviBasic, flashing red (Bolt rupture) and yellow (Pre-set elongation reached) LED lights attached to the sensor	Rock bolt elongation and rupture
CaviCom	CaviSens and Wi-Fi data download	Rock bolt elongation and rupture

The Cavisensor system uses a tiny steel wire located inside a plastic tube looped around the rock bolt to measure the extension of the rock bolt and thus indirectly measure the rock bolt integrity status. The elongation sensors are colour-coded to give warnings of rock bolt elongation above predetermined safe levels; red colour blinks are used for a completely broken rock bolt whereas yellow indicates rock bolt extension greater than acceptable levels.

The CaviLight system has a one-week life if the LED light flashes constantly and a five-year operation lifespan without the flashing LED light. A luminescent bead can also be used to indicate when the rock bolt has reached a pre-set elongation level. The field test of the CaviSens included a cable attached to a battery-powered data collector at the Outokumpu mine, although the authors did not indicate the battery life of the data logger.

3.6.2 Ultrasonic-guided waves

Ultrasonic-guided wave rock anchor evaluation technique has come out as one of the most promising non-destructive cable anchor installations monitoring techniques. The ultrasonic non-destructive testing method involves exciting and propagating guided ultrasonic waves along the entire length of the cable bolt using specialized devices.

Beard and Lowe (2003), in their search for portable non-destructive ultrasonic wave-based equipment, identified usable ultrasonic wave frequencies through modelling software and proved their concept with

laboratory and in-situ tests. The authors concluded low ultrasonic wave frequencies can identify areas of partial or full cable bolt grout encapsulation, and in contrast, asserted that higher-end frequencies can be reliably used to verify installed cable bolt lengths. Figure 3.6-6 is a diagrammatical illustration of the working premise of the ultrasonic wave method.

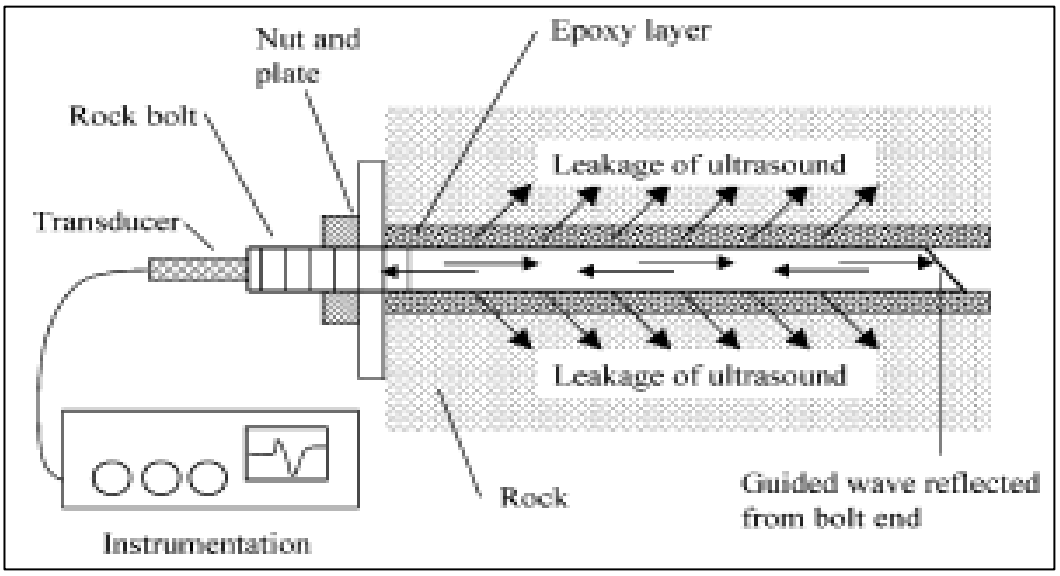


Figure 3.6-6. A diagram showing a rock bolt installation and the set-up of the guided wave method (Beard and Lowe, 2003).

The proposed Beard and Lowe (2003) ultrasonic monitoring method is diagrammatically illustrated in Figure 3.6-6 where guided ultrasonic waves are shown travelling through an epoxy resin anchored rock bolt. Sbartai et al (2007) proved the application of direct radar waves in assessing the physical condition of cement-based materials such as grout as a non-

destructive technique. The authors correlated saturation readings of seventy-two concrete samples with radar wave attenuations and validated this method using electrical resistivity measurements showing good correlations between radar attenuations and measured electrical resistances.

Buys et al (2009) provided a comprehensive review of the use of ultrasonic waves to monitor grout integrity. These researchers outlined how guided ultrasonic waves' structure is sensitive to diverse types of grout interface flaws. Thus, rock engineers can use the arrival times of these waves and their velocities to locate areas where grout is defective or calculate the length of the grout column in a rock bolt installation.

Zou et al (2010) conducted a study of how cementitious grout quality disturbs and reduces ultrasonic wave velocity. They found grout strength and air capacity in tested specimens influenced ultrasonic wave propagations revealing the potential of the ultrasonic wave as a non-destructive technique to assess the quality of grout.

Jiang et al (2016) investigated a stress-wave method to monitor the integrity of grout using piezoceramic sensors attached to the ends of a rock tendon. A piezoelectric-lead-zirconate (PZT) transducer placed in the middle of the tendon duct was used to excite stress waves. The authors simulated four possible situations that may occur during grouting operations and included

non-grouted ducts, 50 percent grouted ducts, and 90 percent grouted ducts, as well as full-column grouted ducts.

The analysis of the stress-wave signals showed that the single bottom piezoceramic sensor could only detect 50 percent grouted ducts and upwards, whereas the two upper sensors could only detect fully grouted ducts. This study showed that the proposed stress-wave method can be potentially used for non-destructive monitoring of grouted tendon ducts. Figure 3.6-7 shows the stress-wave signals from the stress-wave method.

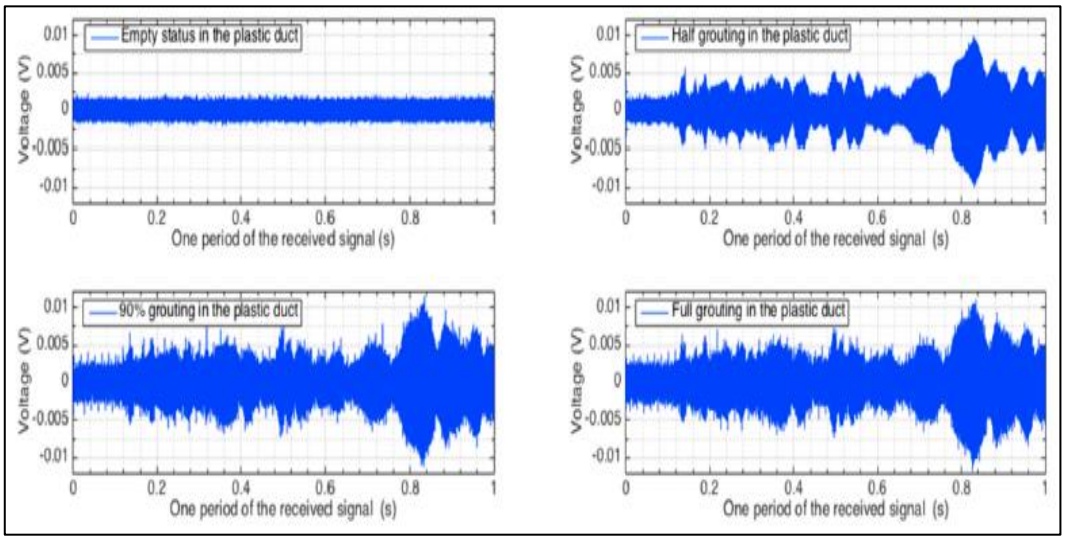


Figure 3.6-7. Plots of the bottom-sensor (PZT1) stress-wave signals recorded from different grouting simulations (Jiang et al., 2016).

Figure 3.6-7 shows the variation of the stress-wave signals for all simulated grouting situations from this study. The generated stress waves had an amplitude (expressed as voltage) of ten Volts and a period of one full

second. The detectability of 50 percent column grouting and upwards can be observed. It is noted that the investigated stress-wave signals presented by Jiang et al (2016) were obtained after five days of grout curing. The stress-wave energy is likely to change as the grout cures further and could impact the detectability of the simulated grouted columns.

Song et al (2017), in their review of cable bolt smart-sensor technologies, asserted that engineers could isolate certain frequencies of ultrasonic guided waves to evaluate cable bolt installations in situ. The engineer can also assess waveforms in the frequency or time domains to find waveform velocities that best describe the length of grout columns in support holes.

Xu et al (2021) used direct stress wave measurements to actively find grout imperfections where they attached PZT patches on the surface of grouted splice sleeve connectors to excite and measure stress wave propagations. These researchers tested the technique on four test samples with varying intensities of artificially induced grout defects as well as on four samples without defects.

Xu et al (2021) recorded an increase in the stress-wave values using PZT sensors in test samples with grout defects compared to specimens without grout defects. The caveat of the study by Xu et al (2021) is that the PZT stress-wave actuators and sensor patches needed to be arranged in a specific fashion over a 300 mm test sample to accurately identify the location and length of the grout imperfections. Underground applications of

this technique would require a different arrangement of PZT patches and thus the technique offers a non-unique solution.

Liu et al (2022) cautioned that wave propagation methods are dependent on the precise identification of the arrival times of reflected waves. They further stated that the detection of direct waves and multiple reflections from the closest point of the cable bolt can muddy the signal and detection of grout defects if one uses one sensor to record the propagated waves.

3.6.3 Optical-fibre methods

Researchers have employed optical-fibre technology in their studies of cable bolts using smart sensor technologies. Optical-fibre methods exploit the fact that light journeying through the fibre element is perturbed by external stimuli such as pressure changes, temperature fluctuations and others.

These perturbations can be ciphered into corresponding alterations of the travelling light that may include the light's wavelength, frequency, and other factors, a demodulation system is used to extract the original information from these travelling light perturbations (Song et al., 2017). The FBG sensors are one of the most employed sensor types in the field of rock engineering.

Tang et al (2018) realized mechanical or electronic sensors in cable and rock bolts are disturbed by electromagnetic waves and dust from harsh

underground environments, as well as corroded by acidic mine water. The authors proposed and installed quasi-distributed FBG sensors on a rock bolt with slots covered with resin to protect and permanently fix the sensors in place for the measurement of axial forces experienced by the rock bolts. The diagram in Figure 3.6-8 shows how the FBG sensors were incorporated into a rock bolt element.

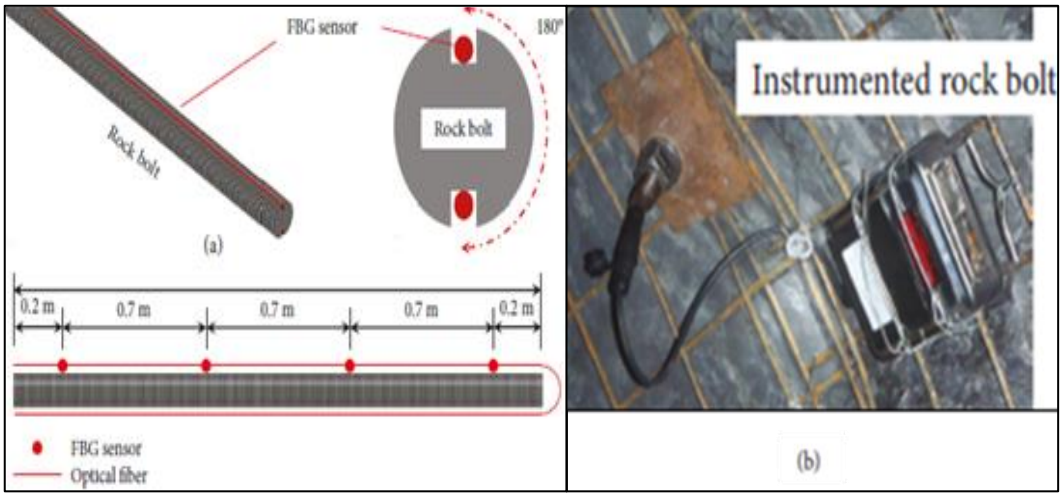


Figure 3.6-8. An illustration of (a) The incorporation of FGB sensors into a rock bolt and (b) An instrumented rock bolt installation in a mine (Tang et al., 2018).

The picture on the right-hand side in Figure 3.6-8 shows an FGB sensor instrumented rock bolt and a data collection module installed in an underground mine. Tang et al (2018) found that roof-installed bolts experienced higher forces compared to bolts installed at other locations. Furthermore, the maximum axial forces were frequently recorded towards

the middle parts of the rock bolts. The authors were able to establish a mine-wide rock bolt excessive load detection system by marrying the FBG sensor rock bolts to the already established detection system of the mine where axial forces greater than one hundred kilo Newtons (kN) triggered an advance-warning alarm on the overloading and imminent rock bolt failure.

Vlachopoulos et al (2018) used a recently developed distributed optical strain sensing technology with a reported resolution of 0.65 mm to document strain values along a rock bolt length. The authors evaluated rock anchors with fibre-optic sensors grouted into 28 days cured concrete. Further, they conducted pull-out testing of the rock anchor samples to assess the effects of different embedment lengths, grout types, and support hole diameters. Vlachopoulos et al (2018) found that the embedment length affected the axial pull-out response of evaluated rock bolts the most.

Forbes et al (2020) demonstrated the use of optical fibre technology for the evaluation of cable anchors during pull-out testing at an underground salt mine. The optical fibre technology was used to continuously record strain data along an entire length of a cable anchor during underground pull-out testing. The strain profiles from Forbes et al (2020) were used to calculate shear stress and deformation profiles for the support anchor thus providing more diagnostic behavioural information beyond the load and displacement usually reported from in-situ pull-out testing. Furthermore, the normal installation methodology for the in-situ pull-out test was not impeded by the

additional sensor installation. Thus, this technique can be readily used to complement pull-out test operations.

3.7 Electrical Resistivity Technology

The novel grout sensor technology evaluated in this research report is based on the electrical resistivity method thus a review of the evaluation of cementitious materials using electrical resistivity is included in this literature survey. The use of electrical resistivity methods in hardening cementitious mixtures dates to the early 1920s (McCarter, 1999). Electrical resistivity methods are well-researched and applied in civil engineering for structural health mapping (identifying damaged areas) of structures constructed from cement-based materials. In contrast to civil engineering research, little to no research work has been conducted on mining engineering applications.

There has also been a lot of work performed to understand the early-age and late-age hydration characteristics of cement-based materials using electrical resistivity methods. It is important to study the hydration characteristics of cement-based mixtures as these characteristics determine the long-term strength, longevity and soundness of cement-based mixtures (Pei et al., 2017; Lu et al., 2018). Klun et al (2021) similarly asserted that the microstructures that develop in concrete, mortar, and cement paste during hydration largely control their mechanical, and physical properties when they have solidified.

Electrical resistivity methods are low-cost, repeatable and non-destructive to the cementitious grout, concrete, and mortar installation; thus electrical methods are well suited as measurement and monitoring techniques (Morsy, 1999; Vincent et al., 2017; Tian et al., 2020; Choo et al., 2021). The electrical resistivity technique can be applied both in the laboratory and field settings to assess the structural health of the cementitious grout, concrete, and mortar installation (Morsy, 1999; Vincent et al., 2017, Tian et al, 2020). In practice, electrical resistivity methods involve the measurement of the electrical resistivity or conductivity of a cement-based material (concrete, mortar, cement paste) using a variety of instruments. An alternating current (AC) is passed through the test specimen and the resistivity of the specimen is measured at each electrode location. The resulting electrical resistivity or conductivity quantity is usually plotted against the test specimen curing or hydration age.

Electrical resistivity measurement methods can be divided into surface and bulk resistivity measurement techniques. The surface resistivity of cementitious grouts, concrete, and mortars is measured directly using mould-fixed electrodes that are directly placed on test specimens. In contrast, the bulk resistivity (the resistivity of the cementitious paste and the cement paste pore-water resistivity) is measured using electrodes embedded into the test specimens. Figure 3.7-1 shows schematic diagrams of various surface and bulk electrical resistivity measurement methods. The grout sensor technology employed evaluated in this research can be

classified as a bulk resistivity technique utilizing electrodes embedded into the grout to record electrical resistivity.

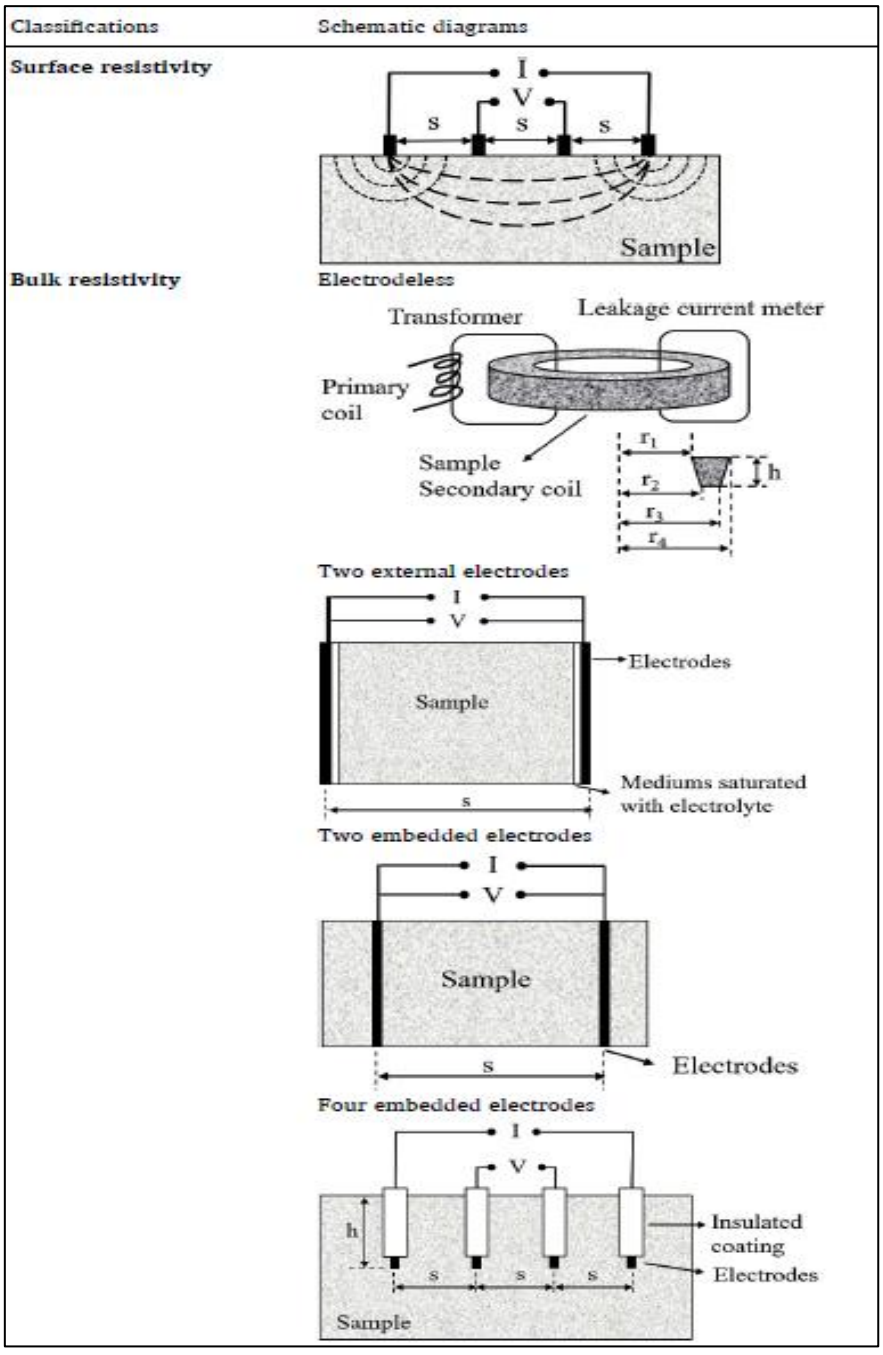


Figure 3.7-1. Diagrams and classification of electrical resistivity measurements (Sang et al., 2022).

Recent years have seen the increasing use of non-electrode resistivity measurement devices. These devices are transformer based and use two coils for resistivity measurements (Sang et al., 2022). Non-electrode or non-contact electrical resistivity methods are more dependable and accurate whereas contact electrical resistivity methods require good contact between the electrode and the test specimen (cementitious grout, concrete, or mortar) and are therefore prone to errors in measurements. Figure 3.7-2 shows a schematic diagram of the non-electrode electrical resistivity measurement method.

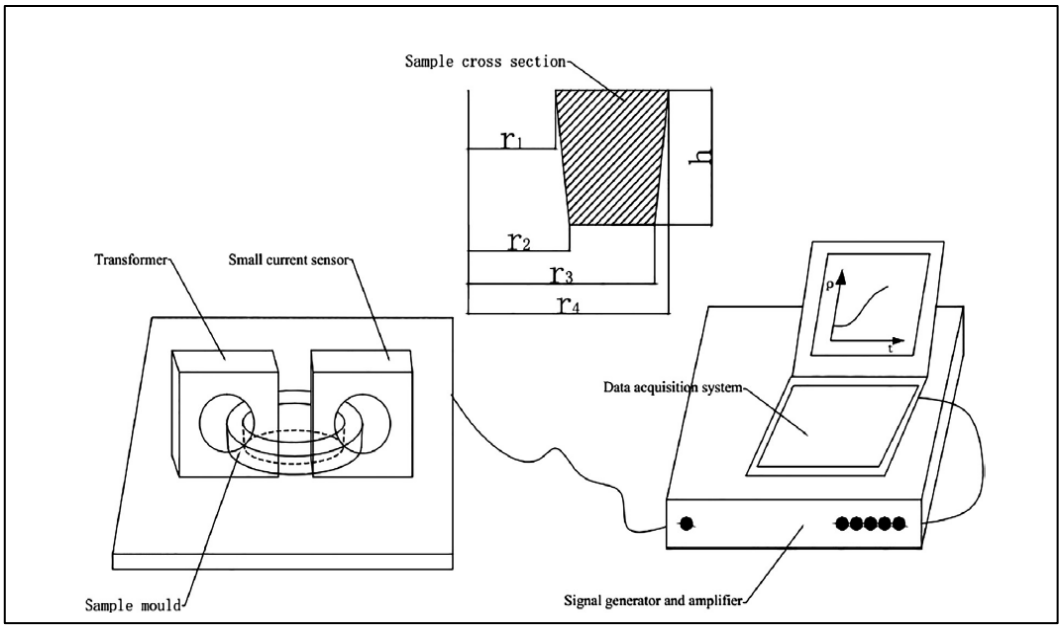


Figure 3.7-2. A diagrammatical illustration of the non-contact electrical resistivity measurement technique (Lu et al., 2018).

Figure 3.7-2 shows the non-contact electrical resistivity method and how the electrical resistivity measurements are read through a data acquisition system to derive resistivity-curing age plots that can be used to study the hydration characteristics of cementitious materials.

3.7.1 Portland cement hydration and electrical resistivity

Most of the cementitious grouts used in the mining industry are manufactured using OPC with added admixtures to influence the performance of the grout under certain mining conditions. Therefore, it is important to understand the hydration process of OPC and how this process can be studied using the electrical resistivity method. Gartner et al (2002) provided an exhaustive review of the OPC hydration chemical reactions and showed how these chemical reactions influence the shape of electrical resistivity/conductivity versus curing age plots.

In essence, a series of complex superimposed chemical reactions (hydration) take place when OPC is added to water resulting in the curing and hardening of the cement paste over time (Morsy, 1999; Gartner et al., 2002). In response to these chemical reactions, the resistivity values measured from the OPC-water paste reflect the concentration of charged ionic particles and the resistivity of the connected pore solution (McCarter, 1999; Morsy, 1999; Heikal et al., 2000; Gartner et al., 2002; Liu et al., 2014; Choo et al., 2021).

Immediately following the mixing of OPC and water (early age) the dominant chemical process taking place is the liberation of charged ionic particles into the OPC-water paste (Liu et al., 2014; Lu et al., 2018; Choo et al., 2021). The early-age hydration process is expressed as low and constantly decreasing resistivity values (high conductivity) in resistivity versus curing age plots reflecting the ease of movement of the liberated charged ions in the OPC-water paste (Liu et al., 2014; Dong et al., 2016; Lu et al., 2018; Choo et al., 2021; Sang et al., 2022).

Then, the OPC paste starts to harden as hydrates are produced from the continual reaction of OPC and water filling up previously-unfilled pore spaces. This chemical process is reflected in an increase in resistivity values with increasing curing age. The increase in resistivity values reflects a hardening OPC molecular structure with disconnected pores that resists the easy flow of electrical current. Figure 3.7-3 shows how the mixing and hardening phases of OPC affect electrical resistivity measurements.

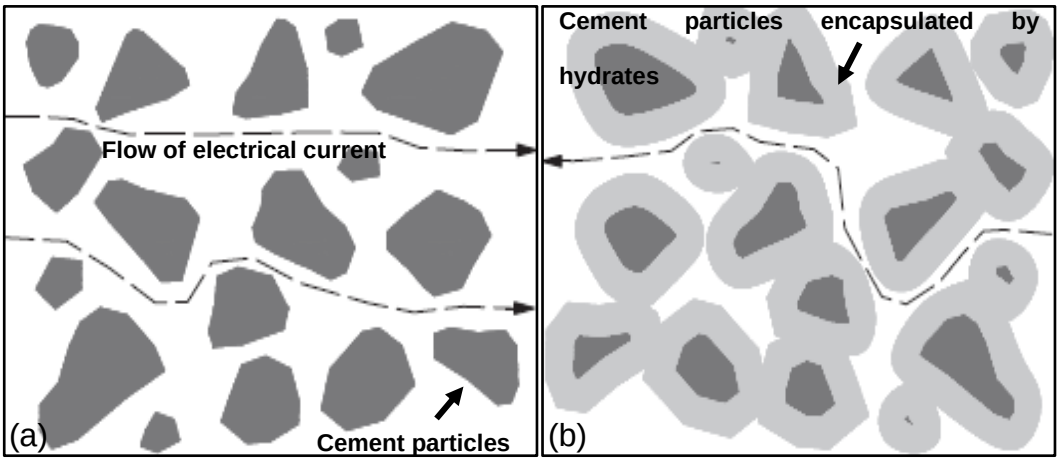


Figure 3.7-3. A schematic illustration of the setting of OPC paste and the effect on electrical resistivity (a) Early-age cement paste permits the easy flow of electrical current = low resistivity values, and (b) Late-age cement paste restricts the easy flow of electrical current = high resistivity values. (Modified from Wei et al., 2012).

Figure 3.7-3 shows how the early-age OPC paste allows the easy flow of electric current through charged ionic particles. Figure 3.7-3 also shows how the change in the hardened OPC molecular structure (hydrates attach themselves to unreacted cement particles) constricts the flow of electrical current. Therefore based on these observations, an idealised cementitious grout electrical resistivity versus curing age can be drawn as shown in Figure 3.7-4.

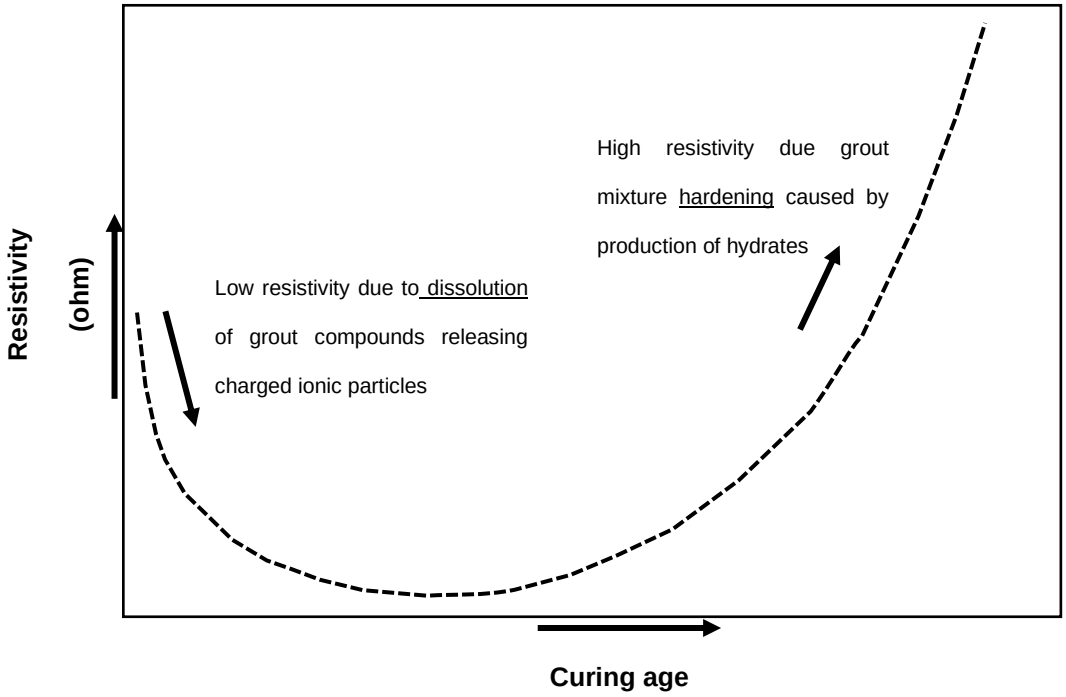


Figure 3.7-4. A plot of the idealised OPC and cementitious grout resistivity versus curing age profile.

Figure 3.7-4 shows how the hydration chemical reactions control the shape of OPC resistivity versus the curing age profile. It can be noticed that an initial curvilinear decrease in resistivity values is followed by a minimum and then a steady rise of OPC resistivity values. Based on the understanding of the OPC hydration reactions, two cementitious grout products with similar mineral compositions will react differently when mixed with water as their mineral constituents may have been refined and prepared differently by different manufacturers (Morsy, 1999; Gartner et al., 2002). These grouts will have different resistivity-curing age profiles due to the difference in chemical reactions taking place. These resistivity-curing age plots can be

studied carefully to understand the hydration characteristics of each grout. This ability outlines the usefulness of the electrical resistivity method to study and differentiate cementitious grouts.

Both surface and bulk resistivity measurement methods can measure the electrical resistivity of cementitious materials at fine intervals (every second or minute) and thus can provide a very comprehensive electrical resistivity dataset. Such comprehensive electrical resistivity datasets can be utilised to study variables that control the integrity and soundness of the solidified cementitious grouts and concretes (Klun et al., 2021). Variables that can be studied include the effects of changing the w/c ratio of cementitious grouts, the effects of variable curing temperatures, the addition of admixtures, and the development of the uniaxial compressive strength in cementitious grouts.

Electrical resistivity measurements are sensitive to the chosen current frequency, voltage, and the positioning of electrodes. High current frequencies tend to underestimate electrical resistivity readings while low current frequencies contribute to the polarization of the electrical current. Polarization describes the difference between measured and actual alternating current values. The frequency limitation can be overcome by using alternating-current spectroscopy methods which use multiple frequencies. McCarter (1999) showed how the complex resistivity signal from AC spectroscopy can be used to study cement pastes, mortars and concrete and capture the effect of changing the w/c ratios and the addition

of aggregates. The ambient temperatures and humidity levels in test environments are also known to affect how ions move about in the cementitious material and thus affect the measured electrical resistivity (Sang et al., 2022). The research work briefly discussed below shows how researchers have applied the electrical resistivity and conductivity measurement methods in their studies of cementitious materials (cement grouts, concrete, and mortars) to highlight salient points of the resistivity methods.

3.7.2 Curing temperatures

Morsy (1999) studied the effect different curing temperatures have on the hydration properties and setting times of blended OPC mixtures. Electrical conductivity values were measured using a coaxial cylinder with an inner and outer electrode ring. Table 3.7-1 shows the blended cement mixture compositions where OPC was progressively replaced by silica fumes by weight per cent.

Table 3.7-1. Silica fume cement mixture compositions (Adapted from Morsy, 1999).

Composition of Silica and Slag Mixtures			
Mix Number	**OPC**	**Silica Fume (%)**	**Slag (%)**
I	100	0	0
II	97.5	2.5	0
III	95	5	0
IV	90	10	0
V	65	0	35
VI	60	0	40
VII	55	0	45

Morsy (1999) found that the electrical conductivity method can be used to effectively study the hydration properties of silica fume and slag blended OPC mixtures. Each resulting conductivity curve documented the initial dissolution of blended OPC where charged ionic particles are liberated increasing conductivity values. All conductivity curves of blended OPC mixtures also showed a steep decline in conductivity values resulting from a steady production of hydrates. Figure 3.7-5 shows the electrical conductivity values recorded from silica fume and slag blended OPC mixtures.

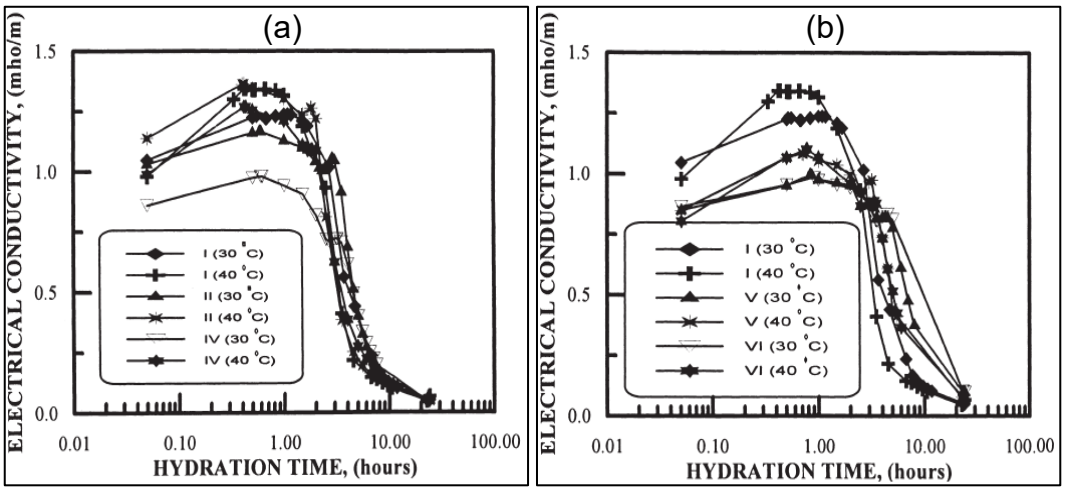


Figure 3.7-5. Plots of electrical conductivity versus hydration time of (a) Silica fume blended OPC and (b) Slag blended OPC (Morsy, 1999).

Figure 3.7-5 shows the initial increase and later decrease of electrical conductivity values documenting the hydration process of OPC. It can also be observed from Figure 3.7-5 that increased hydration temperatures increase the electrical conductivity values (or decreases the electrical resistivity). Further, electrical conductivity values can be observed to decrease with the increasing addition of silica and slag to OPC mixtures.

Morsy (1999) also found that higher curing temperatures resulted in the faster setting of all cement mixtures. The study also found that increasing amounts of cement replacement with silica fume and slag resulted in longer setting times for each blended mixture. This study is especially important for deep mines with high geothermal gradients and mine using blended grouts

where the setting time of OPC-derived grouts will be impacted by rock temperatures. Figure 3.7-6 illustrates the effect curing temperature had on blended cement mixtures containing varying mixtures of silica fume by weight per cent from Morsy (1999).

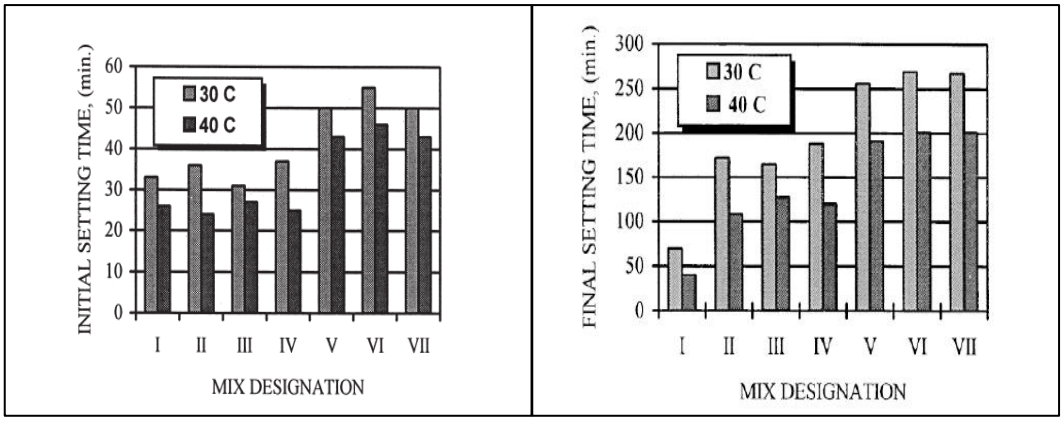


Figure 3.7-6. A plot of initial and final setting time plots of OPC mixtures with different amounts of added silica fumes and slag cured at different temperatures (Morsy, 1999).

It can be observed in Figure 3.7-6 that there is a noticeable reduction in the initial and final setting times of the silica fume and slag-added OPC mixtures when curing takes place under higher temperatures. Another interesting study on curing temperatures and electrical resistivity is that by Teixeira et al (2016). The authors studied how curing temperatures affect the hydration, the evolution of the microstructure and pore structure, and the development of compressive strength in cement paste modified with titanium oxide nanoparticles. Nanomaterials are increasingly used by the construction

industry to provide durability to cement-based materials and improve their performance. In this study, normal and titanium oxide nanoparticles-modified cement pastes were prepared and cured at room temperature, 40 degrees Celsius, and 60 degrees Celsius between three, 14, and 28 curing days. An electrical impedance spectroscopy device was used to conduct the electrical resistivity measurements. Figure 3.7-7 shows the electrical resistivity versus curing age of normal and blended cement pastes over a 28-day curing interval.

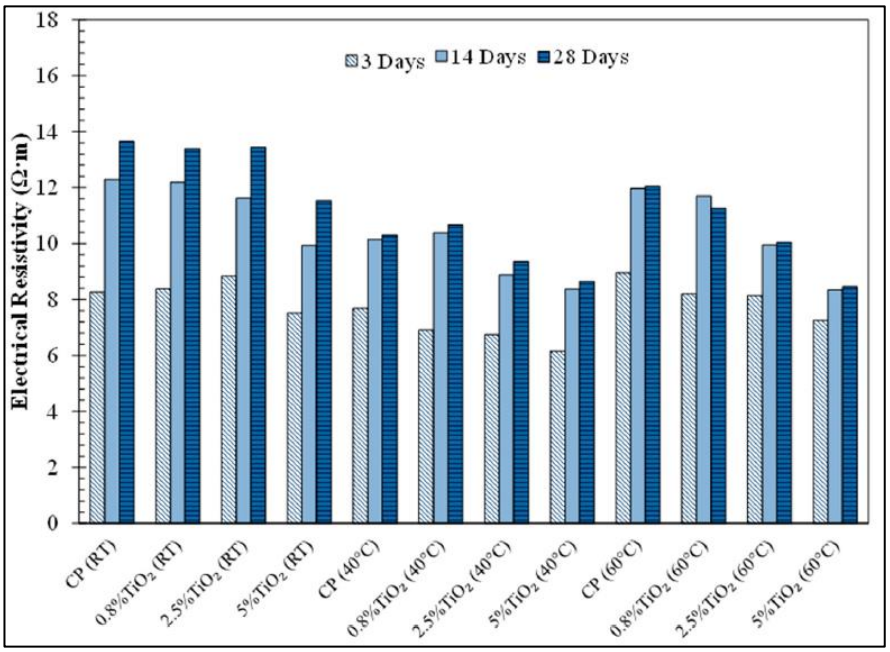


Figure 3.7-7. A plot of electrical resistivity versus curing age of normal and titanium oxide-modified cement pastes cured at different temperatures over a 28-day interval (Teixeira et al., 2016).

It can be observed in Figure 3.7-7 that all electrical resistivity values show an increase with increasing curing age irrespective of curing temperature or nanoparticle addition. It can also be observed that normal and blended cement paste resistivity values cured at 40 degrees and 60 degrees Celsius are reduced compared to those measured at room temperature and that the reduction is more pronounced at 28 curing days. Further, the increasing addition of titanium oxide nanoparticles to the cement pastes resulted in an increasing amount of reduction of the cement paste electrical resistivity values.

3.7.3 Water-cement ratio

Dong et al (2016) investigated the effect of an increasing cement-paste w/c ratio on electrical resistivity measurements. The authors prepared cement mixtures with w/c ratios of 0.25, 0.3, 0.4 and 0.5. These mixtures were placed into a moulding device and the electrical resistivity was recorded at five-second intervals for a full day while maintaining an atmospheric temperature of 20 degrees Celsius using a non-electrode measurement device. UCS testing was also conducted on 40 x 40 x 40 mm cement sample cubes (12, 18, 24 hours as well as three-, 14-, and 28-day curing ages). The non-electrode device used by Dong et al (2016) is shown in Figure 3.7-8.



Figure 3.7-8. A non-electrode electrical resistivity mould and measurement device (Dong et al., 2016).

In Figure 3.7-8, the non-electrode mould and measurements device is shown connected to a workstation to download and process the recorded resistivity data. The authors found a decrease in electrical resistivity values with increasing w/c ratio of cement paste. The authors then plotted the cement UCS values against the electrical resistivity data. A linear equation was fitted through the datasets to describe the cement UCS - electrical resistivity relationship collected over one day. Figure 3.7-9 shows a plot of the different w/c ratio cement pastes electrical resistivity measurements conducted over 24 hours.

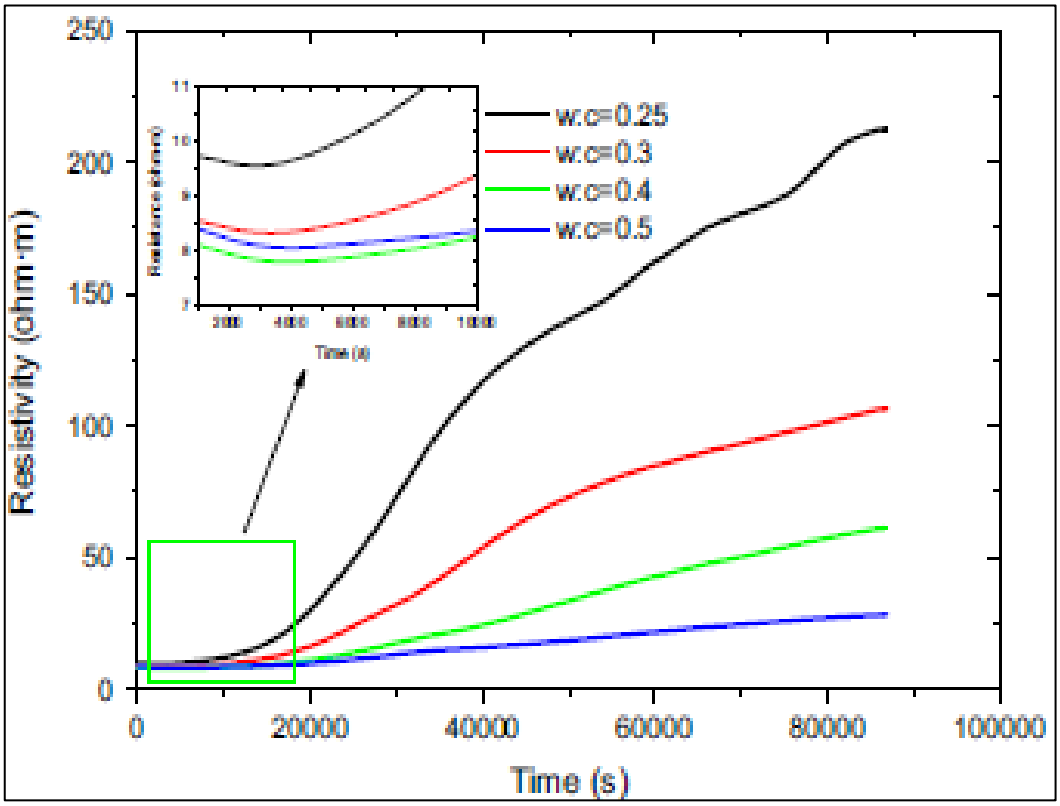


Figure 3.7-9. A plot of electrical resistivity measurements versus curing age in seconds shows the effect of an increasing w/c ratio on the electrical resistivity values (Dong et al., 2016).

It can be observed in Figure 3.7-9 that higher electrical resistivity values of cement paste are obtained at a lower w/c ratio, the insert figure is a magnification of the first three curing minutes. This study showed that the early-age electrical resistivity measurements are sensitive to and can capture the changes in cement paste w/c ratios. Furthermore, this study showed that electrical resistivity measurements can be successfully used to predict the compressive strengths of early-set cementitious materials.

Zhang and Li (2017) compared and contrasted the measured early-age electrical resistivities of OPC and Calcium Sulfoaluminate cement (CSA) with a w/c ratio range of 0.3 to 0.55 using a contactless electromagnetic induction-based electrical resistivity measurement tool. The authors represented the OPC and CSA cement samples at the w/c ratio range of 0.3 to 0.55 using the notation P03 – P055 and S03 – S055, respectively.

The authors obtained distinctly different electrical resistivity curves for the OPC and CSA cement variants. The CSA showed higher resistivity values than the OPC over the same w/c ratios of tested mixtures. Furthermore, the study found that an increase in the w/c ratio depressed the electrical resistivity values and delayed the occurrence of the first resistivity minima before a further increase in the resistivity values. The early age resistivities of CSA and OPC are shown in Figures 3.7-10 and 3.7-11, respectively.

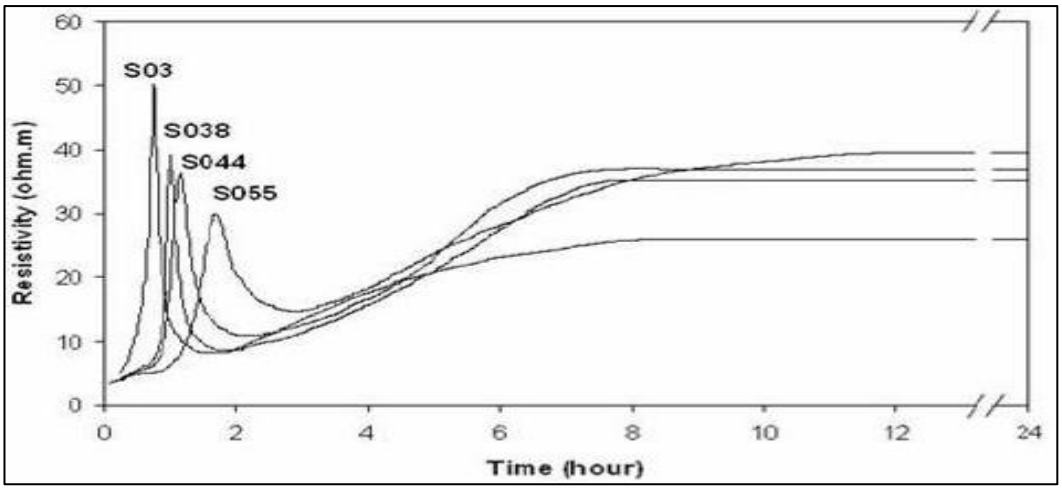


Figure 3.7-10. A plot of resistivity values recorded from different w/c ratio CSA mixtures over the first 24 hours of curing (Zhang and Li, 2017).

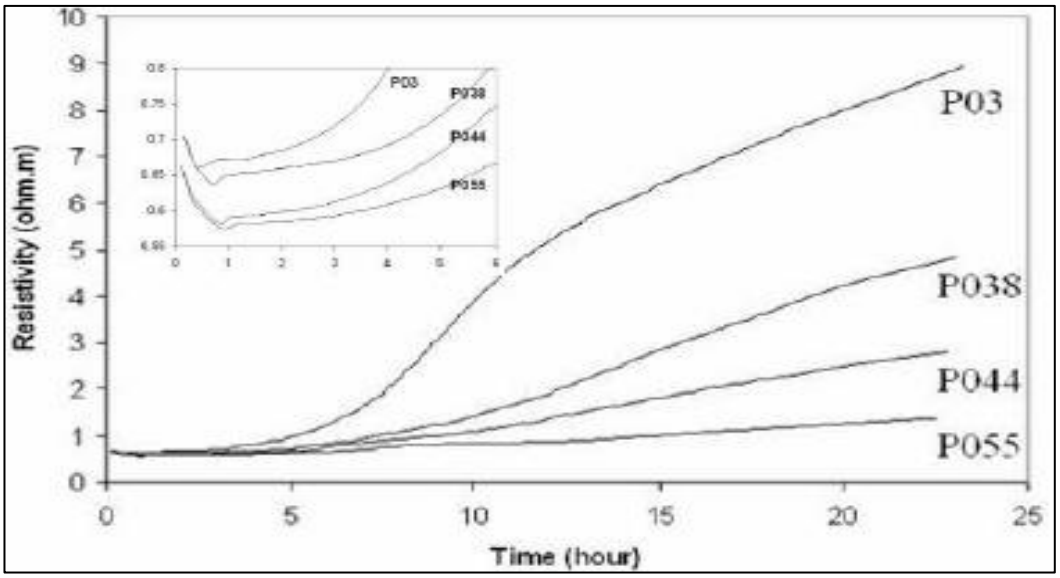


Figure 3.7-11. A plot of resistivity values recorded from different w/c ratio OPC mixtures over the first 24 hours of curing (Zhang and Li, 2017).

Figures 3.7-10 and 3.7-11 show the electrical resistivity versus curing age profiles for CSA and OPC types of cement. It can be noticed in Figure 3.7-10 that the relationship between cement resistivity and the w/c ratio is not clear. However, Figure 3.7-10 illustrates that the CSA cement attained resistivity values between 10 and 50 ohms. In contrast, Figure 3.7-11 illustrates a clear relationship between OPC resistivity values to the w/c ratio. The insert in Figure 3.7-11 shows a plot of resistivity versus curing age illustrating the details of the resistivity decreases over the first curing hour. This study showed that electrical resistivity measurements are sensitive to and can capture the hydration process and the variation of w/c ratios between two different cement types.

3.7.4 Compressive strength

Wei et al (2012) initiated a study to find a quick method that can predict the compressive strength of cement within a day of casting. The authors prepared and assessed three grades of cement (32.5 MPa; 42.5 MPa and 52.5 MPa) with eight samples of cement procured from different suppliers. All resistivity and compressive strength samples were prepared with a w/c ratio of 0.4. Electrical resistivity measurements were conducted for one full day using non-contact electrical resistivity equipment. Figure 3.7-12 shows the non-contact electrical resistivity equipment used by Wei et al (2012). The equipment maintained the tested cement pastes at a temperature of 20 ± 2 degrees Celsius to minimize the effects of temperatures on the recorded resistivities.

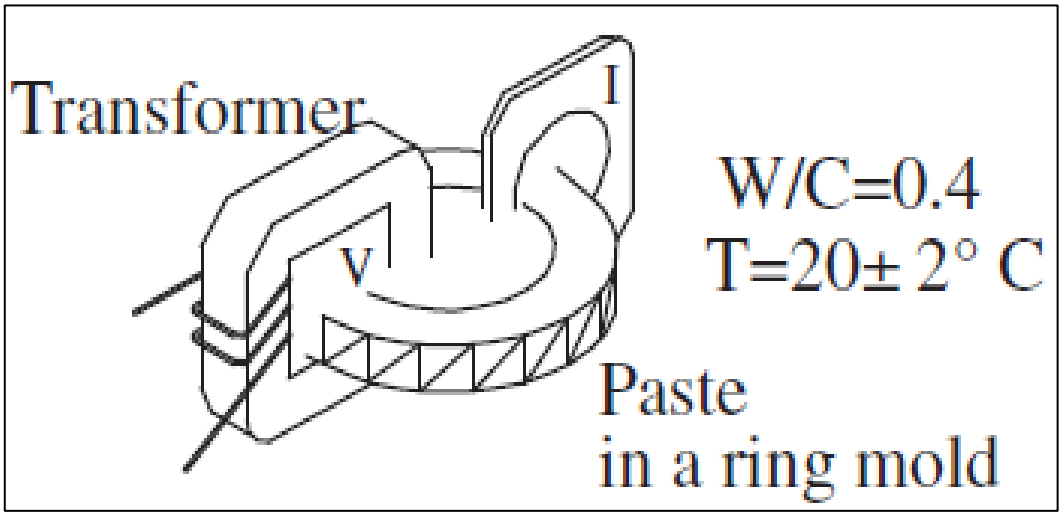


Figure 3.7-12. A diagram of a non-contact transformer-based electrical resistivity measurement equipment (Wei et al., 2012).

Figure 3.7-13 shows the plot of electrical conductivity against the 24 hours of cement curing from the Wei et al (2012) study.

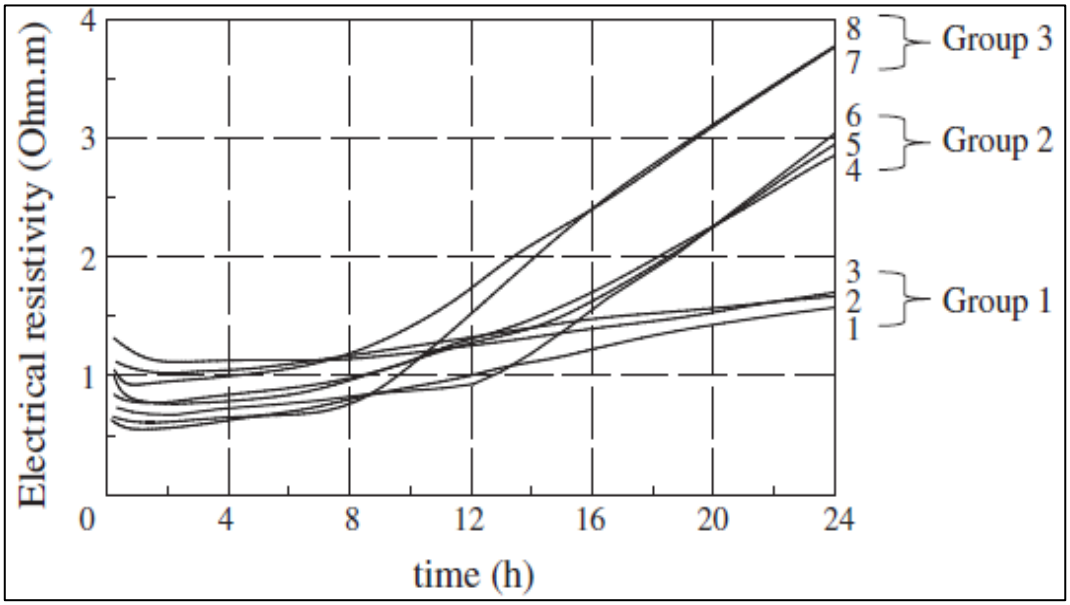


Figure 3.7-13. A plot of electrical resistivity recorded over 24 hours in eight different cement mixtures with a w/c ratio of 0.4 (Wei et al., 2012).

Figure 3.7-13 shows that higher grades of cement (group 3) have higher electrical resistivity readings when compared to lower grades of cement (group one). The three-way grouping of the cement electrical resistivity curves according to cement grade can also be observed in Figure 3.7-13. The prediction of the cement mortar compressive strength from early-age (24 hours) electrical resistivity measurements is illustrated in Figure 3.7-14, albeit with a few data points. The authors were able to establish a linear

equation describing cement sample strength at 28 days with resistivity measurements collected over the first 24 hours of cement casting.

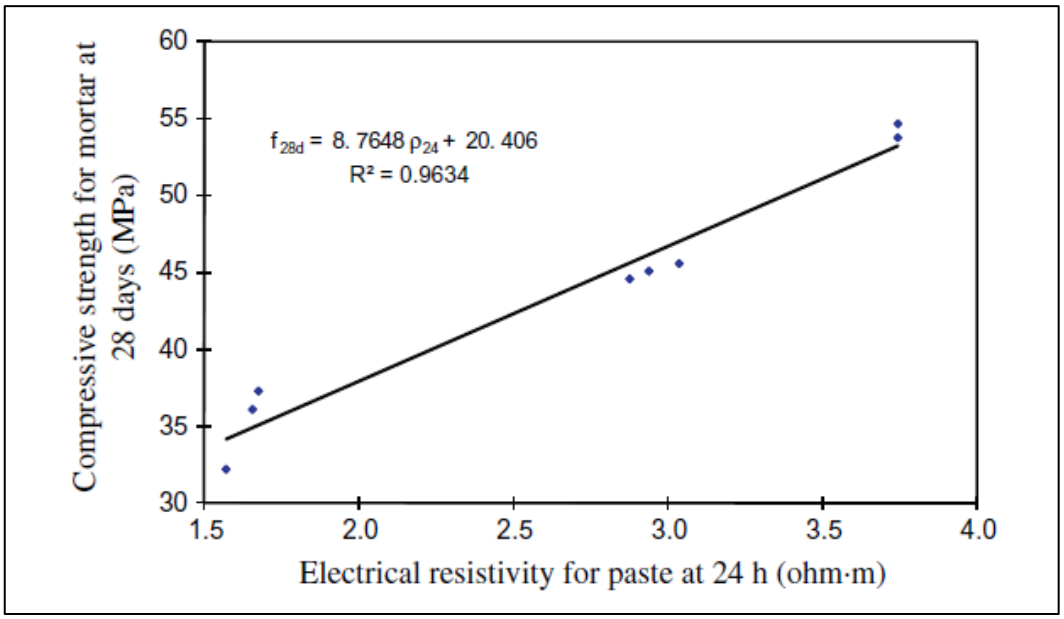


Figure 3.7-14. A plot of the 28-day cement mortar compressive strength against the 24-hour electrical resistivity values (Wei et al., 2012).

Wei et al (2012) concluded that electrical resistivity measurements can capture the differences in cement grade under a fixed w/c ratio. Furthermore, this study demonstrated the use of early-age electrical resistivity measurements to predict the 28-day compressive strength of cement mortars.

Choo et al (2021) investigated the relationship between grout UCS and grout w/c ratio to the measured electrical conductivity values in cement grout stabilized sands. Choo et al (2021) conducted UCS tests and recorded electrical conductivity data for up to 28 to 35 days on three silica micro-cement types. The three silica micro-cements (designated as K-4, K-5, and K-6) were each made into grout slurries with w/c ratios of 1.0, 1.5, and 2.0, respectively. The authors repeated the electrical resistivity data and UCS collection three times and the average values from these tests were used. Figure 3.7-15 is a plot of electrical conductivity versus curing age in days for the cement grout stabilized sands at a constant w/c ratio of 1.5.

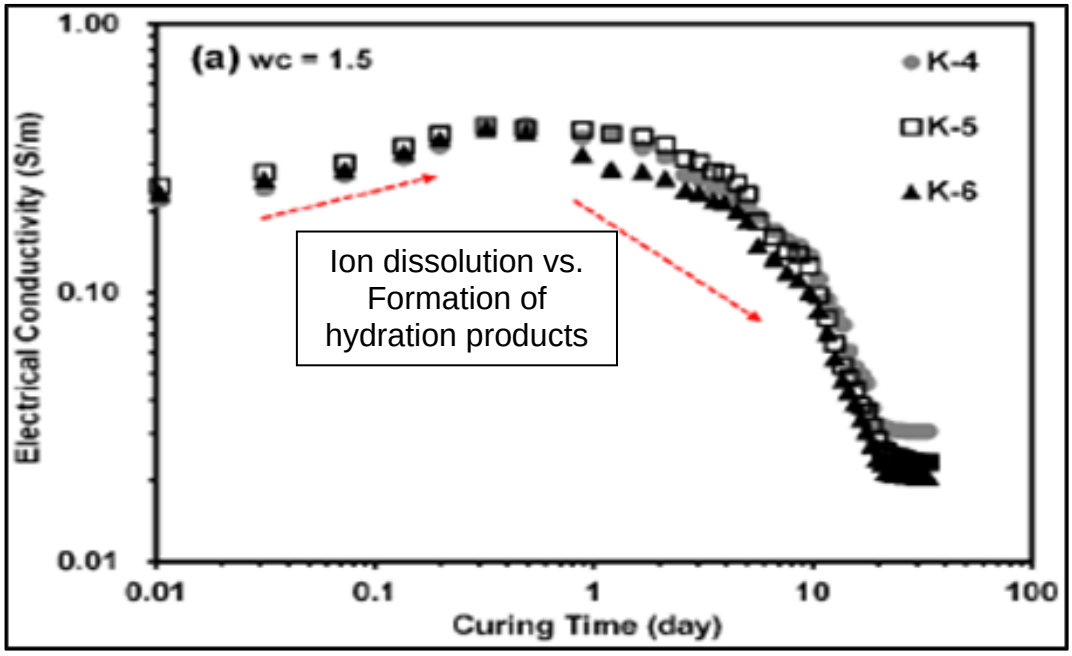


Figure 3.7-15. A plot of electrical conductivity recorded from three-cement grout stabilized sands with a w/c ratio of 1.5 (Choo et al., 2021).

The electrical conductivity versus curing age plot in Figure 3.7-15 shows an initial increase in electrical conductivity driven by increased charged ions in the watery cement grout paste. As the cement grout sands cured further the electrical conductivity started dropping off caused by the formation of hydrates. This plot shows that electrical conductivity measurements are sensitive to and can capture the curing process (microscopical changes) of cement grouts. The UCS test results showed a non-linear UCS increase with curing age at different cement grout w/c ratios. The UCS tests further revealed increased UCS values with decreasing w/c ratios.

The authors attributed this relationship to the availability of more cement grains to create strong bonds of cement-grouted geomaterials. The authors then plotted electrical resistivity against the UCS values of the tested cement sands and fitted a linear equation that describes the UCS and electrical resistivity relationship. Figure 3.7-16 shows the effect of increasing the w/c ratio on the UCS measured on different cement grout stabilized sands.

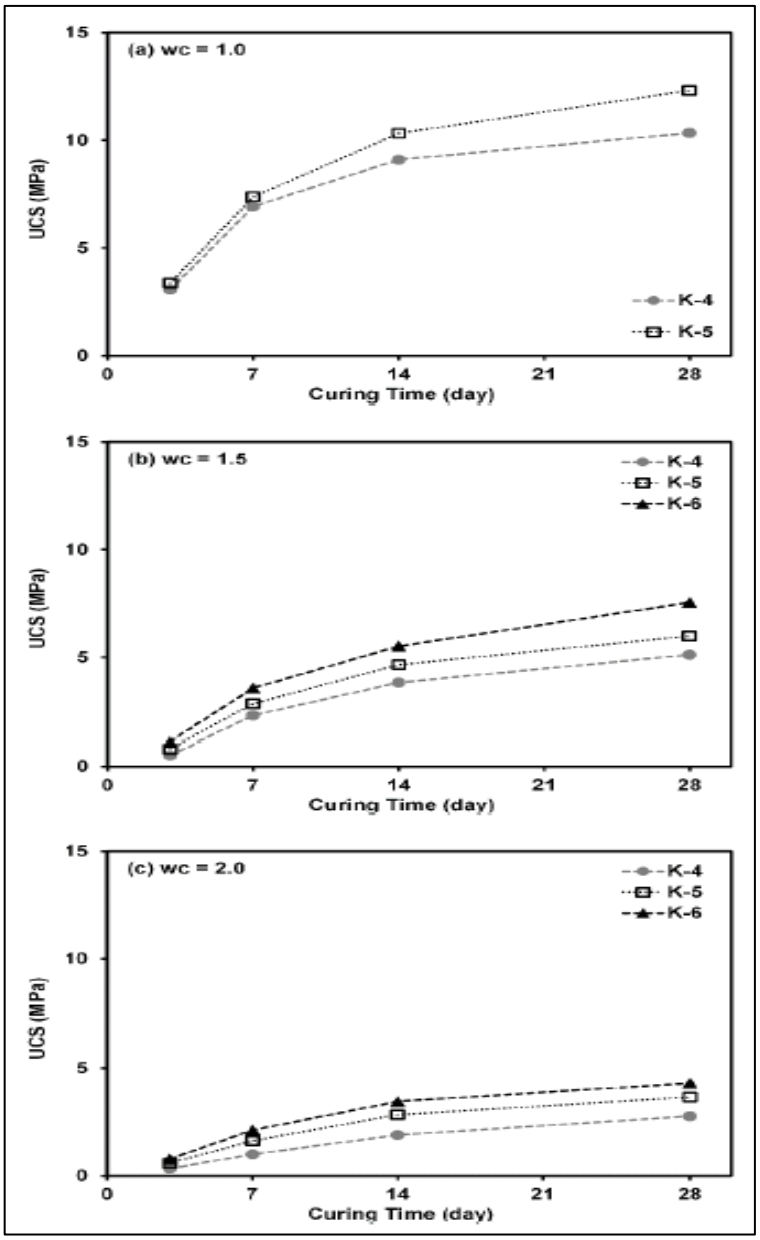


Figure 3.7-16. Plots of UCS versus curing age for different cement stabilized sands mixed at different w/c ratios (Choo et al., 2021).

Figure 3.7-16 demonstrates the non-linearity of UCS values increase over curing time at different w/c ratios. Figure 3.7-17 shows a plot of electrical resistivity versus UCS sorted by cement grout stabilized sands (particle size).

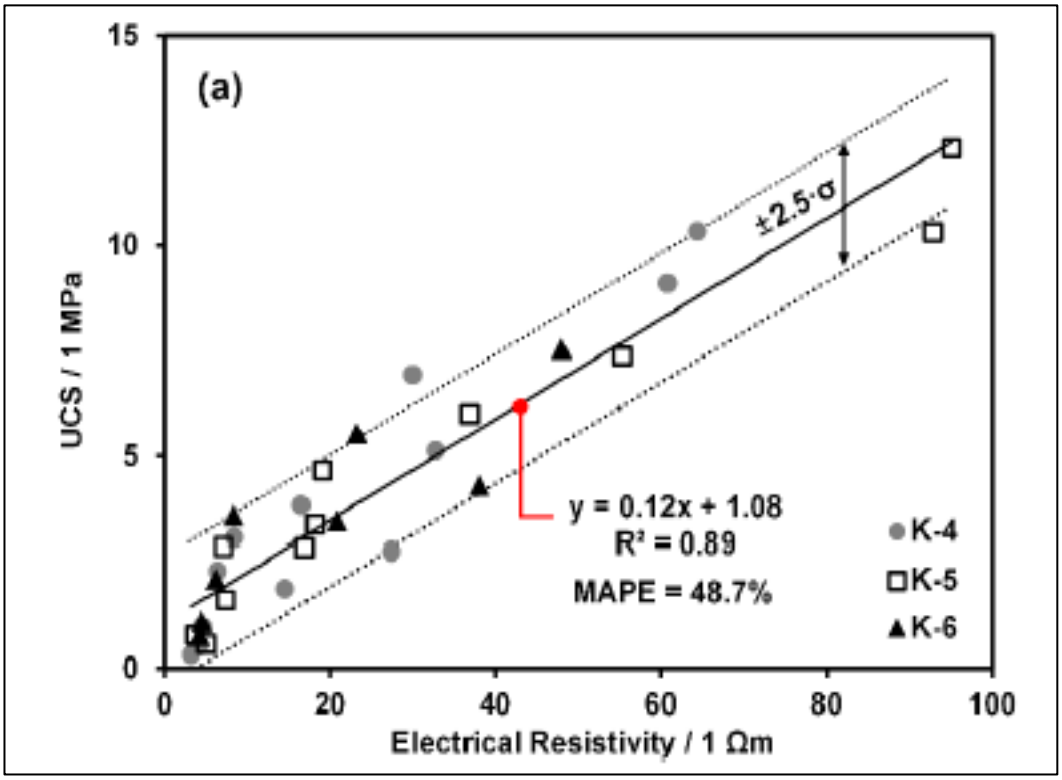


Figure 3.7-17. A plot of electrical resistivity against the UCS of cement grout stabilized sand (Choo et al., 2021).

In Figure 3.7-17, the UCS and electrical resistivity relationship is expressed as a linear equation through linear regression of the UCS-electrical resistivity data (sorted by particle size). A large data scatter (up to 2.5 standard deviations) can be observed in Figure 3.7-17. The authors refined

the UCS-electrical resistivity relationship using an equation by Carino (1984) and Yoon et al (2020). Choo et al (2021) obtained a lower mean absolute percentage error (MAPE) when plotting the estimated and predicted grout UCS from electrical resistivity using this new equation.

This study demonstrated that the cement grout curing process is a complex kinematic interplay between the increase in ionized particles during cement dissolution in water and the formation of hydration compounds over curing time. Furthermore, this study showed through careful data analysis electrical resistivity (or conductivity) measurements can be used to predict grout compressive strength.

3.8 Chapter Summary

The widespread use of cable bolts in the mining and civil engineering industries has been briefly reviewed. It has been highlighted how these reinforcement elements are crucial for the stability of underground and civil excavations, the safety of mining persons and the protection of mining equipment. The cable bolt system was shown to comprise of the cable, grouting media, faceplate, and fastening nut. These components need to work together and share the rock deformation load for effective rock mass support.

The research work presented in this chapter demonstrated the flexibility, cost-effectiveness, and adaptability of cables in reinforcing and stabilizing a wide range of mining excavations. Cable bolts have also been shown to

mobilize the rock's inherent strength more effectively when pre-tensioned (it is recommended to tension to approximately 70 percent of the ultimate tensile strength) after installation into support holes. The need for and importance of full-column grouting of cables for the prevention of anchor corrosion, maintaining good bonding behaviour to the rock mass, as well as enhancing the load transfer mechanism was also discussed. Research work on corroded rock bolts and cables was used to show that these support units can lose their reinforcement capacity and as a consequence can lead to rock falls in underground mines posing a safety threat to mining operations worldwide.

The prevalent use of Portland cement grouts in the mining industry to fully encapsulate cables and rock bolts has also been discussed. It has been shown that Portland cement grouts are used for full-column grouting of cables into support holes for steel corrosion prevention and the enhancement of the load transfer mechanism. This chapter has also discussed the use of admixture to enhance grouts physical, mechanical, and chemical attributes. The w/c of grout has been shown to have a negative correlation to the compressive strength of grout and thus needs to be regulated carefully during grouting operations. This chapter has demonstrated that it is best to use grouts at w/c ratios between 0.35 and 0.40 to optimize the load-carrying capacity of support units as well as ensure flowable grout that can bond well to the rock mass.

The two main methods of pumping grouts into support holes are the breather and grout tube methods. The successful use of these methods has been shown to depend on the use of appropriate drilling practices and the use of appropriate w/c ratio grouts. It has also been noted that grouted cables experience issues during grouting operations. Research work reviewed in this chapter cited grouting problems such as improperly sized borehole annulus and depth, the use of poor-quality grout, as well as the pumping of insufficient grout columns in support holes.

Cementitious grouts undergo shrinkage inside support holes as they cure resulting in a volume change of the cementitious grout mixture. Support holes annuluses are confined spaces, and the shrinkage of cementitious grout can be detrimental to the load-bearing capacity and corrosion protection of support anchors. Constrained shrinkage in tight borehole annular spaces can impact tensile stress on the cement grout mixture possibly leading to the cracking of grout inside the support hole. The complex cement superimposed reactions have been shown to impact further thermal strain on the grout. The reviewed research work has underlain the importance of undertaking grout shrinkage and cracking studies to better understand the corrosion of cables and bolts.

Research work presented in this chapter has shown the importance of relative humidity and curing temperatures on the development of linear shrinkage and the cracking of grout. Other research studies have presented different standards for measuring the length of change in prism-shaped test

specimens. It has also been shown that different curing conditions outlined in different testing standards have a huge influence on shrinkage measurements. Prism-shaped specimens under the ASTM C 157/C 157M testing standard can be used to measure shrinkage by determining the relative length change under carefully controlled curing temperatures and humidity. Studies of autogenous shrinkage are important for engineers to assess how cementitious grouts will perform in support hole installations as the mining fraternity does not generally perform and report grout shrinkage studies. Furthermore, the studies can be used to verify the non-shrink grout claim by most mining and civil engineering manufacturers.

The review of pull-out testing research work has shown how varied experiments, analytical and numerical solutions have been proposed to study the bonding behaviour of cables, the bond strength of the cable–grout–rock mass interfaces, factors controlling the pull-out behaviour of cables and bolts, as well as the corrosion of cables and bolts. Many authors have detailed the preparation of pull-test cylindrical test samples to be evaluated in common and specially built devices and contraptions to simulate underground failure mechanisms. Pull-test results have been reviewed and shown to be useful for refining the support design capacity of cables and bolts as well as double-checking listed cable bolt loads among the many uses of pull-tests.

Research work presented in this chapter has shown the development of a strong cable-to-grout bond in stiff rock masses and in higher compressive

strength grouts as well as in cables or bolts that promote higher frictional resistance to the grout. Other pull test research work has focused on assessing the effects of different embedment lengths, confining pressure, cable and bolt surface profiles, and support hole optimum diameter on the recorded axial resistance of cables and bolts and how this impacts the load transfer mechanism. Research work that sought to quantify the loss of supportive capacity by corroded anchors has also been presented as well, this type of study further outlined the importance of decent quality grouting operations underground.

The load and bond stress distributions along the partially or fully grouted length of the rock anchor have been noted in this chapter to be non-uniform. This is a major drawback of pull-testing as the non-uniformity of load and bond stress distributions does not constitute a good test of the efficiency of the grout to rock anchor bond strength. Research work has also shown that pull-testing load and displacement information is of limited use in assessing the anchor-to-grout bond strength as the strength of this interface is controlled by many variable factors.

The emergence of smart sensor technologies has come about due to the need for non-destructive and long-term monitoring of cables and rock bolts. This chapter discussed smart-sensor methods such as strain gauges, radar and ultrasonic waves, as well as fibre-optic methods. All these techniques are capable of monitoring parameters such as rock bolt and cable exerted axial strain loads, detecting nearby drilling activity, strain values along the

entire length of rock tendon and, the identification of partial or full column grouting.

This chapter also briefly discussed how strain sensors have been cleverly incorporated into cables and rock bolts to measure strains along the full length of a rock tendon during pull-out testing for a more sophisticated characterization of the strength of the rock anchor – grout–rock mass interfaces. Researchers have sought to take full advantage of the internet of things. Smart rock bolts researched in this regard have been shown to record and wirelessly transmit pockets of rock bolt and cable strain data. Other sensor systems are capable of detecting grout cavities and can be incorporated with LED warning lights when excessive rock bolt loads are detected. High-end versions of such systems can be installed with Wi-Fi for data download, although such systems are limited by the bulky sensor equipment and the use of limited battery life power modules.

Ultrasonic methods, using wave excitement devices and sensor recording devices, have been shown to possess the ability to measure embedded lengths of cables and rock bolts and detect locations and lengths of non-grouted areas in support holes. The use of PZT sensor patches has proven to be popular when using ultrasonic wave techniques. The drawbacks of ultrasonic methods include the use of specialized devices, the complex processing of recorded wave signals, and the required specific arrangement of excitement devices and sensors.

FBG sensors have also proven popular with mining and civil engineering researchers as a non-destructive technique for the assessment of rock tendons. These sensors can also be integrated into rock tendons and installed into support holes to record strain data from the roofs and side walls of mining excavations, and temperature and pressure values in support holes. FGB sensors have also been used to record continuous strains for shear stress calculation during rock bolt testing thus providing more diagnostic behavioural information beyond the load and displacement usually reported from in-situ pull-out testing.

FGB sensors can be easily damaged if not covered by a protective casing when used in harsh mining environments. Furthermore, discretely placed fibre-optic strain gauges can leave unmonitored gaps along the length of the rock anchor where locally occurring strain events may go unrecorded. The reviewed techniques cannot perform long-term monitoring with an easy method of data collection and processing under harsh mining conditions. Smart sensor systems also require the use of bulky monitoring tools, have a limited battery, and are prone to incorrect applications in the field. The glaring gap that these smart sensor systems cannot fill currently is the confirmation of the height of grout in a support hole.

The use of electrical resistivity methods were also briefly reviewed. These methods are mainly used in civil engineering applications to monitor the health of concrete and other cement-based materials. Little to no electrical resistivity research has been conducted in underground mines to assess

the integrity of grout in support hole installations. Electrical methods were shown to fall into the surface and internal electrode bulk resistivity methods. The reviewed research work showed that measured electrical resistivities (or conductivity) of cementitious materials are normally plotted against curing age. These plots are characterized by resistivity (or conductivity) decrease and increase driven by the multiple superimposed cement hydration reactions taking place. It has also been shown that the electrical resistivity method is sensitive to and can document the hydration process of cementitious materials over time thus lending itself useful for studying and differentiating between cementitious materials.

Some of the electrical resistivity research work has focused on capturing the effect curing temperatures have on the recorded resistivity values and the setting time of cementitious materials. Other researchers have evaluated how changing the cement w/c ratio impacts recorded resistivities whereas other research work has focused on the prediction of cementitious material compressive strength from electrical resistivity measurements. An informative summary of the common factors that affect electrical resistivity measurements gleaned from the review of electrical resistivity methods in cementitious materials is given in Table 3.8-1. The results of grout sensor technology recordings will be benchmarked against these observations.

Table 3.8-1. Summary of the factors that impact electrical resistivity measurements in cement-based materials.

Factor Affecting Electrical Resistivity	
Curing Temperatures	Early-age resistivity decreases with increased curing temperatures and later increases
Water Content	Resistivity decreases with increased water content
Curing Age	Resistivity initially decreases and then steeply increases with increasing curing age

The research methodology, devised based on the preceding critical review of relevant literature, seeks to address the key research questions and is presented in the next chapter.

4 RESEARCH METHODOLOGY

4.1 Introduction

The literature survey presented in Chapter 3 was used to identify factors that contribute to the ineffective grouting of cable anchor support holes in underground mines. These factors have been used to establish the research methods described in this chapter and are summarized in Table 4.1-1. Each investigation method, conducted in the laboratory and underground, aimed to fully address a critical aspect of fully grouted cable anchor support holes.

Table 4.1-1. Factors contributing to ineffective grouting installations, impact, investigation method, and study site.

Contributing Factor	Impact on Cable Installation	Investigation Method
Grout Invisibility Inside a Support Hole	Unconfirmed grout column; Unmonitored in-support hole loss of grout during pumping or grout shrinkage over time	(1) Grout Sensor Technology
Inconsistent Water-Cement Ratio	Reduced grout to support unit bond strength	(2) Short Encapsulation Pull-Out Testing
Grout Shrinkage	Reduced grout to support unit bond strength and corrosion protection of support unit	(3) Standardized Grout Linear Shrinkage Measurements

Grouts A, B, C and Portland cement were sourced from two different manufacturers to compose the different quality mixtures evaluated in this research report. Grout or cement mixtures are often prepared in large quantities to perform the grouting of as many support holes as possible in one pass. This practice usually occurs in parts of underground mines where rigs capable of both drilling and grouting functions are not readily available.

To make grout or cement mixtures easier to mix in hand pump grout mixers miners often add extra amounts of water. This action is identified as sub-standard grouting practise. Therefore, to capture the sub-standard grouting of support units in underground mines, a good, fair, and bad-quality grout mixture has been prepared for each supplied grout product.

Grout C was supplied along with a specialized pump that enabled the mixing and pumping of workable thick mixes of this particular grout and thus slightly different w/c ratios were used to compose the good, fair, and bad-quality grout C mixtures. Table 4.1-2 presents descriptions of the grout and cement products as well as the w/c ratios used to compose the good, fair, and bad-quality mixtures.

Table 4.1-2. Descriptions and w/c ratio ranges of the grouts and Portland cement mixtures used in this study.

Sample	Description	Water-Cement Ratios
Grout A	Portland cement-based medium-strength grout	0.4 (G) – 0.5 (F) – 0.6 (B)
Grout B	Portland cement-based high-strength grout	0.4 (G) – 0.5 (F) – 0.6 (B)
Grout C	Portland cement-based high-strength grout	0.14 (F) – 0.27 (G) – 0.52 (B)
Portland Cement	High early-strength Portland cement	0.4 (G) – 0.5 (F) – 0.6 (B)
KEY G = Good-quality mixture, F = Fair-quality mixture, B = Bad-quality mixture		

The following sections describe how shrinkage measurements and short encapsulation pull-out testing were conducted as well as how grout sensor technology data was recorded in the laboratory and underground at the study sites.

4.2 Grout Shrinkage

Shrinkage measurements were conducted in the laboratory to quantify the linear change in good, fair, and bad-quality grout samples under controlled temperature and humidity conditions. Shrinkage was measured in grouts A, B, C and Portland cement samples using the ASTM C157 standard test for

a change of length evaluation in cementitious materials outlined in section 3.4 of the literature survey chapter. ASTM C157 is a well-established method for measuring shrinkage in cementitious materials and the results of grout shrinkage are complementary to the verification of the quality and performance of grout. Three shrinkage samples were prepared per grout for a total of 12 samples. These shrinkage test specimens were prepared as good, fair, and bad-quality mixtures for each grout. All mixtures were carefully poured into a three-gang mould to form test prisms with dimensions of 25 x 25 x 285 mm. Each mixture was then levelled off with a chisel and placed into a curing chamber. The curing chamber comprised storage racks with good air circulation and a controlled temperature and humidity environment of 23 degrees Celsius and 50 percent, respectively. Figure 4.2-1 shows the moulding and drying of grout shrinkage prisms in the laboratory.



Figure 4.2-1. A three-gang mould apparatus (left), the casting of shrinkage samples (middle), and the curing of grout shrinkage samples (right).

The test prisms were de-moulded after 24 hours of curing following the mixing and casting process. All test prisms were then immersed in limewater for 30 minutes to reduce the change of length induced by temperature fluctuations during the moulding process. Figure 4.2-2 shows the curing chamber that was used to store shrinkage test prisms.

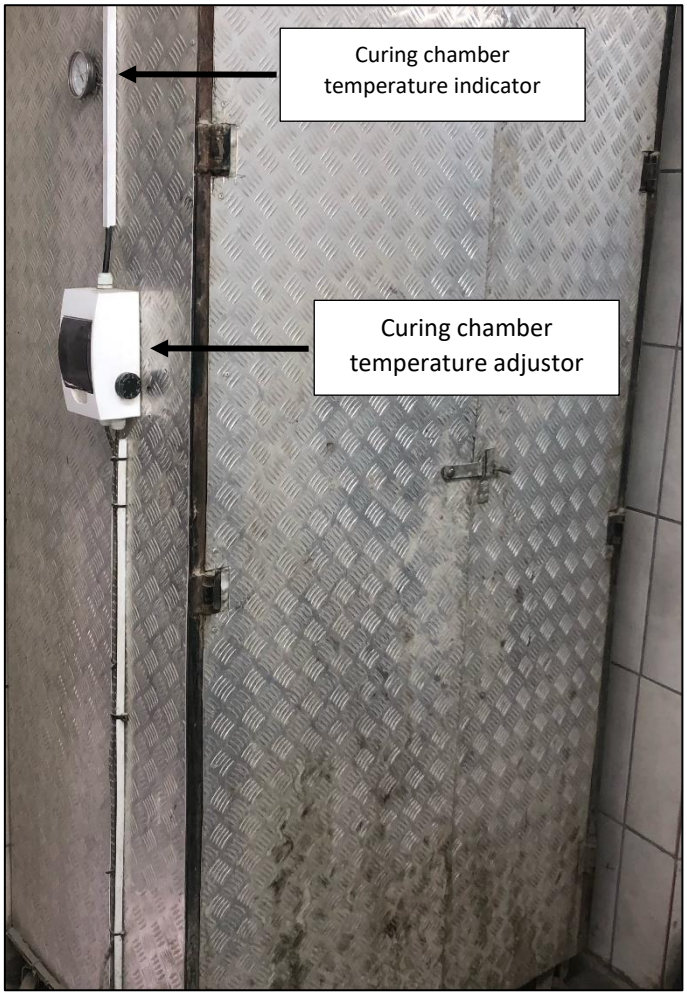


Figure 4.2-2. A temperature and humidity-controlled curing chamber used to cure shrinkage test prisms.

The initial prism length measurements were then taken using a digital length comparator. While taking measurements using the digital length comparator, each test prism was rotated twice to get a consistent change in length measurement. Following these initial measurements, the prism specimens were returned to the curing chamber. The subsequent change of length measurements was then taken after four, seven, 14, and 28 curing days had elapsed as specified by the ASTM C157 standard. The shrinkage measurement results are reported as a graph of linear shrinkage (or expansion) plotted against curing age in days.

4.3 SEPT

The pull-out tests were conducted in the laboratory to quantify the development of the grout-cable anchor interface bond strength over a 35-day curing period for different quality grout mixtures. Short encapsulation pull-out testing also sought to quantify the grout-cable anchor bond strength for good, fair, and bad quality grout mixtures using grout sensor data collected over a similar curing interval.

A single type of an 18 mm diameter, 36 tonnes (t) tensile strength cable anchor was used to conduct pull-out tests. It is assumed that the recorded axial resistances obtained from the pull testing were solely due to the frictional strength of the cable-grout bond developed over the grout-encapsulated sections. Equation 4.3-1 was used to convert the recorded peak axial resistance values into cable-grout bond strength values.

$$Bond\ Strength = \frac{Maximum\ Pull-Out\ Resistance}{\pi\ x\ C_d\ x\ C_l}$$ Equation 4.3-1

Variables C_d and C_l are the cable anchor diameter and embedded length, respectively. The cable anchor diameter and embedment length variables were kept constant such that the bond strength could be expressed as a function of the maximum axial pull-out resistance recorded from different-quality grout mixtures for a single type of cable anchor.

A total of sixty samples were prepared for pull-out testing in the laboratory. These samples were prepared by casting 1.5 m tall cable anchors into 200 mm tall steel cylinders sealed at their bases. Each test sample was prepared by filling up test cylinders with either good, fair, or bad-quality grout and Portland cement mixtures. The cable anchors were kept centred to allow an even grout mixture to be poured around each cable anchor. Then, the pull-out testing samples were stored in a dry curing chamber kept at room temperature. Figure 4.3-1 shows a schematic of the short encapsulation pull-out testing sample.

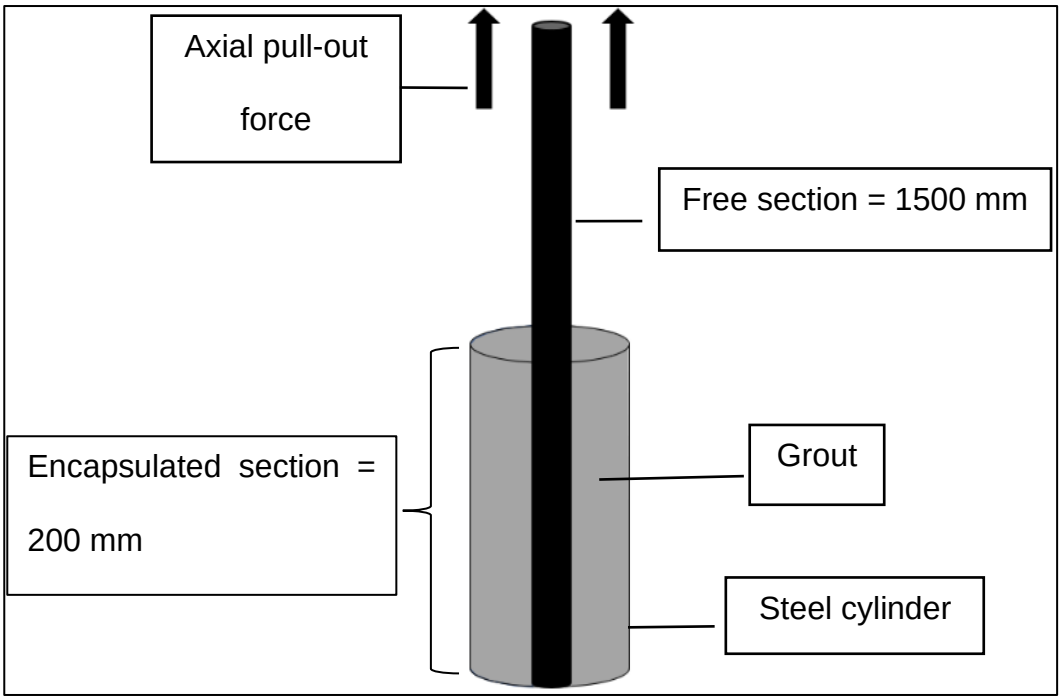


Figure 4.3-1. A schematic of a short-encapsulation pull-out testing sample (not to scale).

It can be observed from Figure 4.3-1 that the cable anchor-free section is 1500 mm in length and the test section is 200 mm in length. Each test cylinder mimics the confinement that rock masses in underground excavations exert around support holes. Figure 4.3-2 shows the preparation of short encapsulation pull-out testing samples in the laboratory.



Figure 4.3-2. Pictures of the SEPT samples prepared in the laboratory.

In the laboratory, a 25-tonne bench was used to conduct axial pull-out tests and record the peak axial resistance information from different quality grout samples. Peak axial resistances were measured through a load cell device and were displayed digitally on the read-out unit. Figure 4.3-3 shows a picture of the 25-tonne pull-out testing bench used in the laboratory.



Figure 4.3-3. A picture of the 25-tonne pull-out testing bench.

4.4 Grout Sensor Technology

Grout sensor technology comprises up to three sacrificial grout sensors, a signal receiver assembly, and a hand-held grout signal citation as well as a grout detector meter (GDT100 meter). These grout sensors are based on the electrical resistivity method and utilize a positive and a negative terminal

to obtain a grout signal. These grout sensors can be easily constructed using cheaply available electrical wiring material that can withstand harsh mining conditions over long periods. This is a major advantage in comparison to the complex sensor solutions presented in the literature survey. The grout sensors are housed in an adjustable-length breather tube which permits the flexible positioning of these sensors inside different-length support holes. Figure 4.4-1 shows a picture of a sample of the novel grout sensor technology comprising grout sensors and a grout signal receiver assembly.

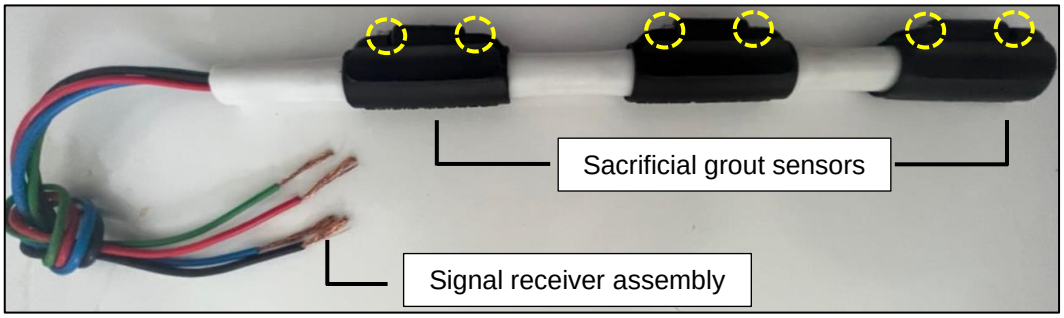


Figure 4.4-1. A sample of the novel grout sensor technology. Yellow circles indicate exposed positive and negative terminals that are used to record grout resistivity signals.

In this research study, a lower, middle and upper grout sensor was installed and positioned at 30 percent, 65 percent, and 95 percent of the support hole lengths used in the laboratory and underground. These grout sensors were used to confirm the full column grouting of all support holes as well as to record and store in memory the resistivity of each different quality column

of grout at three independent points over time. Figure 4.4-2 is a diagrammatical representation of the installation of grout sensor technology.

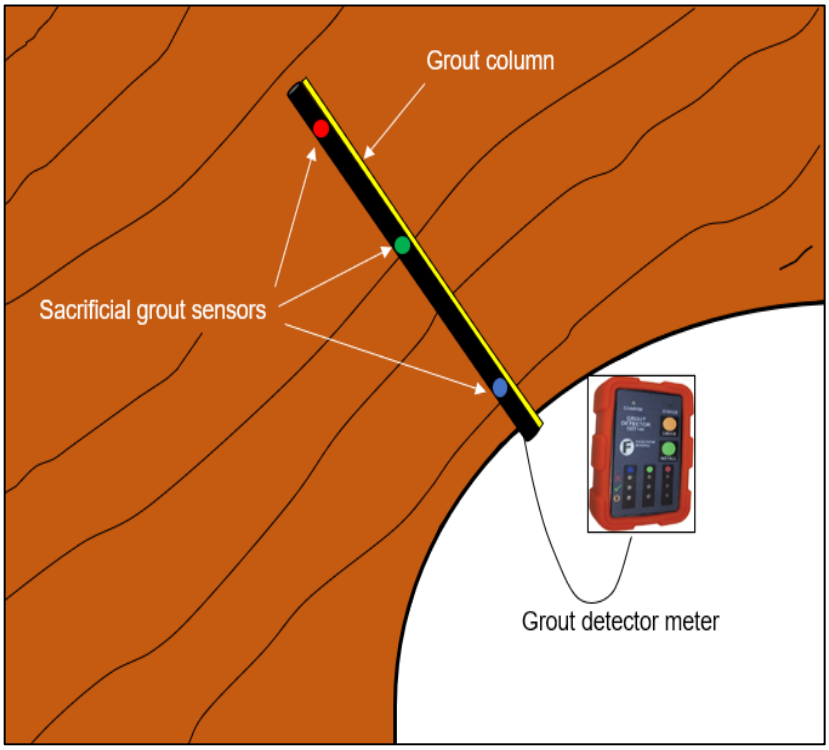


Figure 4.4-2. A diagrammatical representation of the installation of grout sensor technology.

Table 4.4-1 shows the placement (in metres) of the grout sensors in the simulated support holes in the laboratory and in underground experimental support holes. Intuitively, the placement of grout sensors in the 4 m simulated support holes in the laboratory is more akin to the 4.5 m underground support holes. It is important to note that the discrete nature of the sensors along the length of each support hole does leave unmonitored gaps in between the sensors.

Table 4.4-1. The placement of sacrificial grout sensors in different-length support holes.

Sensor Location	Control Support Holes (4 m length)	Experimental Support Holes (1.2 m length)
Lower Sensor (30%)	1.2	0.36
Middle Sensor (65%)	2.6	0.78
Upper Sensor (95%)	3.8	1.14

Figure 4.4-3 shows a picture of the GDT100 meter. The GDT100 meter has a connection point at the bottom that fits the signal receiver assembly from each cable anchor support hole.

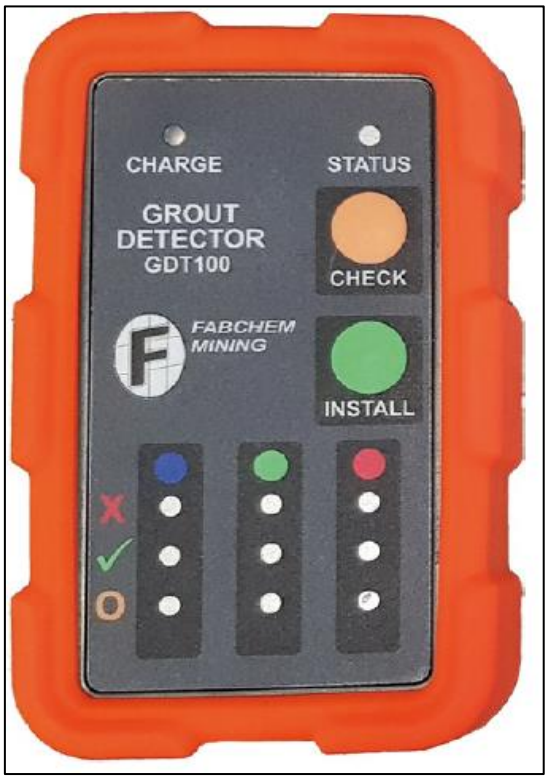


Figure 4.4-3. A picture of the GDT100 grout detector meter (Fabchem Mining Product Brochure, 2022).

It can be seen in Figure 4.4-3 that the GDT100 meter is fitted with Install and Check buttons as well as an array of LED indicator lights that correspond to the lower, middle, and upper sensors (blue, green, and red channels). When using the grout detector meter to take grout readings, the presence of a full column of grout inside the support hole is indicated by flashing green LED lights [√] across all three sensor channels. When there is no grout present in the support hole it is indicated by red flashing LED lights [O] across all three sensor channels. In addition, red-flashing LED lights [X] in one or more of the grout sensor channels indicate a short circuit

in the system. Short-circuiting can be caused by the sensor terminals touching against the support unit or the grout sensor receiver wires coming into contact.

A single press of the Check button allows an operator to check whether all of the grout sensors installed into each support hole are operational before the commencement of the grouting operations. Following this check, the Install button is pressed and the pumping of grout into the support hole can begin. LED lights on the GDT100 meter corresponding to the lower, middle, and upper sensors will light up in sequence as the grout column moves past all these sensors.

During grouting operations conducted in the laboratory and underground, the appearance of a grout resistivity signal from the topmost sensor was taken to indicate 95 percent column grouting. Then, grout was continuously pumped into each support hole until grout appeared at the collar of each support hole in the breather tube housing the grout sensors to ensure the full immersion of the support unit in the grout. All the resistivity values recorded from the different-quality grout mixtures, the time as well as the date stamp when grout resistivity was recorded in each grout sensor position were stored as a comma-separated value (CSV) file by the GDT100 meter. This CSV file was downloaded onto a desktop PC and all the recorded grout resistivity data was organized in a Microsoft Excel spreadsheet.

Grout sensor technology is simple in its design and does not require bulky, complex battery and signal excitation modules. Grout sensor technology, however, in its current form does not permit the continuous recording of grout sensor data from each support hole. Instead, a manual connection must be made for each support hole to register a reading. This is in stark contrast to the laboratory measurements made for civil engineering applications where continuous, long-term resistivity recordings can be made. These specialised recording devices, however, can only be used in the laboratory and not in support holes at underground mines.

The bond strength was described in the literature survey as being non-uniform over the length of each grout column. Thus, the use of three grout sensors forms an opportunity to study the bond strength (using the resistivity of grout) at three independent measuring points. Furthermore, the installation of three sacrificial grout sensors allows for the monitoring of the loss of grout during grouting operations as well as the detection of grout shrinkage over time. Therefore, grout sensor technology allows the reconciliation of the grout shrinkage and short-encapsulation pull-out testing research methodologies to form a unified view of the importance of verifying the quality and performance of grout in support hole installations.

The recording of grout sensor technology data from different quality grout mixtures in the laboratory comprised the control group of the hypotheses proposed in this study. The hypotheses were further evaluated experimentally by recording grout sensor technology data from

underground support holes filled with different quality grout mixtures. The recording of grout sensor data in the laboratory is discussed next.

4.4.1 Laboratory Grout Sensor Data Recording

4 m tall, 43 mm diameter PVC pipes were installed in the laboratory to simulate underground support holes and their lengths. Grout tubes were inserted at the bottom of these pipes to conduct grouting operations using the grout tube method. The top and base of each pipe were plugged to stop the grout mixtures from running out of the pipes. The recording methodology of grout sensor technology in the laboratory is summarized in Table 4.4-2 and shows the number of pipes, testing purposes, and testing intervals.

Table 4.4-2. Laboratory grout sensor technology data recording methodology.

No. of Simulated Support Holes	12
Simulated Support Hole Lengths (m)	4
Laboratory Support Hole Purposes	
Record grout resistivity from different quality grout mixtures under controlled conditions using novel grout sensor technology	
Grout Sensor Data Recording Interval	
Record grout resistivity during grouting operations and every 10 minutes for an hour. Thereafter, record grout resistivity once a week for up to three months for each different-quality grout mixture	

Figure 4.4-4 shows a picture that depicts the set-up of support holes in the laboratory.

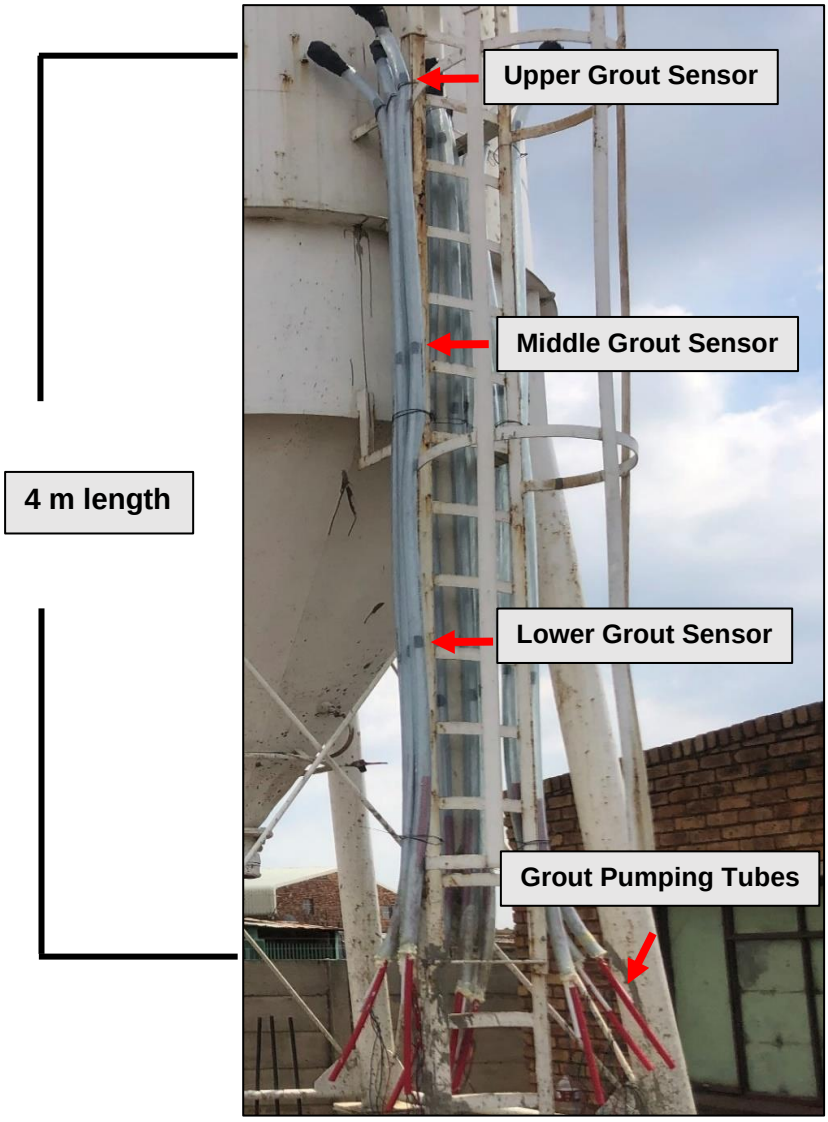


Figure 4.4-4. A picture of the simulated support holes in the laboratory showing grout tubes and grout sensor positioning.

It can be seen in Figure 4.4-4 that the sacrificial grout sensors show up as black dots in each of the clear PVC pipes. The simulated support holes used

in the laboratory represented the idealised full-column grouting of underground support holes with a visible full-column of grout. However, rock masses that are commonly encountered underground have fractures where grout can be lost during pumping. Thus, to complete the testing of the hypothesis proposed in this research report, underground experiments were conducted at the South Deep mine study site. The recording of underground grout sensor technology data is discussed next.

4.4.2 Underground Grout Sensor Data Recording

Figure 4.4-5 shows a locality map of the underground testing site at the South Deep gold mine.

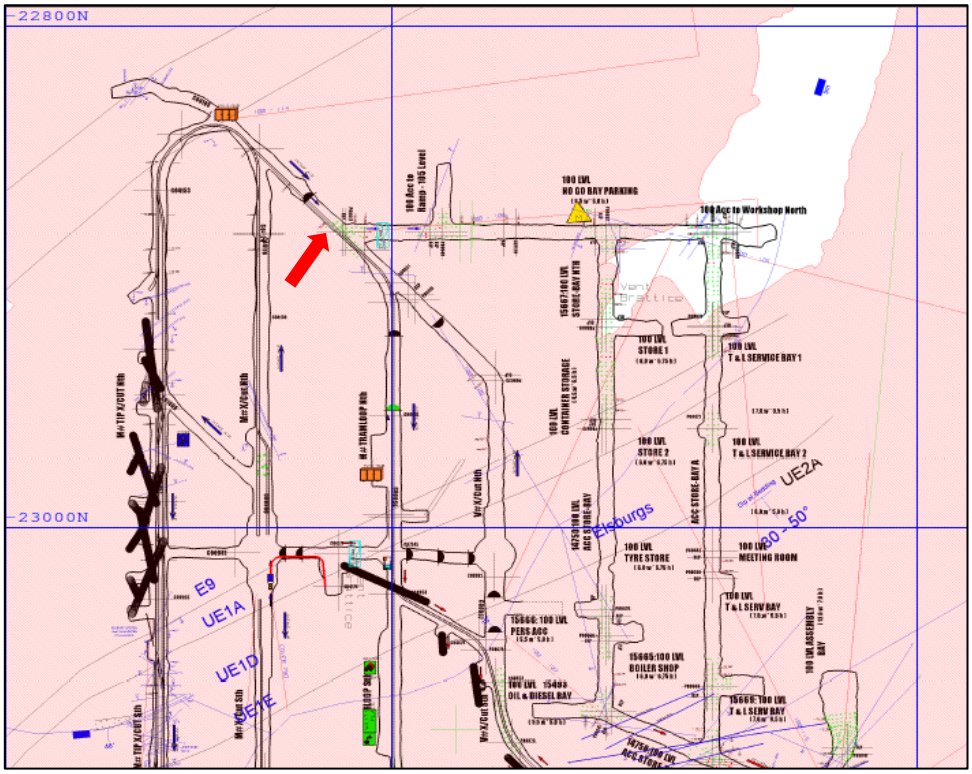


Figure 4.4-5. A mine map of the testing site (red arrow) at South Deep.

The test site was located in a 5 m tall, 6 m wide service tunnel at a depth of 2733 m below ground. The main rock formation encountered at the test site was a brittle and generally fractured Witwatersrand quartzite and thus it was expected some grout would be lost into near-borehole fractures during grouting. The number of support holes drilled underground, their purposes, and recording intervals are summarized in Table 4.4-3.

Table 4.4-3. Underground grout sensor technology data recording.

No. of Simulated Support Holes	24
Simulated Support Hole Lengths (m)	1.2 and 4.5
Experimental Support Hole Purposes	
Experimental evaluation of the recording of resistivity from different quality grout mixtures in different length support holes using novel grout sensor technology	
Grout Sensor Data Recording Interval	
Record grout resistivity during grouting operations and every 10 minutes for an hour. Thereafter, record grout resistivity once a week for up to three months for each different-quality mixture	

A total of 24 support holes were drilled using a percussion drill into the sidewall of the tunnel at the test locality; each support hole was cleaned of all drilling rock fragments in preparation for the installation of support anchors. 12 of these support holes were fitted with 1.5 m cable anchors and

grout sensor tubes; another 12 support holes were fitted with 4.8 m long cable anchors and grout sensor tubes. These 24 support holes were then each full-column grouted with different quality grout mixtures.

The placement of grout sensors in breather tubes facilitated the grouting of the support holes via the breather tube method. The breather tube method allows the withdrawal of air bubbles (which form voids in the grout) during the pumping of grout into each support hole. This action ensured that each different grout mixture's quality was unaffected during grout installation. Figure 4.4-6 is a diagrammatical illustration of the 1.2 and 4.5 m long underground test holes equipped with grout sensors.

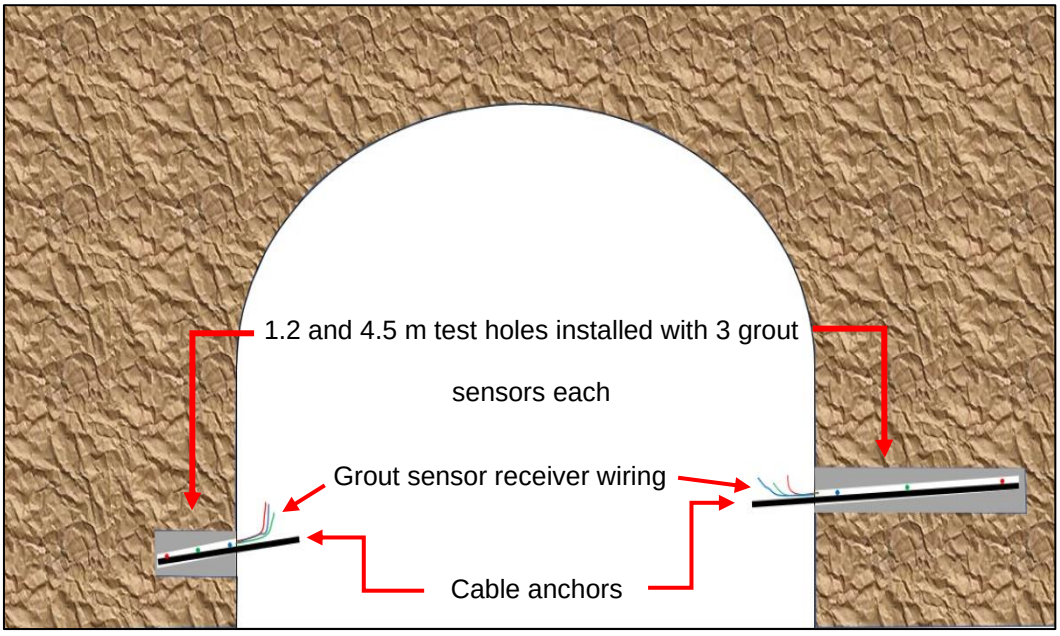


Figure 4.4-6. Diagram of the underground 1.2 m and 4.5 m support test holes.

Grout sensor resistivity from each support hole was recorded for one full hour at ten-minute intervals using the GDT100 meter. Thereafter, weekly grout sensor readings were taken for a total recording time of three months. Figure 4.4-7 shows the installation of grout sensor technology at the underground testing site.

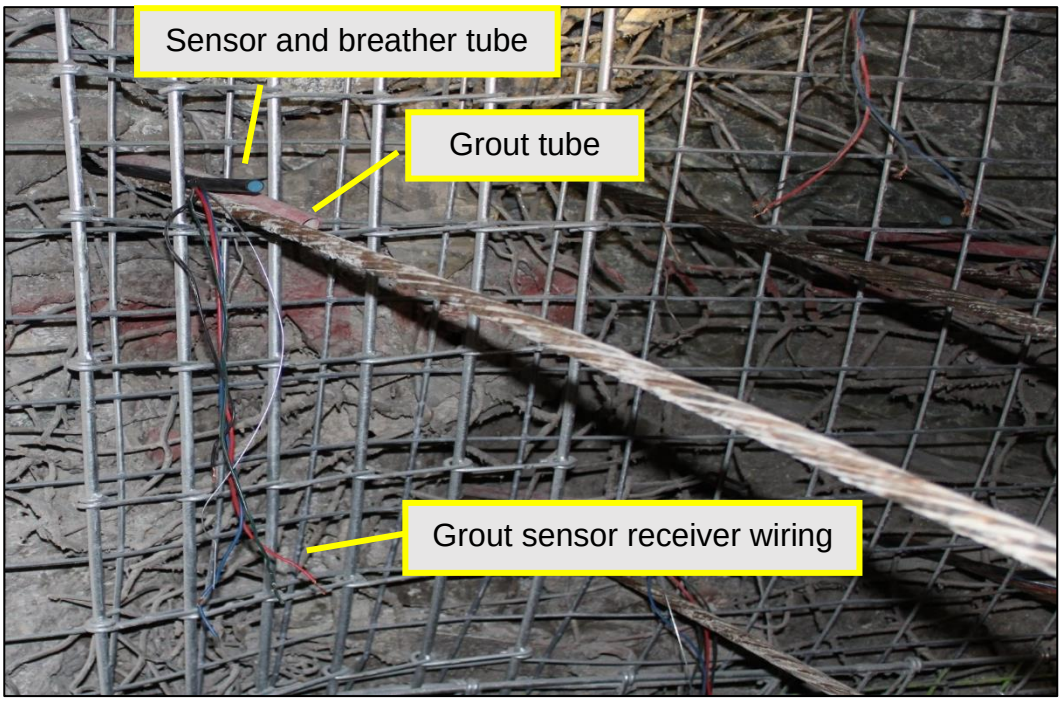


Figure 4.4-7. A picture showing grout sensor technology installations at the South Deep gold mine.

In Figure 4.4-7, the grout sensor (black tube) and grout tubes (red tube) can be observed as well as the grout sensor receiver assemblies at the collar of each support hole. During grouting operations, similar to those conducted

in the laboratory, the GDT100 meter LED lights illuminated in a sequence indicating the movement of the column of grout past all sensors in each of the test support holes. When the GDT100 meter indicated that the grout column had reached the top sensor, grout was continuously pumped into each support hole until it appeared at the collar of each support hole in the cable housing the grout sensors. The continuous pumping of the grout procedure was used to ensure the full immersion of the cable anchor in the grout. Figure 4.4-8 shows pictures of the GDT100 meter in use during underground grouting operations.



Figure 4.4-8. Pictures of the GDT100 meter in use during underground grouting operations.

In the left-hand-hand side picture of Figure 4.4-8, all three GDT100 meter LED lights are illuminated in red indicating there is no grout in the support hole before the pumping of grout could be initiated. The right-hand side picture shows that the column of the grout had moved past the lower and middle sensors during underground grouting operations. All the underground support holes were successfully full-column grouted and using all three-grout sensor positions the grouted column could be confirmed during, and immediately following the end of grouting operations as well as over time.

This is in stark contrast to common practices where a miner only needs to fold and bend the grout tube at the end of grouting operations to indicate they have fully grouted the support hole. Routine underground visits by strata control officers rely on visually observing these bent grout tubes as an indication of full-column grouting. The use of novel grout sensor technology evaluated in this research report aims to eliminate these ineffective visual confirmation of the full grouting of ground support units at South Deep and other underground mines.

The research methodologies used to conduct grout shrinkage measurements, short encapsulation pull-out tests, and record grout sensor data have been presented in this chapter. The results of all measurements based on the research methodology are presented to critically address the key research questions posed in this research report.

5 RESULTS AND DISCUSSION

5.1 Introduction

The results of the grout shrinkage measurements (laboratory), short encapsulation pull-out testing (laboratory) and grout resistivity recordings (laboratory and underground) are presented in this chapter. The appendix contains the full-suite of grout sensor data recorded in the laboratory as well as underground.

5.2 Grout Shrinkage

The grout shrinkage measurements conducted in the laboratory sought to quantify the amount of shrinkage that occurs in different quality grout mixtures under controlled temperature and humidity conditions. The results of the grout shrinkage measurements are reported in this research report as linear changes (in percent) of length in good, fair, and bad-quality grout samples. Table 5.2-1 shows the results of the grout shrinkage measurements.

Table 5.2-1. A table showing measured grout linear shrinkage and expansion values in cm. Naming convention = shrinkage/sample name.

Linear length measurements (cm)		Initial (24 hours)	Day 4	Day 7	Day 14	Day 28
Sample name	SH/A04	15.389	15.548	15.303	15.205	15.188
	SH/A05	15.532	15.601	15.351	15.093	14.990
	SH/A06	15.442	14.789	14.583	14.112	14.023
	SH/B04	15.486	15.980	15.476	15.240	14.620
	SH/B05	15.694	15.810	15.264	14.724	14.238
	SH/B06	15.496	14.826	14.604	14.232	13.791
	SH/CE04	15.284	14.716	14.698	14.688	13.674
	SH/CE05	15.256	14.556	14.104	13.860	13.504
	SH/CE06	15.396	14.100	13.786	13.590	13.542
	SH/C14	14.078	14.392	14.606	15.857	16.124
	SH/C27	14.906	15.488	14.248	13.753	13.656
	SH/C54	15.436	14.728	13.780	14.037	14.221

Figure 5.2-1 is a plot of the linear change of length in different quality grout samples composed from grouts A and B over 28 curing days.

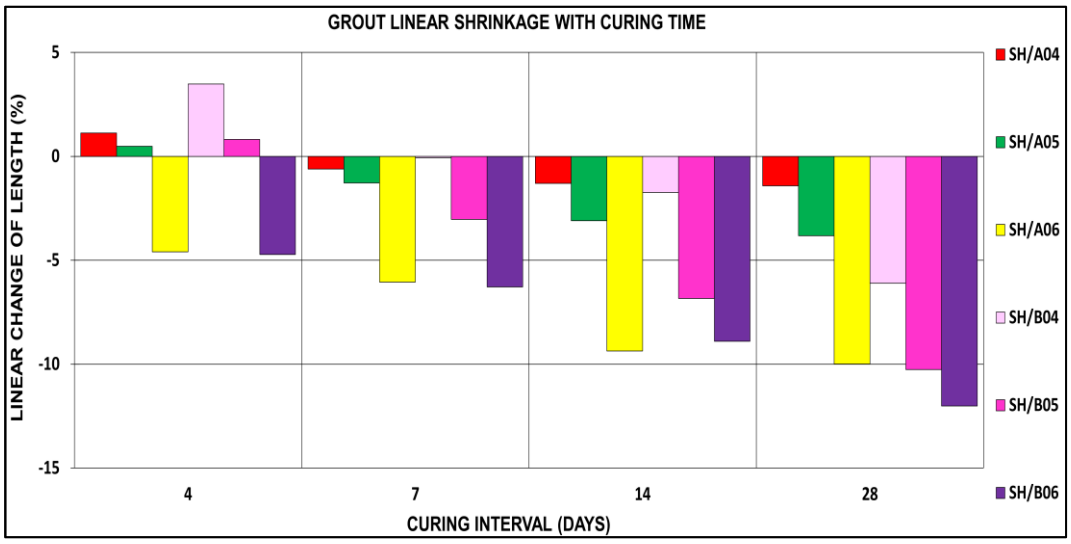


Figure 5.2-1. A plot of the linear change of length in grouts A and B samples.

Bad-quality grout samples from grouts A and B shrink over the first four curing days as shown in Figure 5.2-1. In contrast, grouts A and B good and fair-quality samples expand over the first four curing days. Thereafter, grouts A and B good, fair, and bad-quality samples show increasing shrinkage with increasing curing age. Moreover, it can be noticed that there is an increasing amount of shrinkage taking place in grouts A and B samples when the quality of the grout mixture is decreased (increasing w/c ratio). Figure 5.2-2 is a plot of the linear change of length in different quality grout samples composed from grout C and Portland cement over 28 curing days.

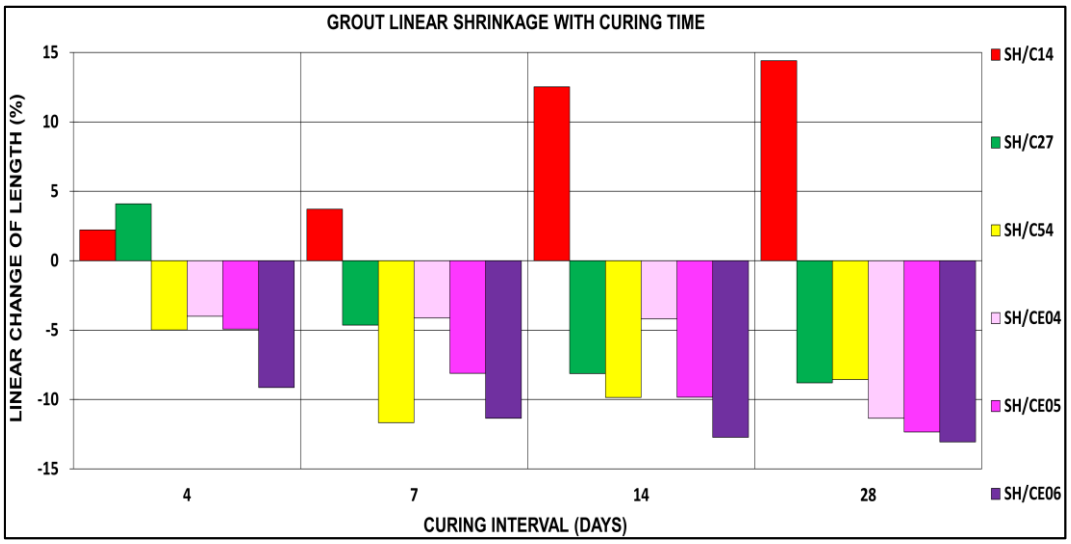


Figure 5.2-2. A plot of the linear change of length in grout C and Portland cement samples.

It can be observed in Figure 5.2-2 that the good and fair quality grout samples composed from grout C undergo expansion over the first four curing days. Thereafter, all grout C samples undergo increasing shrinkage with increasing curing age bar the fair-quality grout sample (SH/C14) which undergoes increasing expansion with increasing curing age. In contrast, the good, fair, and bad-quality grout samples from the Portland cement show increasing shrinkage over the entire curing period.

Similar to grouts A and B, the increase in shrinkage in grout C and Portland cement can be correlated to an increase in the w/c ratio of the grout mixture. Table 5.2-2 shows the reduction of grout columns in 4 m, 1.2 m and 4.5 m support holes using the maximum shrinkage/expansion values shown in

Figures 5.2-1 and 5.2-2. It is assumed that the column of grout inside the support hole shrinks linearly at one end of the support hole. Where grout expansion occurs a full column of grout is assumed to be retained in the support hole.

It can be observed from Table 5.2-2 that the shrinkage values measured in different quality grout samples would result in a significant reduction of the columns of grout inside support holes of different lengths. This is especially true where Portland cement is used during grouting operations.

It is also important to note that under increased temperature and humidity conditions that are typically encountered at the South Deep mine the different quality grout mixtures can be expected to undergo expansion as outlined in section 3.4 of the literature survey. Grout linear shrinkage is not desirable as it results in the exposure of the support unit to potentially corrosive groundwater.

Table 5.2-2. Lengths of grout columns after 28 curing days in different length support holes. Green shading = no shrinkage, red shading = maximum shrinkage, and asterisk (*) = net expansion.

Sample Name	Maximum Shrinkage	4 m hole	1.2 m hole	4.5 m hole
SH/A04	1.40%	3.943 m	1.183 m	4.436 m
SH/A05	3.80%	3.847 m	1.154 m	4.328 m
SH/A06	10.00%	3.600 m	1.080 m	4.050 m
SH/B04	6.10%	3.756 m	1.127 m	4.225 m
SH/B05	10.30%	3.590 m	1.077 m	4.038 m
SH/B06	12.00%	3.520 m	1.056 m	3.960 m
SH/CE04	11.30%	3.546 m	1.064 m	3.990 m
SH/CE05	12.30%	3.506 m	1.052 m	3.945 m
SH/CE06	13.10%	3.478 m	1.043 m	3.912 m
SH/C14	*14.40%	4.000 m	1.200 m	4.500 m
SH/C27	8.80%	3.648 m	1.094 m	4.104 m
SH/C54	8.60%	3.658 m	1.097 m	4.115 m

Grout expansion, as noted in the fair-quality grout C sample (SH/C14), is not desirable either as it may lead to the cracking of the installed grout column during expansion against the stiffer surrounding rock mass. A cracked column of grout, similar to a shrunken grout column, can provide pathways for groundwater to reach the installed support unit. Over time, corroded anchors can lose their supportive capacity potentially leading to undesirable falls of ground thus posing a safety risk underground.

5.2.1 Grout shrinkage summary

It can be summarized that, over a 28-day curing period under controlled temperature and humidity conditions, different quality grout prism composed from grouts A, B, C and Portland cement will typically shrink and expand in length by up to 13 percent. The results of shrinkage measurements also show that low-quality grout and Portland cement samples undergo the highest reduction in length due to shrinkage. Thus, the w/c ratio is an important consideration when preparing grout mixture for use in support holes underground to protect support units from corrosion. Moreover, the results of shrinkage measurements also show that standardized testing methods are useful as differentiators of grout quality and can be used to compare different cementitious grouts.

5.3 SEPT

The short encapsulation pull-out tests sought to quantify the development of the grout-cable anchor interface bond strength over a 35-day curing period in different quality grout mixtures. The results of the short encapsulation pull-out tests are reported in this research report as a plot of the bond strength values against curing age. Curing age intervals of one, seven, 14, 28, and 35 days are used in each of the bond strength versus curing age plots. The main mechanism of failure observed during the short encapsulation pull-out tests was the failure of the grout-cable anchor interface in all test samples irrespective of grout mixture quality. Figure 5.3-1 shows pictures of the failure of the grout column during pull-out testing conducted in the laboratory.

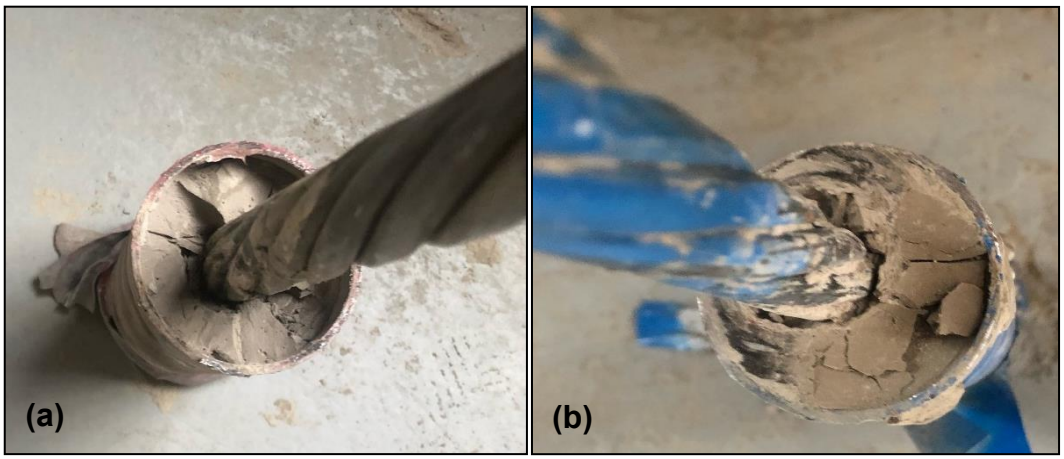


Figure 5.3-1. Pictures showing the failure of the grout column during short encapsulation pull-out testing of grout test samples, (a) Grout B fair-quality mixture sample, and (b) Grout A good-quality mixture sample.

It can be noticed in Figure 5.3-1 that the failed grout-cable anchor interface shows radially propagated cracks. The grout-cable anchor interface in each test sample was fully split similar to what was described in section 3.5 of the literature survey. It is thought that the grout cracks formed during the dilation of the grout-cable anchor interface as an axial-loading force was continually applied. The grout-cable anchor interface has a lower strength and thus failed first before the failure of the grout-to-steel cylinder interface or before the tensile failure of each 36t cable anchor. It is important to note that combined loading conditions (axial, shear, axial and shear, and compression) are more commonly encountered in underground mines. Thus, the failure mode is likely to change from what is observed in these laboratory pull-out tests.

Table 5.3-1 shows the bond strength values of grouts A, B and C as well as Portland cement plotted over the first curing day. It can be noticed in Table 5.3-1 that the different-quality grout samples evaluated in this study have low bond strengths in the first 24 hours of installation (less than 1.4 MPa). Based on section 3.5 of the literature survey, it is thought that these low bond strengths are not uniformly distributed and likely to be lower or higher along the length of the 200 mm tall test cylinders. The low bond strength values are such that the grout-cable anchor interface is unlikely to exert enough frictional resistance to arrest any rock mass movement that occurs near the supported area unless the density of support is increased drastically. Further, if mining activities are conducted over the first grout curing day the associated stress changes could further lower the bond strength in support holes installed in working areas thus putting the safety of miners at serious risk.

Table 5.3-1. Grouts A, B, C and Portland cement cable anchor to grout bond strength on the first curing day.

Sample Name	Bond Strength (MPa)
BS/A04	0.20
BS/A05	0.13
BS/A06	0.01
BS/B04	0.42
BS/B05	0.18
BS/B06	0.03
BS/C27	1.38
BS/C14	0.53
BS/C54	0.46
BS/CE04	0.11
BS/CE05	0.03
BS/CE06	0.02

The bond strengths obtained over a 200 mm grout encapsulated length over the first curing day have been upscaled to reflect bond strength values that would be obtained in 1.2 and 4.5 m long support holes. Table 5.3-2 shows the values of cable anchor to grout bond strength calculated for different quality mixtures composed from grouts A, B, and C as well as Portland cement over the first curing day. Table 5.3-2 shows that at long encapsulation lengths, the fair and bad-quality Portland cement as well as bad-quality grouts A and B mixtures would retain low bond strengths. In contrast, the good-quality Portland cement as well as fair and good-quality grouts A and B mixtures would attain reasonable bond strength values. In addition, it can be noticed that grout C bond strength values are anomalous over the entire curing interval.

Table 5.3-2. Bond strengths for the first curing day in different length support holes.

Grout Name	Sample Name	Bond Strength (MPa)		
		200 mm	1.2 m	4.5 m
Grout A	BS/A04	0.20	1.20	4.49
	BS/A05	0.13	0.78	2.93
	BS/A06	0.01	0.07	0.27
Grout B	BS/B04	0.42	2.55	9.56
	BS/B05	0.18	1.09	4.10
	BS/B06	0.03	0.18	0.68
Grout C	BS/C27	0.53	3.17	11.90
	BS/C14	1.38	8.27	31.02
	BS/C54	0.46	2.76	10.34
Portland Cement	BS/CE04	0.11	0.65	2.44
	BS/CE05	0.03	0.16	0.59
	BS/CE06	0.02	0.13	0.49

The upscaling of bond strength values is not as straightforward as indicated above. A brittle and fractured rock mass buried at depth is likely to offer a different type of radial confinement which affects the peak bond strength of the grout-cable anchor interface. Nonetheless, it is informative to illustrate how these low bond strength values could manifest themselves at long encapsulation lengths. Figure 5.3-2 shows the seven to 35 curing day cable anchor to grout bond strength values calculated for different quality mixtures composed from grouts A and B.

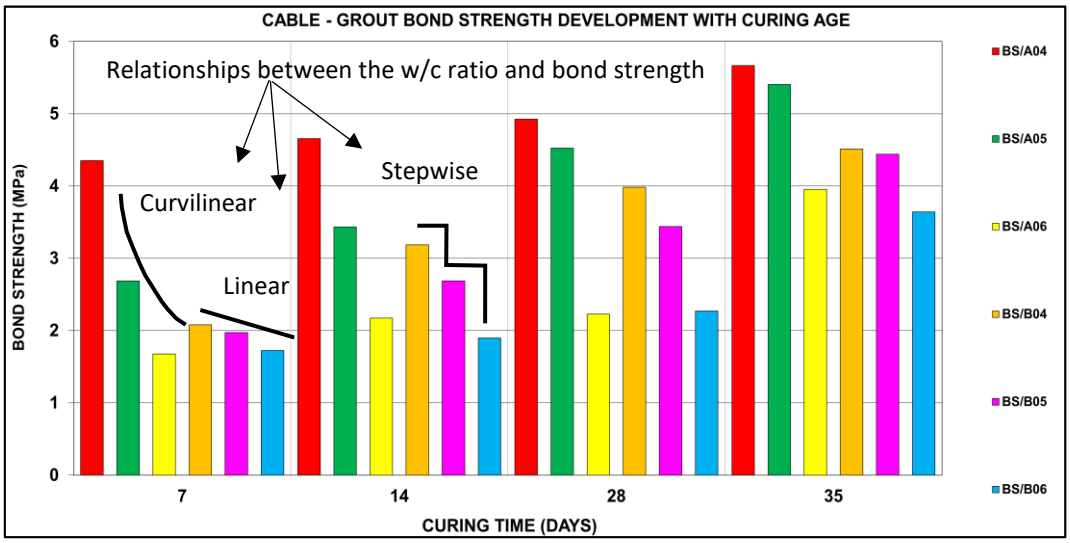


Figure 5.3-2. A plot of the cable anchor to grout bond strengths for grouts A and B with different w/c ratios. Curvilinear, linear and stepwise relationships between the w/c and bond strength are indicated.

It can be observed from Figure 5.3-2 that grouts A and B bond strength values decrease with an increasing w/c ratio (decreasing grout quality). A

combination of step-wise decrease, linear, and curvilinear lines can be drawn through the bond strength values from grouts A and B good, fair, and bad-quality mixtures. It can also be observed that the curvilinear grout to cable bond strength – grout w/c ratio relationship yields a drastic reduction of the cable-grout bond strength when the grout w/c ratio is increased slightly. Thus, over curing time there exist both small and large differences in bond strengths of good, fair, and bad-quality grout mixtures depending on the quality of the grout. Figure 5.3-3 shows the seven to 35 curing day cable anchor to grout bond strength values calculated for good, fair, and bad-quality mixtures composed from grout C and Portland cement.

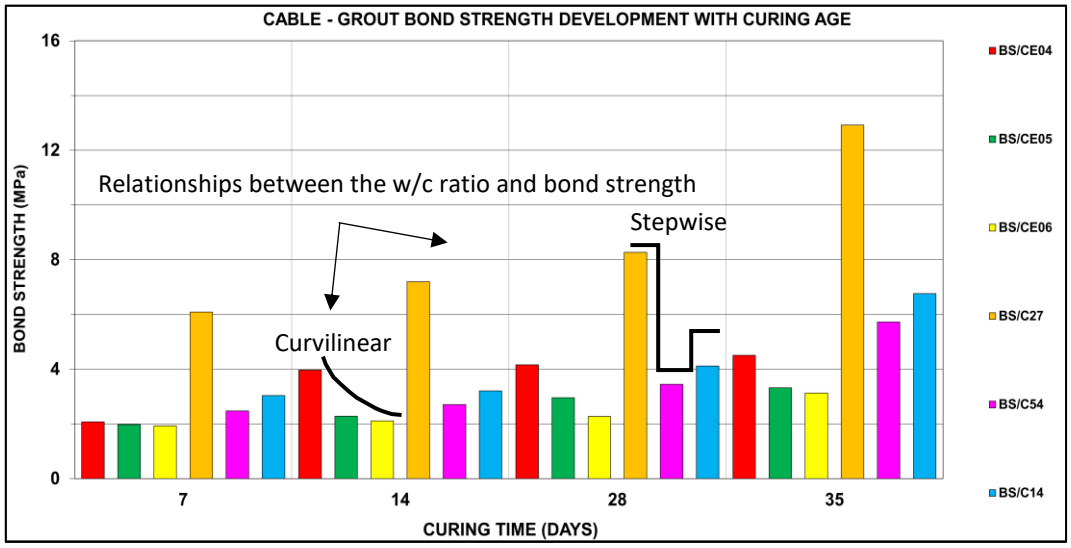


Figure 5.3-3. A plot of the cable anchor to grout bond strengths for grout C and Portland cement with different w/c ratios. Curvilinear and stepwise relationships between the w/c and bond strength are indicated.

It can be noticed from Figure 5.3-3 that the bond strength values of the good-quality mixture from grout C (BS/C27) are anomalous (50 percent larger than the highest bond strength value at any curing age) in comparison to the rest of the bond strength values. Between 14 and 35 days curing there exists a stepwise decrease-increase and a curvilinear bond strength to grout quality relationship in grout C and Portland cement, respectively. These relationships result in both subtle and dramatic differences in bond strength values of good, fair, and bad-quality grout mixtures.

It is common practice in the engineering fraternity to report grout/cement bond strength and curing characteristics at 28 days. Inherent in the use of 28-day reporting is the assumption that grouts and types of cement have a minimal gain in bond strength after 28 curing days. To test this assumption, the percentage gain in the bond strength of different quality grout mixtures has been tabled for grouts A, B, C and Portland Cement between one- and 35-days curing. It is assumed the 35-day bond strength values represent the ultimate bond strength.

Table 5.3-3 shows the gain in bond strength over each curing interval of up to 35 days in different quality grout mixtures. It can be noticed in Table 5.3-3 that the good, fair, and bad-quality grout mixtures gain between one to 10 percent in bond strength over the first curing day. At the end of 28 curing days, the different quality grout mixtures gain between 57 to 92 percent of their bond strength depending on the type of grout and its mixture quality. Additionally, Table 5.3-3 shows that the good-quality grout mixtures have

higher gains in bond strength over any curing interval and that after 28 days good-quality grout mixtures gain less than 13 percent bond strength (bar all grout C mixture BS/C27). In contrast, fair and bad-quality grout mixtures gain up to 44 percent in bond strength post 28 curing days. The significant post 28-day gain in bond strength in these bad-quality grout samples is attributed to the extra amount of water in these mixtures and thus a longer curing time is required for the hydration process to be completed.

Table 5.3-3. The gain in bond strength by different quality grout mixtures over curing intervals as a percentage of the 35-day bond strength.

Grout Mixture Name and Quality	Curing Interval (Days)				
	1	7	14	28	35
BS/A04	3.5%	76.8%	82.2%	86.9%	13.1%
BS/A05	2.4%	49.7%	63.5%	83.7%	16.3%
BS/A06	0.3%	42.4%	54.9%	56.4%	43.6%
BS/B04	9.4%	46.1%	70.6%	88.3%	11.7%
BS/B05	4.1%	44.4%	60.5%	77.5%	22.5%
BS/B06	0.8%	47.4%	52.1%	62.4%	37.6%
BS/C27	10.7%	47.1%	60.9%	64.0%	36.0%
BS/C14	7.8%	44.9%	47.4%	60.9%	39.1%
BS/C54	8.0%	43.2%	47.3%	60.3%	39.7%
BS/CE04	2.4%	46.0%	87.9%	92.3%	7.7%
BS/CE05	0.8%	59.5%	68.8%	89.2%	10.8%
BS/CE06	0.7%	61.6%	67.5%	72.7%	27.3%

It is thus apparent that badly-mixed (high w/c ratios) grout and Portland cement mixtures (A06, B06, C54, & CE06) will require longer curing times

to fully gain their strengths. The percentage gain bond strength table shows that grouts or Portland cement attain gain their full strength approximately between 28 and 35 curing days. This curing period can be used as a guide for civil and mining applications.

5.3.1 SEPT Summary

The axial loading of short-length cable anchors embedded in different w/c grout samples results in the failure of the grout-cable anchor interface irrespective of the w/c ratio used to mix each grout. Short encapsulation pull-out tests also showed that the bond strengths of good, fair, and bad-quality grout mixtures have a varied (curvilinear, linear, and stepwise) relationship to the w/c ratio. In addition, fair and bad-quality grout mixtures (high w/c ratio) have reduced bond strengths that would result in reduced frictional resistances to arrest rock mass movements in supported areas under axial loading conditions, especially over the first curing day. Furthermore, the analysis of the bond strength gain after 28 curing days showed that it is more appropriate to report bond strength values up to 35 curing days instead of 28 days.

5.4 Grout Sensor Technology

The results and discussion of the grout sensor technology recordings are presented in the following subsections that seek to critically address the key research questions posed in this research report. In the analyses of grout quality, the setting of grout and the effectiveness of grout, a variety of grout resistivity versus curing age are presented. In addition, grout resistivity

summary tables and diagrams are also presented in an attempt to answer each of the three main research questions posed in this research report. Table 5.4.1 outlines the naming convention to present the results of the grout sensor data analysis.

Table 5.4-1. Grout recordings sample naming convention (recording location/sample name/support hole length).

Grout Name	Laboratory Recordings	Underground Recordings	
A	L/A04/40	U/A04/12	U/A04/45
	L/A05/40	U/A05/12	U/A05/45
	L/A06/40	U/A06/12	U/A06/45
B	L/B04/40	U/B04/12	U/B04/45
	L/B05/40	U/B05/12	U/B05/45
	L/B06/40	U/B06/12	U/B06/45
C	L/C14/40	U/C14/12	U/C14/45
	L/C27/40	U/C27/12	U/C27/45
	L/C54/40	U/C54/12	U/C54/45
Portland Cement	L/CE04/40	U/CE04/12	U/CE04/45
	L/CE05/40	U/CE05/12	U/CE05/45
	L/CE06/40	U/CE06/12	U/CE06/45

5.4.1 Grout quality

The grout resistivity values recorded from grout A, B, C and Portland cement over a 12 weeks observation period are presented here. To ensure clarity of each of the grout resistivity-curing age plots, only the bi-weekly data is shown. The grout resistivity trends noted in this bi-weekly data are representative of the 12-week observation period dataset. It was found that good, fair, and bad-quality grout mixtures have different resistivity values and can be differentiated from each in the laboratory as well as

underground. It was also found that grout resistivity values recorded from grouts A to C and Portland cement decrease over the first curing hour and then immediately increase with increasing curing age following a path that can be approximated with a concave upward line. This approximation line is similar to the grout resistivity-curing age profiles presented in section 3.7 of the literature survey. Furthermore, the resistivity values recorded underground are shown to be lower in magnitude than those recorded in the laboratory. An expanded discussion of the comparison of grout resistivity magnitudes and causes is included in subsection 5.4-3.

Furthermore, a grout quality signature that is defined by the increase or decrease of grout resistivity values with an increase in the w/c ratio has been identified (using the full grout sensor dataset) for grout A, B, and C as well as in the Portland cement. Section 3.7 of the literature survey showed that the resistivity values of cementitious materials decrease with an increase in the w/c ratio; this is the expected grout signature.

The analysis of grout A resistivity recordings is presented first. Figures 5.4-1 to 5.4-3 show the resistivity values recorded from good, fair, and bad-quality (0.4 – 0.5 – 0.6 w/c) grout A mixtures in 4 m long simulated support holes in the laboratory as well as in underground 1.2 m and 4.5 m long experimental support holes.

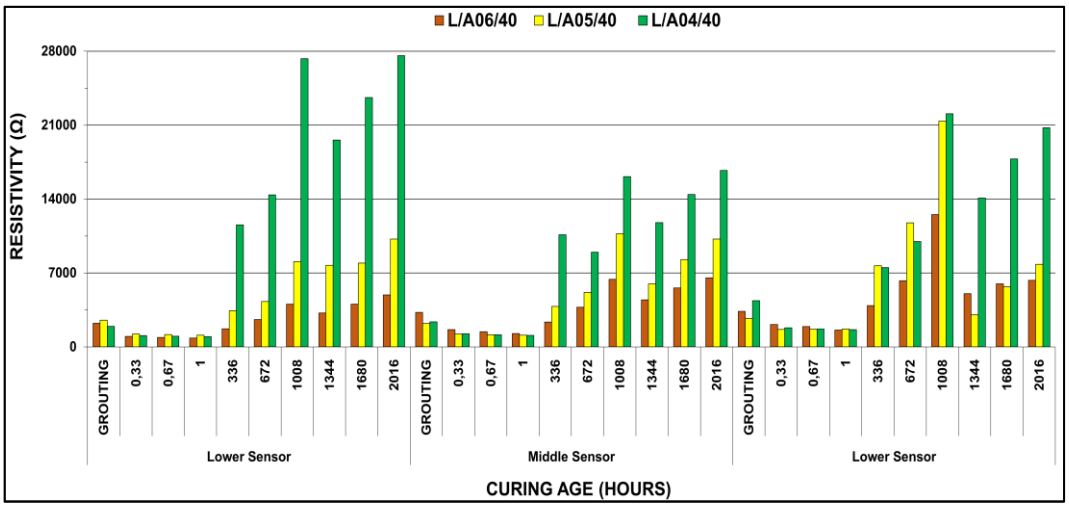


Figure 5.4-1. Electrical resistivity recorded from good, fair, and bad-quality grout A mixtures in 4 m long simulated support holes in the laboratory.

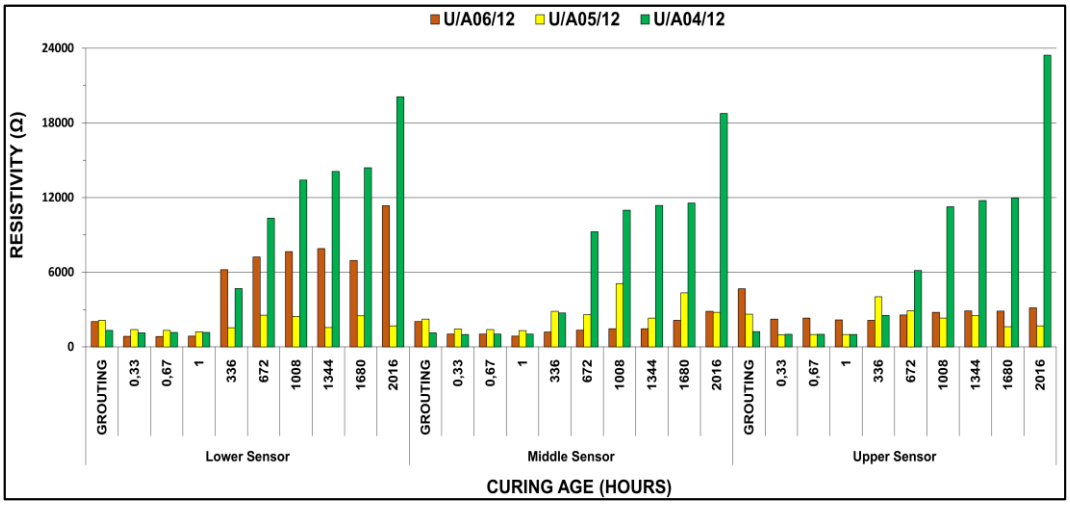


Figure 5.4-2. Electrical resistivity recorded from good, fair, and bad-quality grout A mixtures in 1.2 m long underground support holes.

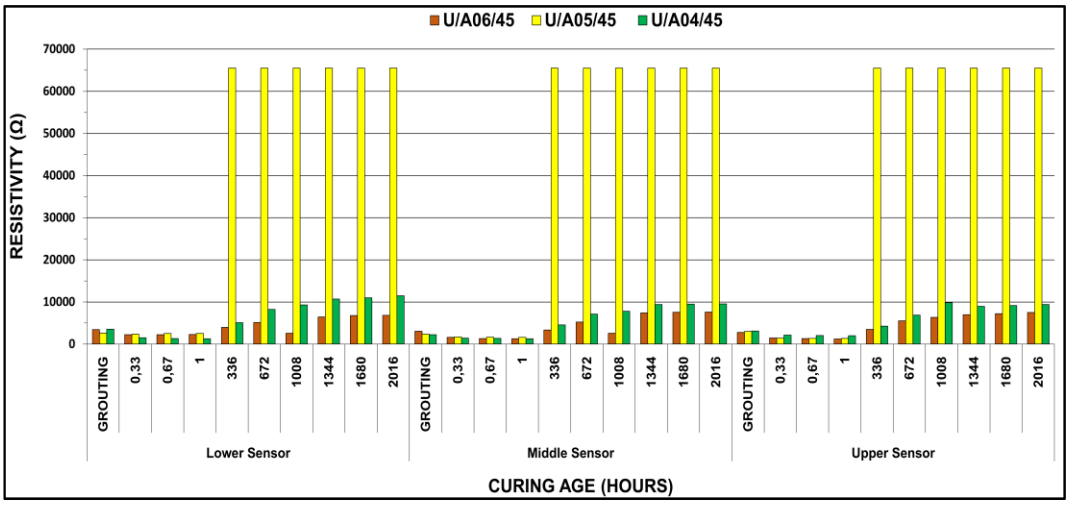


Figure 5.4-3. Electrical resistivity recorded from good, fair, and bad-quality grout A mixtures in 4.5 m long underground support holes.

It can be observed from Figures 5.4-1 to 5.4-3 that the grout A resistivity values decrease over the first curing hour. Grout resistivity decreases as the grout A compounds are broken down during hydration which releases electrically conductive ionic particles. It can also be observed from Figures 5.4-1 to 5.4-3 that grout A's good, fair, and bad-quality mixtures show an increasing resistivity trend with increasing curing age. In Figure 5.4-3, the high resistivity values indicate the shrinkage of grout (an expanded discussion of how grout sensor technology captures grout shrinkage is included in subsection 5.4-5).

The grout resistivity values increase with curing age as each good, fair, and bad-quality grout mixture hardens becoming more electrically resistive. In addition, it can also be observed that the different quality grout A mixtures immediately attain different resistivity values during grouting operations and remain differentiated over time when evaluated under controlled conditions in the laboratory as well as under experimental conditions at the underground study site.

Table 5.4-2 shows the grout A quality signature identified from grout sensor data recorded in the laboratory and underground. It can be noticed in Table 5.4-2 that grout A shows a decrease in grout resistivity values with an increasing w/c ratio in laboratory recordings. This grout A quality signature is similar to that garnered from the literature survey.

In underground recordings, grout A shows an increase in grout resistivity values with an increasing w/c ratio apart from the decrease in grout resistivity with an increase in the w/c ratio (0.4 to 0.5) seen in the lower and middle grout sensors of the 4.5 m long support hole recordings.

Table 5.4-2. Grout A quality signature identified from laboratory and underground grout sensor recordings.

Support Hole Length	Grout Quality Change (w/c ratio)	Lower Sensor	Middle Sensor	Upper Sensor
4 m	**Good (0.4) – Fair (0.5)**	Decrease	Decrease	Decrease
	Good (0.4) – Bad (0.6)	Decrease	Decrease	Decrease
U/G – 1.2 m	**Good (0.4) – Fair (0.5)**	Increase	Increase	Increase
	Good (0.4) – Bad (0.6)	Increase	Increase	Decrease
U/G – 4.5 m	**Good (0.4) – Fair (0.5)**	Decrease	Decrease	Increase
	Good (0.4) – Bad (0.6)	Increase	Increase	Increase

The analysis of grout B resistivity recordings is presented next. Figures 5.4-4 to 5.4-6 show the resistivity values recorded from good, fair, and bad-quality (0.4 – 0.5 – 0.6 w/c) grout B mixtures in 4 m long simulated support holes in the laboratory as well as in underground 1.2 m and 4.5 m long experimental support holes.

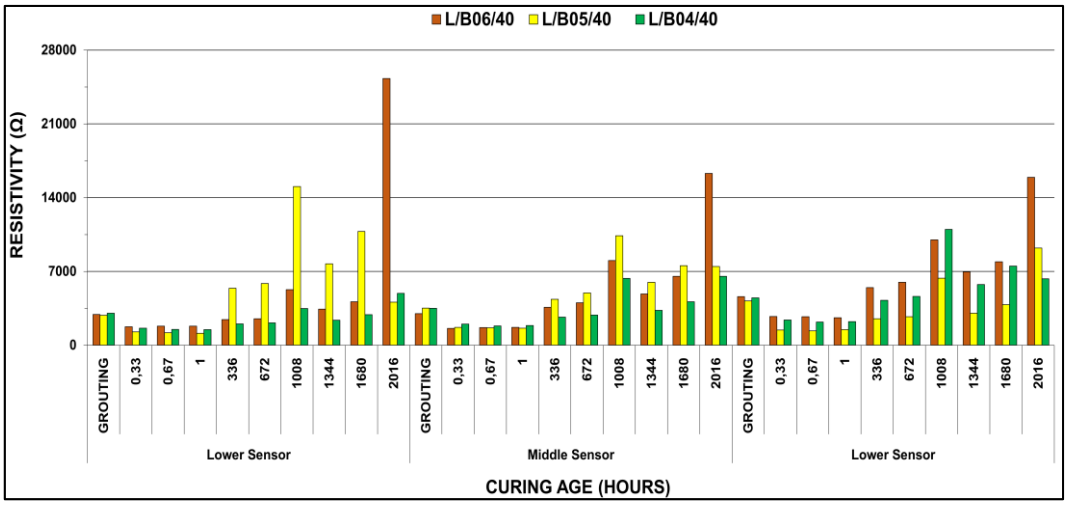


Figure 5.4-4. Electrical resistivity recorded from good, fair, and bad-quality grout B mixtures in 4 m long simulated support holes in the laboratory.

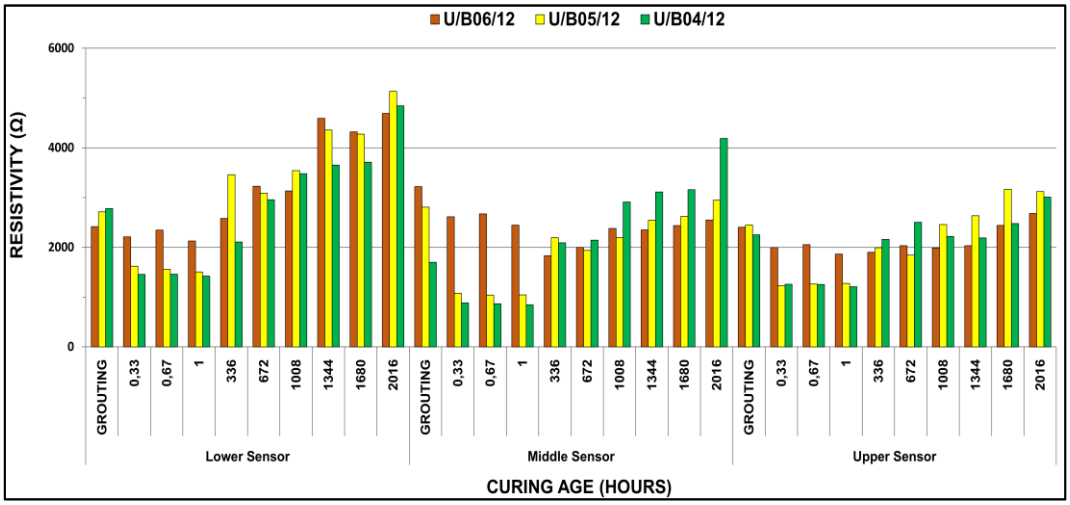


Figure 5.4-5. Electrical resistivity recorded from good, fair, and bad-quality grout B mixtures in 1.2 m long underground support holes.

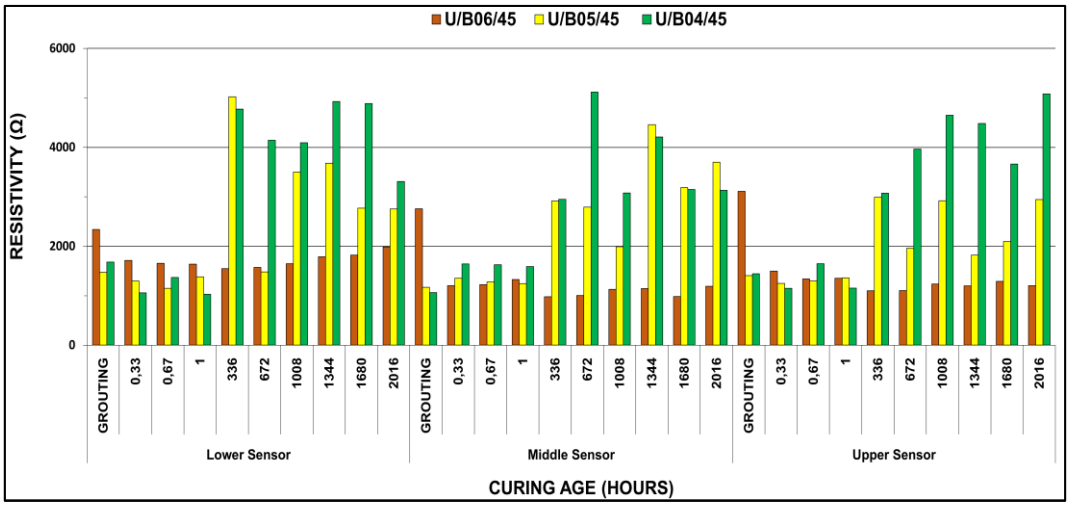


Figure 5.4-6. Electrical resistivity recorded from good, fair, and bad-quality grout B mixtures in 4.5 m long underground support holes.

Figures 5.4-4 to 5.4-6 show how grout B resistivity decreases over the first hour of curing, and then increases immediately afterward. These grout B resistivity trends results from the abundance of charged ions in the wet grout mixture phase and the continual hardening of grout with increasing curing age, respectively. It can also be observed that the grout B good, fair, and bad-quality mixture can be differentiated from each other during grouting operations and over three months in both laboratory and underground recordings of grout resistivity.

Table 5.4-3 shows the grout B quality signature identified from grout sensor data recorded in the laboratory and underground in different-length support holes. It can be noticed in Table 5.4-3 that grout B shows a decrease in

grout resistivity with an increase in the w/c ratio from 0.4 to 0.6 in both the 4 m long laboratory support hole recordings and 1.2 m long underground support hole recordings of grout resistivity. This grout quality signature is similar to that noted in the literature survey. In contrast, the change in the w/c ratio from 0.4 to 0.5 in the 4 m long laboratory support hole recordings and 1.2 m long underground support hole recordings shows mixed increases and decreases in grout resistivity. Furthermore, the 4.5 m long underground support hole recordings show an increase in grout resistivity with an increase in the w/c between 0.4 and 0.6.

Table 5.4-3. Grout B quality signature identified from laboratory and underground grout sensor recordings.

Support Hole Length	Grout Quality Change (w/c ratio)	Lower Sensor	Middle Sensor	Upper Sensor
4 m	**Good (0.4) – Fair (0.5)**	Decrease	Decrease	Increase
	Good (0.4) – Bad (0.6)	Decrease	Decrease	Decrease
U/G – 1.2 m	**Good (0.4) – Fair (0.5)**	Decrease	Increase	Decrease
	Good (0.4) – Bad (0.6)	Decrease	Decrease	Decrease
U/G – 4.5 m	**Good (0.4) – Fair (0.5)**	Increase	Increase	Increase
	Good (0.4) – Bad (0.6)	Increase	Increase	Increase

The analysis of grout C resistivity recordings is discussed next. Figures 5.4-7 to 5.4-9 show the resistivity values recorded from good, fair, and bad-quality (0.14 – 0.27 – 0.54 w/c) grout C mixtures in 4 m long simulated support holes in the laboratory as well as in underground 1.2 m and 4.5 m long experimental support holes.

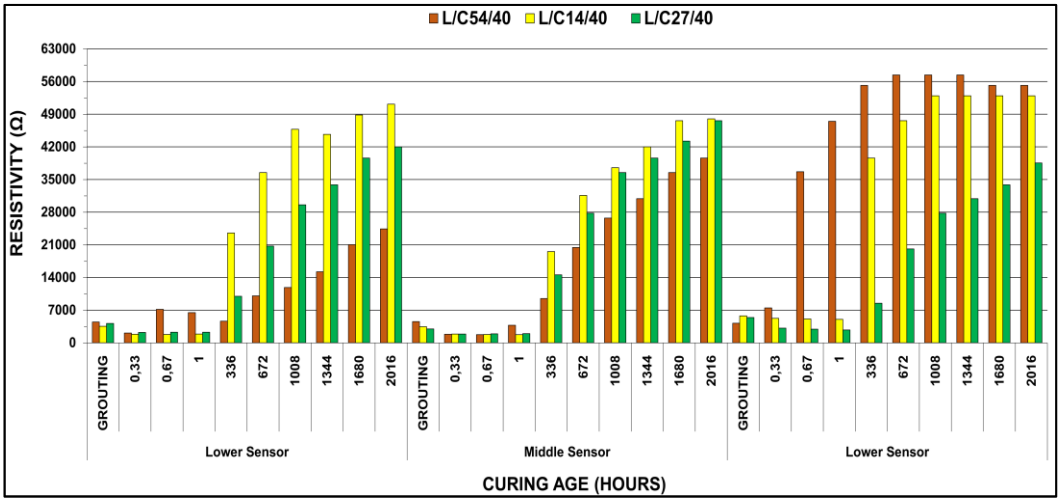


Figure 5.4-7. Electrical resistivity recorded from good, fair, and bad-quality grout C mixtures in 4 m long simulated support holes in the laboratory.

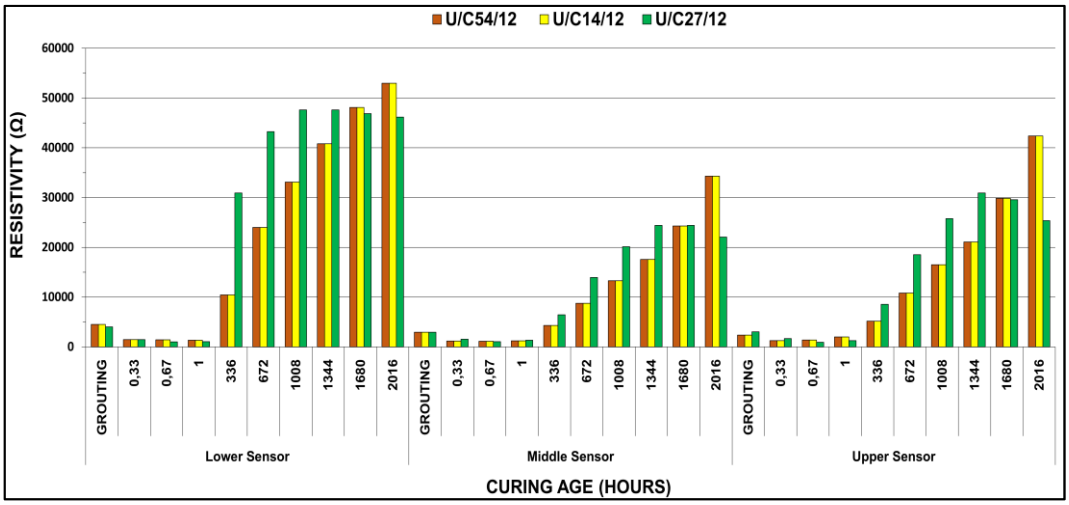


Figure 5.4-8. Electrical resistivity recorded from good, fair, and bad-quality grout C mixtures in 1.2 m long underground support holes.

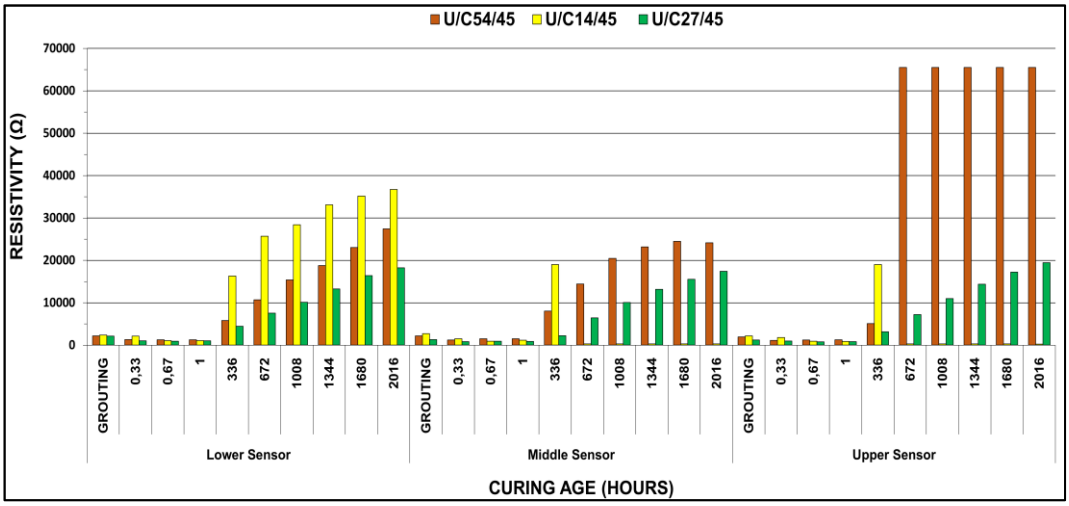


Figure 5.4-9. Electrical resistivity recorded from good, fair, and bad-quality grout C mixtures in 4.5 m long underground support holes.

It can be observed from Figures 5.4-7 to 5.4-9 that the grout C good, fair, and bad-quality mixtures show a decrease in grout resistivity over the first curing hour followed by immediate and steep increases in grout resistivity over each grout sensor position. It can also be observed that, during grouting operations and over time, the different quality grout C mixtures have different resistivity values and remain differentiated over time when evaluated under controlled conditions in the laboratory as well as under experimental underground conditions. In Figure 5.4-9, the bad-quality grout resistivity values are high and anomalous indicating the shrinkage of grout over the upper grout sensor position.

Table 5.4-4 shows the grout C quality signature identified from grout sensor data recorded in the laboratory and underground in different-length support holes. It can be noticed in Table 5.4-4 that grout C largely shows a decrease in grout resistivity values with both an increase and a decrease in the w/c ratio; the decrease in grout resistivity is similar to what has been observed from the literature survey. Exceptions to these grout C quality signatures exist over the middle grout sensor of the 4 m long simulated support holes (w/c ratio change from 0.27 to 0.54) and across all grout sensor positions of the 1.2 m long underground support holes (w/c ratio change from 0.27 to 0.54).

Table 5.4-4. Grout C quality signature identified from laboratory and underground grout sensor recordings.

Support Hole Length	Grout Quality Change (w/c ratio)	Lower Sensor	Middle Sensor	Upper Sensor
4 m	**Good (0.27) – Fair (0.14)**	Decrease	Decrease	Decrease
	Good (0.27) – Bad (0.54)	Decrease	Increase	Decrease
U/G – 1.2 m	**Good (0.27) – Fair (0.14)**	Decrease	Decrease	Decrease
	Good (0.27) – Bad (0.54)	Increase	Increase	Increase
U/G – 4.5 m	**Good (0.27) – Fair (0.14)**	Decrease	Decrease	Decrease
	Good (0.27) – Bad (0.54)	Decrease	Decrease	Decrease

The analysis of Portland cement quality using grout sensor technology recordings is discussed next. Figures 5.4-10 to 5.4-12 show the resistivity values recorded from good, fair, and bad-quality (0.4 – 0.5 – 0.6 w/c) Portland cement mixtures in 4 m long simulated support holes in the laboratory as well as in underground 1.2 m and 4.5 m long experimental support holes.

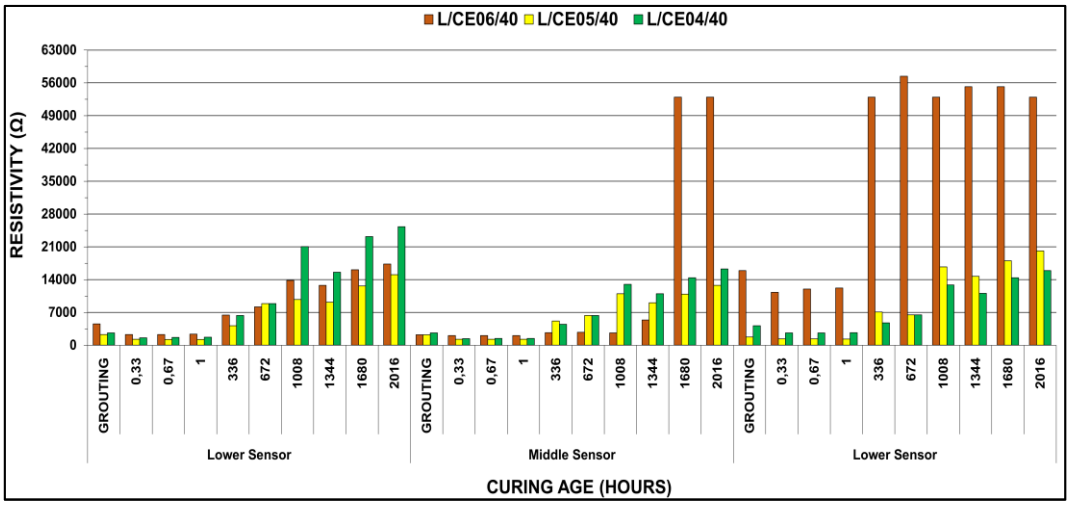


Figure 5.4-10. Electrical resistivity recorded from good, fair, and bad-quality Portland cement mixtures in 4 m long simulated support holes in the laboratory.

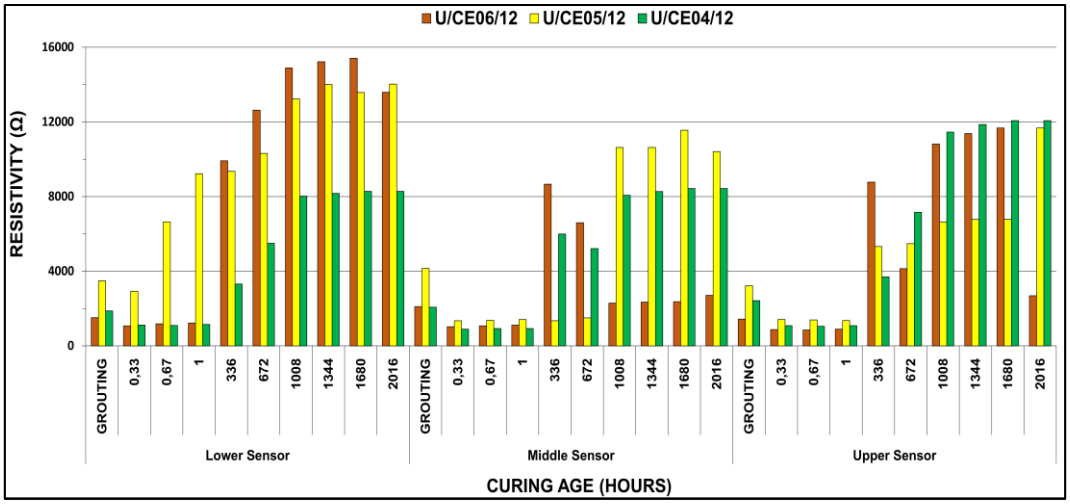


Figure 5.4-11. Electrical resistivity recorded from good, fair, and bad-quality Portland cement mixtures in 1.2 m long underground support holes.

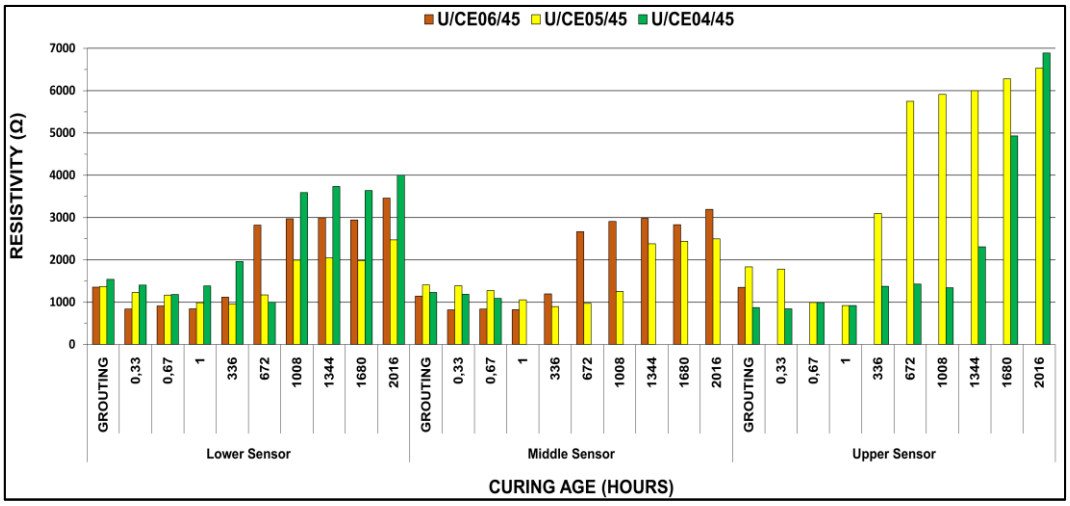


Figure 5.4-12. Electrical resistivity recorded from good, fair, and bad-quality Portland cement mixtures in 4.5 m long underground support holes.

It can be observed from Figures 5.4-10 to 5.4-12 that the Portland cement resistivity values decrease following the end of grouting operations and increase thereafter across all grout sensor positions similar to grouts A, B, and C. There are, however, several “spikes” in grout resistivity present in both laboratory and underground recordings. It can also be noticed that the good, fair, and bad-quality Portland cement mixtures can be differentiated from each other over a three-month observation period in laboratory and underground experimental support holes.

Table 5.4-5 shows the Portland cement quality signature identified from grout sensor data recorded in the laboratory and underground in different-

length support holes. It can be noticed in Table 5.4-5 that the Portland cement largely shows mixed increases and decreases of cement resistivity with an increasing w/c ratio. A single instance of a decrease in Portland cement resistivity with an increase in the w/c (0.4 to 0.6) that is pervasive across all the grout sensors can be seen in the 4 m long simulated support hole recordings.

Table 5.4-5. Portland cement quality signature identified from laboratory and underground grout sensor recordings.

Support Hole Length	Grout Quality Change (w/c ratio)	Lower Sensor	Middle Sensor	Upper Sensor
4 m	**Good (0.4) – Fair (0.5)**	Increase	Increase	Decrease
	Good (0.4) – Bad (0.6)	Decrease	Decrease	Decrease
U/G – 1.2 m	**Good (0.4) – Fair (0.5)**	Decrease	Increase	Increase
	Good (0.4) – Bad (0.6)	Decrease	Increase	Increase
U/G – 4.5 m	**Good (0.4) – Fair (0.5)**	Increase	Increase	Decrease
	Good (0.4) – Bad (0.6)	Increase	Decrease	Decrease

Grouts A to C and Portland cement resistivity-curing age plots have been presented to show that good, fair, and bad-quality grout mixtures can be differentiated from each other using three independent recording points inside long cable anchor support holes. Grout quality signature tables have also been presented to show how grouts A to C and Portland cement

resistivity values vary when the w/c ratio changes over the range 0.14 – 0.6. This is a novel output and it validates the hypothesis that different quality grout mixes have different grout sensor data signatures that indicate their quality.

Grout resistivity-curing age plots show both an increase and decrease in resistivity with an increasing w/c ratio. In contrast, the resistivity-curing age plots presented in the literature survey showed a decrease in resistivity with an increase in the w/c ratio. It is possible that the grout sensor data recorded in weekly intervals does not have enough resolution to capture the long-term hydration of each of the evaluated grouts and Portland cement where a consistent change in grout resistivity with a change in the w/c ratio can be recorded.

An equally important possibility is that grout sensor technology offers an opportunity to study the curing profiles of 1.2 m, 4 m, and 4.5 m long grout columns at three independent points and it is likely that the curing profiles at these points are different. The resistivity methods presented in the literature survey recorded the bulk resistivity values of samples contained in cylindrical moulds thus the scale (volume and studied length) of measurements is different. Based on the observation that each column of grout has a different resistivity versus curing age profile over each sensor, it is put forward that different parts of a column of grout inside the support hole will cure at different rates over the length of the support hole.

In that respect, it is postulated that thixotropic grout mixtures become immediately stratified (due to shearing against rough support hole walls) as they are pumped into support holes where they retain different curing and gain in strength profiles across the length of each column of grout. The differential gain in strength implies that the load-transfer mechanism and bond strength may be non-uniform along the length of each support hole and thus support holes, especially those grouted with poor-quality grout mixtures, will generally not offer efficient support in mining excavations. Grout sensor technology, therefore, offers three unique and independent points to study the quality of a column of grout inside different-length support holes. This concept is explored further in subsection 5.4-3 where the effectiveness of grout is analysed using sensor technology.

The verification of the quality of grout aims to eliminate the need for the ineffective visual quality of grouting in underground mines. In this regard, the grout quality signature is a particularly useful index that can be used during the routine quality of support holes equipped with grout sensor technology. Recorded grout resistivity values from underground support holes equipped with grout sensor technology can be verified for the installed grout quality. Using a comprehensive library of pre-recorded perfect w/c ratio grout resistivity values, a shift (increase or decrease in grout resistivity values) away from the ideal w/c ratio can be calculated for each grout sensor position. This way, the sub-standard grouting of any length support hole can

be identified during a routine quality inspection of fully grouted long cable anchor support holes.

5.4.2 Grout quality summary

The differentiation of grout mixture quality using grout sensor technology installed in simulated support holes in the laboratory and in underground experimental support holes has been presented as grout resistivity-curing age plots and grout quality signature tables. Figures 5.4-1 to 5.4-12 showed that over the lower, middle, and upper grout sensor positions the good, fair, and bad-quality grout mixtures can be differentiated during grouting operations as well as over a three-month observation period. It has also been observed that grout resistivity values, irrespective of mixture quality and support hole length, decrease in the early curing age and then start increasing with increasing curing age. The grout resistivity values recorded in the laboratory and underground respectively reach upwards of 57 000 ohms and 52 000 ohms towards the end of the observation period.

Furthermore, depending on the position of the grout sensor, laboratory and underground grout resistivity recordings show unique grout quality signatures concerning an increasing w/c ratio over the three months observation period. This grout quality signature identified from grout resistivity can be potentially used to identify the sub-standard grouting of long cable anchor support holes in mines.

5.4.3 The setting of grout

Cementitious grouts cure differently under different temperature and humidity conditions. It was thus anticipated that there would be a difference in the grout and Portland cement resistivity values recorded in the laboratory to those recorded underground. It was also anticipated that the grout resistivity magnitude difference will vary over each grout sensor location owing to the discrete placement of grout sensors into the rock mass underground.

Column charts have been plotted to compare the differences between laboratory and underground resistivity readings for all good, fair, and bad-quality grout mixtures to demonstrate the sensitivity of grout sensor technology to the setting of grout. In addition, the plots of grout resistivity over five curing weeks for all good, fair, and bad-quality grout and Portland cement mixtures are presented to demonstrate the sensitivity of grout sensor technology to the setting of grout over a curing period where there is a rapid development of grout strength. Figure 5.4-13 is a plot of the average resistivity differences between underground and laboratory recordings of good-quality grout mixtures over three months.

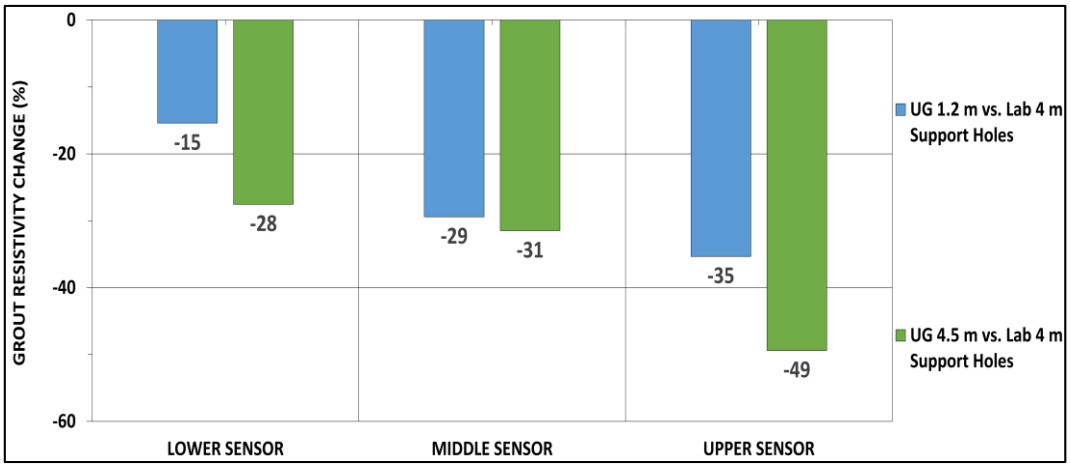


Figure 5.4-13. A plot of the average resistivity differences between good-quality grout mixtures recorded from underground support holes to those recorded in the laboratory over a three-month period.

It can be noticed from Figure 5.4-13 that the grout resistivity recordings from 1.2 m and 4.5 m long underground support holes are lower in magnitude by up to 49 percent when compared to those recorded in the laboratory across all the grout sensor positions. It can also be noticed that the magnitude of the grout resistivity reduction in both the 1.2 m and 4.5 m long support holes amplifies with increasing distance into the rock mass. Additionally, the underground 4.5 m long support hole grout resistivity recordings show a larger decrease in grout resistivity across all the grout sensor positions. Figure 5.4-14 is a plot of the average resistivity differences between underground and laboratory recordings of fair-quality grout mixtures over three months.

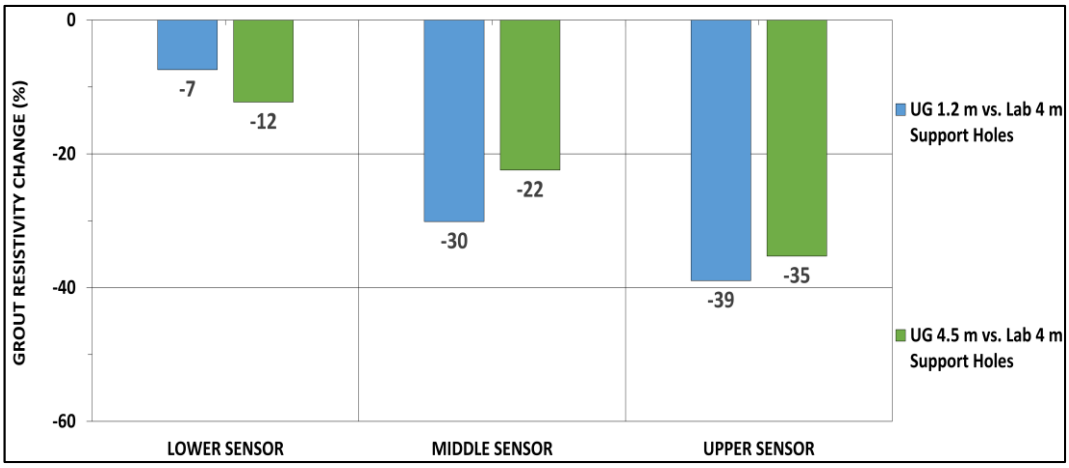


Figure 5.4-14. A plot of the average resistivity differences between fair-quality grout mixtures recorded from underground support holes to those recorded in the laboratory over a three-month period.

It can be observed in Figure 5.4-14 that the 1.2 m and 4.5 m long support hole grout resistivity recordings are lower in magnitude across all the grout sensor positions when compared to laboratory recordings. It can also be noticed that the magnitude of the grout resistivity decrease in both the 1.2 m and 4.5 m long support holes amplifies with increasing distance into the rock mass. In addition, the underground 4.5 m long support hole grout resistivity recordings show a larger decrease when compared to laboratory grout resistivity recordings over the lower grout sensor position. In contrast, the 1.2 m long support hole grout resistivity recordings show a larger decrease in grout resistivity over the middle and upper grout sensors. Figure 5.4-15 is a plot of the average resistivity differences between underground and laboratory recordings of bad-quality grout mixtures over three months.

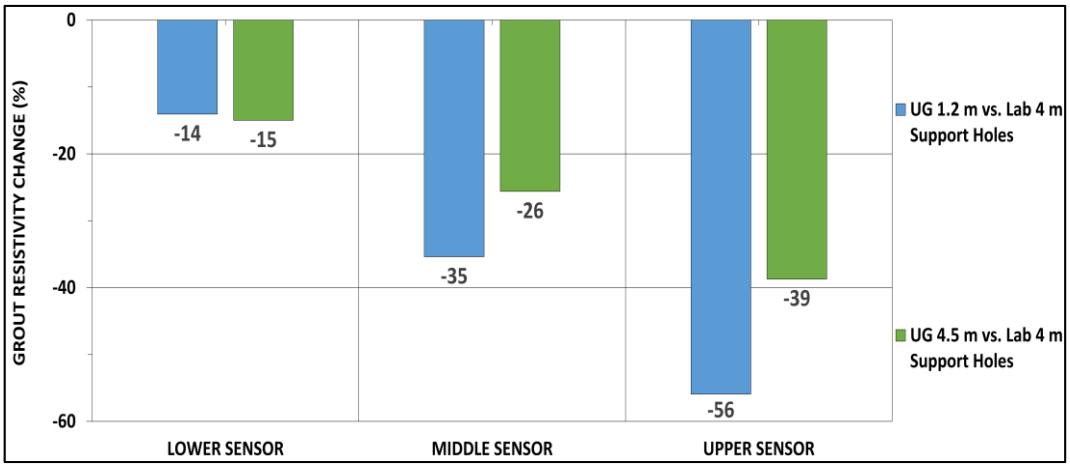


Figure 5.4-15. A plot of the average resistivity differences between fair-quality grout mixtures recorded from underground support holes to those recorded in the laboratory over a three-month period.

Figure 5.4-15, in likeness to Figures 5.4-13 and 5.4-14, shows that all the 1.2 m and 4.5 m long support hole grout resistivity recordings are lower in magnitude when compared to laboratory grout resistivity recordings across all the grout sensors. In further likeness, the bad-quality grout resistivity values show an increasing reduction with increasing grout sensor positioning into the rock mass irrespective of support hole length.

In addition, it can also be observed that, over the lower grout sensor, the underground 4.5 m long support hole grout resistivity recordings show a larger decrease in grout resistivity. In contrast, the 1.2 m long support hole grout resistivity recordings show a larger decrease in grout resistivity over middle and upper grout sensor positions.

The modifying factor resulting in the lowering of the underground support hole grout resistivity values is thought to be the presence of a small temperature gradient inside each support hole. A small temperature increase can modify the rate of grout hydration and the overall setting characteristics of a mixture of grout. This effect is expressed as a heightening decrease in grout resistivity values recorded underground in comparison to those recorded in the laboratory with increasing grout sensor distance into each support hole. It is, however, not clear why there are larger reductions in grout resistivity in longer-length support holes grouted with good-quality grout mixtures only. In support holes grouted with fair and bad-quality grout mixtures, the larger reduction of grout resistivity in longer (4.5 m) support holes occurs over the lower grout sensor positions only.

Based on observations made from Figures 5.4-13 to 5.4-15 it is evident that grout sensor technology installed into laboratory and underground support holes is sensitive to the setting of the column of grout (under different temperature conditions). These observations are aligned with those found in the Morsy (1999) and Teixeira et al (2016) studies where higher curing temperatures were shown to increase and decrease measured conductivity and resistivity values, respectively.

To further test the sensitivity of grout sensor technology to the setting of grout, grout resistivities from different quality grout mixtures have been plotted over 35 curing days (one plot of laboratory resistivity recordings and two from the underground recordings) to illustrate the sensitivity of grout

sensor technology to the setting of grout. The grout resistivity values recorded in the laboratory as well as underground were expected to increase rapidly between the completion of grouting operations up to a curing age of 35 days.

The rapid increase in grout resistivity over this period occurs as the curing grout mixture changes from a wet mixture to a solid phase forming a tight molecular structure. This tight molecular structure provides a complex pathway for an electric charge to be transmitted across the hardening grout mixture. Figure 5.4-16 shows the resistivity values recorded from good quality grout mixtures composed from grouts A, B, and C as well as Portland cement in 4 m long simulated support holes in the laboratory.

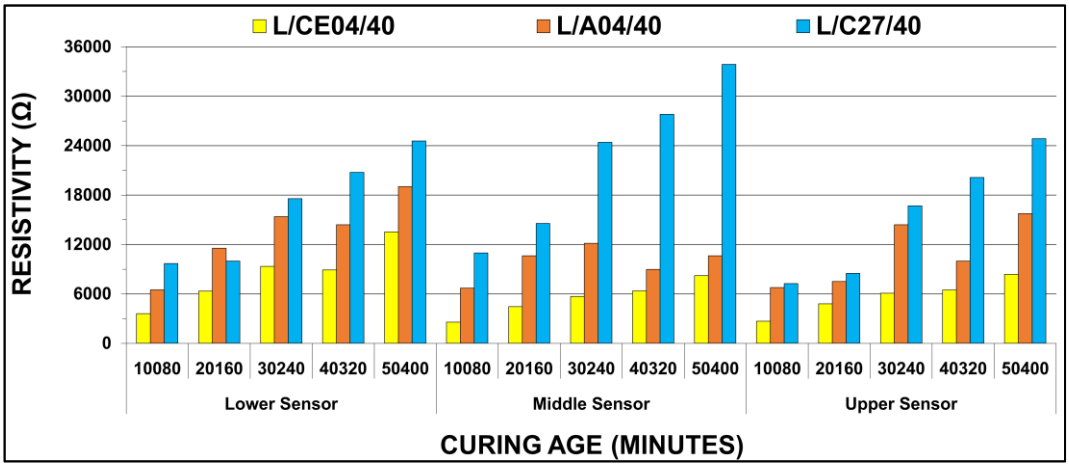


Figure 5.4-16. Grout resistivity measurements conducted on good-quality grout A, B, and C as well as Portland cement mixtures grouted into 4 m long simulated support holes over 35 curing days.

In Figure 5.4-16, there is a steep increase in grout resistivity in all good-quality mixtures as they cured over 35 days. It can also be noticed that, for each different quality grout mixture over each grout sensor position, the resistivity values increase at different rates of change in response to the complex evolution of each grout's microstructure during the curing process.

Figure 5.4-17 shows the grout resistivity values recorded from good, fair, and bad quality grout C mixtures installed into 1.2 m long underground support holes.

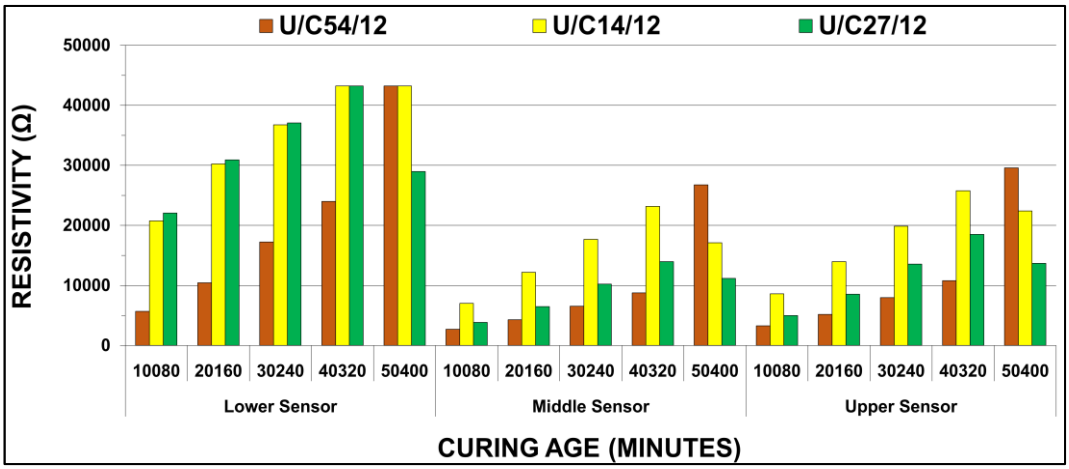


Figure 5.4-17. Grout resistivity measurements conducted on good, fair, and bad-quality grout C mixtures grouted into 1.2 m long underground support holes over 35 curing days.

It can be observed from Figure 5.4-17 that there is an increase in the resistivity values recorded from different quality grout C mixtures with

increasing curing age over each grout sensor location. However, good-quality grout C resistivity values decrease slightly between curing weeks 4 and 5 across all the grout sensor positions. Further, fair-quality grout C resistivity also show a slight decrease between curing weeks four and five over the middle and upper grout sensors. It can also be noticed that, for each good, fair, and bad-quality grout mixture over each grout sensor position, the grout resistivity values increase at different rates of change.

Figure 5.4-18 shows the grout resistivity values recorded from good-quality mixtures of grout A, B, and C installed into 4.5 m long underground support holes.

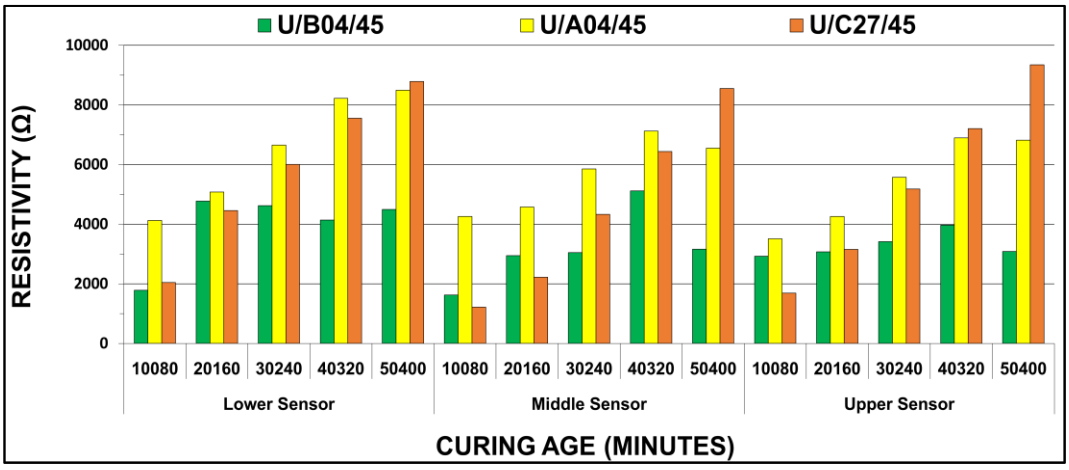


Figure 5.4-18. Grout resistivity measurements conducted on good-quality grout A, B and C mixtures grouted into 4.5 m long underground support holes over 35 curing days.

Similar to the laboratory 4m long support hole recordings and 1.2 m long underground support hole recordings, the 4.5 m long support hole grout resistivity recordings shown in Figure 5.4-18 show an increase in grout resistivity with increasing curing age (grout B values are characterised by intermittent decrease and increases in grout resistivity). In addition, the 4.5 m long support hole grout resistivity recordings shown in Figure 5.4-18 have different rates of resistivity development over the lower, middle, and upper grout sensors.

The identification of the lowering of grout resistivity values recorded underground compared to those recorded in the laboratory as well as the identification of rapid increases in grout resistivity over the first 35 curing days are novel outputs. These outputs both adequately answer the research question on whether grout sensor technology is sensitive to the setting of grout.

5.4.4 The setting of grout summary

The differences in grout resistivity magnitude when good, fair, and bad-quality grout mixtures are cured under controlled conditions in the laboratory as well as under experimental underground conditions have been presented to illustrate the sensitivity of grout sensor technology to the setting of grout. Observations made from Figures 5.4-13 to 5.4-15 showed that the 1.2 m and 4.5 m long experimental support hole recordings of grout resistivity are lower in magnitude than those recorded under controlled conditions in the laboratory over the lower, middle and upper grout sensor positions. It was

also noted that there was an increase in the lowering of grout resistivity values with an increasing distance into the rock face. This effect was thought to be caused by increasing temperatures into the rock face which modify the rate of grout hydration.

Furthermore, the sensitivity of grout sensor technology to the setting of good, fair, and bad-quality grout mixtures has also been presented as grout resistivity column charts plotted over a 35-day curing period. Examination of Figures 5.4-16 to 5.4-18 revealed a rapid increase in grout resistivity values over a curing period where there is a rapid gain in grout strength that occurred irrespective of grout mixture quality and grout sensor position.

The rapid increase in grout resistivities recorded in the laboratory as well as underground took place in response to the complex evolution of grout microstructures as they hardened. This evolution of the grout microstructure is expressed as a rapid increase and large rate of change in grout resistivity.

Grout sensor technology, installed in laboratory and underground support holes, is therefore sensitive to the setting of grout where the sensitivity is measurable using three independent grout sensors installed into each support hole.

5.4.5 The effectiveness of grout

The effectiveness of grout inside a support hole is defined by the full encapsulation of a support unit, the minimal to zero loss of grout through

rock fractures as well as the minimal long-term shrinkage of grout. The analysis of the effectiveness of grout using sensor technology is presented here with a focus on how the loss of grout and shrinkage in support holes can be detected using grout sensor technology. The effectiveness of grout is also presented as the prediction of the bond strength developed between the interfaces of cable anchors and different quality grout mixtures using grout resistivity data.

The three grout sensors installed into each support hole in the laboratory as well as underground were positioned to ensure each support hole can be adequately monitored over three months. Table 5.4-6 shows the overall performance of grout sensor technology in laboratory support holes as well as in experimental underground support holes. It can be noticed in Table 5.4-6 that grout sensor technology performed robustly and that faulty grout sensor readings only occurred during the installation and monitoring of 4.5 m long underground support holes.

Table 5.4-6. The performance of grout sensor technology in the laboratory and underground over a three-month observation period.

Grout Sensor Readings Taken	**Faulty Grout Sensor Readings**	**Overall Grout Sensor Technology Performance (%)**
2160	36	98
Laboratory Sensor Performance (%)	**Underground Sensor Performance – 1.2 m (%)**	**Underground Sensor Performance – 4.5 m (%)**
100	100	95

Over a three-month observation period, the grout sensor data recorded under controlled conditions in the laboratory shows that all three sensors in each of the 12 simulated support holes remained fully covered with grout. The see-through PVC pipes enabled the visual inspection and confirmation of full-column grouting in each simulated support hole over three months. Grout sensor recordings also show that all 1.2 m long underground experimental support holes remained fully grouted over three months. Table 5.4-7 is a snapshot of a grout sensor technology datasheet that shows the grout sensor data recorded in the laboratory. Table 5.4-7 shows that when there is grout present inside the support hole, grout sensor technology shows grout resistivity values greater than 800 Ω and an “OK” grout detection status in the grout datasheet stored in memory.

Table 5.4-7. A grout sensor technology excel sheet compiled from laboratory support hole resistivity recordings.

Elapsed Time (Hours)	Time Stamp	Status	Resistivity	Time Stamp	Status	Resistivity	Time Stamp	Status	Resistivity
SENSOR CHECK	12:25:24	OK	59631	12:25:24	OK	52953	12:25:24	OK	52953
GROUT IN	12:25:55	OK	4557	12:26:00	OK	2253	12:26:30	OK	15950
0,167	12:36:11	OK	2343	12:36:11	OK	2155	12:36:11	OK	11697
0,33	12:44:40	OK	2271	12:44:40	OK	2050	12:44:40	OK	11315
0,5	12:55:11	OK	2297	12:55:11	OK	2048	12:55:11	OK	11275
0,67	13:04:52	OK	2280	13:04:52	OK	2061	13:04:52	OK	12014
0,83	13:15:12	OK	2359	13:15:12	OK	2092	13:15:12	OK	12319
1	13:25:38	OK	2369	13:25:38	OK	2077	13:25:38	OK	12222
168	13:35:06	OK	4276	13:35:06	OK	2648	13:35:06	OK	52953
336	09:45:26	OK	6435	09:45:26	OK	2668	09:45:26	OK	52953
504	13:18:00	OK	7553	13:18:00	OK	2694	13:18:00	OK	57405
672	09:43:47	OK	8174	09:43:47	OK	2784	09:43:47	OK	57405
840	12:53:00	OK	10072	12:53:00	OK	2792	12:53:00	OK	52953
1008	09:35:15	OK	13822	09:35:15	OK	2639	09:35:15	OK	52953
1176	13:31:32	OK	11765	13:31:32	OK	5294	13:31:32	OK	55179
1344	09:24:37	OK	12778	09:24:37	OK	5384	09:24:37	OK	55179
1512	09:55:26	OK	14422	09:55:26	OK	5296	09:55:26	OK	52953
1680	08:46:21	OK	16122	08:46:21	OK	52953	08:46:21	OK	55179
1848	09:57:09	OK	14555	09:57:09	OK	52953	09:57:09	OK	52953
2016	08:53:59	OK	17353	08:53:59	OK	52953	08:53:59	OK	52953

In contrast to the laboratory and underground 1.2 m long support hole grout resistivity recordings, three of the 4.5 m long underground experimental support holes experienced the loss and shrinkage of grout over time following the end of grouting operations. In addition, a total of 36 faulty sensor readings were noted in the 4.5 m long underground support holes.

An underground 4.5 m long support hole that was grouted with a good quality mixture of Portland cement (U/45/CE04) showed the loss of the Portland cement mixture in the middle of the support hole fifty minutes after grouting operations were concluded. It is hypothesised that a small volume of the relatively wet cement mixture escaped via a near-support hole fracture resulting in the loss of the grout signal over the middle grout sensor position.

Grout sensor technology, when there is no grout present inside the support hole, shows high and unvarying grout resistivity values (> 60 KΩ) and an “OPEN” grout detection status in the grout datasheet stored in memory. Figure 5.4-19 is a grout resistivity versus curing age plot that shows the grout resistivity values recorded in an underground 4.5 m long support hole filled with a good quality Portland cement mixture.

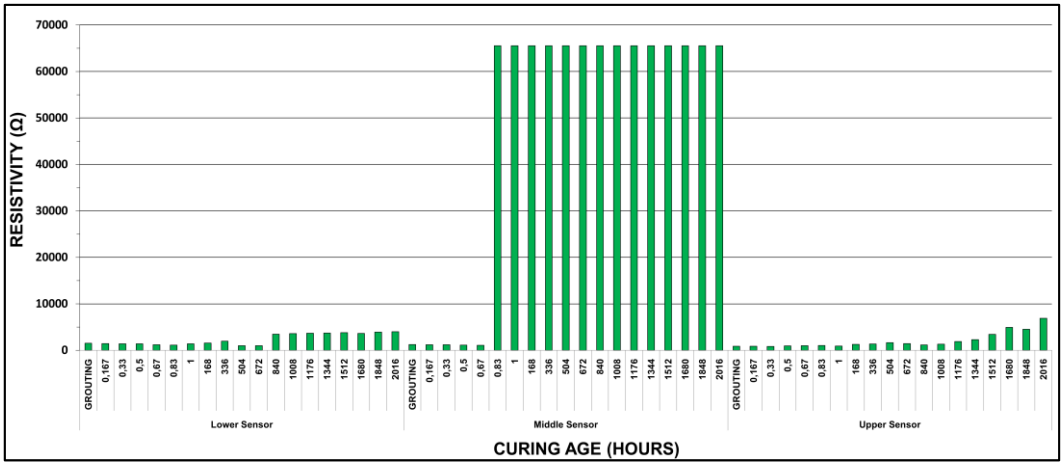


Figure 5.4-19. Electrical resistivity recorded from a good-quality Portland cement mixture in an underground 4.5 m long support hole.

It can be seen in Figure 5.4-19 that the middle grout sensor resistivity profile is high and unvarying values of approximately 65 K Ω beginning at fifty minutes (time stamp when grout was lost from the support hole) and extending to the end of the observation period. A separate 4.5 m long underground support hole grouted with a fair-quality grout A mixture (U/45/A05) showed a loss of grout signal over the lower, middle, and upper grout sensors during the reading of underground grout sensor data after two weeks following the conclusion of grouting operations. A grout mixture at the curing age of two weeks is likely to be solidified and unlikely to escape through a system of near-support hole rock fractures.

Table 5.4-8 shows the grout sensor technology datasheet of the 4.5 m long support hole grouted with the U/45/A05 mixture. In Table 5.4-8, all grout sensors show an open grout detection status (no grout present) after two weeks (336 hours) following the conclusion of grouting operations underground. It is postulated that the grout sensors malfunctioned. When recalling the results of grout shrinkage measurements, grout A's fair-quality mixture (SH/A05) was shown to shrink by approximately 3.8% under controlled conditions in the laboratory (section 4.2 of the results and discussion chapter).

Table 5.4-8. A grout sensor technology excel sheet compiled from the underground 4.5 m long support hole recordings showing an OPEN grout detection status on all sensors on the 3rd week following grouting operations.

Elapsed Time (Hours)	Time Stamp	Status	Resistivity	Time Stamp	Status	Resist	Time Stamp	Status	Resistivity
SENSOR CHECK	12:58:09	OK	59631	12:58:09	OK	59631	12:58:09	OK	55179
1	13:58:12	OK	2526	13:58:12	OK	1593	13:58:12	OK	1387
168	09:53:26	OK	4612	09:53:26	OK	3620	09:53:26	OK	3880
336	10:24:18	OPEN	65535	10:24:18	OPEN	65535	10:24:18	OPEN	65535
504	09:15:16	OPEN	65536	09:15:16	OPEN	65536	09:15:16	OPEN	65536
672	09:27:16	OPEN	65535	09:27:16	OPEN	65535	09:27:16	OPEN	65535
840	09:39:16	OPEN	65535	09:39:16	OPEN	65535	09:39:16	OPEN	65535
1008	09:04:01	OPEN	65535	09:04:01	OPEN	65535	09:04:01	OPEN	65535
1176	09:12:16	OPEN	65535	09:12:16	OPEN	65535	09:12:16	OPEN	65535
1344	09:30:59	OPEN	65535	09:30:59	OPEN	65535	09:30:59	OPEN	65535
1512	09:35:40	OPEN	65535	09:35:40	OPEN	65535	09:35:40	OPEN	65535
1680	09:19:55	OPEN	65535	09:19:55	OPEN	65535	09:19:55	OPEN	65535
1848	09:44:27	OPEN	65535	09:44:27	OPEN	65535	09:44:27	OPEN	65535
2016	09:13:41	OPEN	65535	09:13:41	OPEN	65535	09:13:41	OPEN	65535

Underground at the South Deep mine, the combination of higher rock temperatures and higher air humidity is likely to increase the amount of shrinkage taking place. Thus, it is also possible that this grout mixture shrunk inside the support hole to such an extent that the positive and negative terminals of the grout sensors lost contact with the column of the grout. A possible means of verifying and confirming these postulations are the overcoring of the support hole installations to inspect the column of grout and the grout sensors. This capability was, however, not available during the recording and monitoring of underground support holes at the mine.

Figure 5.4-20 shows a support hole drawing to illustrate how the shrinkage of a column of grout inside a support hole can lead to a loss of contact with the installed grout sensors.

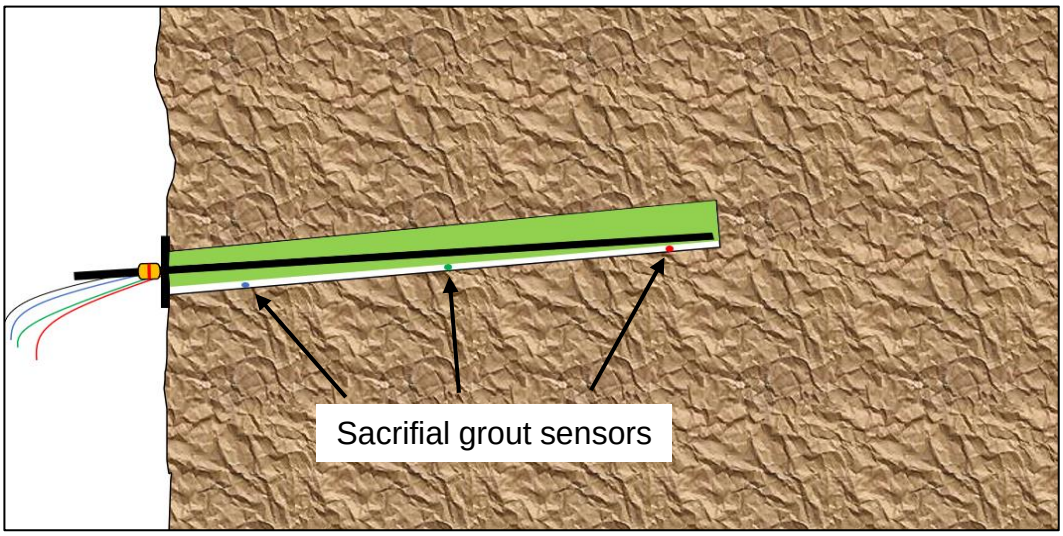


Figure 5.4-20. Support hole two-dimensional drawing showing the shrinkage of grout.

In further analysis of the effectiveness of grout, the prediction of the frictional resistance (bond strength) developed over the grout-cable anchor interface using grout sensor technology is presented. Grout resistivity data recorded over the lower, middle, and upper grout sensors in simulated support holes in the laboratory have been plotted against the grout-cable anchor bond strengths calculated from pull-out tests conducted using different quality grout and Portland cement mixtures. It is thought appropriate to use the

short-encapsulation pull-out test results due to the fact all test samples failed by yielding of the grout-cable anchor interface.

Separate plots have been constructed for grouts A, B, and C as well as Portland cement. A similar curing interval (one, seven, 14, 28, and 35 curing days) was used to plot the grout resistivity data versus the grout-cable anchor bond strength. Each plot of grout resistivity versus the grout–cable anchor bond strength has been fitted with a linear regression trendline that minimizes the sum of errors through the plotted dataset.

The linear regression equations are used to predict the bond strength of the grout-cable anchor interface over the lower, middle, and upper parts of the support hole. This workflow builds on the concept of the differential gain in grout strength presented in subsection 5.4-2 of the results and discussion chapter.

In the analysis of the effectiveness of grout, it was found that the grout resistivity to grout-cable anchor bond strength dataset recorded over the first curing day was full of estimation errors. These errors are thought to stem from the inability of grout resistivity data recorded over one curing hour to accurately describe the bonding behaviour of a grout mixture cured over one full day. As a result, the one-hour grout resistivity and one-day bond strength datasets are not included in the following analysis of bond strength prediction from grout resistivity. Figure 5.4-21 is a plot of the grout resistivity values recorded from all the good-quality grout mixtures in the laboratory

versus the grout-cable anchor bond strength values. The plotted values are coloured by the positioning of the grout sensors (lower–blue channel, middle–green channel, and upper–red channel).

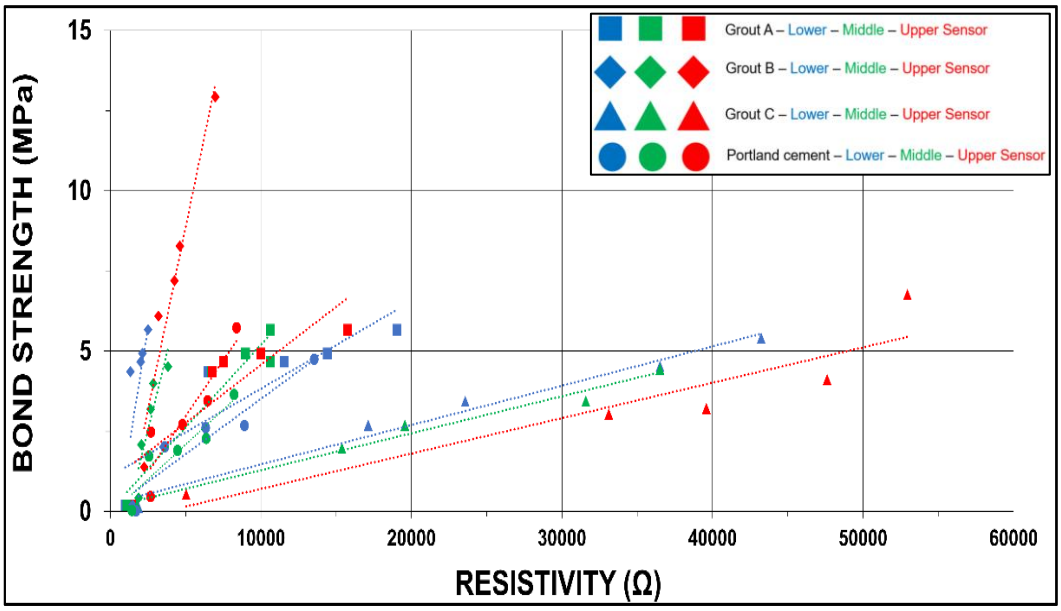


Figure 5.4-21. A plot of the lower, middle, and upper sensor resistivity versus the grout–cable anchor bond strength in all good-quality grout mixtures.

It can be seen in Figure 5.4-21 that grouts A, B, C and Portland cement plot in distinct sectors of the bond strength – grout resistivity dataset. A linear regression trendline has been fitted through each of the lower, middle, and upper sensor grout resistivity to grout-cable anchor bond strength datasets. To better understand the data scatter and estimation errors a mean average percentage error (MAPE) has been computed for each linear regression trendline using equation 5.4-1.

$$MAPE = \frac{1}{n}\sum_{t=1}^{n}\frac{Actual\ Value_t - Forecast\ Value_t}{Actual\ Value_t}$$ *Equation 5.4-1*

In Equation 5.4-1, the forecast value is the forecasted grout-cable anchor bond strength from grout resistivity using a linear regression trendline. Similarly, the actual value is the actual bond strength value calculated from short-encapsulation pull-out testing. MAPE, thus, is a measure of the predictive accuracy of the grout resistivity to grout-cable anchor bond strength linear regression trendline. A lower MAPE value means that the grout-cable anchor bond strength can be estimated fairly confidently from the grout sensor resistivity dataset with only a few errors present.

Table 5.4-9 shows the good-quality grout linear regression correlation confidences for each grout sensor position and the MAPE computed for each linear regression trendline. It can be observed that all linear regression trendlines show a high degree of correlation (> 75 percent) between grout resistivity and the grout-cable anchor bond strength. Green shading in the MAPE column highlights relatively low grout-cable anchor bond strength prediction errors. Therefore, based on this classification scheme, the good-quality grout-cable anchor bond strengths can be estimated confidently with only a few errors (<21 percent) present across all the grout sensor positions.

Table 5.4-9. Good-quality grout linear regression trendline correlation confidence and MAPE.

Grout	Sensor Position	Linear Regression Trendline Correlation Confidence (%)	MAPE (%)
A	Lower	78	16
	Middle	91	13
	Upper	74	15
B	Lower	83	14
	Middle	81	15
	Upper	95	7
C	Lower	98	20
	Middle	98	14
	Upper	85	12
PORTLAND CEMENT	Lower	89	21
	Middle	86	19
	Upper	83	18

Figure 5.4-22 is a plot of the grout resistivity values recorded from all the fair-quality grout mixtures in the laboratory versus the grout–cable anchor bond strength values. The values are coloured by the positioning of the grout sensors (lower–blue channel, middle–green channel, and upper–red channel).

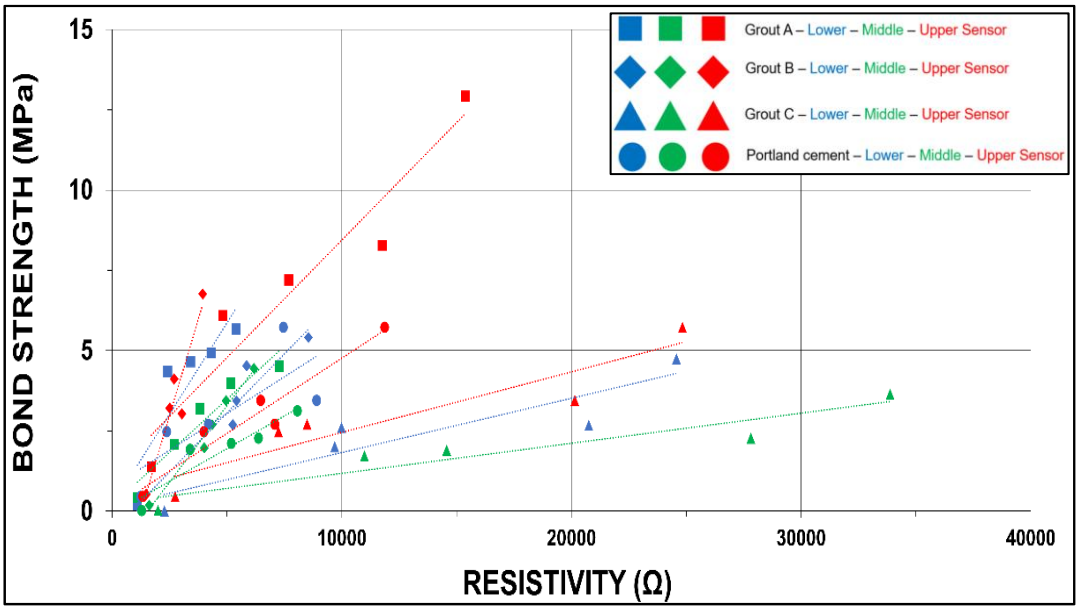


Figure 5.4-22. A plot of the lower, middle, and upper sensor resistivity versus the grout–cable anchor bond strength in all fair-quality grout mixtures.

It can be observed in Figure 5.4-22 that grout C plots in the lower right-hand half of the chart whereas grout A and B as well as Portland cement plot towards the centre. A linear regression trendline has been fitted through each of the lower, middle, and upper sensor grout resistivity to grout-cable anchor bond strength datasets. Table 5.4-10 shows the fair-quality grout linear regression correlation confidences for each grout sensor position and the MAPE computed for each linear regression trendline.

It can be seen in Table 5.4-10 that the grout resistivity to grout-cable anchor bond strength correlation confidence is generally high (apart from the Portland cement lower grout sensor position correlation confidence).

Furthermore, Table 5.4-10 shows that the fair-quality grout-cable anchor bond strengths can be predicted with a few errors present (<33 percent) in each grout sensor position.

Table 5.4-10. Fair-quality grout linear regression trendline correlation confidence and MAPE.

Grout	Sensor Position	Linear Regression Trendline Correlation Confidence (%)	MAPE (%)
A	**Lower**	77	15
	Middle	92	8
	Upper	92	21
B	**Lower**	93	11
	Middle	98	10
	Upper	90	17
C	**Lower**	82	22
	Middle	88	19
	Upper	86	18
PORTLAND CEMENT	**Lower**	62	25
	Middle	88	12
	Upper	94	33

Figure 5.4-23 is a plot of all of the lower, middle, and upper sensor grout resistivity values recorded from all the bad-quality grout mixtures in the

laboratory versus the grout–cable anchor bond strength values. The values are coloured by the positioning of the grout sensors (lower–blue channel, middle–green channel, and upper–red channel).

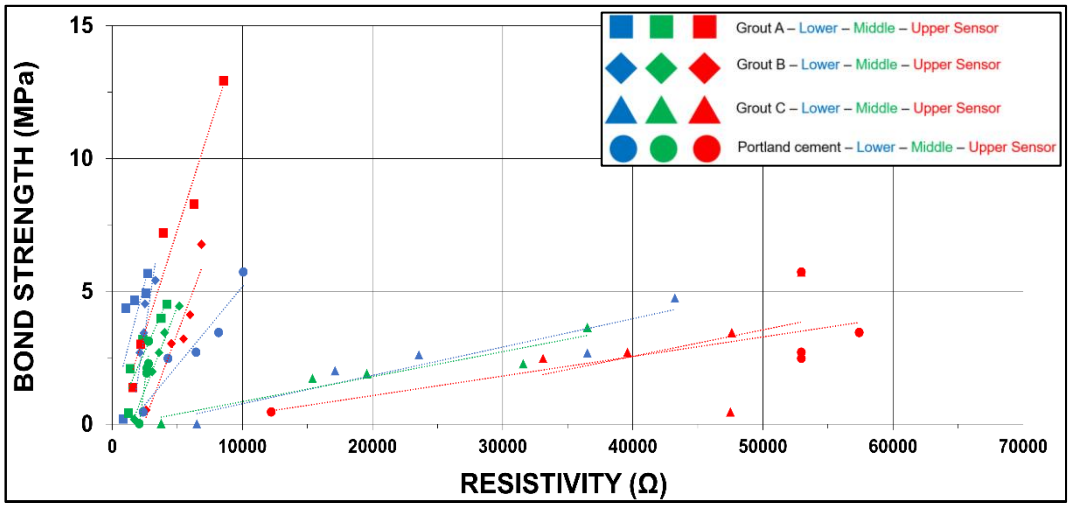


Figure 5.4-23. A plot of the lower, middle, and upper sensor resistivity versus the grout–cable anchor bond strength in all bad-quality grout mixtures.

Figure 5.4-23 shows that grout A and B as well as Portland Cement and Grout C plot in separate quadrants of the grout resistivity-bond strength dataset. A linear regression trendline has been fitted through each of the lower, middle, and upper sensor grout resistivity to grout-cable anchor bond strength datasets as previously performed in the good and fair-quality grout resistivity versus bond strength plots. Table 5.4-11 shows the bad-quality grout linear regression correlation confidences for each grout sensor position and the MAPE computed for each linear regression trendline. It can be concluded from Table 5.4-11 that the bad-quality grout bond strengths

can be predicted with very few errors (<27 percent) present over each grout sensor position using a highly correlated (>74 percent) dataset.

Table 5.4-11. Bad-quality grout linear regression trendlines, correlation confidence and MAPE.

Grout	Sensor Position	Linear Regression Trendline Correlation Confidence (%)	MAPE (%)
A	Lower	78	18
	Middle	91	21
	Upper	74	27
B	Lower	83	13
	Middle	81	6
	Upper	95	15
C	Lower	98	23
	Middle	98	18
	Upper	85	17
PORTLAND CEMENT	Lower	89	17
	Middle	86	10
	Upper	83	26

The prediction of the strength of the grout-cable anchor interface (thereby the effectiveness of grout) can form an invaluable strata quality control tool in underground mines. In comparison to work by other authors, the

prediction of the bond strength is similar to the work by Wei et al (2012) and Choo et al (2021) presented in the literature survey where these researchers used electrical resistivity recordings to find cement mortar and cement-sands compressive strength predictive functions.

The detection of grout loss and shrinkage as well as the prediction of grout effectiveness using in-support hole grout sensor technology are novel outputs that validate the research question on whether grout sensor technology can be used to determine the effectiveness of grout over time.

5.4.6 The effectiveness of grout summary

The analysis of the determination of the effectiveness of grout using grout sensor technology has been presented to show how grout loss and grout shrinkage can be detected in underground support hole installations. Observations made from Figures 5.4-19 – 5.4-22 showed that the shrinkage or loss of grout inside support holes can be detected over the lower, middle, and upper grout sensors during and immediately following grouting operations as well as over time. This ability outlines the value of using in-support hole sacrificial sensor technology to verify the effectiveness of grout over time.

The effectiveness of grout analysis also showed how the bond strengths of different quality grouts can be predicted using in-support hole grout sensor technology. In this regard, it has been shown that the bond strengths of good, fair, and bad-quality grouts to the cable anchor interfaces can be

determined over time with reasonable accuracy (generally less than 33% MAPE) using grout sensor technology installed in support holes.

5.5 Shortcomings of Grout Sensor Technology

This section discusses the shortcomings of grout sensor technology encountered at the South Deep mine during the recording of grout sensor data. The preceding section showed how grout sensor technology can detect the loss and shrinkage of grout using grout sensors placed at 30 percent, 65 percent, and 95 percent of each support hole length. However, the in-support hole discrete grout sensor placement leaves unmonitored gaps in between the grout sensors.

Table 5.5-1 shows the lengths of unmonitored gaps between grout sensors in control and experimental support holes to illustrate the shortcoming of grout sensor technology (a grout sensor is 5.5 cm in length). It can be noticed from Table 5.5-1 that the loss of small amounts of grout or its shrinkage inside the support hole in-between grout sensors can go undetected.

Table 5.5-1. Unmonitored lengths in support and experimental support holes equipped with grout sensor technology.

Unmonitored Length Position	Control Support Hole (4 m)	Experimental Support Hole (1.2 m)	Experimental Support Hole (4.5 m)
SC - LS	1.2	0.36	1.35
LS - MS	1.35	0.37	1.52
MS - US	1.15	0.31	1.3
US - TSH	0.15	0.01	0.17
SC – support hole collar, LS – lower sensor, MS – middle sensor, US – upper sensor, and TSH – top of the support hole.			

Figure 5.5-1 is a support hole schematic that shows gaps that may go unmonitored when small amounts of grout escape from the support hole or shrink in support holes equipped with grout sensor technology.

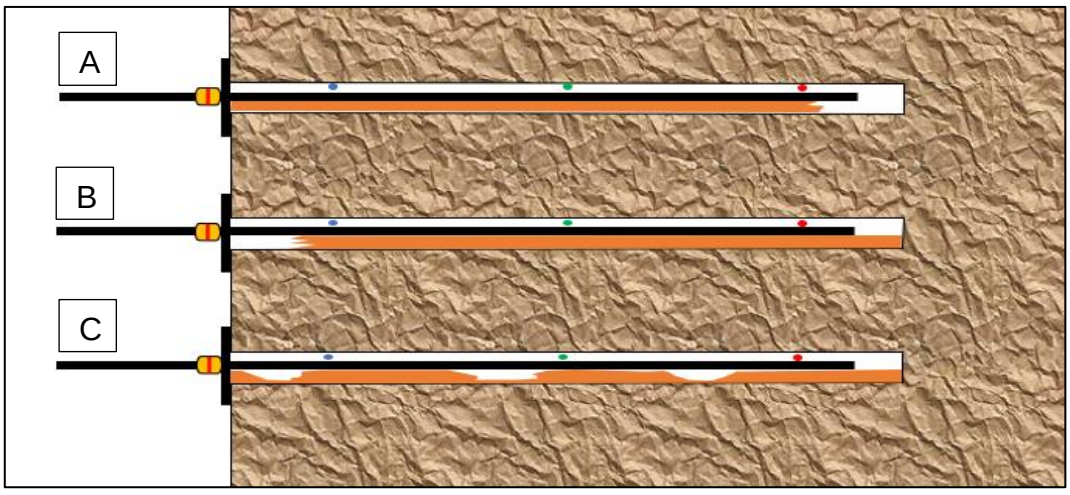


Figure 5.5-1. A generic length support hole schematic showing potentially unmonitored occurrences of in-support hole shrinkage (A) top support hole grout shrinkage; (B) bottom support hole grout shrinkage; and (C) grout shrinkage between sensor locations.

Another shortcoming is that grout sensor resistivity data when read using the GDT100 meter connected to each support hole is not viewable in situ. The grout detector meter only provides in-situ information on whether a support hole is full-column grouted or not. This means that diagnostic information on the quality and effectiveness of a column of grout cannot be analysed in situ to perform quality control and assurance of ground support units.

Another shortfall is that grout sensor technology does not permit the continuous recording of grout sensor data from underground support holes. This is a shortfall since a detailed study of the physical changes taking place in a curing grout mixtures can only be conducted using continuously recorded resistivity datasets.

It was also noted that during the installation of the cables housing the grout sensors that the exposed positive and negative terminals are prone to damage as the cables are forced inside underground support holes. Furthermore, the grout sensors installed into each support hole are prone to short-circuiting when one or more sensor terminals touches the cable anchor or the steel wire in the cable anchor shell anchor mechanism. Table 5.5-2 shows a snapshot of a grout sensor technology data log sheet for an underground support hole with short-circuited grout sensors.

In Table 5.5-2, the short-circuiting of the upper grout sensor (red channel) occurred ten minutes (0.167 hours) after the conclusion of grouting

operations. Grout sensor technology, when there is a short circuit, shows low grout resistivity values (< 800 Ω) in the grout datasheet stored in memory as well as shows a “SHORT” grout detection status on the grout detection meter. A short-circuited grout sensor is irrecoverable therefore that section of the support hole will remain unmonitored indefinitely.

Table 5.5-2. A grout sensor technology datasheet showing short-circuiting in the upper grout sensor.

Elapsed Time (Hours)	Time Stamp	Status	Resistivity	Time Stamp	Status	Resistivity	Time Stamp	Status	Resistivity
SENSOR CHECK	10:50:00	OK	43240	10:50:00	OK	57405	10:50:00	OK	43240
GROUTING	11:05:13	OK	1357	11:05:13	OK	1145	11:05:14	OK	1350
0,167	11:15:39	OK	837	11:15:39	OK	834	11:15:39	SHORT	701
0,33	11:25:40	OK	840	11:25:40	OK	821	11:25:40	SHORT	674
0,5	11:35:14	OK	852	11:35:14	OK	879	11:35:14	SHORT	707
0,67	11:44:42	OK	910	11:44:42	OK	838	11:44:42	SHORT	681
0,83	11:53:25	OK	932	11:53:25	OK	854	11:53:25	SHORT	691
1	12:04:42	OK	845	12:04:42	OK	825	12:04:42	SHORT	668
168	12:14:33	OK	1058	12:14:33	OK	1132	12:14:33	SHORT	675
336	10:30:15	OK	1117	10:30:15	OK	1197	10:30:15	SHORT	762
504	10:14:14	OK	1875	10:14:14	OK	1683	10:14:14	SHORT	719
672	09:35:51	OK	2824	09:35:51	OK	2666	09:35:51	SHORT	726
840	09:45:10	OK	2917	09:45:10	OK	2834	09:45:10	SHORT	710
1008	09:14:23	OK	2973	09:14:23	OK	2911	09:14:23	SHORT	763
1176	10:56:37	OK	2990	10:56:37	OK	2951	10:56:37	SHORT	703
1344	10:07:41	OK	2998	10:07:41	OK	2983	10:07:41	SHORT	751
1512	09:29:50	OK	3103	09:29:50	OK	3013	09:29:50	SHORT	775
1680	09:40:33	OK	2945	09:40:33	OK	2833	09:40:33	SHORT	714
1848	10:42:11	OK	3288	10:42:11	OK	3099	10:42:11	SHORT	763
2016	09:38:33	OK	3461	09:38:33	OK	3193	09:38:33	SHORT	750

Another shortfall is that to read grout resistivity data a manual connection of the grout detector meter needs to be made to the wires that form the grout receiver unit located at the collar of each support hole. This labouring task

means that for support holes located at heights in tall excavations, a ladder or climbing onto uneven excavation walls is required to reach the support hole, make a connection, and take a grout sensor recording. Further, the grout receiver unit wiring at the collar of each support hole is easily damaged when applying a faceplate and wedge onto a cable anchor to pre-tension the cable anchor.

Lastly, but more critically, grout sensor technology readings cannot distinguish between a water-grout solution flushed support hole and one filled with a well-mixed grout mixture. A single underground 1.2 m long support hole equipped with grout sensor technology was filled with a solution of mine water with a tiny amount of grout added to it. Then, grout resistivity data were recorded for one full hour from this support hole.

This support hole filled with a grout-water solution showed similar resistivity values to those recorded from genuine good, fair, and bad-quality grout mixtures. This means that grout sensor technology is unable to distinguish between a normal grout mixture and a grout-water solution. A tiny amount of grout added to water is enough to register a “grout reading.” Therefore, support holes filled with grout-water solutions can go undetected. This shortcoming of grout sensor technology has huge safety implications as poor grout installations can be erroneously assessed as having passed routine quality control inspections of fully grouted cable anchor installations underground. Figure 5.5-2 is a plot of good and fair quality grout mixture, as

well as grout-water solution resistivity values recorded in an underground 1.2 m long support hole and plotted over the first curing hour.

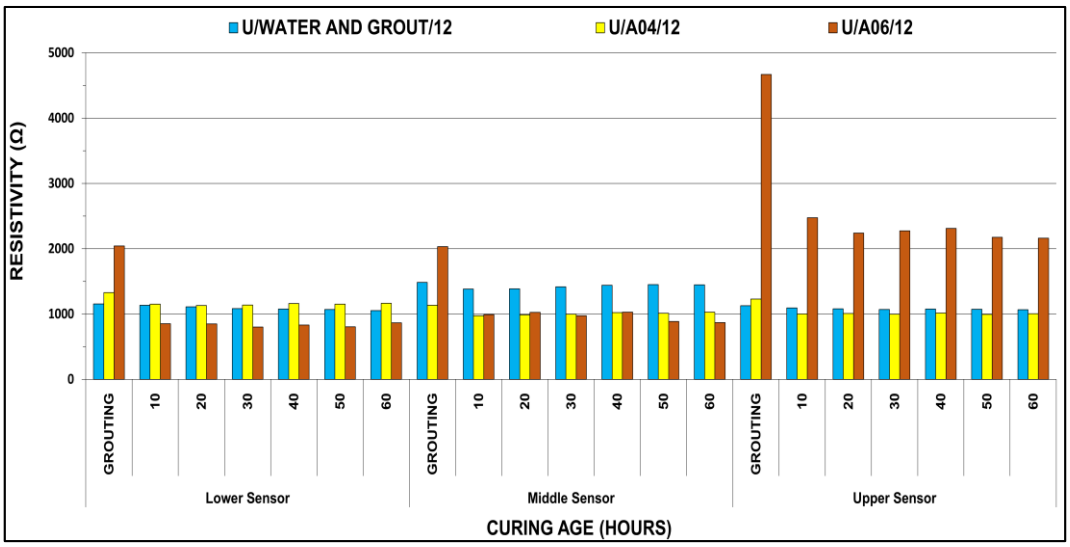


Figure 5.5-2. A comparison of grout A good (yellow) and bad (brown) quality mixture to grout-water solution (blue) resistivity values recorded from an underground 1.2 m support hole.

It can be observed from Figure 5.5-2 that the grout-water solution produces similar resistivity values to those recorded from good and bad-quality grout A mixtures and would go undetected during routine analysis of grout sensor recordings.

5.5.1 Grout sensor technology shortcomings summary

The shortcomings of grout sensor technology have been presented to outline weak points of the technology that can be potentially improved in the

future. Firstly, the use of three discrete grout sensors was shown to leave unmonitored gaps in between the grout sensors where the loss and shrinkage of grout can go unmonitored. Secondly, the recorded grout resistivity data is not viewable in-situ, to read grout resistivity data underground requires making a labouring manual connection for each support hole, and that the grout sensor exposed terminals are prone to damage and short-circuiting during installation. Lastly, grout sensor technology is unable to distinguish between well-prepared grout mixture and grout-water solutions. All mixtures with tiny amounts of grout added to them will erroneously register as a grout signal similar to a genuinely mixed grout mixture.

6 CONCLUSIONS AND RECOMMENDATIONS

6.1 Introduction

This chapter presents the conclusions and recommendations of this research study based on the results presented in the preceding chapter. This chapter also presents the limitations encountered during the recording of the grout sensor technology dataset. Recommendations are also presented as well as suggestions for further work to be carried out at the mine study site.

The problem statement presented in this research report stated how the quality, loss, and shrinkage of cementitious grout inside the support hole are important but often overlooked considerations during the installation and quality control of fully grouted long cable anchor support holes. As a first study of its kind in the South African mining fraternity, this study conducted grout linear shrinkage measurements, short encapsulation pull-out testing, and the recording of grout sensor technology datasets to address these overlooked critical aspects of fully grouted long cable anchor support holes.

6.2 Grout Shrinkage

Grout linear shrinkage was measured using a precise digital length comparator in short-length test prisms under controlled conditions specified by the ASTM C157 standard over a 28-day curing period. This was done to quantify the amount of shrinkage that occurs in different w/c ratio grout samples. The use of the ASTM C 157 standard method is in line with the

literature survey (Menu et al., 2017; Mohan et al., 2021) as the preferred method of measuring the linear change of length in cementitious materials.

Grout shrinkage measurement results have shown that different quality grout mixtures will shrink and expand by up to 13 percent when cured under 23 degrees Celsius and 50 percent temperature and humidity conditions over 28 curing days. Grout shrinkage measurement results also showed that the amount of grout shrinkage and expansion that occurred in different quality samples increased with increasing curing age. In addition, the increase in the amount of grout shrinkage that occurred in different quality test prisms was shown to be correlated to an increase in the w/c ratio or a decrease in the quality of the grout mixture. Further, when the grout shrinkage measurements were extrapolated to 1.2 m, 4 m, and 4.5 m long support holes it was shown that grout columns in these support holes could be significantly reduced in length due to grout shrinkage. A reduced column of grout lowers the corrosion protection of installed support units.

The development of corrosion in support units results in the loss of supportive capacity and poses significant safety risks in underground mines when undetected. Grout shrinkage and expansion values measured under controlled conditions in the laboratory were postulated to be higher for grout columns inside support holes installed at the underground mine study site where damp and high humidity conditions prevail. Similar findings were noted in the literature survey (Lura et al., 2003; Newlands et al., 2008); the

authors found that measured shrinkage/expansion values typically increased with increasing humidity.

It can thus be concluded that the quality (w/c ratio) of grout exerts a large control of the development of grout shrinkage inside support holes and should be well regulated for optimal corrosion protection of cable and rock bolt support units.

6.3 SEPT

The short encapsulation pull-out tests conducted in the laboratory sought to quantify the development of the grout-cable anchor interface bond strength over a 35-day curing period in different quality (w/c ratio) grout mixtures. In this regard, testing comprised the axial loading of short-length cable anchors encapsulated in good, fair, and bad-quality grout mixtures in the laboratory.

Short encapsulation pull-out test results showed that the grout-cable anchor interface is the weaker interface and will fail first under axial loads irrespective of the quality of the grout mixture. Short encapsulation pull-out testing also showed that most of the evaluated different quality grout mixtures in the first 24 curing hours have an exceptionally low grout-cable anchor interface bond strength. Then, with increasing curing age, the w/c ratio exerted a large control on the magnitude of the cable-grout interface bond strength where fair and bad-quality grout mixtures (high w/c ratio) have reduced bond strengths. Therefore, where sub-standard grout mixing has

been conducted, the installed fully grouted support unit may not be effectively bonded to the grout column and is likely to offer reduced frictional resistance to arrest rock mass movements in supported areas under axial loading conditions.

It was also shown that a column of grout, between 28 and 35 curing days, could gain as much as 44 percent bond strength depending on the quality of the grout mixture thereby illustrating the importance of curing grout mixtures up to at least 35 days for a full gain in strength. The residual bond strength gain between 28 and 35 curing days also outlined the importance of using the correct w/c ratios when preparing grout mixtures in underground mines.

It can thus be concluded that the quality (w/c ratio) of grout exerts a large control of the development of grout-cable anchor interface bond strength and should be carefully regulated before grouting operations for the optimal performance of cable and rock bolt support units.

6.4 Grout Sensor Technology

This research report aimed to answer three key research questions that addressed the verification of the quality and performance of grout using sensor technology. In formulating the research hypothesis, control and experimental conditions were set up to evaluate grout sensor technology in the laboratory and at the mine study site, respectively.

The first research question was whether grout sensor technology can differentiate between good and poor-quality grout.

In-support hole sensor technology comprising of three sacrificial grout sensors and a grout detector meter (GDT100) was used to record the resistivity of good, fair, and bad-quality grout mixtures installed into laboratory 4 m long as well as in underground 1.2 m and 4.5 m long support holes. Grout resistivity values recorded in the laboratory and underground were presented as grout resistivity versus curing age plots. These grout resistivity-curing age plots showed that, over the lower, middle, and upper grout sensor positions, good, fair, and bad-quality mixtures can be differentiated from each other during grouting operations as well as over a three-month observation period. The differentiation of grout quality using sensor technology is a novel output for the mining industry.

The grout resistivity-curing age plots also showed that grout resistivity values, irrespective of mixture quality (w/c ratio), decrease initially and then start increasing with increasing curing age reaching magnitude up to 57 000 ohms forming a unique resistivity profile over each grout sensor position. In addition, each grout resistivity-curing age plot formed a u-shape (over each grout sensor) that described the microstructural changes taking place in a grout mixture as it hardens over time.

Based on the occurrence of different grout resistivity-curing age profiles over each sensor, it was put forward that the lower, middle and upper regions of a column of grout inside the support hole will cure and gain their bond strengths at different rates leading to an inefficient load-transfer mechanism during rock mass loading. Furthermore, grout resistivity-curing age plots showed that the Portland cement and grouts A, B, and C have different signatures concerning the grout mixture quality in each of the grout sensor positions.

It can therefore be concluded that, laboratory and underground grout sensor technology installations yield unique, to each grout, resistivity signatures with changing grout quality over curing time. This conclusion validates the hypothesis that there are different signatures to different quality grout mixes.

The second research question was whether grout sensor technology is sensitive to or accurate to the setting of grout.

In the analysis of the setting of grout, plots of the average change in different quality grout resistivity values between control and experimental support holes over three curing months were presented. Observations made from these plots showed that all good, fair, and bad-quality grout mixture resistivities recorded from underground experimental support holes are lower in magnitude when compared to similar-quality grout mixture resistivity values recorded in control support holes in the laboratory. The lowering of underground grout resistivity values is thought to be caused by

high rock temperatures that modify the grout hydration reactions. It was also noted that there was an amplified lowering of grout resistivity values with an increasing distance into the rock face thought to be caused by an increase in temperature with increasing distance into the rock face.

Further analysis focused on the sensitivity of grout sensor technology in capturing the rapid curing of grout over 35 days. Grout resistivity plotted over a 35-day curing period revealed a rapid increase in grout resistivity values that occurred irrespective of grout mixture quality and grout sensor position. The rapid increases in grout resistivity over this period were thought to be caused by the formation of a hardened mixture that is resistive to the flow of electrical current. It was also observed in the grout resistivity-curing age plots that each different quality grout mixture has a different rate of resistivity change over the lower, middle and upper grout sensors.

It can thus be concluded that grout sensor technology installed into support holes is sensitive to the setting of the column of the grout and is measurable using three independent grout sensors installed into each support hole.

The third research question was whether grout sensor technology can be used to determine the effectiveness of grout over time.

The analysis of the effectiveness of grout using grout sensor technology focused on detecting the loss of grout during grouting operations of 1.2 m

and 4.5 m long support holes underground and the shrinkage of grout over time. The results of the detection of grout loss and shrinkage showed that the loss and shrinkage of grout inside underground experimental support holes can be detected immediately following grouting operations and over time in support holes equipped with grout sensor technology. In this respect, grout sensor technology log sheets stored in memory of the GDT100 meter showed high and unvarying grout resistivity values (> 60 KΩ) and an “OPEN” grout detection status when there was no grout present inside the support hole due to loss and shrinkage.

The effectiveness of grout was also presented as the prediction of the bond strength developed between the interface of an 18 mm diameter cable anchor and good, fair, and bad-quality grout mixtures using grout resistivity data. This workflow was found to be similar to that used by Wei et al (2012) and Choo et al (2021) presented in the literature survey where these researchers used electrical resistivity recordings to find cement mortar and cement-sands compressive strength predictive functions. The results of the bond strength prediction from grout resistivity showed that the bond strengths of good, fair, and bad-quality grout mixtures to the cable anchor interface can be determined over time with reasonable accuracy (generally less than 33% MAPE) using grout sensor technology.

It can thus be concluded that grout sensor technology can be used to determine the effectiveness of grout over time. This conclusion validates the hypothesis that grout sensor data recorded in the background can be

analyzed to answer all research questions posed in this research study. Overall, it can be concluded that the novel grout sensor technology can be used to verify the quality and performance of grout helping to eliminate the sub-standard grouting of long cable and rock bolt support holes at the South Deep mine thus improving the health and safety aspects of mining.

6.5 Research Limitations

- There was limited access to the mine study site which limited the recording of grout sensor data to one data point per week as opposed to recording a high-density grout resistivity dataset. A denser grout resistivity dataset can more accurately describe the quality and performance of different quality grout mixtures.
- The recording of grout sensor data underground was limited to support holes drilled into the sidewalls of excavations whereas in the laboratory grout sensor data was recorded in vertical simulated support holes. It is possible that the underground recordings experiments could be modified by the orientation of the support hole thus introducing extra variables into the scientific hypothesis testing.

6.6 Recommendations

It is recommended that grout sensor technology should incorporate more than three grout sensors to reduce the unmonitored length along the column of grout installed inside the support hole. In this regard, it is recommended to install 3 grout sensors per metre length of each support hole.

It is also recommended that the grout detector meter and its functionalities be converted to a tablet-installed easy-to-use grout sensor program to allow the capture and the real-time display of resistivity on-site during quality control of underground support holes. Each tablet should feature means to easily connect to a support hole to take grout sensor readings.

6.7 Further Work

Further work is suggested to be carried out at the underground study site. It is suggested that a set of vertical 1.2 m, 4.5 m, and 6.5 m long support holes be drilled and evaluated using grout sensor technology near advancing mining faces as well as in stopes before backfilling. This will assess the use, performance and suitability of grout sensor technology in different-length support holes under active mining conditions as well assess the shrinkage documented in long-hole stopes over time.

It is also suggested that grout sensor data be recorded for a few hours per day to accumulate a high-density grout sensor dataset to refine the one-day grout resistivity to grout–cable anchor bond strength correlations. Further work is suggested to include the overcoring of several support holes to verify and confirm the full-column grouting, grout loss, and grout shrinkage documented by grout sensor technology.

In addition, further work is suggested to include compressive strength testing of different quality grout cubes/cylinders. Compressive strength is a

readily usable index to describe the strength of grout and Portland cement and can be easily correlated to grout sensor technology resistivity data.

Lastly, pull-out testing of support holes equipped with grout sensor technology is suggested as further work to understand the pull-out resistance of cable anchors grouted in different quality mixtures when both a cable anchor and grout cables are installed into a support hole.

REFERENCE LIST

ASTM D4435, 2014. *Standard test method for rock bolt anchor pull test,* West Conshocken, PA, USA: ASTM International.

ASTM-C157, 2014. *Standard test method for length change of hardened hydraulic-cement mortar and concrete,* West Conshocken, PA, USA: ASTM International.

Bacic, M; Gavin, K; Konacevic, M S, 2018. Trends in non-destructive testing of rock bolts. *Gradevinar,* 71(10), pp. 823-831.

Bawden, W. F., Dube, S. & Hyett, A. J., 1994. *A laboratory study on the capacity of fully grouted cable bolts subjected to combined axial and lateral loads,* Kingston, Ontario, Canado: Report to URIF.

Beard, M. D. & Lowe, M. J. S., 2003. Non-destructive testing of rockbolts using guided ultrasonic waves. *International Journal Of Rock Mechanics & Mining Sciences,* Volume 40, pp. 527-536.

Benmokrane, B., Chennouf, A. & Mitri, H. S., 1995. Laboratory evaluation of cement-based grouts and grouted rock anchors. *International Journal Of Rock Mechanics And Mining Sciences & Geomechanics,* 32(7), pp. 633-642.

Bentz, D. P., Jones, S. Z., Peltz, M. A. & Stutzman, P. E., 2015. Mitigation of autogenous shrinkage in repair mortars via internal curing. *Concrete in Australia,* 41(4), pp. 35-39.

Bohloli, B. et al., 2019. Cements for tunnel grouting - Rheology and flow properties tested at different temperatures. *Tunnelling and Underground Space Technology,* Volume 91, pp. 1-10.

Buys, B. J., Heyns, P. S. & Loveday, P. W., 2009. Rock bolt condition monitoring using ultrasonic guided waves. *The Journal of The Southern African Institute of Mining and Metallurgy,* Volume 108, pp. 95-105.

Carino, N. J., 1984. The maturity method: theory and application. *Cement Concrete Aggregates,* 6(2), pp. 61-73.

Chekired, M., Benmokrane, B. & Mitri, H. S., 1997. Laboratory evaluation of a new cable bolt tension measuring device. *International Journal of Rock Mechanics & Mining Science,* 34(3-4).

Chen, J., Hagan, P. C. & Serkan, S., 2016. Parametric study on the axial performance of a fully grouted cable bolt with a new pull-out test. *International Journal of Mining Science and Technology,* Volume 26, pp. 53-58.

Chen, J., He, F. & Zhang, S., 2020. A study of the load transfer behavior of fully grouted rock bolts with analytical modelling. *International Journal Of Mining Science And Technology,* Volume 30, pp. 105-109.

Choo, H., Lee, W. & Lee, C., 2021. Impact of curing time on UCS-electrical resistivity relation of cement grouted sands. *Geomechanics And Engineering,* 27(3), pp. 253-262.

Craig, P. et al., 2021. Stress corrosion cracking of rockbolts: An in-situ testing approach. *Construction and Building Materials,* Volume 269, p. 121275.

De la Varga, I. & Graybeal, B., 2016. *Dimensional stability of grout-type materials used as connections for prefabricated bridge elements,* Washington, DC: Federal Highway Administration.

De la Varga, I., Haber, Z. B. & Graybeal, B. A., 2018. Enhancing shrinkage properties and bond performance of prefabricated bridge deck connection grouts: material and component testing. *Journal of Materials in Civil Engineering,* 30(4).

Dong, B. et al., 2016. Evolutionary trace for early hydration of cement paste using electrical resistivity method. *Construction and Building Materials,* Volume 119, pp. 16-20.

Dorion, J. F., 2019. *Corroded rock support issues: implementation of an investigation and rehabilitation program.* Sudbury, Canada, Australian Centre for Geomechanics.

Elliasson, J. et al., 2014. A feasibility study of SOA-enabled networked rock bolts. *IEEE Emerging Technology and Factory Automation,* pp. 1-8.

Fabchem Mining, 2022. *Fabchem Mining.* [Online] Available at: https://www.fabchem.co.za/wp-content/uploads/2022/08/Fabchem-Mining-Product-Brochure.pdf [Accessed 18 10 2022].

Feng, X., Zhang, N., Li, G. & Guo, G., 2017. Pullout test on fully grouted bolt sheathed by different length of segmented steel tubes. *Shock And Vibration,* Volume 2017.

Forbes, B., Vlachopoulos, N., Diederichs, M. S. & Aubertin, J., 2020. Augmenting the in-situ rock bolt pull test with disturbed optical fiber strain sensing. *International Journal of Rock Mechanics and Mining Sciences,* Issue 26.

Gartner, E. M., Young, J. F., Damidot, D. A. & Jawed, I., 2002. Hydration of Portland cement. In: J. Bensted & P. Barnes, eds. *Structure and performance of cements.* New York: Spon Press, pp. 57-108.

Gold Fields, 2020. *Gold Fields minerals resources and mineral reserves supplement ,* Johannesburg: Gold Fields.

Gustafsson, L. K., 2016. *Sensor techniques to monitor installation and status of rock bolts.* Kulturens Hus, Luleå, Sweden, In Proceedings of the Eighth International Symposium on Ground Support in Mining and Underground Construction: “Ground Support 2016”.

Hadjigeorgiou, J. & Tomasone, P., 2018. *Characterising the behaviour of rockbolts based on in situ pull tests.* Perth, Australia, Caving 2018: Proceedings of the Fourth International Symposium on Block and Sublevel Caving.

Hagen, A. S., Larsen, T., Berghorst, A. & Knox, G., 2020. Full-scale rockbolt testing in the laboratory: Analysis Of Recent Results. *The Journal of the Southern African Institute of Mining and Metallurgy,* Volume 120, pp. 1-6.

Heikal, M., El-Didamony, H. & Morsy, M. S., 2000. Limestone-filled pozzolanic cement. *Cement and Concrete Research,* Volume 30, pp. 1827-1834.

Hoek, E. & Brown, E. T., 1980. Underground excavations in rock. *London Institution of Mining and Metallurgy,* p. 527.

Hoek, E., Kaiser, P. K. & Bawden, W. F., 2000. *Support of Underground Excavations in Hard Rock.* 1st Edition ed. s.l.:CRC Press.

Hoek, E. & Wood, D. F., 1987. Support in underground hard rock mines. *Underground Support Systems,* Volume 35, pp. 1-6.

Hudson, J. A. & Harrison, J. P., 1997. *Engineering rock mechanics: An introduction to the principles.* 1st Edition ed. s.l.:Elsevier Science.

Hutchison, D. J. & Diederichs, M. S., 1996. *Cablebolting In Underground Mines.* Richmond: Bi Tech Publishers.

Hyett, A. J., Bawden, W. F. & Reichert, R. D., 1992. The effect of rock mass confinement on the bond strength of fully grouted cable bolts. *International Journal Of Rock Mechanics And Mineral Sciences & Geomechanics Abastracts,* 29(5), pp. 503-524.

Jalalifar, H., 2011. An analytical solution to predict axial load along fully grouted bolts in an elasto-plastic rock mass. *The Journal of The Southern African Institute Of Mining And Metallurgy,* Volume 111, pp. 809-814.

Jiang, T. et al., 2016. Monitoring of grouting compactness in a post-tensioning tendon duct using piezoceramic transducers. *Sensors,* Volume 16, p. 1343.

Kelly, A. M. & Jager, A. J., 1996. *Critically evaluate techniques for the in situ tetsing of steel tendon grouting effectiveness as a basis for reducing fall of ground injuries and fatalities,* Johannesburg, South Africa: Safety In Mines Research Advisory Committee (SIMRAC).

Kilic, A., Yasar, E. & Celik, A. G., 2002. Effect of grout properties on the pull-out load capacity of fully grouted rock bolt. *Tunnelling And Underground Space Technology,* Volume 17, pp. 355-362.

Kim, H. et al., 2019. Classification of factors affecting the performance of fully grouted rock bolts with empirical classification systems. *Applied Sciences,* 9(22).

Klun, M., Bosiljkov, V. & Bokan-Bosiljkov, V., 2021. The Relation between concrete, mortar and paste early age properties. *Materials,* Volume 14, p. 1569.

Kucharczykova, B. et al., 2017. Comparison of Measurements Methods Intended to Determination of the Shrinkage Development in Polymer Cement Mortars. *Procedia Engineering,* Volume 195, pp. 17-23.

Lecieux, Y. et al., 2018. Towards a 3D shrinkage measurement in concrete using an embedded strain sensor. *Smart Materials and Structures,* Volume 27.

Li, C. C., 2017. Rockbolting: Prinicples and Applications. *Journal of Rock Mechanics And Geotechnical Engineering,* Volume 9, pp. 396-414.

Li, C. C., Kristjansson, G. & Hoien, A. H., 2016. Critical embedment length and bond strength of fully encapsulated rebar rockbolts. *Tunnelling and Underground Space Technology,* Volume 59, pp. 16-23.

Littlejohn, G. S. & Bruce, D. A., 1975. Rock anchors - state of the art. *Ground Engineering,* 8(3), pp. 25-32.

Li, X. et al., 2022. Effect of pretension on the performance of cable bolts and its optimisation in underground coal mines with various geological conditions. *International Journal of Rock Mechanics and Mining Sciences,* Volume 152.

Liu, L., Li, S., Jiang, X. & Tao, F., 2022. A new two-sensor non-destructive testing method of grouted rock bolts. *Construction and Building Materials,* Volume 317.

Liu, Z., Zhang, Y. & Jiang, Q., 2014. Continuous tracking of the relationship between resistivity and pore structure of cement pastes. *Construction and Building Materials,* Volume 53, pp. 26-31.

Lu, Y. et al., 2018. Study on the effect of chloride ion on the early age hydration process of concrete by a non-contact monitoring method. *Construction and Building Materials,* Volume 172, pp. 499-508.

Lura, P., Jensen, O. M. & van Breugel, K., 2003. Autogenous shrinkage in high-performance cement paste: An evaluation of basic mechanisms. *Cement and Concrete Research,* Volume 33, pp. 223-232.

Maepa, T. G. & Zvarivadza, T., 2017. Installation of resin-grouted rockbolts in hard rock mining:challenges and solutions for improved safety. *The Journal of the Southern Institute of Mining and Metallurgy,* Volume 117, pp. 329-336.

Mark, C., Compton, C. S., Dolinar, D. R. & Oyler, D. C., 2003. *Field performance testing of fully grouted roof bolts.* Cincinnati, Ohio, SME Annual Meeting, pp. 1-8.

Martin, L. B., Tijani, M., Hadj-Hassen, F. & Noiret, A., 2013. Assessment Of The Bolt Grout Interface Behaviour Of Fully Grouted Rockbolts From Laboratory Experiments Under Axial Loads. *International Journal Of Rock Mechanics & Mining Sciences,* Volume 63, pp. 50-61.

Martin, L., Pakalnis, R. & Milne, D., 2002. *Determination of physical properties of cable bolts in cement grout pull tests using instrumented*

king wires. Vancouver, British Columbia, Canadian Institute of Mining Annual Conference.

McCarter, W. J., 1999. *The application of impedance spectroscopy to cementitious systems,* s.l.: Solatron Limited.

Menu, B., Jolin, M. & Bissonnette, B., 2017. Studies on the influence of drying shrinkage test procedure, specimen geometry, and boundary conditions on free shrinkage. *Advances in Materials Science and Engineering,* Volume 2017.

Minerals Council, 2021. *Facts and figures 2021, changing mines, changing lives.* [Online]
Available at: https://www.mineralscouncil.org.za/industry-news/publications/facts-and-figures
[Accessed 11 7 2022].

Mohan, M. K., Pillai, R. G., Santhanam, M. & Gettu, R., 2021. High-performance cementitious grout with fly ash for corrosion protection of post-tensioned concrete structures. *Construction and Building Materials,* Volume 281.

Morsy, M. S., 1999. Effect of temperature on electrical conductivity of blended cement pastes. *Cement And Concrete Research,* Volume 29, pp. 603-606.

Newlands, M. D., Paine, K. A., Vemuri, N. A. & Dhir, R. K., 2008. A linear test method for determining early-age shrinkage of concrete. *Magazine of Concrete Research,* 60(10), pp. 747-757.

Pei, H., Shao, H. & Li, Z., 2017. A novel early-age shrinkage measurement method based on non-contact electrical resistivity and FBG sensing techniques. *Construction and Building Materials,* Volume 156, pp. 1158-1162.

Permeh, S., Lau, K. & Tansel, B., 2021. Moisture and ion mobilization and stratification in post-tensioned (PT) grout during hydration. *Case Studies in Construction Materials,* 15(18).

Preston, R. P., Roy, J. M. & Bewick, R. P., 2019. *Rusty bolts: planning for corrosion of ground support in underground mines.* Perth, Australia, Australian Centre for Geomechanics.

Reny, S., Pena Cruz, J. & Clements, W., 2019. *Development of a new cementitious grout for permafrost conditions.* Sudbury, Canada, Australian Centre for Geomechanics.

Ryder, J. A. & Jager, A. J., 2002. *A textbook on rock mechanics for tabular hard rock mines.* Johannesburg: Safety In Mines Research Advisory Committee.

Sang, Y., Yang, Y. & Zhao, Q., 2022. Electrical resistivity of plain cement-based materials based on ionic conductivity: A review of applications and conductive models. *Journal of Building Engineering,* Volume 46.

Satyarno, I. et al., 2014. Practical method for mix design of cement-based grout. *Procedia Engineering,* Volume 95, pp. 356-365.

Sbartai, Z. M. et al., 2007. Using radar direct wave for concrete condition assessment: Correlation with electrical resistivity. *Journal of Applied Geophysics,* Volume 62, pp. 361-374.

Shamsuddoha, M. et al., 2019. Long-term mechanical and shrinkage properties of cementitious grouts for structural repair. *RILEM Technical Letters,* Volume 4, pp. 9-15.

Singh, D. R., Agrawal, H. & Manna, C., 2016. Analysis of un-tensioned fully grouted rock bolt: A case study. *Recent Advances in Rock Engineering ,* pp. 110-117.

Singh, P., Jang, H. & Spearing, A. J., 2022. Improving the numerical modelling of in-situ rock bolts using axial and bending strain data from instrumented bolts. *Geotechnical and Geological Engineering,* Volume 40, pp. 2631-2655.

Singh, S. & Srivastava, A. K., 2021. Numerical simulation of pull-out test on cable bolts. *Materials Today: Proceedings,* Volume 45, pp. 6332-6340.

Skrzypkowski, K., Korzeniowski, W., Zagorski, K. & Zagorska, A., 2020. Modified rock bolt support for mining method with controlled roof bending. *Energies,* Volume 13, p. 1868.

Song, G., Li, W., Wang, B. & Ho, S. C., 2017. A review of rock bolt monitoring using smart sensors. *Journal Of Sensors,* 17(4), p. 776.

Stacey, T. R., 2012. A philosophical view on the testing of rock support for rockburst conditions. *The Journal of The Southern African Institute Of Mining And Metallurgy,* Volume 112, pp. 703-710.

Tang, B. et al., 2018. Application of a FBG-based instrumented rock bolt in a TBM-excavated coal mine roadway. *Journal of Sensors,* Volume 2018.

Teixeira, K. P. et al., 2016. The effect of curing temperature on the properties of cement pastes modified with TiO2 nanoparticles. *Materials,* Volume 9, p. 952.

Terzioglu, T. et al., 2018. Nondestructive evaluation of grout defects in internal tendons of post-tensioned girders. *NDT and E International,* Volume 99, pp. 23-35.

Thenevin, I. et al., 2017. Laboratory pull-out tests on fully grouted rock bolts and cable bolts: Results and lessons learned. *Journal of Rock Mechanics and Geotechnical Engineering,* Volume 9, pp. 843-855.

Thompson, A. G., 2004. *Performance of cable bolt anchors - An update.* Santiago, Chile, Instituto de Ingenerios de Chile Santiago, pp. 317-323.

Thompson, A. G. & Villaescusa, E., 2014. Case studies of rock reinforcement components and systems testing. *Rock Mechanics and Rock Engineering,* 47(5), pp. 1589-1602.

Tian, Y. et al., 2020. A mathematical model for the electrical resistivity of cement paste at early ages considering the partially saturated state. *Materials,* 13(15), p. 3306.

Tomasone, P., Bahrani, N. & Hadjigeorgiou, J., 2020. Practical considerations in the modelling of resin-grouted rockbolts. *Journal of the Southern African Institute of Mining and Metallurgy,* 120(6), pp. 385-392.

Vallati, O., Roach, W. & Weaver, S., 2020. *Ground support and strata monitoring: what is needed?.* Perth, Australia, Proceedings of the Second International Conference on Underground Mining Technology, pp. 285-296.

Vasumithran, M., Anand, K. B. & Sathyan, D., 2020. Effects of fillers on the properties of cement grouts. *Construction and Building Materials,* Volume 246.

Villaescusa, E., Hassell, R. & Thompson, A. G., 2008. Development of a corrosivity classification for cement grouted cable strand In uinderground hard-rock mining. *Journal Of The Southern African Institute Of Mineralogy And Metallurgy,* 108(6), pp. 301-308.

Vincent, N. A., Shivashankar, R., Lokesh, K. N. & Jacob, J. M., 2017. Laboratory electrical resistivity studies on cement stabilized soil. *International Scholarly Research Notices,* Volume 1, pp. 1-15.

Vlachopoulos, N., Cruz, D. & Forbes, B., 2018. Utilizing a novel fiber optic technology to capture the axial responses of fully grouted rock bolts. *Journal of Rock Mechanics and Geotechnical Engineering,* Volume 10, pp. 222-235.

Wei, X., Xiao, L. & Li, Z., 2012. Prediction of standard compressive strength of cement by the electrical resistivity measurement. *Construction And Building Materials,* Volume 31, pp. 341-346.

Windsor, C. R., 1997. Rock reinforcement systems. *International Journal of Rock Mechanics & Mining Sciences,* 34(6), pp. 919-951.

Xu, B. et al., 2021. Experimental study on grout defects detection for grouted splice sleeve connectors using stress wave measurement. *Construction and Building Materials,* Volume 274.

Yazici, S. & Kaiser, P. K., 1992. Bond strength of grouted cable bolts. *International Journal Of Rock Mechanics, Mineral Sciences & Geomechanics Abstracts,* 29(3), pp. 279-292.

Yoo, D.-Y., Ryu, G.-S., Yuan, T. & Koh, K.-T., 2017. Mitigating shrinkage cracking in posttensioning grout using shrinkage-reducing admixture. *Cement and Concrete Composites,* Volume 81, pp. 97-108.

Yoon, B., Lee, W., Lee, C. & Choo, H., 2020. Time-dependent variations of compressive strength and small-strain stiffness of sands grouted with microfine cement. *Journal of Geotechnical and Geoenvironmental Engineering,* 146(4).

Zhang, J. & Li, Z., 2017. *Comparison of early age resistivity development between Ordinary Portland Cement and Calcium Sulfoaluminate Cement.* Montreal, Canada, National Research Council of Canada.

Zhang, S., Qiao, W.-G., Chen, P.-C. & Xi, K., 2019. Rheological and mechanical properties of microfine-cement-based grouts mixed with microfine fly ash, colloidal nanosilica and superplasticizer. *Construction and Building Materials,* Volume 212, pp. 10-18.

Zhao, X., Li, H., Zhang, S. & Yang, X., 2019. Stability analyses and cable bolt support design for a deep large-span stope at the Hongtoushan mine, China. *Sustainability,* Volume 11, p. 6134.

Zou, D. H., Cheng, J., Yue, R. & Sun, X., 2010. Grout quality and its impact on guided ultrasonic waves In grouted rock bolts. *Journal Of Applied Geophysics,* Volume 72, pp. 102-106.

APPENDIX

A. Grout Sensor Technology Datasets

Table_A-1. Grout sensor technology datasets recorded in the laboratory and underground.

LABORATORY GROUT SENSOR DATA								
CE06								
BLUE_TimeStamp	**BLUE_Status**	**BLUE_Resist**	**GREEN_TimeStamp**	**GREEN_Status**	**GREEN_Resist**	**RED_TimeStamp**	**RED_Status**	**RED_Resist**
12:25:24	OK	59631	12:25:24	OK	52953	12:25:24	OK	52953
12:25:55	OK	4557	12:26:00	OK	2253	12:26:30	OK	15950
12:36:11	OK	2343	12:36:11	OK	2155	12:36:11	OK	11697
12:44:40	OK	2271	12:44:40	OK	2050	12:44:40	OK	11315
12:55:11	OK	2297	12:55:11	OK	2048	12:55:11	OK	11275
13:04:52	OK	2280	13:04:52	OK	2061	13:04:52	OK	12014
13:15:12	OK	2359	13:15:12	OK	2092	13:15:12	OK	12319
13:25:38	OK	2369	13:25:38	OK	2077	13:25:38	OK	12222
13:35:06	OK	4276	13:35:06	OK	2648	13:35:06	OK	52953
09:45:26	OK	6435	09:45:26	OK	2668	09:45:26	OK	52953
13:18:00	OK	7553	13:18:00	OK	2694	13:18:00	OK	57405
09:43:47	OK	8174	09:43:47	OK	2784	09:43:47	OK	57405
12:53:00	OK	10072	12:53:00	OK	2792	12:53:00	OK	52953
09:35:15	OK	13822	09:35:15	OK	2639	09:35:15	OK	52953
13:31:32	OK	11765	13:31:32	OK	5294	13:31:32	OK	55179
09:24:37	OK	12778	09:24:37	OK	5384	09:24:37	OK	55179
09:55:26	OK	14422	09:55:26	OK	5296	09:55:26	OK	52953
08:46:21	OK	16122	08:46:21	OK	52953	08:46:21	OK	55179
09:57:09	OK	14555	09:57:09	OK	52953	09:57:09	OK	52953
08:53:59	OK	17353	08:53:59	OK	52953	08:53:59	OK	52953
CE05								
BLUE_TimeStamp	**BLUE_Status**	**BLUE_Resist**	**GREEN_TimeStamp**	**GREEN_Status**	**GREEN_Resist**	**RED_TimeStamp**	**RED_Status**	**RED_Resist**
13:33:22	OK	59631	13:33:22	OK	52953	13:33:22	OK	52953
13:33:51	OK	2299	13:33:51	OK	2245	13:33:51	OK	1768

13:44:08	OK	1281	13:44:08	OK	1297	13:44:08	OK	1461
13:52:58	OK	1260	13:52:58	OK	1272	13:52:58	OK	1369
14:02:52	OK	1246	14:02:52	OK	1274	14:02:52	OK	1357
14:13:40	OK	1236	14:13:40	OK	1277	14:13:40	OK	1353
14:23:34	OK	1228	14:23:34	OK	1279	14:23:34	OK	1339
14:33:58	OK	1233	14:33:58	OK	1287	14:33:58	OK	1332
14:43:36	OK	2375	14:43:36	OK	3390	14:43:36	OK	3997
09:52:57	OK	4184	09:52:57	OK	5190	09:52:57	OK	7087
13:15:38	OK	5101	13:15:38	OK	6785	13:15:38	OK	8845
09:49:11	OK	8901	09:49:11	OK	6371	09:49:11	OK	6466
12:49:32	OK	7457	12:49:32	OK	8068	12:49:32	OK	11863
09:34:01	OK	9762	09:34:01	OK	10981	09:34:01	OK	16715
13:29:56	OK	8435	13:29:56	OK	9344	13:29:56	OK	14403
09:26:13	OK	9213	09:26:13	OK	9083	09:26:13	OK	14716
09:57:16	OK	9985	09:57:16	OK	10136	09:57:16	OK	15175
08:45:00	OK	12644	08:45:00	OK	10888	08:45:00	OK	18040
09:55:58	OK	10460	09:55:58	OK	10376	09:55:58	OK	16319
08:53:11	OK	15050	08:53:11	OK	12764	08:53:11	OK	20143

CE04

BLUE_TimeStamp	BLUE_Status	BLUE_Resist	GREEN_TimeStamp	GREEN_Status	GREEN_Resist	RED_TimeStamp	RED_Status	RED_Resist
10:34:39	OK	59631	10:34:39	OK	52953	10:34:39	OK	52953
10:35:06	OK	2642	10:35:11	OK	2613	10:35:16	OK	4154
10:45:06	OK	1588	10:45:06	OK	1460	10:45:06	OK	2784
10:55:01	OK	1600	10:55:01	OK	1422	10:55:01	OK	2613
11:04:51	OK	1648	11:04:51	OK	1439	11:04:51	OK	2607
11:14:19	OK	1667	11:14:19	OK	1449	11:14:19	OK	2639
11:24:53	OK	1686	11:24:53	OK	1443	11:24:53	OK	2654
11:36:16	OK	1692	11:36:16	OK	1431	11:36:16	OK	2672
11:46:52	OK	3607	11:46:52	OK	2562	11:46:52	OK	2689
09:49:16	OK	6337	09:49:16	OK	4458	09:49:16	OK	4795
13:11:29	OK	9344	13:11:29	OK	5702	13:11:29	OK	6087
09:49:11	OK	8901	09:49:11	OK	6371	09:49:11	OK	6466
12:44:09	OK	13536	12:44:09	OK	8223	12:44:09	OK	8379
09:32:36	OK	21068	09:32:36	OK	13019	09:32:36	OK	12892
13:27:08	OK	18040	13:27:08	OK	10460	13:27:08	OK	10488
09:20:41	OK	15568	09:20:41	OK	10981	09:20:41	OK	11070
09:53:13	OK	18515	09:53:13	OK	13139	09:53:13	OK	12764
08:35:28	OK	23188	08:35:28	OK	14403	08:35:28	OK	14403
09:53:51	OK	18782	09:53:51	OK	13274	09:53:51	OK	12764
08:51:44	OK	25303	08:51:44	OK	16306	08:51:44	OK	15925

A06								
BLUE_TimeStamp	BLUE_Status	BLUE_Resist	GREEN_TimeStamp	GREEN_Status	GREEN_Resist	RED_TimeStamp	RED_Status	RED_Resist
13:24:02	OK	59631	13:24:02	OK	52953	13:24:02	OK	52953
13:24:14	OK	2231	13:24:14	OK	3267	13:24:14	OK	3367
13:37:11	OK	1056	13:37:11	OK	1682	13:37:11	OK	2100
13:44:16	OK	1003	13:44:16	OK	1628	13:44:16	OK	2125
13:54:04	OK	938	13:54:04	OK	1538	13:54:04	OK	2053
14:03:49	OK	888	14:03:49	OK	1437	14:03:49	OK	1923
14:14:40	OK	848	14:14:40	OK	1316	14:14:40	OK	1668
14:24:08	OK	832	14:24:08	OK	1261	14:24:08	OK	1598
14:34:59	OK	1038	14:34:59	OK	1383	14:54:59	OK	2202
10:01:06	OK	1716	10:01:06	OK	2359	10:01:06	OK	3914
13:35:03	OK	2403	13:35:03	OK	4629	13:35:03	OK	6435
10:05:40	OK	2588	10:05:40	OK	3763	10:05:40	OK	6271
13:07:03	OK	2721	13:07:03	OK	4215	13:07:03	OK	8549
09:14:34	OK	4039	09:14:34	OK	6401	09:14:34	OK	12530
13:37:50	OK	3163	13:37:50	OK	4893	13:37:50	OK	10626
09:34:56	OK	3211	09:34:56	OK	4455	09:34:56	OK	5036
10:03:59	OK	3837	10:03:59	OK	5281	10:03:59	OK	5723
08:55:02	OK	4053	08:55:02	OK	5594	08:55:02	OK	5972
10:02:08	OK	3916	10:02:08	OK	4836	10:02:08	OK	4557
08:39:19	OK	4914	08:39:19	OK	6535	08:39:19	OK	6307
A05								
BLUE_TimeStamp	BLUE_Status	BLUE_Resist	GREEN_TimeStamp	GREEN_Status	GREEN_Resist	RED_TimeStamp	RED_Status	RED_Resist
12:08:20	OK	59631	12:08:20	OK	52953	12:08:20	OK	52953
12:08:40	OK	2523	12:08:43	OK	2212	12:08:47	OK	2708
12:18:11	OK	1298	12:18:11	OK	1261	12:18:11	OK	1648
12:28:17	OK	1229	12:28:17	OK	1236	12:28:17	OK	1651
12:39:39	OK	1194	12:39:39	OK	1191	12:39:39	OK	1695
12:48:31	OK	1165	12:48:31	OK	1152	12:48:31	OK	1667
12:57:33	OK	1138	12:57:33	OK	1124	12:57:33	OK	1693
13:08:04	OK	1104	13:08:04	OK	1105	13:08:04	OK	1703
13:18:33	OK	2415	13:18:33	OK	2709	13:18:33	OK	4813
09:55:11	OK	3419	09:55:11	OK	3836	09:55:11	OK	7680
13:33:49	OK	4421	13:33:49	OK	5776	13:33:49	OK	10888
10:08:27	OK	4307	10:08:27	OK	5165	10:08:27	OK	11755
13:09:13	OK	5395	13:09:13	OK	7290	13:09:13	OK	15384
09:30:00	OK	8068	09:30:00	OK	10715	09:30:00	OK	21385
13:42:06	OK	6305	13:42:06	OK	8549	13:42:06	OK	8603

09:49:41	OK	7732	09:49:41	OK	5972	09:49:41	OK	3039
10:07:29	OK	7775	10:07:29	OK	8435	10:07:29	OK	4993
09:06:47	OK	7937	09:06:47	OK	8273	09:06:47	OK	5694
10:04:13	OK	8722	10:04:13	OK	8610	10:04:13	OK	5231
08:41:54	OK	10217	08:41:54	OK	10217	08:41:54	OK	7821

A04

BLUE_TimeStamp	BLUE_Status	BLUE_Resist	GREEN_TimeStamp	GREEN_Status	GREEN_Resist	RED_TimeStamp	RED_Status	RED_Resist
10:59:22	OK	59631	10:59:22	OK	52953	10:59:22	OK	52953
11:03:48	OK	1955	11:03:48	OK	2370	11:03:48	OK	4373
11:13:12	OK	1309	11:13:12	OK	1391	11:13:12	OK	1974
11:23:03	OK	1065	11:23:03	OK	1240	11:23:03	OK	1815
11:33:01	OK	1036	11:33:01	OK	1186	11:33:01	OK	1742
11:43:01	OK	1011	11:43:01	OK	1147	11:43:01	OK	1697
11:53:31	OK	989	11:53:31	OK	1117	11:53:31	OK	1653
12:02:55	OK	980	12:02:55	OK	1099	12:02:55	OK	1632
12:12:21	OK	6498	12:12:21	OK	6707	12:12:21	OK	6785
10:05:43	OK	11555	10:05:43	OK	10626	10:05:43	OK	7502
13:30:50	OK	15384	13:30:50	OK	12142	13:30:50	OK	14403
10:02:24	OK	14403	10:02:24	OK	8978	10:02:24	OK	9985
13:04:53	OK	19029	13:04:53	OK	10634	13:04:53	OK	15741
09:31:27	OK	27288	09:31:27	OK	16122	09:31:27	OK	22078
13:39:35	OK	21385	13:39:35	OK	12422	13:39:35	OK	18515
09:32:48	OK	19586	09:32:48	OK	11765	09:32:48	OK	14108
10:06:06	OK	23252	10:06:06	OK	13552	10:06:06	OK	16503
09:01:32	OK	23610	09:01:32	OK	14436	09:01:32	OK	17793
10:03:14	OK	22841	10:03:14	OK	12193	10:03:14	OK	14251
08:43:40	OK	27578	08:43:40	OK	16715	08:43:40	OK	20751

B06

BLUE_TimeStamp	BLUE_Status	BLUE_Resist	GREEN_TimeStamp	GREEN_Status	GREEN_Resist	RED_TimeStamp	RED_Status	RED_Resist
13:07:43	OK	59631	13:07:43	OK	52953	13:07:43	OK	52953
13:08:42	OK	2924	13:08:48	OK	2990	13:08:57	OK	4610
13:18:44	OK	1739	13:18:44	OK	1618	13:18:44	OK	2695
13:29:40	OK	1755	13:29:40	OK	1605	13:29:40	OK	2719
13:38:22	OK	1792	13:38:22	OK	1640	13:38:22	OK	2674
13:48:40	OK	1809	13:48:40	OK	1669	13:48:40	OK	2709
13:58:23	OK	1824	13:58:23	OK	1704	13:58:23	OK	2669
14:08:24	OK	1817	14:08:24	OK	1688	14:08:24	OK	2601
14:18:02	OK	2116	14:18:02	OK	3075	14:18:02	OK	4539
09:29:56	OK	2431	09:29:56	OK	3597	09:29:56	OK	5473

13:26:24	OK	3257	13:26:24	OK	5066	13:26:24	OK	6900
09:58:28	OK	2515	09:58:28	OK	4030	09:58:28	OK	5976
13:00:32	OK	3313	13:00:32	OK	5150	13:00:32	OK	6862
09:38:04	OK	5264	09:38:04	OK	8030	09:38:04	OK	9995
13:37:05	OK	3658	13:37:05	OK	5788	13:37:05	OK	7468
09:31:14	OK	3425	09:31:14	OK	4863	09:31:14	OK	6975
10:00:28	OK	3588	10:00:28	OK	5981	10:00:28	OK	8022
08:49:51	OK	4117	08:49:51	OK	6547	08:49:51	OK	7926
10:01:09	OK	3132	10:01:09	OK	5066	10:01:09	OK	6896
08:51:44	OK	25303	08:51:44	OK	16306	08:51:44	OK	15925

B05

BLUE_TimeStamp	BLUE_Status	BLUE_Resist	GREEN_TimeStamp	GREEN_Status	GREEN_Resist	RED_TimeStamp	RED_Status	RED_Resist
11:44:35	OK	59631	11:44:35	OK	52953	11:44:35	OK	52953
11:45:08	OK	2838	11:45:16	OK	3515	11:45:25	OK	4199
11:54:26	OK	1449	11:54:26	OK	1874	11:54:26	OK	1773
12:04:54	OK	1270	12:04:54	OK	1701	12:04:54	OK	1433
12:14:14	OK	1238	12:14:14	OK	1742	12:14:14	OK	1436
12:23:54	OK	1186	12:23:54	OK	1662	12:23:54	OK	1360
12:35:04	OK	1160	12:35:04	OK	1645	12:35:04	OK	1422
12:44:15	OK	1121	12:44:15	OK	1616	12:44:15	OK	1484
12:54:03	OK	5255	12:54:03	OK	4012	12:54:03	OK	3035
09:37:25	OK	5419	09:37:25	OK	4356	09:37:25	OK	2505
13:23:54	OK	7874	13:23:54	OK	6367	13:23:54	OK	4053
09:56:20	OK	5859	09:56:20	OK	4956	09:56:20	OK	2700
12:58:50	OK	8549	12:58:50	OK	6181	12:58:50	OK	3941
09:39:23	OK	15050	09:39:23	OK	10383	09:39:23	OK	6367
13:34:28	OK	9914	13:34:28	OK	7047	13:34:28	OK	4322
09:49:41	OK	7732	09:49:41	OK	5972	09:49:41	OK	3039
09:58:51	OK	9281	09:58:51	OK	7011	09:58:51	OK	3675
08:48:40	OK	10803	08:48:40	OK	7549	08:48:40	OK	3848
09:58:38	OK	7801	09:58:38	OK	6091	09:58:38	OK	2956
08:46:55	OK	4086	08:46:55	OK	7468	08:46:55	OK	9221

B04

BLUE_TimeStamp	BLUE_Status	BLUE_Resist	GREEN_TimeStamp	GREEN_Status	GREEN_Resist	RED_TimeStamp	RED_Status	RED_Resist
10:28:27	OK	59631	10:28:27	OK	52953	10:28:27	OK	52953
10:38:59	OK	3040	10:38:59	OK	3503	10:38:59	OK	4487
10:47:45	OK	2622	10:47:45	OK	3139	10:47:45	OK	4014
10:58:34	OK	1608	10:58:34	OK	2006	10:58:34	OK	2401
11:08:15	OK	1523	11:08:15	OK	1863	11:08:15	OK	2259

11:17:57	OK	1505	11:17:57	OK	1833	11:17:57	OK	2203
11:28:34	OK	1509	11:28:34	OK	1838	11:28:34	OK	2174
11:39:12	OK	1476	11:39:12	OK	1870	11:39:12	OK	2243
11:49:57	OK	1342	11:49:57	OK	2056	11:49:57	OK	3191
09:41:46	OK	2019	09:41:46	OK	2660	09:41:46	OK	4261
13:18:57	OK	2526	13:18:57	OK	4084	13:18:57	OK	7047
09:53:22	OK	2127	09:53:22	OK	2854	09:53:22	OK	4629
12:54:31	OK	2495	12:54:31	OK	3825	12:54:31	OK	6975
09:36:31	OK	3485	09:36:31	OK	6341	09:36:31	OK	10994
13:33:49	OK	2674	13:33:49	OK	4217	13:33:49	OK	7830
09:28:03	OK	2381	09:28:03	OK	3318	09:28:03	OK	5751
10:02:25	OK	2593	10:02:25	OK	3676	10:02:25	OK	6785
08:47:26	OK	2909	08:47:26	OK	4128	08:47:26	OK	7507
09:59:55	OK	2376	09:59:55	OK	3193	09:59:55	OK	6153
08:39:19	OK	4914	08:39:19	OK	6535	08:39:19	OK	6307

C27

BLUE_TimeStamp	BLUE_Status	BLUE_Resist	GREEN_TimeStamp	GREEN_Status	GREEN_Resist	RED_TimeStamp	RED_Status	RED_Resist
12:28:04	OK	55179	12:28:04	OK	52953	12:28:04	OK	52953
12:28:34	OK	4154	12:28:44	OK	2990	12:28:53	OK	5442
12:38:10	OK	2302	12:38:10	OK	1904	12:38:10	OK	3258
12:47:37	OK	2248	12:47:37	OK	1867	12:47:37	OK	3169
12:58:58	OK	2237	12:58:58	OK	1857	12:58:58	OK	3006
13:08:56	OK	2260	13:08:56	OK	1935	13:08:56	OK	2953
13:17:56	OK	2274	13:17:56	OK	2005	13:17:56	OK	2805
13:30:19	OK	2273	13:30:19	OK	1994	13:30:19	OK	2743
13:40:03	OK	9694	13:40:03	OK	10981	13:40:03	OK	7246
12:16:47	OK	9985	12:16:47	OK	14565	12:16:47	OK	8491
10:07:32	OK	17565	10:07:32	OK	24413	10:07:32	OK	16701
09:05:49	OK	20751	09:05:49	OK	27812	09:05:49	OK	20143
08:43:02	OK	24575	08:43:02	OK	33873	08:43:02	OK	24835
10:20:52	OK	29580	10:20:52	OK	36515	10:20:52	OK	27812
14:00:27	OK	21731	14:00:27	OK	30916	14:00:27	OK	24413
08:46:00	OK	33873	08:46:00	OK	39597	08:46:00	OK	30916
09:43:39	OK	35634	09:43:39	OK	40811	09:43:39	OK	31584
08:43:47	OK	39597	08:43:47	OK	43240	08:43:47	OK	33873
10:23:18	OK	36515	10:23:18	OK	43389	10:23:18	OK	32347
08:39:00	OK	42025	08:39:00	OK	47611	08:39:00	OK	38569

C54

BLUE_TimeStamp	BLUE_Status	BLUE_Resist	GREEN_TimeStamp	GREEN_Status	GREEN_Resist	RED_TimeStamp	RED_Status	RED_Resist

13:19:11	OK	55179	13:19:11	OK	52953	13:19:11	OK	57405
13:19:47	OK	4452	13:19:55	OK	4574	13:20:02	OK	4228
13:30:19	OK	2273	13:30:19	OK	1994	13:30:19	OK	2743
13:42:19	OK	2120	13:42:19	OK	1839	13:42:19	OK	7507
13:52:34	OK	5029	13:52:34	OK	1817	13:52:34	OK	25567
14:02:08	OK	7170	14:02:08	OK	1758	14:02:08	OK	36661
14:12:08	OK	8500	14:12:08	OK	2400	14:12:08	OK	42000
14:22:08	OK	6500	14:22:08	OK	3760	14:22:08	OK	47500
14:32:39	OK	3863	14:32:39	OK	5802	14:32:39	OK	55179
14:42:51	OK	4629	14:42:51	OK	9484	14:42:51	OK	55179
10:10:54	OK	8223	10:10:54	OK	16503	10:10:54	OK	55179
09:08:23	OK	10066	09:08:23	OK	20434	09:08:23	OK	57405
08:47:48	OK	10298	08:47:48	OK	24413	08:47:48	OK	52953
10:22:23	OK	11863	10:22:23	OK	26764	10:22:23	OK	57405
14:01:11	OK	12061	14:01:11	OK	17599	14:01:11	OK	52953
08:47:41	OK	15223	08:47:41	OK	30916	08:47:41	OK	57405
09:42:33	OK	18515	09:42:33	OK	33873	09:42:33	OK	55179
08:42:31	OK	21068	08:42:31	OK	36515	08:42:31	OK	55179
10:24:19	OK	19296	10:24:19	OK	33551	10:24:19	OK	52953
08:37:49	OK	24413	08:37:49	OK	39597	08:37:49	OK	55179

C14

BLUE_TimeStamp	BLUE_Status	BLUE_Resist	GREEN_TimeStamp	GREEN_Status	GREEN_Resist	RED_TimeStamp	RED_Status	RED_Resist
13:46:32	OK	57405	13:46:32	OK	52953	13:46:32	OK	55179
13:46:52	OK	3549	13:47:11	OK	3461	13:47:35	OK	5782
13:57:12	OK	1966	13:57:12	OK	2009	13:57:12	OK	5105
14:07:55	OK	1859	14:07:55	OK	1893	14:07:55	OK	5235
14:17:16	OK	1838	14:17:16	OK	1837	14:17:16	OK	5252
14:27:16	OK	1809	14:27:16	OK	1795	14:27:16	OK	5125
14:35:22	OK	1844	14:35:22	OK	1779	14:35:22	OK	5050
14:47:24	OK	1879	14:47:24	OK	1763	14:47:24	OK	5035
14:57:28	OK	17125	14:57:28	OK	15384	14:57:28	OK	33110
12:27:24	OK	23570	12:27:24	OK	19563	12:27:24	OK	39597
10:13:19	OK	34753	10:13:19	OK	29580	10:13:19	OK	47611
09:11:56	OK	36515	09:11:56	OK	31584	09:11:56	OK	47611
08:50:17	OK	43240	08:50:17	OK	36515	08:50:17	OK	52953
10:23:31	OK	45789	10:23:31	OK	37542	10:23:31	OK	52953
14:02:33	OK	36515	14:02:33	OK	32448	14:02:33	OK	52953
08:48:48	OK	44697	08:48:48	OK	42025	08:48:48	OK	52953
09:39:56	OK	47611	09:39:56	OK	43240	09:39:56	OK	52953
08:41:19	OK	48835	08:41:19	OK	47611	08:41:19	OK	52953
10:25:12	OK	48989	10:25:12	OK	45318	10:25:12	OK	52953

08:34:37	OK	51172	08:34:37	OK	47999	08:34:37	OK	52953

UNDERGROUND GROUT SENSOR DATA (1,2 m UNITS)								
U12CE06								
BLUE_TimeStamp	**BLUE_Status**	**BLUE_Resist**	**GREEN_TimeStamp**	**GREEN_Status**	**GREEN_Resist**	**RED_TimeStamp**	**RED_Status**	**RED_Resist**
11:05:40	OK	57405	11:05:40	OK	57405	11:05:40	OK	59631
11:46:06	OK	1510	11:46:04	OK	2101	11:46:03	OK	1434
11:56:29	OK	977	11:56:29	OK	993	11:56:29	OK	884
12:06:23	OK	1071	12:06:23	OK	1032	12:06:23	OK	876
12:16:25	OK	1122	12:16:25	OK	1051	12:16:25	OK	858
12:26:23	OK	1186	12:26:23	OK	1072	12:26:23	OK	855
12:36:19	OK	1209	12:36:19	OK	1093	12:36:19	OK	873
12:46:32	OK	1225	12:46:32	OK	1112	12:46:32	OK	895
09:24:35	OK	25772	09:24:35	OK	3968	09:24:35	OK	2561
09:34:35	OK	9914	09:34:35	OK	8661	09:34:35	OK	8778
10:44:01	OK	4081	10:44:01	OK	2498	10:44:01	OK	2468
09:08:37	OK	35634	09:08:37	OK	6601	09:08:37	OK	4139
09:45:54	OK	36515	09:45:54	OK	6635	09:45:54	OK	4214
10:08:22	OK	14899	10:08:22	OK	2288	10:08:22	OK	10816
11:42:29	OK	15050	11:42:29	OK	2320	11:42:29	OK	11172
09:29:44	OK	15223	09:29:44	OK	2347	09:29:44	OK	11373
09:43:11	OK	15407	09:43:11	OK	2352	09:43:11	OK	11564
09:52:01	OK	15407	09:52:01	OK	2369	09:52:01	OK	11672
10:06:17	OK	13865	10:06:17	OK	2566	10:06:17	OK	2243
10:11:57	OK	13584	10:11:57	OK	2712	10:11:57	OK	2686
U12CE05								
BLUE_Time Stamp	**BLUE_Status**	**BLUE_Resist**	**GREEN_TimeStamp**	**GREEN_Status**	**GREEN_Resist**	**RED_Time Stamp**	**RED_Status**	**RED_Resist**
11:07:24	OK	57405	11:07:24	OK	59631	11:07:24	OK	52953
11:47:04	OK	3492	11:47:03	OK	4150	11:47:01	OK	3230
11:58:16	OK	2762	11:58:16	OK	1310	11:58:16	OK	1457
12:08:17	OK	2927	12:08:17	OK	1351	12:08:17	OK	1409
12:18:15	OK	6063	12:18:15	OK	1353	12:18:15	OK	1384
12:28:16	OK	6644	12:28:16	OK	1368	12:28:16	OK	1390
12:38:11	OK	7129	12:38:11	OK	1377	12:38:11	OK	1392
12:47:39	OK	9221	12:47:39	OK	1416	12:47:39	OK	1354
09:12:39	OK	7554	09:12:39	OK	1299	09:12:39	OK	1438

09:32:26	OK	9353	09:32:26	OK	1342	09:32:26	OK	5322
10:45:30	OK	4627	10:45:30	OK	2548	10:45:30	OK	2758
09:09:10	OK	10309	09:09:10	OK	1497	09:09:10	OK	5475
09:46:37	OK	10556	09:46:37	OK	1511	09:46:37	OK	5761
10:07:42	OK	13240	10:07:42	OK	10626	10:07:42	OK	6639
11:43:00	OK	12401	11:43:00	OK	9923	11:43:00	OK	6743
09:32:30	OK	14001	09:32:30	OK	10626	09:32:30	OK	6780
09:44:13	OK	13240	09:44:13	OK	10890	09:44:13	OK	6891
09:53:17	OK	13578	09:53:17	OK	11549	09:53:17	OK	6788
10:07:23	OK	18332	10:07:23	OK	10626	10:07:23	OK	11564
10:12:44	OK	14027	10:12:44	OK	10412	10:12:44	OK	11672

U12CE04

BLUE_Time Stamp	BLUE_S tatus	BLUE_R esist	GREEN_Tim eStamp	GREEN_ Status	GREEN_ Resist	RED_Time Stamp	RED_St atus	RED_R esist
11:03:35	OK	59631	11:03:35	OK	59631	11:03:35	OK	57405
11:44:35	OK	1875	11:44:13	OK	2067	11:44:11	OK	2421
11:55:05	OK	1161	11:55:05	OK	907	11:55:05	OK	1272
12:05:17	OK	1119	12:05:17	OK	900	12:05:17	OK	1085
12:15:02	OK	1094	12:15:02	OK	919	12:15:02	OK	1047
12:25:05	OK	1097	12:25:05	OK	931	12:25:05	OK	1052
12:35:14	OK	1117	12:35:14	OK	944	12:35:14	OK	1065
12:44:56	OK	1149	12:44:56	OK	933	12:44:56	OK	1088
09:40:14	OK	3540	09:40:14	OK	3250	09:40:14	OK	4260
09:36:14	OK	3311	09:36:14	OK	5998	09:36:14	OK	3699
10:46:11	OK	3475	10:46:11	OK	5278	10:46:11	OK	1895
09:11:34	OK	5495	09:11:34	OK	5213	09:11:34	OK	7162
09:47:01	OK	5620	09:47:01	OK	5281	09:47:01	OK	7327
10:08:59	OK	8022	10:08:59	OK	8068	10:08:59	OK	11452
11:43:40	OK	8174	11:43:40	OK	8223	11:43:40	OK	11755
09:35:17	OK	8174	09:35:17	OK	8273	09:35:17	OK	11858
09:45:38	OK	8277	09:45:38	OK	8073	09:45:38	OK	11966
09:54:40	OK	8279	09:54:40	OK	8435	09:54:40	OK	12074
10:08:30	OK	8277	10:08:30	OK	8383	10:08:30	OK	11966
10:13:59	OK	8279	10:13:59	OK	8435	10:13:59	OK	12074

U12A06

BLUE_Time Stamp	BLUE_S tatus	BLUE_R esist	GREEN_Tim eStamp	GREEN_ Status	GREEN_ Resist	RED_Time Stamp	RED_St atus	RED_R esist
11:21:32	OK	55179	11:21:32	OK	57405	11:21:32	OK	59631
11:35:22	OK	2043	11:35:23	OK	2034	11:38:12	OK	4668
11:47:56	OK	854	11:47:56	OK	992	11:47:56	OK	2476
11:58:43	OK	849	11:58:43	OK	1025	11:58:43	OK	2241

12:08:40	OK	803	12:08:40	OK	974	12:08:40	OK	2276
12:19:00	OK	833	12:19:00	OK	1029	12:19:00	OK	2313
12:28:33	OK	805	12:28:33	OK	888	12:28:33	OK	2176
12:38:21	OK	867	12:38:21	OK	871	12:38:21	OK	2161
09:37:24	OK	823	09:37:24	OK	1031	09:37:24	OK	2144
09:17:24	OK	6210	09:17:24	OK	1191	09:17:24	OK	2130
09:10:10	OK	6976	09:10:10	OK	1250	09:10:10	OK	2455
09:21:55	OK	7233	09:21:55	OK	1344	09:21:55	OK	2566
09:24:13	OK	6340	09:24:13	OK	1476	09:24:13	OK	2178
10:07:27	OK	7652	10:07:27	OK	1455	10:07:27	OK	2781
10:10:40	OK	8124	10:10:40	OK	1599	10:10:40	OK	2602
11:34:29	OK	7899	11:34:29	OK	1467	11:34:29	OK	2888
12:10:40	OK	8427	12:10:40	OK	1899	12:10:40	OK	2943
12:13:09	OK	6945	12:13:09	OK	2136	12:13:09	OK	2879
12:42:47	OK	8996	12:42:47	OK	2485	12:42:47	OK	2934
11:15:51	OK	11345	11:15:51	OK	2863	11:15:51	OK	3135

U12A05

BLUE_Time Stamp	BLUE_Status	BLUE_Resist	GREEN_TimeStamp	GREEN_Status	GREEN_Resist	RED_Time Stamp	RED_Status	RED_Resist
11:04:14	OK	59631	11:04:14	OK	59631	11:04:14	OK	55179
11:18:06	OK	2143	11:18:02	OK	2231	11:18:04	OK	2624
11:29:06	OK	1395	11:29:06	OK	1442	11:29:06	OK	1010
11:39:30	OK	1402	11:39:30	OK	1443	11:39:30	OK	986
11:49:04	OK	1374	11:49:04	OK	1422	11:49:04	OK	991
11:59:05	OK	1323	11:59:05	OK	1387	11:59:05	OK	996
12:09:07	OK	1257	12:09:07	OK	1350	12:09:07	OK	1001
12:19:28	OK	1218	12:19:28	OK	1305	12:19:28	OK	1001
09:19:28	OK	1144	09:19:28	OK	1294	09:19:28	OK	995
09:16:05	OK	1547	09:16:05	OK	2856	09:16:05	OK	4036
09:11:02	OK	2427	09:11:02	OK	1752	09:11:02	OK	3089
09:22:59	OK	2552	09:22:59	OK	2591	09:22:59	OK	2916
09:25:40	OK	2573	09:25:40	OK	3312	09:25:40	OK	2813
10:08:39	OK	2444	10:08:39	OK	5084	10:08:39	OK	2309
10:11:58	OK	2634	10:11:58	OK	4369	10:11:58	OK	3689
11:35:50	OK	1559	11:35:50	OK	2323	11:35:50	OK	2515
12:11:44	OK	1320	12:11:44	OK	1713	12:11:44	OK	2099
12:14:18	OK	2506	12:14:18	OK	4348	12:14:18	OK	1632
12:44:01	OK	2688	12:44:01	OK	3694	12:44:01	OK	4062
11:17:01	OK	1691	11:17:01	OK	2775	11:17:01	OK	1686

U12A04

BLUE_Time Stamp	BLUE_S tatus	BLUE_R esist	GREEN_Tim eStamp	GREEN_ Status	GREEN_ Resist	RED_Time Stamp	RED_St atus	RED_R esist
10:53:34	OK	59631	10:53:34	OK	59631	10:53:34	OK	52953
11:08:13	OK	1328	11:08:13	OK	1136	11:08:13	OK	1230
11:16:04	OK	1152	11:16:04	OK	977	11:16:04	OK	1004
11:25:47	OK	1132	11:25:47	OK	990	11:25:47	OK	1008
11:36:23	OK	1140	11:36:23	OK	1000	11:36:23	OK	1000
11:43:34	OK	1162	11:43:34	OK	1024	11:43:34	OK	1015
11:56:00	OK	1151	11:56:00	OK	1013	11:56:00	OK	995
12:06:09	OK	1167	12:06:09	OK	1030	12:06:09	OK	1005
09:36:14	OK	1405	09:36:14	OK	3280	09:36:14	OK	4324
10:36:14	OK	4689	10:36:14	OK	2723	10:36:14	OK	2530
09:12:05	OK	7972	09:12:05	OK	7166	09:12:05	OK	7372
09:23:50	OK	10344	09:23:50	OK	9260	09:23:50	OK	6140
09:27:01	OK	8328	09:27:01	OK	11234	09:27:01	OK	11334
10:09:50	OK	13409	10:09:50	OK	10981	10:09:50	OK	11261
10:12:58	OK	13957	10:12:58	OK	11261	10:12:58	OK	11755
11:37:01	OK	14108	11:37:01	OK	11359	11:37:01	OK	11755
12:12:37	OK	14403	12:12:37	OK	11461	12:12:37	OK	11755
12:15:27	OK	14403	12:15:27	OK	11564	12:15:27	OK	11971
12:45:40	OK	17834	12:45:40	OK	15233	12:45:40	OK	20058
11:18:12	OK	20097	11:18:12	OK	18768	11:18:12	OK	23441

U12B06

BLUE_Time Stamp	BLUE_S tatus	BLUE_R esist	GREEN_Tim eStamp	GREEN_ Status	GREEN_ Resist	RED_Time Stamp	RED_St atus	RED_R esist
11:42:21	OK	59631	11:42:21	OK	59631	11:42:21	OK	57405
11:45:14	OK	2415	11:45:05	OK	3220	11:45:17	OK	2403
11:54:09	OK	2192	11:54:09	OK	2641	11:54:09	OK	2023
12:04:58	OK	2209	12:04:58	OK	2614	12:04:58	OK	1998
12:14:45	OK	2109	12:14:45	OK	2469	12:14:45	OK	1862
12:24:36	OK	2347	12:24:36	OK	2672	12:24:36	OK	2055
12:34:45	OK	2064	12:34:45	OK	2393	12:34:45	OK	1814
12:43:00	OK	2127	12:43:00	OK	2444	12:43:00	OK	1866
09:21:21	OK	3059	09:21:21	OK	2040	09:21:21	OK	1903
09:04:45	OK	2580	09:04:45	OK	1831	09:04:45	OK	1903
09:07:45	OK	2990	09:07:45	OK	1789	09:07:45	OK	1943
09:33:28	OK	3230	09:33:28	OK	2000	09:33:28	OK	2035
09:10:17	OK	3494	09:10:17	OK	2119	09:10:17	OK	2134
09:38:00	OK	3134	09:38:00	OK	2380	09:38:00	OK	1987
09:56:19	OK	3774	09:56:19	OK	2413	09:56:19	OK	2294
09:10:50	OK	4592	09:10:50	OK	2349	09:10:50	OK	2034
09:18:39	OK	4250	09:18:39	OK	2371	09:18:39	OK	2421

10:55:31	OK	4321	10:55:31	OK	2438	10:55:31	OK	2440
09:40:57	OK	4157	09:40:57	OK	2320	09:40:57	OK	2589
09:21:35	OK	4693	09:21:35	OK	2549	09:21:35	OK	2679

U12B05

BLUE_Time Stamp	BLUE_S tatus	BLUE_R esist	GREEN_Tim eStamp	GREEN_ Status	GREEN_ Resist	RED_Time Stamp	RED_St atus	RED_R esist
11:29:58	OK	59631	11:29:58	OK	59631	11:29:58	OK	57405
11:31:01	OK	2715	11:31:54	OK	2810	11:31:56	OK	2451
11:41:57	OK	1766	11:41:57	OK	1214	11:41:57	OK	1301
11:51:53	OK	1621	11:51:53	OK	1079	11:51:53	OK	1232
12:01:03	OK	1596	12:01:03	OK	1055	12:01:03	OK	1243
12:11:23	OK	1558	12:11:23	OK	1042	12:11:23	OK	1262
12:21:59	OK	1530	12:21:59	OK	1043	12:21:59	OK	1283
12:31:49	OK	1508	12:31:49	OK	1045	12:31:49	OK	1274
09:22:47	OK	2191	09:22:47	OK	1812	09:22:47	OK	1766
09:03:48	OK	3460	09:03:48	OK	2195	09:03:48	OK	1993
09:06:09	OK	3664	09:06:09	OK	2031	09:06:09	OK	2131
09:32:14	OK	3090	09:32:14	OK	1940	09:32:14	OK	1845
09:09:23	OK	4012	09:09:23	OK	2445	09:09:23	OK	1923
11:19:01	OK	3540	11:19:01	OK	2200	11:19:01	OK	2458
09:55:20	OK	3987	09:55:20	OK	2327	09:55:20	OK	2780
09:09:58	OK	4356	09:09:58	OK	2544	09:09:58	OK	2637
09:17:02	OK	4455	09:17:02	OK	2358	09:17:02	OK	2839
10:56:20	OK	4276	10:56:20	OK	2623	10:56:20	OK	3167
09:39:11	OK	4087	09:39:11	OK	2512	09:39:11	OK	2944
09:20:22	OK	5137	09:20:22	OK	2949	09:20:22	OK	3123

U12B04

BLUE_Time Stamp	BLUE_S tatus	BLUE_R esist	GREEN_Tim eStamp	GREEN_ Status	GREEN_ Resist	RED_Time Stamp	RED_St atus	RED_R esist
11:24:02	OK	59631	11:24:02	OK	52953	11:24:02	OK	57405
11:24:16	OK	2781	11:24:16	OK	1700	11:24:16	OK	2252
11:34:28	OK	1459	11:34:28	OK	909	11:34:28	OK	1267
11:44:32	OK	1458	11:44:32	OK	886	11:44:32	OK	1261
11:54:53	OK	1456	11:54:53	OK	872	11:54:53	OK	1252
12:04:30	OK	1462	12:04:30	OK	868	12:04:30	OK	1255
12:14:21	OK	1482	12:14:21	OK	856	12:14:21	OK	1236
12:24:26	OK	1425	12:24:26	OK	847	12:24:26	OK	1208
09:19:34	OK	1612	09:19:34	OK	1926	09:19:34	OK	2124
09:05:38	OK	2106	09:05:38	OK	2093	09:05:38	OK	2163
09:09:12	OK	2624	09:09:12	OK	2370	09:09:12	OK	2321
09:35:01	OK	2958	09:35:01	OK	2143	09:35:01	OK	2504
09:11:32	OK	2870	09:11:32	OK	2702	09:11:32	OK	2757
10:11:55	OK	3481	10:11:55	OK	2910	10:11:55	OK	2220

09:58:11	OK	3951	09:58:11	OK	3540	09:58:11	OK	2583
09:08:44	OK	3651	09:08:44	OK	3112	09:08:44	OK	2190
09:15:24	OK	3945	09:15:24	OK	3310	09:15:24	OK	2623
10:58:23	OK	3711	10:58:23	OK	3159	10:58:23	OK	2477
09:38:40	OK	3845	09:38:40	OK	3945	09:38:40	OK	2713
09:19:17	OK	4845	09:19:17	OK	4189	09:19:17	OK	3011

U12C27

BLUE_Time Stamp	BLUE_S tatus	BLUE_R esist	GREEN_Tim eStamp	GREEN_ Status	GREEN_ Resist	RED_Time Stamp	RED_St atus	RED_R esist
10:32:04	OK	59631	10:32:04	OK	52953	10:32:04	OK	57405
10:32:36	OK	4037	10:33:28	OK	2956	10:41:23	OK	3022
10:51:34	OK	1551	10:51:34	OK	1558	10:51:34	OK	1821
11:01:14	OK	1461	11:01:14	OK	1534	11:01:14	OK	1664
11:10:00	OK	1253	11:10:00	OK	1400	11:10:00	OK	1750
11:19:11	OK	1010	11:19:11	OK	1061	11:19:11	OK	932
11:29:12	OK	1040	11:29:12	OK	1227	11:29:12	OK	1137
11:39:08	OK	1048	11:39:08	OK	1356	11:39:08	OK	1273
12:55:40	OK	22078	12:55:40	OK	3836	12:55:40	OK	4973
09:13:56	OK	30916	09:13:56	OK	6466	09:13:56	OK	8545
10:53:16	OK	37078	10:53:16	OK	10212	10:53:16	OK	13560
09:10:28	OK	43240	09:10:28	OK	13957	09:10:28	OK	18515
09:15:14	OK	28990	09:15:14	OK	11163	09:15:14	OK	13679
08:59:23	OK	47611	08:59:23	OK	20143	08:59:23	OK	25772
09:02:07	OK	47611	09:02:07	OK	22078	09:02:07	OK	28990
09:27:34	OK	47611	09:27:34	OK	24413	09:27:34	OK	30916
09:05:23	OK	47611	09:05:23	OK	26764	09:05:23	OK	32347
10:15:49	OK	46883	10:15:49	OK	24421	10:15:49	OK	29556
09:50:26	OK	46154	09:50:26	OK	22078	09:50:26	OK	26764
10:35:12	OK	46154	10:35:12	OK	22078	10:35:12	OK	25344

U12C54

BLUE_Time Stamp	BLUE_S tatus	BLUE_R esist	GREEN_Tim eStamp	GREEN_ Status	GREEN_ Resist	RED_Time Stamp	RED_St atus	RED_R esist
11:02:11	OK	57405	11:02:11	OK	52953	11:02:11	OK	57405
11:02:35	OK	4511	11:03:01	OK	2941	11:04:35	OK	2392
11:11:58	OK	1443	11:11:58	OK	1208	11:11:58	OK	1649
11:21:14	OK	1448	11:21:14	OK	1173	11:21:14	OK	1274
11:31:33	OK	1458	11:31:09	OK	1186	11:31:09	OK	1193
11:41:17	OK	1405	11:41:17	OK	1152	11:41:17	OK	1383
11:49:08	OK	1091	11:49:08	OK	1435	11:49:08	OK	1538
12:04:09	OK	1349	12:04:09	OK	1236	12:04:09	OK	1990
12:53:20	OK	5696	12:53:20	OK	2700	12:53:20	OK	3269
09:16:10	OK	10460	09:16:10	OK	4291	09:16:10	OK	5167
10:33:20	OK	17226	10:33:20	OK	6535	10:33:20	OK	7985
09:08:25	OK	23991	09:08:25	OK	8778	09:08:25	OK	10803

09:13:29	OK	43240	09:13:29	OK	26764	09:13:29	OK	29580
09:01:39	OK	33110	09:01:39	OK	13274	09:01:39	OK	16503
09:04:08	OK	38569	09:04:08	OK	15384	09:04:08	OK	19029
09:30:17	OK	40811	09:30:17	OK	17565	09:30:17	OK	21068
09:08:12	OK	43240	09:08:12	OK	19586	09:08:12	OK	23188
10:08:14	OK	48097	10:08:14	OK	24288	10:08:14	OK	29852
09:52:58	OK	52953	09:52:58	OK	28990	09:52:58	OK	36515
10:32:40	OK	52953	10:32:40	OK	34289	10:32:40	OK	42365
U12C14								
BLUE_Time Stamp	**BLUE_S tatus**	**BLUE_R esist**	**GREEN_Tim eStamp**	**GREEN_ Status**	**GREEN_ Resist**	**RED_Time Stamp**	**RED_St atus**	**RED_R esist**
10:46:39	OK	59631	10:46:39	OK	52953	10:46:39	OK	52953
10:48:54	OK	3159	10:48:57	OK	2455	10:49:05	OK	3210
10:59:15	OK	1163	10:59:15	OK	1410	10:59:15	OK	1967
11:14:12	OK	1309	11:14:12	OK	1395	11:14:12	OK	1708
11:24:15	OK	1333	11:24:15	OK	1426	11:24:15	OK	1835
11:34:26	OK	1314	11:34:26	OK	1430	11:34:26	OK	1896
11:44:15	OK	1333	11:44:15	OK	1353	11:44:15	OK	1944
11:54:09	OK	1349	11:54:09	OK	1260	11:54:09	OK	1527
12:54:36	OK	20751	12:54:36	OK	7006	12:54:36	OK	8603
09:15:13	OK	30248	09:15:13	OK	12188	09:15:13	OK	13957
10:15:33	OK	36744	10:15:33	OK	17688	10:15:33	OK	19865
09:09:34	OK	43240	09:09:34	OK	23188	09:09:34	OK	25772
09:11:36	OK	43240	09:11:36	OK	17125	09:11:36	OK	22425
09:00:17	OK	47611	09:00:17	OK	28990	09:00:17	OK	32347
09:03:08	OK	47611	09:03:08	OK	30916	09:03:08	OK	34753
09:28:54	OK	47611	09:28:54	OK	33110	09:28:54	OK	36515
09:06:49	OK	47611	09:06:49	OK	34753	09:06:49	OK	36515
10:06:02	OK	50282	10:06:02	OK	35634	10:06:02	OK	38056
09:51:52	OK	52953	09:51:52	OK	36515	09:51:52	OK	39597
10:30:47	OK	52953	10:30:47	OK	39375	10:30:47	OK	41123

UNDERGROUND GROUT SENSOR DATA (4,5 m UNITS)								
U45CE06								
BLUE_Time Stamp	**BLUE_S tatus**	**BLUE_R esist**	**GREEN_Tim eStamp**	**GREEN_ Status**	**GREEN_ Resist**	**RED_Time Stamp**	**RED_St atus**	**RED_R esist**
10:50:00	OK	43240	10:50:00	OK	57405	10:50:00	OK	43240
11:05:13	OK	1357	11:05:13	OK	1145	11:05:14	OK	1350
11:15:39	OK	837	11:15:39	OK	834	11:15:39	SHORT	701

11:25:40	OK	840	11:25:40	OK	821	11:25:40	SHORT	674
11:35:14	OK	852	11:35:14	OK	879	11:35:14	SHORT	707
11:44:42	OK	910	11:44:42	OK	838	11:44:42	SHORT	681
11:53:25	OK	932	11:53:25	OK	854	11:53:25	SHORT	691
12:04:42	OK	845	12:04:42	OK	825	12:04:42	SHORT	668
12:14:33	OK	1058	12:14:33	OK	1132	12:14:33	SHORT	675
10:30:15	OK	1117	10:30:15	OK	1197	10:30:15	SHORT	762
10:14:14	OK	1875	10:14:14	OK	1683	10:14:14	SHORT	719
09:35:51	OK	2824	09:35:51	OK	2666	09:35:51	SHORT	726
09:45:10	OK	2917	09:45:10	OK	2834	09:45:10	SHORT	710
09:14:23	OK	2973	09:14:23	OK	2911	09:14:23	SHORT	763
10:56:37	OK	2990	10:56:37	OK	2951	10:56:37	SHORT	703
10:07:41	OK	2998	10:07:41	OK	2983	10:07:41	SHORT	751
09:29:50	OK	3103	09:29:50	OK	3013	09:29:50	SHORT	775
09:40:33	OK	2945	09:40:33	OK	2833	09:40:33	SHORT	714
10:42:11	OK	3288	10:42:11	OK	3099	10:42:11	SHORT	763
09:38:33	OK	3461	09:38:33	OK	3193	09:38:33	SHORT	750

U45CE05

BLUE_Time Stamp	BLUE_S tatus	BLUE_R esist	GREEN_Tim eStamp	GREEN_ Status	GREEN_ Resist	RED_Time Stamp	RED_St atus	RED_R esist
10:59:16	OK	57405	10:59:16	OK	55179	10:59:16	OK	55179
11:10:01	OK	1372	11:10:09	OK	1407	11:10:14	OK	1835
11:18:28	OK	1345	11:18:28	OK	1392	11:18:28	OK	1776
11:28:48	OK	1229	11:28:48	OK	1390	11:28:48	OK	1780
11:38:43	OK	1243	11:38:43	OK	1270	11:38:43	OK	1043
11:48:21	OK	1167	11:48:21	OK	1276	11:48:21	OK	995
11:58:21	OK	1044	11:58:21	OK	1134	11:58:21	OK	967
12:08:21	OK	987	12:08:21	OK	1057	12:08:21	OK	923
12:15:40	OK	896	11:08:01	OK	973	11:08:01	OK	803
10:32:31	OK	953	10:32:31	OK	899	10:32:31	OK	3100
10:15:11	OK	1139	10:15:11	OK	973	10:15:11	OK	3163
09:36:33	OK	1171	09:36:33	OK	974	09:36:33	OK	5748
09:45:59	OK	1919	09:45:59	OK	1229	09:45:59	OK	5856
09:15:05	OK	1996	09:15:05	OK	1257	09:15:05	OK	5912
10:57:13	OK	2034	10:57:13	OK	2299	10:57:13	OK	6041
10:08:40	OK	2048	10:08:40	OK	2380	10:08:40	OK	5998
09:30:41	OK	2065	09:30:41	OK	2415	09:30:41	OK	6258
09:41:13	OK	1987	09:41:13	OK	2438	09:41:13	OK	6279
10:43:20	OK	2194	10:43:20	OK	2461	10:43:20	OK	6291
09:39:34	OK	2472	09:39:34	OK	2499	09:39:34	OK	6532

U45CE04

BLUE_Time Stamp	BLUE_S tatus	BLUE_R esist	GREEN_Tim eStamp	GREEN_ Status	GREEN_ Resist	RED_Time Stamp	RED_St atus	RED_R esist
10:55:12	OK	59631	10:55:12	OK	59631	10:55:12	OK	52953
11:09:55	OK	1542	11:09:55	OK	1230	11:09:55	OK	872
11:19:12	OK	1445	11:19:12	OK	1201	11:19:12	OK	883
11:29:40	OK	1403	11:29:40	OK	1189	11:29:40	OK	844
11:39:14	OK	1390	11:39:14	OK	1100	11:39:14	OK	956
11:49:01	OK	1183	11:49:01	OK	1090	11:49:01	OK	994
11:59:56	OK	1123	11:59:56	OPEN	65535	11:59:56	OK	1048
12:09:25	OK	1386	12:09:25	OPEN	65535	12:09:25	OK	923
12:16:22	OK	1549	12:16:22	OPEN	65535	12:16:22	OK	1280
10:31:50	OK	1959	10:31:50	OPEN	65535	10:31:50	OK	1374
10:15:59	OK	1006	10:15:59	OPEN	65535	10:15:59	OK	1644
09:37:47	OK	997	09:37:47	OPEN	65535	09:37:47	OK	1429
09:46:30	OK	3461	09:46:30	OPEN	65535	09:46:30	OK	1149
09:16:00	OK	3593	09:16:00	OPEN	65535	09:16:00	OK	1341
10:59:55	OK	3674	10:59:55	OPEN	65535	10:59:55	OK	1897
10:09:21	OK	3734	10:09:21	OPEN	65535	10:09:21	OK	2307
09:31:13	OK	3784	09:31:13	OPEN	65535	09:31:13	OK	3429
10:31:13	OK	3638	10:31:13	OPEN	65535	10:31:13	OK	4931
11:31:13	OK	3940	11:31:13	OPEN	65535	11:31:13	OK	4538
12:31:13	OK	4003	12:31:13	OPEN	65535	12:31:13	OK	6891
U45A06								
BLUE_Time Stamp	BLUE_S tatus	BLUE_R esist	GREEN_Tim eStamp	GREEN_ Status	GREEN_ Resist	RED_Time Stamp	RED_St atus	RED_R esist
13:00:43	OK	59631	13:00:43	OK	59631	13:00:43	OK	52953
13:03:49	OK	3428	13:03:52	OK	3050	13:03:31	OK	2757
13:13:46	OK	2278	13:13:46	OK	1789	13:13:46	OK	1491
13:23:29	OK	2225	13:23:29	OK	1605	13:23:29	OK	1451
13:33:38	OK	2238	13:33:38	OK	1433	13:33:38	OK	1397
13:43:29	OK	2256	13:43:29	OK	1346	13:43:29	OK	1316
13:53:30	OK	2269	13:53:30	OK	1306	13:53:30	OK	1266
14:03:31	OK	2293	14:03:31	OK	1287	14:03:31	OK	1226
09:55:23	OK	3219	09:55:23	OK	2473	09:55:23	OK	2723
10:27:25	OK	3969	10:27:25	OK	3335	10:27:25	OK	3504
09:16:11	OK	4546	09:16:11	OK	4294	09:16:11	OK	4523
09:28:21	OK	5122	09:28:21	OK	5253	09:28:21	OK	5542
09:40:45	OK	5516	09:40:45	OK	5887	09:40:45	OK	6271
09:19:26	OK	2577	09:19:26	OK	2580	09:19:26	OK	6359
09:11:01	OK	5723	09:11:01	OK	5913	09:11:01	OK	6673
09:29:40	OK	6470	09:29:40	OK	7413	09:29:40	OK	7006
09:34:36	OK	6677	09:34:36	OK	7457	09:34:36	OK	7124

09:18:17	OK	6785	09:18:17	OK	7544	09:18:17	OK	7204
09:43:10	OK	6819	09:43:10	OK	7574	09:43:10	OK	7246
09:12:22	OK	6856	09:12:22	OK	7590	09:12:22	OK	7530

U45A05

BLUE_Time Stamp	BLUE_S tatus	BLUE_R esist	GREEN_Tim eStamp	GREEN_ Status	GREEN_ Resist	RED_Time Stamp	RED_St atus	RED_R esist
12:58:09	OK	59631	12:58:09	OK	59631	12:58:09	OK	55179
12:58:39	OK	2618	12:58:44	OK	2369	12:58:54	OK	3022
13:08:06	OK	2308	13:08:06	OK	1462	13:08:06	OK	1788
13:18:06	OK	2404	13:18:06	OK	1725	13:18:06	OK	1421
13:28:03	OK	2488	13:28:03	OK	1724	13:28:03	OK	1390
13:38:05	OK	2518	13:38:05	OK	1682	13:38:05	OK	1383
13:48:05	OK	2532	13:48:05	OK	1633	13:48:05	OK	1385
13:58:12	OK	2526	13:58:12	OK	1593	13:58:12	OK	1387
09:53:26	OK	4612	09:53:26	OK	3620	09:53:26	OK	3880
10:24:18	OPEN	65535	10:24:18	OPEN	65535	10:24:18	OPEN	65535
09:15:16	OPEN	65536	09:15:16	OPEN	65536	09:15:16	OPEN	65536
09:27:16	OPEN	65535	09:27:16	OPEN	65535	09:27:16	OPEN	65535
09:39:16	OPEN	65535	09:39:16	OPEN	65535	09:39:16	OPEN	65535
09:04:01	OPEN	65535	09:04:01	OPEN	65535	09:04:01	OPEN	65535
09:12:16	OPEN	65535	09:12:16	OPEN	65535	09:12:16	OPEN	65535
09:30:59	OPEN	65535	09:30:59	OPEN	65535	09:30:59	OPEN	65535
09:35:40	OPEN	65535	09:35:40	OPEN	65535	09:35:40	OPEN	65535
09:19:55	OPEN	65535	09:19:55	OPEN	65535	09:19:55	OPEN	65535
09:44:27	OPEN	65535	09:44:27	OPEN	65535	09:44:27	OPEN	65535
09:13:41	OPEN	65535	09:13:41	OPEN	65535	09:13:41	OPEN	65535

U45A04

BLUE_Time Stamp	BLUE_S tatus	BLUE_R esist	GREEN_Tim eStamp	GREEN_ Status	GREEN_ Resist	RED_Time Stamp	RED_St atus	RED_R esist
12:44:18	OK	59631	12:44:18	OK	52953	12:44:18	OK	55179
12:49:44	OK	3549	12:52:09	OK	2262	12:53:07	OK	3110
12:59:16	OK	1729	12:59:16	OK	1525	12:59:16	OK	2350
13:08:53	OK	1495	13:08:53	OK	1406	13:08:53	OK	2163
13:19:03	OK	1400	13:19:03	OK	1379	13:19:03	OK	2087
13:29:03	OK	1340	13:29:03	OK	1354	13:29:03	OK	2035
13:39:31	OK	1289	13:39:31	OK	1315	13:39:31	OK	1989
13:49:00	OK	1274	13:49:00	OK	1297	13:49:00	OK	1981
09:57:44	OK	4128	09:57:44	OK	4261	09:57:44	OK	3514
10:29:54	OK	5081	10:29:54	OK	4575	10:29:54	OK	4260
09:16:38	OK	6652	09:16:38	OK	5850	09:16:38	OK	5576
09:29:27	OK	8223	09:29:27	OK	7124	09:29:27	OK	6891

10:38:15	OK	8493	10:38:15	OK	6553	10:38:15	OK	6816
09:05:15	OK	9296	09:05:15	OK	7793	09:05:15	OK	9853
09:13:19	OK	9620	09:13:19	OK	8379	09:13:19	OK	7919
09:31:53	OK	10715	09:31:53	OK	9412	09:31:53	OK	8959
09:36:22	OK	10803	09:36:22	OK	9478	09:36:22	OK	9088
09:21:07	OK	10981	09:21:07	OK	9499	09:21:07	OK	9148
09:45:59	OK	11075	09:45:59	OK	9511	09:45:59	OK	9239
09:15:11	OK	11502	09:15:11	OK	9549	09:15:11	OK	9385

U45B06

BLUE_Time Stamp	BLUE_S tatus	BLUE_R esist	GREEN_Tim eStamp	GREEN_ Status	GREEN_ Resist	RED_Time Stamp	RED_St atus	RED_R esist
10:42:38	OK	55179	10:42:43	OK	55179	10:42:10	OK	55179
11:43:38	OK	2342	11:43:43	OK	2760	11:43:10	OK	3112
11:53:55	OK	1628	11:53:55	OK	1258	11:53:55	OK	1733
12:03:17	OK	1714	12:03:17	OK	1204	12:03:17	OK	1500
12:13:32	OK	1740	12:13:32	OK	1231	12:13:32	OK	1386
12:25:10	OK	1655	12:25:10	OK	1226	12:25:10	OK	1342
12:36:29	OK	1827	12:36:29	OK	1367	12:36:29	OK	1421
12:46:54	OK	1640	12:46:54	OK	1328	12:46:54	OK	1355
09:35:14	OK	1406	09:35:14	OK	2573	09:35:14	OK	1906
10:50:41	OK	1547	10:50:41	OK	978	10:50:41	OK	1101
12:04:31	OK	1533	12:04:31	OK	986	12:04:31	OK	1113
11:06:01	OK	1572	11:06:01	OK	1005	11:06:01	OK	1106
10:18:57	OK	1613	10:18:57	OK	1098	10:18:57	OK	1050
11:35:30	OK	1649	11:35:30	OK	1129	11:35:30	OK	1238
11:26:58	OK	1501	11:26:58	OK	1177	11:26:58	OK	1299
10:54:51	OK	1789	10:54:51	OK	1145	10:54:51	OK	1199
12:18:11	OK	1599	12:18:11	OK	1093	12:18:11	OK	1236
10:55:31	OK	1823	10:55:31	OK	984	10:55:31	OK	1290
10:40:57	OK	1846	10:40:57	OK	893	10:40:57	OK	1372
10:43:35	OK	1989	10:43:35	OK	1193	10:43:35	OK	1204

U45B05

BLUE_Time Stamp	BLUE_S tatus	BLUE_R esist	GREEN_Tim eStamp	GREEN_ Status	GREEN_ Resist	RED_Time Stamp	RED_St atus	RED_R esist
11:50:39	OK	52953	11:50:39	OK	65535	11:50:39	OK	52953
12:00:48	OK	1475	12:00:48	OK	1169	12:00:48	OK	1408
12:00:53	OK	1180	12:00:53	OK	1007	12:00:53	OK	1098
12:20:19	OK	1300	12:20:19	OK	1353	12:20:19	OK	1250
12:31:21	OK	1331	12:31:21	OK	1207	12:31:21	OK	1351
12:41:13	OK	1150	12:41:13	OK	1277	12:41:13	OK	1301
12:51:59	OK	1364	12:51:59	OK	1470	12:51:59	OK	1319

13:01:32	OK	1381	13:01:32	OK	1245	13:01:32	OK	1361
09:36:33	OK	4789	09:36:33	OK	2721	09:36:33	OK	2960
10:51:45	OK	5023	10:51:45	OK	2915	10:51:45	OK	2992
12:05:50	OK	1449	12:05:50	OK	2771	12:05:50	OK	1942
11:07:13	OK	1483	11:07:13	OK	2792	11:07:13	OK	1958
10:19:47	OK	3570	10:19:47	OK	2830	10:19:47	OK	3058
11:36:52	OK	3501	11:36:52	OK	1993	11:36:52	OK	2919
11:27:51	OK	3276	11:27:51	OK	2681	11:27:51	OK	2374
10:55:59	OK	3678	10:55:59	OK	4459	10:55:59	OK	1820
12:19:04	OK	3806	12:19:04	OK	4838	12:19:04	OK	4222
10:56:42	OK	2773	10:56:42	OK	3185	10:56:42	OK	2097
10:42:33	OK	4325	10:42:33	OK	1802	10:42:33	OK	3049
10:44:50	OK	2755	10:44:50	OK	3702	10:44:50	OK	2946

U45B04

BLUE_Time Stamp	BLUE_S tatus	BLUE_R esist	GREEN_Tim eStamp	GREEN_ Status	GREEN_ Resist	RED_Time Stamp	RED_St atus	RED_R esist
11:40:08	OK	55179	11:40:08	OK	55179	11:40:08	OK	55179
11:45:56	OK	1679	11:46:04	OK	1065	11:46:17	OK	1445
11:55:11	OK	1035	11:55:11	OK	966	11:55:11	OK	1380
12:05:52	OK	1057	12:05:52	OK	1645	12:05:52	OK	1149
12:15:05	OK	1346	12:15:05	OK	1369	12:15:05	OK	1635
12:25:08	OK	1370	12:25:08	OK	1627	12:25:08	OK	1647
12:35:56	OK	1580	12:35:56	OK	1129	12:35:56	OK	1401
12:45:05	OK	1031	12:45:05	OK	1591	12:45:05	OK	1156
09:37:59	OK	1787	09:37:59	OK	1626	09:37:59	OK	2926
10:52:58	OK	4774	10:52:58	OK	2948	10:52:58	OK	3075
12:07:11	OK	4624	12:07:11	OK	3049	12:07:11	OK	3418
11:05:44	OK	4142	11:05:44	OK	5117	11:05:44	OK	3967
10:21:02	OK	4495	10:21:02	OK	3160	10:21:02	OK	3086
11:37:59	OK	4094	11:37:59	OK	3079	11:37:59	OK	4649
12:28:58	OK	4377	12:28:58	OK	3798	12:28:58	OK	3834
10:57:01	OK	4929	10:57:01	OK	4210	10:57:01	OK	4484
12:21:33	OK	4230	12:21:33	OK	3728	12:21:33	OK	4473
10:57:57	OK	4885	10:57:57	OK	3148	10:57:57	OK	3662
10:44:01	OK	4009	10:44:01	OK	4659	10:44:01	OK	3812
10:46:07	OK	3312	10:46:07	OK	3131	10:46:07	OK	5081

U45C27

BLUE_Time Stamp	BLUE_S tatus	BLUE_R esist	GREEN_Tim eStamp	GREEN_ Status	GREEN_ Resist	RED_Time Stamp	RED_St atus	RED_R esist
12:19:56	OK	57405	12:19:56	OK	52953	12:19:56	OK	55179
12:20:12	OK	2125	12:20:18	OK	1312	12:20:37	OK	1204

12:31:58	OK	985	12:31:58	OK	840	12:31:58	OK	984
12:40:51	OK	1023	12:40:51	OK	825	12:40:51	OK	978
12:50:54	OK	1027	12:50:54	OK	851	12:50:54	OK	986
13:05:33	OK	951	13:05:33	OK	921	13:05:33	OK	801
13:14:20	OK	1079	13:14:20	OK	923	13:14:20	OK	984
13:22:23	OK	1013	13:22:23	OK	911	13:22:23	OK	851
12:48:44	OK	2042	12:48:44	OK	1219	12:48:44	OK	1692
08:57:27	OK	4455	08:57:27	OK	2221	08:57:27	OK	3154
08:57:40	OK	6004	08:57:40	OK	4328	08:57:40	OK	5179
09:02:40	OK	7553	09:02:40	OK	6435	09:02:40	OK	7204
08:59:48	OK	8785	08:59:48	OK	8549	08:59:48	OK	9344
08:53:42	OK	10143	08:53:42	OK	10072	08:53:42	OK	10981
08:51:15	OK	11863	08:51:15	OK	11765	08:51:15	OK	12530
09:21:19	OK	13274	09:21:19	OK	13154	09:21:19	OK	14403
09:15:45	OK	15050	09:15:45	OK	14565	09:15:45	OK	15925
09:34:22	OK	16422	09:34:22	OK	15534	09:34:22	OK	17220
10:05:22	OK	17793	10:05:22	OK	16503	10:05:22	OK	18515
09:53:24	OK	18232	09:53:24	OK	17432	09:53:24	OK	19450

U45C54

BLUE_Time Stamp	BLUE_S tatus	BLUE_R esist	GREEN_Tim eStamp	GREEN_ Status	GREEN_ Resist	RED_Time Stamp	RED_St atus	RED_R esist
13:18:53	OK	52953	13:18:53	OK	52953	13:18:53	OK	52953
13:19:05	OK	2212	13:19:18	OK	2211	13:19:26	OK	1966
13:29:07	OK	1153	13:29:07	OK	1243	13:29:07	OK	1040
13:38:53	OK	1322	13:38:53	OK	1230	13:38:53	OK	1139
13:49:43	OK	1299	13:49:43	OK	1445	13:49:43	OK	1215
13:59:42	OK	1290	13:59:42	OK	1532	13:59:42	OK	1227
14:09:48	OK	1266	14:09:48	OK	1530	14:09:48	OK	1249
14:20:48	OK	1267	14:20:48	OK	1540	14:20:48	OK	1271
12:45:53	OK	3773	12:45:53	OK	4504	12:45:53	OK	3032
08:56:06	OK	5830	08:56:06	OK	8068	08:56:06	OK	5101
08:57:33	OK	8276	08:57:33	OK	11245	08:57:33	OK	8133
09:00:33	OK	10722	09:00:33	OK	14422	09:00:33	OPEN	65535
09:02:50	OK	13019	09:02:50	OK	17581	09:02:50	OPEN	65535
08:52:39	OK	15384	08:52:39	OK	20460	08:52:39	OPEN	65535
08:49:48	OK	17793	08:49:48	OK	22460	08:49:48	OPEN	65535
09:19:17	OK	18782	09:19:17	OK	23188	09:19:17	OPEN	65535
09:14:30	OK	20751	09:14:30	OK	25772	09:14:30	OPEN	65535
09:34:49	OK	23027	09:34:49	OK	24480	09:34:49	OPEN	65535
10:03:49	OK	25303	10:03:49	OK	23188	10:03:49	OPEN	65535
09:51:02	OK	27445	09:51:02	OK	24134	09:51:02	OPEN	65535

U45C14								
BLUE_Time Stamp	BLUE_Status	BLUE_Resist	GREEN_TimeStamp	GREEN_Status	GREEN_Resist	RED_Time Stamp	RED_Status	RED_Resist
12:41:36	OK	57405	12:41:36	OK	52953	12:41:36	OK	59631
12:42:08	OK	2393	12:42:12	OK	2729	12:42:50	OK	2212
12:53:34	OK	2219	12:53:34	OK	1938	12:53:34	OK	2140
13:00:55	OK	2148	13:00:55	OK	1529	13:00:55	OK	1816
13:10:18	OK	1096	13:10:18	OK	947	13:10:18	OK	1047
13:20:59	OK	1087	13:20:59	OK	926	13:20:59	OK	958
13:32:45	OK	996	13:32:45	OK	993	13:32:45	OK	878
13:42:56	OK	1080	13:42:56	OK	1170	13:42:56	OK	900
12:47:51	OK	9478	12:47:51	OK	10460	12:47:51	OK	11075
08:58:48	OK	16306	08:58:48	OK	19029	08:58:48	OK	19029
08:57:33	OK	25700	08:57:33	OK	29489	08:57:33	OK	30104
09:05:33	OK	25699	09:05:33	SHORT	285	09:05:33	SHORT	287
09:05:39	OK	25772	09:05:39	SHORT	281	09:05:39	SHORT	282
08:54:50	OK	28401	08:54:50	SHORT	288	08:54:50	SHORT	288
08:52:57	OK	31584	08:52:57	SHORT	285	08:52:57	SHORT	287
09:23:05	OK	33110	09:23:05	SHORT	290	09:23:05	SHORT	290
09:16:57	OK	33873	09:16:57	SHORT	281	09:16:57	SHORT	281
09:34:39	OK	35194	09:34:39	SHORT	287	09:34:39	SHORT	291
10:06:39	OK	36515	10:06:39	SHORT	283	10:06:39	SHORT	283
09:49:18	OK	36726	09:49:18	SHORT	287	09:49:18	SHORT	277